Study of the Creeping Motion of a Sphere in the Presence of a Deformable Fluid/Fluid Interface

Thesis by

Clarke Berdan II

In Partial Fulfillment of the Requirements
for the Degree of
Doctor of Philosophy

California Institute of Technology
Pasadena, California

1982

(Submitted September 22, 1981)

To my wife, Karen, and our daughter, Louise.

ACKNOWLEDGMENTS

I wish to express my appreciation to my advisor, Professor L. G. Leal, for suggesting this research topic and for his guidance throughout. He was a constant source of new perspectives and encouragement. It was a pleasure to work with all the members of Dr. Leal's research group, as well as to interact with all the graduate students, many of whom contributed greatly to my growth. I specifically would like to acknowledge my debt to Paul Chan, Tony Geller, Seong Lee, Bill Moonan, and Art Stelson for the many discussions of both scientific and social value.

Much of the credit for the success of the experiments belongs to George Griffith, John Yehle, Seichi Nakawatase, and Ray Reed for their fine work and many ideas that went into the apparatus.

To my parents are due many thanks for their love and encouragement they have provided for as long as I can remember.

And to my wife, who suffered with me through my failures and never could fully enjoy my successes, for all the love and support I owe everything.

ABSTRACT

The creeping motion of a rigid sphere in the presence of a deformable fluid/fluid interface has been considered using theoretical, experimental and numerical techniques. Solutions for small perturbations in shape, for an initially flat interface, are obtained to calculate the additional forces and torques on a sphere rotating and translating both normal to and parallel with a slightly deformed interface. The interfacial shape as well as the forces and torques are calculated as a function of sphere position and interfacial deformation parameters; viscosity ratio, capillary number, and ratio of Bond number to capillary number. The interface deformation was found to yield no correction to the torque or parallel force on the sphere for any combination of sphere motion. The interface deformation did yield a force directed way from the interface for all sphere motions which generate a deformation for the interface.

A new direct force measurement experimental apparatus is used to study the normal motion of a rigid sphere approaching a deformable interface under conditions of constant interfacial deformation parameters. The sphere was lowered at a constant velocity and the force on the body was measured as a function of the interface shape and values of the deformation parameters.

Study of the translation of a nonrotating sphere parallel with a fluid/fluid interface, experiencing finite amplitude deformations, utilizes a numerical collocation technique. The forces and torques on the body are calculated as a function of body displacement from the interface and the interface deformation parameter (ratio of Bond number to capillary number). The interface shapes are determined and the forces and torques on the sphere are calculated.

TABLE OF CONTENTS

CHAPTER I:

INTRODUCTION

The creeping motion of bubbles, drops and particles through a viscous medium near a fluid interface has long been of interest in industrial applications. For example, in metallurgical processes the transfer of contaminant materials from the molten metal to the molten slag involves the motion of small particulates near much larger gas bubbles. In this process the fluid motion and interfacial properties can affect the rate of contaminant removal and a first approximation to the problem is obtained by considering the motion of a particle near an interface which is flat in its undeformed state. Other processes which involve coalescence phenomena are concerned with the passage of a body across a fluid/fluid interface. In this case we would normally be concerned with the relative motion of two drops. However, for the case of one drop much larger than the other, the problem can again be treated as the motion of a drop near a 'flat' fluid/fluid interface.

These phenomena indicate that the motion of a sphere in the presence of a deformable interface is of interest as a model problem. The details of the sphere/interface interaction are of primary concern, particularly the mechanism of penetration of the interfacial boundary for a particle which moves normal to the undeformed surface. Two alternative mechanisms of penetration exist, depending upon whether the interface breaks at the leading surface of the body or breaks behind the body. The first case corresponds to the well-known film drainage configuration, in which a thin film is formed along the leading surface and rupture occurs somewhere in this film. The second mechanism is associated with the formation of a tail of fluid following the sphere for the case of large deformations. The penetration process is completed in this case when this tail breaks. The motion of the sphere can be studied in either of two modes, fixed velocity or moving freely under the action of external forces. It is expected that the "free" motion of the body is more realistic for practical applications, however, the fixed velocity problem provides a more convenient vehicle for study

over a wide range of values of the dimensionless groups since these are easily adjustable by simply changing the velocity of the particle.

There has been a considerable amount of theoretical and experimental work related to the general problem of particle motion near an interface. Brenner (1961) solved the creeping flow problem of both translation and rotation of a rigid sphere near a nondeformable flat interface where the second fluid is either rigid or inviscid. This work was extended to arbitrary viscosity for the second fluid in the work by Lee, Chadwick, and Leal (1979). Their solution involved a series representation for the velocity field for large values of the dimensionless distance to the interface. An exact solution in terms of bipolar coordinates for this same problem was presented by Lee and Leal (1980). These solutions for motion near a flat interface are relevant only in limiting circumstances when the interface remains approximately flat. In the general case of a fluid/fluid interface it is necessary to take into account any interfacial deformation which is present. Some aspects of this more general problem involving the deformation of the interface have been studied experimentally by Princen (1963) and Hartland (1969). In both of these investigations, the primary focus was in the dynamics of film drainage in circumstances when the sphere is very near the interface. In order to carry out these studies, the sphere was placed initially very near the interface and the gap between the sphere and the interface was measured as the sphere moved closer to the interface under the action of gravity. Bart (1968) studied the "free fall" of a sphere toward a deformable interface starting from large distances and continuing up to a distance of two body lengths from the undeformed interface. Shah, Wasan, and Kintner (1972) later studied the mechanism of interface penetration, but only for a relatively limited number of cases. Finally, Lee and Leal (1981) calculated interface shapes and forces on a sphere for the normal approach to a deformable interface in the creeping flow limit using a numerical solution scheme.

Their work provides the first study for which the entire normal approach of a sphere to the interface has been investigated (albeit, numerically).

To this point, there have been no complete analytic solutions for motion of a sphere near a deformable interface. The primary difficulty is that the interface shape is unknown. However, such an analytic solution would provide valuable insight into the dependence of the motion of the sphere on interfacial properties. The most obvious candidate for analytic solution is the limiting case of small but nonzero deformations. The obvious limitations of considering only a small deformations are offset, for the most part, by this potential application of the solution to arbitrary particle motion. In particular, in the limit of a nearly flat interface, solutions for translation normal and parallel to the interface can be superposed, together with solutions for rotation normal and parallel to the interface, to obtain results for an arbitrary particle motion.

In this investigation we study the general problem of the creeping motion of a sphere in the presence of a deformable interface, both theoretically and experimentally. From the governing equations and boundary conditions we can identify the dimensionless groups that are important for the general problem. In the creeping motion limit, the equations of motion for steady Stokes' flow in the two fluids on either side of the interface are

$$\begin{aligned} 0 &= -\nabla p_1 + \mu_1 \nabla^2 \mathbf{u}_1 \\ 0 &= \nabla \cdot \mathbf{u}_1 \end{aligned} \qquad \text{for Fluid 1} \qquad (1)$$

and

$$\begin{aligned} 0 &= -\nabla p_2 + \mu_2 \nabla^2 \mathbf{u}_2 \\ 0 &= \nabla \cdot \mathbf{u}_2 \end{aligned} \qquad \text{for Fluid 2} \qquad (2)$$

where μ is the viscosity, $\mathbf{u}$ is the velocity and $p_i = p - \rho_i g z$, i=1,2, where p is the thermodynamic pressure and we have removed the hydrostatic head as

measured from the undeformed interface. The two fluids are designated by subscripts 1 and 2. The sphere has radius a and velocity U (or Ω for rotation, with resulting characteristic velocity Ω a), and is located initially in fluid 2. It is assumed in the present work that it remains wholly in that fluid. The boundary conditions are,

$$\mathbf{u}_1,\ \mathbf{u}_2 \to 0 \qquad \text{as } |\mathbf{x}| \to \infty, \tag{3}$$

$$\mathbf{u}_2 \text{ specified on the sphere surface,} \tag{4}$$

and on the interface,

$$\mathbf{u}_1 = \mathbf{u}_2, \tag{5}$$

$$\mathbf{n}\cdot\mathbf{u}_1 = \mathbf{n}\cdot\mathbf{u}_2 = \frac{1}{|\nabla f|}\frac{\partial f}{\partial t}, \tag{6}$$

$$\mu_1\,\mathbf{n}\cdot\mathbf{T}_1 - \mu_2\,\mathbf{n}\cdot\mathbf{T}_2 = g(\rho_2-\rho_1)\,f\mathbf{n} - \gamma\left(\frac{1}{R_1}+\frac{1}{R_2}\right)\mathbf{n}, \tag{7}$$

where the interface position is given by the scalar function

$$F \equiv z - f(\rho, \varphi, t) = 0 \tag{8}$$

for the cylindrical coordinate system (ρ, φ, z). The densities are represented as ρ_1 and ρ_2, while the interfacial tension is γ, and g is the acceleration due to gravity. We also have $\mathbf{T}_i \equiv -p_i\mathbf{I} + \tau_i$, where $\mathbf{T}_i$ is the stress tensor in fluid i, τ_i is the viscous stress tensor and i=1,2. It can be seen in equation (7) that the change in pressure at the interface associated with the hydrostatic head in the presence of deformation has been separated from the left hand side. This points out the role of the density difference across the interface as it relates to the stress jump. Finally, R_1 and R_2 are the principal radii of curvature at the interface.

We take the particle radius, a, and velocity, U, as the characteristic length and velocity respectively. While the characteristic stress is given as, $\frac{\mu_2 U}{a}$. This yields the dimensionless equations of motion,

$$0 = -\nabla p_1 + \mu_1 \nabla^2 \mathbf{u}_1$$
$$0 = \nabla \cdot \mathbf{u}_1 \qquad \text{for Fluid 1} \tag{9}$$

and

$$0 = -\nabla p_2 + \mu_2 \nabla^2 \mathbf{u}_2$$
$$0 = \nabla \cdot \mathbf{u}_2 \qquad \text{for Fluid 2} \tag{10}$$

$$\nabla \cdot \mathbf{u}_2 = 0,$$

with boundary conditions,

$$\mathbf{u}_1,\ \mathbf{u}_2 \to 0 \qquad \text{as } |\mathbf{x}| \to \infty, \tag{11}$$

$$\mathbf{u}_2 \text{ specified on the sphere surface,} \tag{12}$$

and on the interface,

$$\mathbf{u}_1 = \mathbf{u}_2, \tag{13}$$

$$\mathbf{n}\cdot\mathbf{u}_1 = \mathbf{n}\cdot\mathbf{u}_2 = \frac{1}{|\nabla F|}\frac{\partial f}{\partial t}, \tag{14}$$

$$\lambda\,\mathbf{n}\cdot\mathbf{T}_1 - \mathbf{n}\cdot\mathbf{T}_2 = \frac{1}{Cg} f\mathbf{n} - \frac{1}{Ca}\left(\frac{1}{R_1} + \frac{1}{R_2}\right)\mathbf{n}. \tag{15}$$

The dimensionless groups which appear in equations (9)--(15) are,

$$\lambda \equiv \frac{\mu_1}{\mu_2} \quad \text{Viscosity Ratio,} \tag{16}$$

$$Ca \equiv \frac{\mu_2 U}{\gamma} \quad \text{Capillary Number,} \tag{17}$$

and

$$Cg \equiv \frac{Ca}{B} \equiv \frac{\mu_2 U}{g a^2 (\rho_2 - \rho_1)} \quad \frac{\text{Capillary Number}}{\text{Bond Number}} \tag{18}$$

along with, $\frac{l}{a}$, the dimensionless distance of the sphere from the position of the

undeformed interface. It is obvious that surface tension and/or the density differences in the two fluids will be most effective at retaining a flat interface when the dimensionless parameters, Ca and Cg, are small. Specifically, for small Ca, forces associated with the interfacial tension are large relative to the viscous forces and for small Cg, the forces associated with the density difference across the interface are large relative to the viscous forces. It should be noted that $\alpha \equiv Cg^{-1}$ and $\beta \equiv Ca^{-1}$ in Chapter II.

This general problem of motion of a sphere near a deformable interface is studied in this thesis using three different methods. In Chapter II we study the deformation of the interface under conditions of small Ca or small Cg which results in a small perturbation of the interface from flat. The solution is based on the velocity fields calculated for motion near a flat interface by Lee, Chadwick and Leal (1979), which consist of the leading two terms in a series solution with respect to l^{-1}. It may be noted that $\frac{\partial f}{\partial t}$ is taken as zero in equation (14) corresponding to the assumption of a flat interface in the solution of Lee et al. (1979). Also, the normal component of equation (15) was not used because of the restriction that the interface remain flat. Our goal in Chapter II is thus to provide analytic results for arbitrary motion of a sphere near a slightly deformed interface. The solutions are obtained using the so-called "domain perturbation" technique in which the exact boundary conditions at the deformed interface are replaced by asymptotically equivalent conditions applied at the undeformed interface position. Thus, results for arbitrary motion of the sphere can be constructed from the solutions for rotation and translation parallel and normal to the interface by simple superposition as was noted earlier. The calculation reported here proceeds from the results of Lee, Chadwick, and Leal (1979) to calculation of the interface shape at first order using equation (15) and from this, to a determination of the corresponding corrections to

the forces and torques on the sphere associated with this deformation.

Chapter III reports on a new experimental apparatus designed to measure the force on a sphere as it moves normal to the interface for large interfacial deformation. In the results from this study, the distance from sphere center to the initial undisturbed interface position is given as l, with positive values of l meaning that the center of the sphere has not penetrated the plane of the undesturbed interface, whereas negative values for l indicate the sphere center has actually passed beyond this plane. The experimental work provides a study of the effects of Cg, λ, and l on the force on the body as well as the interface shape. The results for this experimental method indicate promise for future studies of inertial and non-Newtonian effects, again for motion near a deformable interface, and point to the potential importance of the inhibition of interface motion due to surface tension gradients in some cases.

Finally in Chapter IV, numerical solutions are obtained for the creeping motion problem of the translation of a non-rotating sphere parallel to a deformable interface, but with no restriction on the allowable magnitude of deformation. The interface shape, as well as the forces and torques on the sphere, are determined as a function of l and Cg for $Ca \to \infty$ by satisfying equations (9)--(15) at discrete points on all surfaces. This investigation provides a further study of certain features of the small deformation results of Chapter II for the same problem.

References

Bart, E. 1968 The slow unsteady settling of a (fluid, solid) sphere toward a flat interface. Chem. Eng. Sci. **23**, 193.

Brenner, H. 1961 The slow motion of a sphere through a viscous fluid towards a plane surface. Chem. Eng. Sci. **16**, 242.

Hartland, S. 1969 The profile of the draining film between a rigid sphere and a deformable fluid-liquid interface. Chem. Eng. Sci. **24**, 987.

Lee, S. H., Chadwick, R. S. & Leal, L. G. 1979 Motion of a sphere in the presence of a plane interface. Part 1: An approximate solution by generalization of the method of Lorentz. J. Fluid Mech. **93**, 705.

Lee, S. H. and Leal, L. G. 1980 Motion of a sphere in the presence of a plane interface. Part 2: An exact solution in bipolar coordinates. J. Fluid Mech. **98**, 193.

Lee, S. H. and L. G. Leal 1981 The Motion of a Sphere in the Presence of a Deformable Interface Part 2: A Numerical Study of the Translation of a Sphere Normal to an Interface, Submitted **JCIS**.

Princen, H. M. 1963 Shape of a fluid drop at a liquid-liquid interface. J. Coll. Sci. **18**, 178.

Shah, S. T., Wasan, D. T. and Kintner, R. C. 1972 Passage of a liquid drop through a liquid-liquid interface. Chem. Eng. Sci. **27**, 881.

CHAPTER II:

Motion of a Sphere in the Presence of a Deformable Interface.

Part 1. Perturbation of the Interface from Flat:

The Effects on Drag and Torque

(Accepted)

Journal Colloid and Interface Science

Motion of a Sphere in the Presence of a Deformable Interface.

Part 1. Perturbation of the Interface from Flat:

The Effects on Drag and Torque

by

C. Berdan II and L. G. Leal

Department of Chemical Engineering
California Institute of Technology
Pasadena, California 91125

Abstract

We investigate the effect of small deformations of an initially flat fluid interface on the force and torque experienced by a nearby translating and rotating solid sphere. The small deformation problem is reformulated in terms of equivalent boundary conditions on a *flat* interface; this allows a separation of the rotation and translation problems, along with their respective components parallel and normal to the undeformed interface. Results for the force and torque corrections due to interface deformation are thus calculated for the four fundamental cases of translation normal and parallel to the undeformed interface, and rotation with the axis of rotation normal and parallel to the undeformed interface. These results can be superposed to obtain the force and torque on a sphere which is undergoing an arbitrary translational and/or rotational motion near the interface.

I. Introduction

When a small spherical particle translates at very low Reynolds number through an unbounded viscous fluid, it is subjected to a force

$$\underline{F} = 6\pi\mu a\underline{U} \tag{1}$$

as calculated over 100 years ago by Stokes. When the same particle rotates under similar circumstances it experiences a torque

$$\underline{T} = 8\pi\mu a^3\underline{\Omega}. \tag{2}$$

Here we have denoted the velocity of the sphere relative to that of the suspending fluid at large distances from the sphere as $\underline{U}$ and the relative angular velocity as $\underline{\Omega}$. The sphere radius is represented by a, and the viscosity of the fluid by μ.

Recently, Lee, Chadwick, and Leal (1979) have considered the translation and rotation of a rigid sphere in the vicinity of a *flat* fluid interface between two immiscible Newtonian fluids with a viscosity ratio, λ. In this case, both the creeping flow equations and boundary conditions are linear, and the force and torque can be expressed in a dimensionless relationship of the form

$$\underline{F}/\mu aU = \mathbf{K}_T\cdot\hat{\underline{U}} + \mathbf{K}_C^{\dagger}\cdot\hat{\underline{\Omega}}\,\frac{a\Omega}{U} \tag{3}$$

$$\underline{T}/\mu a^3\Omega = \mathbf{K}_C\cdot\hat{\underline{U}}\,\frac{U}{a\Omega} + \mathbf{K}_R\cdot\hat{\underline{\Omega}} \tag{4}$$

where $\hat{\underline{U}}$ and $\hat{\underline{\Omega}}$ are the translational and angular velocities of the particle, scaled with respect to the speeds U and Ω, respectively. The coefficients $\mathbf{K}_T$, $\mathbf{K}_C$ and $\mathbf{K}_R$ are second-rank tensors, known as 'resistance' tensors, where $\mathbf{K}_C^{\dagger}$ is the transpose of $\mathbf{K}_C$. When expressed in terms of Cartesian axes that lie normal and parallel to the interface, these take the relatively simple forms

$$\mathbf{K}_T = 6\pi \begin{pmatrix} K_{\parallel}^T & 0 & 0 \\ 0 & K_{\parallel}^T & 0 \\ 0 & 0 & K_{\perp}^T \end{pmatrix} \tag{5}$$

$$\mathbf{K}_C = 6\pi \begin{pmatrix} 0 & K_C & 0 \\ -K_C & 0 & 0 \\ 0 & 0 & 0 \end{pmatrix} \tag{6}$$

and

$$\mathbf{K}_R = 8\pi \begin{pmatrix} K_{\parallel}^R & 0 & 0 \\ 0 & K_{\parallel}^R & 0 \\ 0 & 0 & K_{\perp}^R \end{pmatrix} \tag{7}$$

The components of these resistance matrices were shown by Lee, Chadwick, and Leal (1979) to be a function of λ, and of the distance between the sphere center and the interface relative to the particle radius, l/a. In the limit, $l/a \to \infty$, $\mathbf{K}_C \to 0$, while $\mathbf{K}_T$ and $\mathbf{K}_R$ both approach the unit matrix, $\mathbf{I}$. Approximate results for the coefficients of these matrices were determined by Lee, Chadwick, and Leal (1979) for large but finite l/a, while exact but more cumbersome results were obtained by Lee and Leal (1980) for arbitrary $l/a > 1$. Not only does the presence of the interface modify the force and torque for simple translation and rotation, but in general, there is a coupling between translational and rotational motions of the sphere. Thus, for example, a particle which is acted upon by a torque will both rotate and translate, while the effect of an external force is likewise to produce both translation and rotation. It may be noted, however, that the basic linearity and symmetry of the Stokes' flow problem for a sphere near a *plane* interface insures that the translational motion produced by an applied force can only be co-linear with the force, and similarly, the rotation due to a torque can only be co-linear with the torque.

All of the results of the preceding paragraph pertain to the case in which the interface remains precisely flat, in spite of the motions induced in the two fluids by the motion of the sphere. Of course, a real interface cannot remain precisely flat since the motions induced in the two fluids by the motion of the sphere yield a normal stress difference across the interface. The results of Lee, Chadwick, and Leal (1979) and Lee and Leal (1980) must, therefore, be recognized as applying only asymptotically in the limit of arbitrarily small interface deformations. Indeed, Lee, Chadwick, and Leal (1979), have stated conditions for this limit to apply, namely

$$\beta^{-1} \equiv \left(\frac{\gamma}{\mu^{(2)}U} \right)^{-1} << 1 \quad \text{or} \quad \alpha^{-1} \equiv \left[\frac{\rho^{(2)} g a^2}{\mu^{(2)}U} \left(1 - \frac{\rho^{(1)}}{\rho^{(2)}} \right) \right]^{-1} << 1 \qquad (8)$$

for arbitrary $l/a \geq 0(1)$. Here, γ and ρ represent the interfacial tension and fluid density, respectively, while g is the acceleration due to gravity. The two fluids are designated by the superscripts (1) and (2), with fluid (1) lying above fluid (2). Lee, Chadwick and Leal's (1979) analysis applies to the case in which the sphere is assumed to be located in fluid (2).

In the present paper, we consider the consequences of small but finite values of α^{-1} or β^{-1}, so that the first effects of interface deformation need be taken into account. Defining a composite small parameter, ε, as

$$\varepsilon \equiv \frac{1}{\alpha + \beta} \qquad (9)$$

we can deal in a simple way with systems where either, or both surface tension and the density difference are significant. The solutions of Lee, Chadwick, and Leal (1979) and Lee and Leal (1980) correspond, then, to the first, 0(1), term in an asymptotic expansion for small ε and satisfy the conditions of continuity of the tangential velocity and stress fields at the undeformed interface, as well as zero normal velocity. However, they do produce an

imbalance in the normal stress components across the flat interface, and thus, to proceed beyond Lee, Chadwick and Leal (1979) and Lee and Leal (1980), it is necessary to first calculate the $O(\varepsilon)$ correction to the interface shape, and then to determine the effect of the predicted interface deformation at $O(\varepsilon)$ on the force and torque which act on the sphere. Although the force and torque corrections will necessarily be small, also $O(\varepsilon)$, they can be calculated rather simply in this asymptotic framework, thus allowing a useful qualitative examination of the effects of interface deformation. It may be noted that the "large" deformation problem, in which the interface deformation is *not* restricted to be small, is highly nonlinear, as a consequence of the normal stress boundary condition, and the rather simple superposition principle inherent in equations (3) and (4) for calculating $\underline{F}$ and $\underline{T}$ for an arbitrary $\underline{U}$ or $\underline{\Omega}$ is lost. In the limit of small ε, however, the problem remains quasi-linear at each order and the basic expressions (3) and (4) for $\underline{F}$ and $\underline{T}$ are still expected to apply, albeit with additional components in the resistance tensors which depend explicitly on ε.

The analysis for small ε proceeds in a straight forward fashion from the results of either Lee, Chadwick, and Leal (1979) or Lee and Leal (1980). However, in the present paper we shall restrict ourselves to the simpler case of small a/l, discussed by Lee, Chadwick, and Leal (1979) where an approximate and relatively simple analytical solution was obtained at $O(1)$. The interface shape can be expressed in terms of a scalar function, F, where

$$F = z - f(\rho, \varphi, t) = 0 \tag{10}$$

and the function, f, which describes the deformation is written in the asymptotic case, $\varepsilon << 1$, as

$$f = \varepsilon f_1 + \varepsilon^2 f_2 + \cdots. \tag{11}$$

The shape function, f, is determined from the zero-order solutions of Lee, Chadwick and Leal (1979) for the velocity and pressure fields, by first calculating the normal stress imbalance at the undeformed interface (which is a consequence of the fact that the interface is approximated as flat at O(1)) and then applying the normal stress condition

$$\underline{n}\cdot[\lambda\underline{n}\cdot\mathbf{T}^{(1)} - \underline{n}\cdot\mathbf{T}^{(2)}]_{z=0} = \mathbf{L}f \tag{12}$$

from which we can obtain an equation that can be solved for f_1. Here, **L** is a differential operator which is defined in the next section and $\mathbf{T} \equiv -p + \tau$ where p is the hydrodynamic pressure and τ is the stress tensor. With f_1 known, the most obvious procedure is then to determine the velocity and pressure distributions in the two fluids at $O(\varepsilon)$, and calculate the corresponding contributions to the force and torque on the particle, again at $O(\varepsilon)$. Although straightforward in principle, this latter calculation is tedious and, fortunately, unnecessary. Instead, we shall see that the effects of interface deformation on the force and torque at $O(\varepsilon)$ can be obtained via the reciprocal theorem directly from the interface shape function f_1 and the solutions of Lee, Chadwick, and Leal (1979) for the velocity and pressure fields at O(1).

II. Governing Equations

We begin by considering the computation of the interface shape at $O(\varepsilon)$ in somewhat more detail, using the normal stress condition (12). In equation (12) we have used **L** to represent the differential operator,

$$\mathbf{L}f \equiv \alpha f + \beta\left(\frac{1}{R_1} + \frac{1}{R_2}\right) \tag{13}$$

where R_1 and R_2 are the principal radii of curvature for the interface. The sum $(1/R_1 + 1/R_2)$ is simply calculated as the divergence of the unit normal to the interface (i.e. $\nabla \cdot \underline{n}$); where,

$$\underline{n} \equiv \frac{\nabla F}{|\nabla F|} = \kappa\left(\underline{i}_z - \frac{\partial f}{\partial \rho}\underline{i}_\rho - \frac{1}{\rho}\frac{\partial f}{\partial \varphi}\underline{i}_\varphi \right) \tag{14}$$

and

$$\kappa \equiv \frac{1}{|\nabla F|} = \left[1 + \left(\frac{\partial f}{\partial \rho}\right)^2 + \frac{1}{\rho^2}\left(\frac{\partial f}{\partial \varphi}\right)^2 \right]^{-1/2} . \tag{15}$$

In order to proceed analytically, we assume that the deformation, f, is small, and that it can be represented asymptotically in the form of equation (11), where ε is the small parameter of the problem, as defined in (9). Similar expansions of the velocity, pressure, and stress fields are then:

$$\underline{u}^{(k)} = \underline{u}_0^{(k)} + \varepsilon \underline{u}_1^{(k)} + \cdots, \tag{16}$$

$$p^{(k)} = p_0^{(k)} + \varepsilon p_1^{(k)} + \cdots, \tag{17}$$

$$\mathbf{T}^{(k)} = \mathbf{T}_0^{(k)} + \varepsilon \mathbf{T}_1^{(k)} + \cdots, \qquad k = 1, 2, \tag{18}$$

where the O(1) terms, designated by the subscript 0, are simply the solutions for a flat fluid interface. A differential equation for the shape function f_1 at $O(\varepsilon)$ follows directly by substitution of (11), (13), and (18) into (12), noting that $\underline{n} = \underline{i}_z$ to O(1) in ε, which yields

$$-\Delta T_{zz} \equiv \left(\lambda T_{zz_0}^{(1)} - T_{zz_0}^{(2)}\right)_{z=0} = \alpha\varepsilon f_1 - \beta\varepsilon\left(\frac{\partial^2 f_1}{\partial \rho^2} + \frac{1}{\rho}\frac{\partial f_1}{\partial \rho} + \frac{1}{\rho^2}\frac{\partial^2 f_1}{\partial \varphi^2} \right) . \tag{19}$$

For convenience, we have denoted the normal stress difference, calculated using the zero order velocity and pressure fields at z=0, as $-\Delta T_{zz}$. It may be noted that ε multiplied by either α or β [see equation (9)] yields at least one O(1) term so that both sides of (19) are O(1). The normal stress difference, $-\Delta T_{zz}$, has been calculated by Lee, Chadwick, and Leal (1979) for the four fundamental problems of translation and rotation both parallel and

perpendicular to an interface which is flat to O(1). Thus, the linear differential equation (19) can be solved directly, together with the appropriate boundary conditions, to obtain f_1 for these four cases.

The normal stress differences calculated by Lee, Chadwick, and Leal (1979) are:

1) *Normal Translation*

$$-\Delta T_{zz} = \frac{9l^3}{R_0^5}\left(1 + \frac{3}{8}\,\frac{2+3\lambda}{1+\lambda}\,\frac{1}{l}\right) + O(l^{-4}) \tag{20a}$$

2) *Parallel Translation*

$$-\Delta T_{zz} = \frac{9l^2\rho\cos\varphi}{R_0^5}\left(1 - \frac{3}{16}\,\frac{2-3\lambda}{1+\lambda}\,\frac{1}{l}\right) + O(l^{-5}) \tag{20b}$$

3) *Normal Rotation*

$$-\Delta T_{zz} = 0 \tag{20c}$$

4) *Parallel Rotation*

$$-\Delta T_{zz} = \frac{12\rho\sin\varphi}{R_0^5}\left(l + \frac{3}{16}\,\frac{1}{1+\lambda}\,\frac{1}{l}\right) + O(l^{-7}) \tag{20d}$$

where $R_0 = (\rho^2 + l^2)^{1/2}$. These equations have been written for the cylindrical coordinate system (ρ, φ, z), and both ρ and l have been made dimensionless by scaling with the particle radius, a. It can be seen from (20c) that there will be no deformation of the interface at $O(\varepsilon)$, and at all higher orders, for rotation normal to the interface since the rotlet constitutes a complete solution which generates no normal stress difference at the interface. We will consider solutions for f_1 in the other three cases in the next section, subject to the conditions that f_1 be bounded everywhere, and approach zero as the distance along the interface from the sphere center approaches infinity (i.e. $\rho \to \infty$).

Let us now turn to the method of calculating corrections to the hydrodynamic forces and torques on the sphere due to the interface deformation at $O(\varepsilon)$. One way to approach this problem is simply to calculate the detailed velocity and pressure fields in the two fluids at $O(\varepsilon)$ and use this result directly to calculate force and torque corrections due to the interface deformation. At $O(\varepsilon)$, the governing differential equations in the two fluids are

$$\nabla p_1^{(k)} = \nabla^2 \underline{u}_1^{(k)} \tag{21a}$$

and

$$\nabla \cdot \underline{u}_1^{(k)} = 0. \tag{21b}$$

At the deformed interface, calculated now to $O(\varepsilon)$, we again require continuity of the tangential stress, along with the continuity of tangential and normal velocity components. An alternative approach is to use a Taylor series approximation to express the boundary conditions at the deformed boundary to $O(\varepsilon)$, in terms of equivalent conditions applied at the *undeformed* interface, $z=0$ [Chan and Leal (1978)]. These "equivalent" boundary conditions are

$$\underline{u}_1^{(1)} + f_1 \frac{\partial \underline{u}_0^{(1)}}{\partial z} = \underline{u}_1^{(2)} + f_1 \frac{\partial \underline{u}_0^{(2)}}{\partial z} \tag{22}$$

$$\underline{i}_z \cdot \underline{u}_1^{(1)} + \underline{i}_z \cdot f_1 \frac{\partial \underline{u}_0^{(1)}}{\partial z} - \underline{i}_\rho \cdot \frac{\partial f_1}{\partial \rho} \underline{u}_0^{(1)} - \underline{i}_\varphi \cdot \frac{1}{\rho} \frac{\partial f_1}{\partial \varphi} \underline{u}_0^{(1)} = \underline{i}_z \cdot \underline{u}_1^{(2)}$$

$$+ \underline{i}_z \cdot f_1 \frac{\partial \underline{u}_0^{(2)}}{\partial z} - \underline{i}_\rho \cdot \frac{\partial f_1}{\partial \rho} \underline{u}_0^{(2)} - \underline{i}_\varphi \cdot \frac{1}{\rho} \frac{\partial f_1}{\partial \varphi} \underline{u}_0^{(2)} = \frac{\partial f_1}{\partial t} = -\left(u \frac{\partial f_1}{\partial x} + v \frac{\partial f_1}{\partial y} \right) \tag{23}$$

and

$$\lambda \underline{i}_z \cdot \mathbf{T}_1^{(1)} - \underline{i}_z \cdot \mathbf{T}_1^{(2)} + \lambda f_1 \underline{i}_z \cdot \frac{\partial \mathbf{T}_0^{(1)}}{\partial z} - f_1 \underline{i}_z \cdot \frac{\partial \mathbf{T}_0^{(2)}}{\partial z} - \lambda \frac{\partial f_1}{\partial \rho} \underline{i}_\rho \cdot \mathbf{T}_0^{(1)} + \frac{\partial f_1}{\partial \rho} \underline{i}_\rho \cdot \mathbf{T}_0^{(2)}$$

$$-\lambda\,\frac{1}{\rho}\frac{\partial f_1}{\partial\varphi}\underline{i}_\varphi\cdot\mathbf{T}_0^{(1)}+\frac{1}{\rho}\frac{\partial f_1}{\partial\varphi}\underline{i}_\varphi\cdot\mathbf{T}_0^{(2)}=\alpha\varepsilon\left[-f_1\Big(\frac{\partial f_1}{\partial\rho}\underline{i}_\varphi+\frac{1}{\rho}\frac{\partial f_1}{\partial\varphi}\underline{i}_\rho\Big)+f_2\underline{i}_z\right]$$

$$+\beta\varepsilon\left[\Big(\frac{\partial^2 f_1}{\partial\rho^2}+\frac{1}{\rho}\frac{\partial f_1}{\partial\rho}+\frac{1}{\rho^2}\frac{\partial^2 f_1}{\partial\varphi^2}\Big)\Big(\frac{\partial f_1}{\partial\rho}\underline{i}_\rho+\frac{1}{\rho}\frac{\partial f_1}{\partial\varphi}\underline{i}_\varphi\Big)\right.$$

$$\left.-\Big(\frac{\partial^2 f_2}{\partial\rho^2}+\frac{1}{\rho}\frac{\partial f_2}{\partial\rho}+\frac{1}{\rho^2}\frac{\partial^2 f_2}{\partial\varphi^2}\Big)\underline{i}_z\right]\ . \tag{24}$$

It may be noted that the velocity at the sphere surface is identically zero at $O(\varepsilon)$, and the governing equations (21a) and (21b) are homogeneous so that the induced velocity and pressure fields at $O(\varepsilon)$ can be viewed as emanating from a nonzero normal velocity at the plane $z = 0$ [corresponding to the condition (23)], as well as from discontinuities in the tangential velocity and stress components at the same plane.

Instead of actually solving (21)--(24), a simpler method can be developed provided that one is interested only in the corrections to the force and torque on the sphere at $O(\varepsilon)$ rather than in a detailed resolution of the velocity and pressure fields. This method is based upon the reciprocal theorem of Lorentz (1907),

$$\int_S d\underline{s}\cdot\pi'\cdot\underline{v}''=\int_S d\underline{s}\cdot\pi''\cdot\underline{v}' \tag{25}$$

where $(\underline{v}',\pi')$ and $(\underline{v}'',\pi'')$ represent the velocity and stress fields corresponding to two creeping flows of the same fluid contained by the same bounding surface, S.

In the present application, our objective is to determine the $O(\varepsilon)$ contribution to the stress at the surface of the sphere which will yield the $O(\varepsilon)$ drag and torque. For this development, we identify $\underline{v}''$ as the $O(\varepsilon)$disturbance flow, $\underline{u}_1^{(k)}$, defined by equations (21)-(24) and the no-slip boundary condition at the sphere surface, while $\underline{v}'$ is the "complementary" Stokes flow velocity field,

$\hat{\underline{u}}^{(k)}$, for either translation or rotation of the particle in a prescribed direction in the presence of a flat fluid interface. It is evident from this definition that $\hat{\underline{u}}^{(k)}$ will be identical with one of the O(1) solutions $\underline{u}_0^{(k)}$ for translation or rotation either parallel or normal to a flat interface. The choice for $\hat{\underline{u}}^{(k)}$ depends upon the force or torque contribution which we require at $O(\varepsilon)$, as we shall explain below in detail. Let us first consider the remaining steps in the derivation of a formula for calculating the $O(\varepsilon)$ contributions to the force or torque for a general disturbance flow, $\underline{u}_1^{(k)}$ and a general "complementary" flow $\hat{\underline{u}}^{(k)}$. For the lower fluid (k=2), the reciprocal theorem is

$$\int_{A_2} (\mathbf{T}_1^{(2)} \cdot \hat{\underline{u}}^{(2)} - \hat{\mathbf{T}}^{(2)} \cdot \underline{u}_1^{(2)}) \cdot \underline{n} \, dA = 0 \tag{26}$$

where A_2 includes the flat interface and sphere surface. Similarly, in the upper fluid

$$\int_{A_1} (\mathbf{T}_1^{(1)} \cdot \hat{\underline{u}}^{(1)} - \hat{\mathbf{T}}^{(1)} \cdot \underline{u}_1^{(1)}) \cdot \underline{n} \, dA = 0 \tag{27}$$

where A_1 includes only the flat interface. Multiplying (27) by λ and subtracting the result from (26), we obtain

$$\int_{A_F} \left(-\lambda \mathbf{T}_1^{(1)} \cdot \hat{\underline{u}}^{(1)} + \lambda \hat{\mathbf{T}}^{(1)} \cdot \underline{u}_1^{(1)} + \mathbf{T}_1^{(2)} \cdot \hat{\underline{u}}^{(2)} - \hat{\mathbf{T}}^{(2)} \cdot \underline{u}_1^{(2)} \right) \cdot \underline{n} \, dA$$

$$= - \int_{A_S} \left(\mathbf{T}_1^{(2)} \cdot \hat{\underline{u}}^{(2)} - \hat{\mathbf{T}}^{(2)} \cdot \underline{u}_1^{(2)} \right) \cdot \underline{n} \, dA \tag{28}$$

where A_F is the undeformed fluid/fluid interface area (i.e. the plane, z=0), and A_S is the surface of the sphere. Now, the disturbance velocity on the sphere surface, i.e. $\underline{u}_1^{(2)}$, is identically equal to zero for any of the problems of translation or rotation. If we choose the complementary problem to be translation with unit velocity,

$$\hat{\underline{u}}^{(2)} \equiv \underline{i}_T \quad \text{on} \quad A_S \tag{29a}$$

where $\underline{i}_T$ indicates the direction of translation, the integral over A_S in (28)

reduces to

$$-\int_{A_S} (\mathbf{T}_1^{(2)}\cdot\underline{n})\cdot\underline{i}_T \, dA \tag{29b}$$

which is simply the force contribution on the sphere in the $\underline{i}_T$ direction at $O(\varepsilon)$ due to the interface deformation at $O(\varepsilon)$. This force can then be calculated by evaluating the left-hand side of (28) for any of the three problems of translation perpendicular or parallel or rotation parallel to the undeformed interface and the complementary velocity field corresponding to (29a). Similarly, if the complementary problem is chosen to be rotation with unit angular velocity in the $\underline{i}_R$ direction,

$$\hat{\underline{u}}^{(2)} \equiv \underline{i}_R \times \underline{r} \quad \text{on } A_S \tag{30a}$$

the integral over the surface of the sphere becomes

$$-\int_{A_S} [\underline{r} \times (\mathbf{T}_1^{(2)}\cdot\underline{n})]\cdot\underline{i}_R \, dA \tag{30b}$$

which is nothing more than the torque on the sphere about the $\underline{i}_R$ axis at $O(\varepsilon)$. Again, evaluating the left hand side of (28) thus yields the torque on the sphere due to interface deformation for any of the three non-trivial problems of translation or rotation parallel or perpendicular to the undeformed interface. This integral over the undeformed interface surface, A_F, can be simplified considerably by application of the boundary conditions (22)-(24). Specifically, the first and third terms in the integrand can be written as

$$\underline{n}\cdot(\mathbf{T}_1^{(2)} - \lambda\mathbf{T}_1^{(1)})\cdot\hat{\underline{u}} \tag{31}$$

where we have used the fact that the complementary velocity field must be continuous across the plane, z = 0. The second and fourth terms combine to yield

$$\underline{n}\cdot(\lambda\hat{\mathbf{T}}^{(1)} - \hat{\mathbf{T}}^{(2)})\cdot\underline{u}_1^{(1)} + \underline{n}\cdot\hat{\mathbf{T}}^{(2)}\cdot(\underline{u}_1^{(1)} - \underline{u}_1^{(2)}) \ . \tag{32}$$

It is evident, by examination of (22)-(24), and the conditions of continuity of velocity and stress for the complementary solutions at the undeformed interface, that the force and/or torque corrections on the sphere at $O(\varepsilon)$ can be calculated knowing only the shape function, f_1, at $O(\varepsilon)$, and the complementary velocity and stress fields for translation or rotation near a *flat* fluid interface [the latter corresponding to one of the $O(1)$ solutions for translation or rotation near the fluid interface, $(\underline{u}_0^{(k)}, \mathbf{T}_0^{(k)})$].

In the next section, we calculate the shape functions, f_1, at $O(\varepsilon)$ for the problems of parallel and normal translation and rotation. Then, in section IV, we utilize equations (28)-(32) to determine the corresponding corrections at $O(\varepsilon)$ to the hydrodynamic force and torque on the sphere.

III. Interface Shape

We now proceed to solve equation (19) for the shape of the interface at $O(\varepsilon)$, i.e. f_1. After combining equation (19) with equations (20a,b,c,d), we obtain:

$$-\beta\varepsilon\left(\frac{\partial^2 f_1}{\partial\rho^2} + \frac{1}{\rho}\frac{\partial f_1}{\partial\rho} + \frac{1}{\rho^2}\frac{\partial^2 f_1}{\partial\varphi^2}\right) + \alpha\varepsilon f_1 = \frac{9l^3}{R_0^5}\left(1 + \frac{3}{8}\frac{2+3\lambda}{1+\lambda}\frac{1}{l}\right) \tag{33}$$

for translation normal to the undisturbed interface;

$$-\beta\varepsilon\left(\frac{\partial^2 f_1}{\partial\rho^2} + \frac{1}{\rho}\frac{\partial f_1}{\partial\rho} + \frac{1}{\rho^2}\frac{\partial^2 f_1}{\partial\varphi^2}\right) + \alpha\varepsilon f_1 = \frac{9l^2\rho\cos\varphi}{R_0^5}\left(1 - \frac{3}{16}\frac{2-3\lambda}{1+\lambda}\frac{1}{l}\right) \tag{34}$$

for translation parallel; and,

$$-\beta\varepsilon\left(\frac{\partial^2 f_1}{\partial\rho^2} + \frac{1}{\rho}\frac{\partial f_1}{\partial\rho} + \frac{1}{\rho^2}\frac{\partial^2 f_1}{\partial\varphi^2}\right) + \alpha\varepsilon f_1 = \frac{12\rho\sin\varphi}{R_0^5}\left(l + \frac{3}{16}\frac{1}{1+\lambda}\frac{1}{l}\right) \tag{35}$$

for rotation, with the axis of rotation parallel to the interface. The case of rotation normal to the interface does not yield any deformation at $O(\varepsilon)$ as we

have already seen. All three of the equations (33)-(35) can be manipulated into modified inhomogeneous Bessel's equations of order zero or one. This is done by rescaling ρ to $\rho^*(\beta/\alpha)^{1/2}$ and then solving either by use of the Green's function or by use of variation of parameter techniques, subject to the boundary conditions discussed in the preceding section. After rescaling back to the original ρ, the solutions are:

1. Normal Translation

$$f_1(\rho) = 9l^3\left(1 + \frac{3}{8}\frac{2+3\lambda}{1+\lambda}\frac{1}{l}\right)\Bigg\{ K_0\left[\left(\frac{\alpha}{\beta}\right)^{1/2}\rho\right] \int_0^{\rho} \frac{x\, I_0\left[\left(\frac{\alpha}{\beta}\right)^{1/2}x\right]dx}{(x^2+l^2)^{5/2}}$$

$$+ I_0\left[\left(\frac{\alpha}{\beta}\right)^{1/2}\rho\right] \int_{\rho}^{\infty} \frac{x\, K_0\left[\left(\frac{\alpha}{\beta}\right)^{1/2}x\right]dx}{(x^2+l^2)^{5/2}}\Bigg\} \qquad (36)$$

2. Parallel Translation

$$f_1(\rho,\varphi) = 9l^2\cos\varphi\left(1 - \frac{3}{16}\frac{2-3\lambda}{1+\lambda}\frac{1}{l}\right)\Bigg\{ K_1\left[\left(\frac{\alpha}{\beta}\right)^{1/2}\rho\right] \int_0^{\rho} \frac{x^2 I_1\left[\left(\frac{\alpha}{\beta}\right)^{1/2}x\right]dx}{(x^2+l^2)^{5/2}}$$

$$+ I_1\left[\left(\frac{\alpha}{\beta}\right)^{1/2}\rho\right] \int_{\rho}^{\infty} \frac{x^2 K_1\left[\left(\frac{\alpha}{\beta}\right)^{1/2}x\right]dx}{(x^2+l^2)^{5/2}}\Bigg\} \qquad (37)$$

3. Parallel Rotation

$$f_1(\rho,\varphi) = 12\sin\varphi\left(l + \frac{3}{16}\frac{1}{1+\lambda}\frac{1}{l}\right)\Bigg\{ K_1\left[\left(\frac{\alpha}{\beta}\right)^{1/2}\rho\right] \int_0^{\rho} \frac{x^2 I_1\left[\left(\frac{\alpha}{\beta}\right)^{1/2}x\right]dx}{(x^2+l^2)^{5/2}}$$

$$+ I_1\left[\left(\frac{\alpha}{\beta}\right)^{1/2}\rho\right] \int_{\rho}^{\infty} \frac{x^2 K_1\left[\left(\frac{\alpha}{\beta}\right)^{1/2}x\right]dx}{(x^2+l^2)^{5/2}}\Bigg\} . \qquad (38)$$

Let us consider these solutions in some detail, starting with the interface shape for translation normal to the undisturbed interface. One feature of interest is the relative effectiveness of interfacial tension forces, measured by the magnitude of β, and density forces, measured by the magnitude of α, in restricting the degree of interface deformation. In order to investigate this

question, and to make comparisons between results for different conditions as meaningful as possible, we have carried out all of our calculations for a fixed value of $\alpha + \beta$ equal to 10. We may note from equation (9) that this represents a constant value for ε. Figure I shows the results for $z=\varepsilon f_1$ as a function of radial distance rescaled with respect to the sphere radius, for a dimensionless distance $l=6$ between the sphere center and the plane (z=0) of the undeformed interface, a viscosity ratio $\lambda=1$ and various values of α/β ranging from 0.01 to ∞. Although $\alpha + \beta$ is held constant, as indicated above, the magnitude of interface deformation is remarkably sensitive to the value of α/β, particularly for small values where the density forces are small relative to the dominant interfacial tension forces. It is obvious, in examining figure I, that a density difference across the interface is much more effective than surface tension at retaining a "flat" interface. In part, this is a consequence of the fact that the density difference acts directly on the degree of displacement from z=0, while the effect of interfacial tension is an indirect consequence of limiting the curvature of the interface.

The limiting behavior of (36) for $\alpha >> \beta$ and $\alpha << \beta$ can be determined easily. The first case is the density dominated limit, and can be considered either by letting α/β go to infinity in equation (36), or by simply setting $\beta=0$ and $\varepsilon=1/\alpha$ in the differential equation (33). In either case, the shape function is given by

$$f_1(\rho) = \frac{9l^3}{(\rho^2 + l^2)^{5/2}}\left(1 + \frac{3}{8}\,\frac{2+3\lambda}{1+\lambda}\,\frac{1}{l}\right) \quad . \tag{39}$$

The second limiting case, $\alpha << \beta$, corresponds to surface tension dominated deformation. Aderogba and Blake (1978) have noted earlier that the equation (33) has a log singularity if α is set identically to zero, and thus has no solution which is both finite at the origin and still vanishing as ρ goes to

infinity. As suggested above, this is a consequence of the fact that large *deformations* are not mathematically restricted by interfacial tension, only surface curvature is restricted. Thus, in this case, it is advantageous to examine directly the behavior of the solution to equation (36), which is exact for any value of α/β, in the limit as α/β goes to zero. Specifically, we consider $(\alpha/\beta)^{1/2}\rho << 1$. In this case,

$$f_1(\rho) \sim 3\left[\ln \frac{(\beta/\alpha)^{1/2}}{l + (\rho^2 + l^2)^{1/2}} + \frac{l}{(\rho^2 + l^2)^{1/2}}\right] \tag{40}$$

for $\beta >> \alpha$, $\varepsilon \sim 1/\beta$, and it is evident that $\varepsilon f_1(\rho)$ is bounded and $0(\varepsilon \ln \varepsilon)$ for any fixed ρ and $\alpha \neq 0$. In other words, as the interfacial tension becomes asymptotically large, the interface deformation approaches zero for any small, but nonzero density difference. On the other hand, for any large but fixed β, $\varepsilon f_1 \to -\ln\alpha$ as $\alpha \to 0$. Thus, for a fixed level of interfacial tension, which may be arbitrarily large as long as it remains bounded, the interface deformation will only remain finite in the presence of a nonzero density difference across the interface. For sufficiently *large* ρ, on the other hand, where $(\alpha/\beta)^{1/2}\rho$ becomes large, εf_1 vanishes in the manner indicated by the limit of equation (39) for large ρ, even if $\alpha/\beta << 1$.

Compared with the dependence of interface deformation on the relative magnitudes of α and β, as outlined above, the effect of particle position is straight forward. In figure II, we show the variation in degree of deformation for normal motion with $\alpha + \beta = 10$, $\alpha/\beta = 1$ and $\lambda=1$ as the particle is moved from $l=9$ to $l=3$. Obviously, as the particle approaches more closely to the interface, the degree of deformation goes up markedly. Finally, we may note that the viscosity difference across the interface plays only a secondary role in the steady-state degree of deformation. An illustrative example of this fact is shown in figure III, where we have plotted $z=\varepsilon f_1$ as a function of the dimension-

less radial position, for $\alpha + \beta = 10$, $\alpha/\beta = 1$, $l=6$, and several values of λ.

Let us next consider the interface shape for translation of a rigid sphere *parallel* to the plane z=0. Results for the interface shape, i.e. for $z = \varepsilon f_1$, evaluated in the plane of motion of the sphere, for l=6, $\alpha + \beta = 10$ and $\lambda=1$ are plotted in figure IV. The two cases $\alpha/\beta = .1$ and 1 were evaluated directly from the equation (37) with $\varphi = 0$. The limiting cases, $\alpha/\beta \to \infty$ and $\alpha/\beta \to 0$, were obtained from the asymptotic forms of (37) for very large and very small values of α/β. For the case of gravity dominated deformation ($\varepsilon=1/\alpha$ and $\alpha/\beta \to \infty$), we obtain

$$f_1(\rho,\varphi) = \frac{9l^2\rho\cos\varphi}{(\rho^2 + l^2)^{5/2}}\left(1 - \frac{3}{16}\,\frac{2-3\lambda}{1+\lambda}\,\frac{1}{l}\right) \quad . \tag{41}$$

It is evident that the same result could have been obtained by inspection from equation (34) with $\beta=0$. In the limit of surface tension dominated deformation ($\varepsilon = 1/\beta$ and $\alpha/\beta \to 0$), the equation (37) yields

$$f_1(\rho,\varphi) = \frac{3l\cos\varphi}{\rho}\left(1 - \frac{l}{(\rho^2 + l^2)^{1/2}}\right)\left(1 - \frac{3}{16}\,\frac{2-3\lambda}{1+\lambda}\,\frac{1}{l}\right) \quad . \tag{42}$$

Unlike the problem of particle motion normal to the interface, the solution for f_1 in the present development, remains perfectly well behaved in the limit $\alpha/\beta \to 0$.

Although the interface shape illustrated in figure IV is fundamentally different from that obtained for motion normal to the interface, the results are in many respects qualitatively similar. First, a density difference across the interface is much more effective than interfacial tension at restricting interface deformation. It is evident that surface tension allows a very broad deformation with small curvature for small values of α/β. Second, the degree of deformation again increases as the sphere moves closer to the interface--though it can be noted that even at $l=3$, the deformation remains less than 1/50 of the sphere

diameter (for $\alpha/\beta = 1$ and $\alpha + \beta = 10$). At the same time, however, the influence of the sphere extends for several body lengths in the ρ direction. Third, and finally, the ratio of viscosities across the interface has very little effect on the degree of deformation. Plots which illustrate these latter two conclusions are contained in Appendix C and show the same effects for the case of motion normal to the interface (i.e. figures II and III). Figure IV illustrates the section of largest deformation, but, of course, the interface shape is fully two-dimensional. Thus, we present, in figure V, a plot showing contours of constant interface elevation relative to the plane of the undeformed interface for the case $l = 6$, $\alpha/\beta = 1$, $\alpha + \beta = 10$ and $\lambda = 1$. It can be seen, from this plot, that the deformation falls off somewhat more slowly in the direction perpendicular to the direction of the sphere's motion than in the plane of that motion. Apart from this, the data represented by the figure V serve mainly to confirm the impression of interface shape which is indicated by figure IV and the equation (37).

Finally, we consider the interface deformation for rotation, with the axis of rotation parallel to the interface. Comparison of equations (34) and (35) shows that the normal stress imbalance is identical in "form" to the case of parallel translation, apart from a rotation of $\pi/2$ in φ. Thus, the interface shapes are completely analogous to those illustrated in figures IV and V. It will be noted from equation (35), however, that the deformation falls off somewhat more rapidly with increase in l than for the case of parallel translation, and the dependence on viscosity ratio, λ, is different in detail. These latter differences are quantified in figure VI where we have plotted the relative magnitude of the deformation for parallel rotation compared to that for parallel translation as a function of the distance between the sphere center and the plane of the undeformed interface for the various values of λ ranging from 0 to ∞. This scaling is valid for the directions of maximum deformation

for the respective cases. It should be remembered that the maximum deformation in the case of parallel rotation is in the yz plane (normal to the axis of rotation), while that for parallel translation is in the xz plane (parallel to the axis of translation).

IV. Force and Torque Corrections

With the interface shape known to $O(\varepsilon)$, we can now use the reciprocal theorem to calculate the corrections at $O(\varepsilon)$ to the force and torque acting on a sphere which is either translating or rotating with a prescribed velocity. It is evident from the detailed derivation in section II that the evaluation of force or torque corrections for a given type of particle motion requires only the interface shape, f_1, at $O(\varepsilon)$, the velocity and stress fields at $O(1)$, and the velocity and stress fields for a "complementary" Stokes problem. The latter is simply the translation or rotation of a sphere with unit velocity in the presence of a flat interface -- i.e. precisely the $O(1)$ solutions already calculated by Lee, Chadwick and Leal (1979). If the "complementary" problem is a translational motion, the reciprocal theorem yields a *force* correction in the direction of the "complementary" translation regardless of whether the interface deformation is due to particle translation or rotation. Thus, for example, if we wish to determine whether the interface deformation from parallel translation results in a force normal to the undisturbed interface, we would use translation normal to a *flat* interface as the "complementary" problem. Similarly, to estimate any modification in the torque for the same case, we would use the solution for rotation near a flat interface to determine the "complementary" velocity and stress fields.

It is useful to observe that the integral over the undeformed interface surface, A_F, in (28) involves integration over φ from zero to 2π. Thus, integrals in odd powers of $\sin\varphi$ and $\cos\varphi$ will be zero. Investigation of all possible

contributions from the flow fields to the integrand [equations (31) and (32)] of equation (28) shows that the complementary problem will introduce a linear dependence on either $\sin\varphi$ or $\cos\varphi$, except for the normal translational motion, which is independent of φ; the disturbance flow, on the other hand, contributes terms involving the products of $\sin\varphi$ and $\cos\varphi$ (for example, $\sin^2\varphi$, $\cos^2\varphi$ or $\sin\varphi\cos\varphi$) except for the case of motion normal to the interface which is independent of φ. Thus, the only nonzero contributions to the integral over A_F in (28) will occur when the "complementary" velocity field is independent of φ -- i.e. when the complementary problem is translation normal to the interface. It thus follows from these considerations that the only nonzero contributions to the force at $O(\varepsilon)$ must be directed *normal* to the interface, independent of whether the particle is translating normal to the interface, or is translating or rotating parallel to the interface. There can be no nonzero contributions to the torque at $O(\varepsilon)$ in any of these cases, and no contributions to the force component parallel to the undisturbed interface at $O(\varepsilon)$.

Thus, the problem of determining contributions to the force or torque on a sphere at $O(\varepsilon)$, due to interface deformation at $O(\varepsilon)$, is reduced to evaluating the normal component of force for the three cases of translation normal to the plane of the undeformed interface, translation parallel to the plane of the undeformed interface, and rotation with the axis of rotation parallel to the interface. The results of evaluating (28) for these three cases all yield nonzero forces normal to the interface which can be represented in the form

$$AI = BI \int_0^\infty [CI \cdot DI + EI \cdot FI]\,d\rho, \qquad I = 1, 2 \text{ or } 3 . \tag{43}$$

For normal motion,

$$A1 = {}_{Def}K_L^T \tag{44}$$

$$B1 = \left(1 + \frac{9}{8}\frac{2+3\lambda}{1+\lambda}\frac{1}{l}\right)\frac{81l^5}{2(1+\lambda)^2} \tag{45}$$

$$C1 = K_0\left[\left(\frac{\alpha}{\beta}\right)^{1/2}\rho\right]\int_0^{\rho}\frac{xI_0\left[\left(\frac{\alpha}{\beta}\right)^{1/2}x\right]dx}{(x^2+l^2)^{5/2}} + I_0\left[\left(\frac{\alpha}{\beta}\right)^{1/2}\rho\right]\int_{\rho}^{\infty}\frac{xK_0\left[\left(\frac{\alpha}{\beta}\right)^{1/2}x\right]dx}{(x^2+l^2)^{5/2}} \tag{46}$$

$$D1 = \frac{1}{(\rho^2+l^2)^5}\left(\rho^5(-2\lambda+2) + \rho^3l^2(6\lambda^2+6\lambda-4) + \rho l^4(2\lambda+2)\right) \tag{47}$$

$$E1 = \left(\frac{\alpha}{\beta}\right)^{1/2}\left\{-K_1\left[\left(\frac{\alpha}{\beta}\right)^{1/2}\rho\right]\int_0^{\rho}\frac{xI_1\left[\left(\frac{\alpha}{\beta}\right)^{1/2}x\right]dx}{(x^2+l^2)^{5/2}}\right.$$

$$\left. + I_1\left[\left(\frac{\alpha}{\beta}\right)^{1/2}\rho\right]\int_{\rho}^{\infty}\frac{xK_1\left[\left(\frac{\alpha}{\beta}\right)^{1/2}x\right]dx}{(x^2+l^2)^{5/2}}\right\} \tag{48}$$

$$F1 = \frac{1}{(\rho^2+l^2)^4}\left(\rho^4(\lambda-1) + 2\rho^2l^2\right) \tag{49}$$

while, for parallel motion,

$$A2 = {}_{Def}K_{zx}^{T} = {}_{Def}K_{zy}^{T} \tag{50}$$

$$B2 = \left(1 + \frac{9}{4}\frac{2+3\lambda}{1+\lambda}\frac{1}{l}\right)\frac{27l^3}{4(1+\lambda)^2} \tag{51}$$

$$C2 = K_1\left[\left(\frac{\alpha}{\beta}\right)^{1/2}\rho\right]\int_0^{\rho}\frac{x^2I_1\left[\left(\frac{\alpha}{\beta}\right)^{1/2}x\right]dx}{(x^2+l^2)^{5/2}}$$

$$+ I_1\left[\left(\frac{\alpha}{\beta}\right)^{1/2}\rho\right]\int_{\rho}^{\infty}\frac{x^2K_1\left[\left(\frac{\alpha}{\beta}\right)^{1/2}x\right]dx}{(x^2+l^2)^{5/2}} \tag{52}$$

$$D2 = \frac{1}{(\rho^2+l^2)^5}\left(\rho^6(-3\lambda-1) + \rho^4l^2(18\lambda^2-6\lambda+1)\right.$$

$$\left. + \rho^2l^4(12\lambda+14) + l^6(3\lambda+3) - (2+4\lambda+2\lambda^2)l^2(\rho^2+l^2)^{5/2}\right) \tag{53}$$

$$E2=\left(\frac{\alpha}{\beta}\right)^{1/2}\Bigg\{-\left(K_0\left[\left(\frac{\alpha}{\beta}\right)^{1/2}\rho\right]+\frac{1}{\left(\frac{\alpha}{\beta}\right)^{1/2}\rho}K_1\left[\left(\frac{\alpha}{\beta}\right)^{1/2}\rho\right]\right)\int_0^{\rho}\frac{x^2I_1\left[\left(\frac{\alpha}{\beta}\right)^{1/2}x\right]dx}{(x^2+l^2)^{5/2}}$$

$$+\left(I_0\left[\left(\frac{\alpha}{\beta}\right)^{1/2}\rho\right]-\frac{1}{\left(\frac{\alpha}{\beta}\right)^{1/2}\rho}I_1\left[\left(\frac{\alpha}{\beta}\right)^{1/2}\rho\right]\right)\int_{\rho}^{\infty}\frac{x^2K_1\left[\left(\frac{\alpha}{\beta}\right)^{1/2}x\right]dx}{(x^2+l^2)^{5/2}}\Bigg\} \tag{54}$$

$$F2=\frac{1}{(\rho^2+l^2)^4}\Big(\rho^5(-\lambda-3)+\rho^3l^2(5\lambda+9)$$

$$+\rho l^4(3\lambda+3)-(2+4\lambda+2\lambda^2)\rho l^2(\rho^2+l^2)^{3/2}\Big) \tag{55}$$

and for parallel rotation,

$$A3={}_{\mathrm{Def}}K_{zx}={}_{\mathrm{Def}}K_{zy} \tag{56}$$

$$B3=\left(1+\frac{3}{8}\frac{2+3\lambda}{1+\lambda}\frac{1}{l}\right)\frac{36l^5}{(1+\lambda)^2} \tag{57}$$

$$C3=C2 \tag{58}$$

$$D3=\frac{1}{(\rho^2+l^2)^5}\Big(\rho^4(3\lambda^2+2\lambda-2)+\rho^2l^2(-3\lambda^2+5)+l^4(-\lambda-1)\Big) \tag{59}$$

$$E3=E2 \tag{60}$$

$$F3=\frac{1}{(\rho^2+l^2)^4}\Big(\rho^3(-2\lambda+2)+\rho l^2(-\lambda-1)\Big)\ . \tag{61}$$

The results represented by equation (43) can be expressed in a general linear form similar to equations (3) and (4),

$$\frac{\underline{F}}{a\mu u}=\left(\mathbf{K}_T^{(0)}+\varepsilon\mathbf{K}_T^{(1)}\right)\cdot\hat{\underline{U}}+\frac{a\Omega}{U}\left(\mathbf{K}_C^{T}+\varepsilon\mathbf{K}_{Def}\right)\cdot\hat{\underline{\Omega}}+O(\varepsilon^2) \tag{62a}$$

$$\frac{\underline{T}}{a^3\mu\Omega}=\mathbf{K}_C\cdot\hat{\underline{U}}\left(\frac{U}{a\Omega}\right)+\mathbf{K}_R\cdot\hat{\underline{\Omega}}\ . \tag{62b}$$

Clearly, the equation (4) for the torque on the sphere is completely unchanged at $O(\varepsilon)$. However, the coupling tensor which relates $\underline{F}$ and $\hat{\underline{\Omega}}$ is no longer equal to

the transpose of the tensor which relates $\underline{T}$ and $\hat{\underline{U}}$ Furthermore, the components of the resistance tensors $\mathbf{K}_T$ and $\mathbf{K}_C^T + \varepsilon\mathbf{K}_{Def}$ no longer conform to the simple forms (5) - (7) which pertain to a flat fluid interface. It may be noted in regard to the first of these facts, that Brenner's (1964) original proof of the reciprocity of the coupling tensors between $\underline{F}$ and $\hat{\underline{\Omega}}$, and $\underline{T}$ and $\hat{\underline{U}}$ applies to bounded systems only if the fluid motion can do no work on the boundaries. Generalization of Brenner's analysis to the present system is discussed in Appendix A.

Let us now consider the results (43) - (61) in more detail starting with the combined resistance tensor, $\mathbf{K}_T^{(0)} + \varepsilon\mathbf{K}_T^{(1)}$, for translational motion. This is most conveniently discussed in terms of its components for a Cartesian coordinate system with axes x and y parallel to the plane of the undeformed interface, and the z axis normal, as was adopted earlier in conjunction with equations (5) - (7). Adopting the same nomenclature as used in (5), the components $K_{\parallel}^T$ are unchanged at $O(\varepsilon)$, while the normal component $K_{\perp}^T$ is either *decreased* or *increased* depending upon whether the sphere is moving *towards* or *away from* the interface. We shall discuss the details of the modifications to $K_{\perp}^T$ shortly. In addition, and more surprising, the off-diagonal components $(K_{\perp}^{(1)})_{zx}$ and $(K_{\perp}^{(1)})_{zy}$ are *nonzero*, thus demonstrating the existence of a force away from the interface, induced by translation parallel to the interface. This result represents a previously "undiscovered" form of "lateral migration", though it should be noted that the situation is somewhat analogous to the well-known lateral migration of a drop in shear flow away from a plane wall due to deformation of the drop shape [Chaffey, Brenner and Mason (1965,1967)]. It may also be noted that Chan (1980) has predicted the existence of lateral migration of a sedimenting drop away from a vertical plane boundary due, again, to shape deformation of the drop -- and this situation is quite closely analogous to the present problem of parallel translation of a sphere near a deformable boundary. Finally, there is,

according to equations (56)-(61), a coupling induced between particle rotation and the force on the particle which leads to migration of a sphere away from the interface when the sphere rotates about an axis parallel to the interface.

Results corresponding to the equations (43)-(61) have been plotted as a function of l in Figures VII-XII. In Figure VII, we show the magnitude of the drag decrease at $O(\varepsilon)$, scaled with respect to Stokes drag, for normal motion *toward* the interface with a fixed value of λ equal to 1 and $\alpha + \beta = 10$. It is evident that the decrease in drag (due to the $O(\varepsilon)$ deformation) is increased as l decreases and this is presumably a consequence of the increased degree of deformation. In addition, the largest decrease in the drag can be seen to occur for the smallest value of α/β, again as a result of the fact that the largest deformation occurs, for a fixed l, λ and $\alpha+\beta$, in the limit as $\alpha/\beta \to 0$ where surface tension dominates over the density difference across the interface. The variation in the $O(\varepsilon)$ drag contribution with λ for fixed $\alpha/\beta = 1$ and $\alpha + \beta = 10$ is shown in Figure VIII. It will be noted that the drag *decrease* is smallest in the limiting case $\lambda = 0$. Since the magnitude of the deformation is essentially independent of λ, this is simply a consequence of the fact that a given level of deformation has less effect on the particle drag when the second fluid has a very low viscosity than it does when the viscosity is large. It is of some potential interest to note that the qualitative role of interface deformation at $O(\varepsilon)$ could have been deduced from the form of the dynamically "equivalent" boundary conditions (22)-(24) which are satisfied at the plane, z=0, of the undeformed interface. Specifically, the condition (23) shows that the deformation induced at $O(\varepsilon)$ by a sphere moving toward the interface is dynamically equivalent to a normally directed velocity at $O(\varepsilon)$

$$u_{1z}|_{z=0} = \frac{27l^4}{(1+\lambda)(\rho^2+l^2)^5}(l^2 - 3\rho^2) \tag{63}$$

at the plane of the undeformed interface. Although this single condition is not

sufficient to completely determine the form of the velocity field, since the conditions (22) and (24) yield a discontinuity in both the tangential velocity and the tangential stress components, the latter are asymptotically small for large l relative to the normal velocity, $u_{1z}|_{z=0}$. Thus, the disturbance velocity field at $O(\varepsilon)$ can be viewed as resulting from a flow through the plane z=0 which is in the same direction as the sphere velocity for $\rho < l / \sqrt{3}$ and in the opposite direction for $\rho > l / \sqrt{3}$. It is evident from the sense of this boundary flow that the force contribution to the sphere at $O(\varepsilon)$ must consist of a decrease in the force component normal to the interface. It is important to note the effects of reversing the direction of motion for the sphere, for motion normal to the interface. Reversing the direction of motion for the particle changes the sign of the integral over the interface in equation (28). Thus, if a particle is moving away from a deformable interface, the drag, due to the deformation, is increased by the same amount as the drag, due to the deformation, is decreased for an approaching sphere. This result can be viewed as a consequence of the linearity of Stokes equations and the fact that the effective induced velocity field at the plane z=0 for a sphere moving away from the interface is the negative of the velocity field for an approaching sphere.

Detailed results for the $O(\varepsilon)$ contribution to the force on a sphere which is translating ***parallel*** to the plane of the undeformed interface are presented in Figures IX and X. For all values of α/β and λ, this force is directed normal to the interface. In Figure IX, we have plotted the normal force scaled with respect to Stokes drag as a function of l for $\lambda = 2/3$, $\alpha + \beta = 10$ and various values of α/β in the range 0.01 to 10. For all $l > 2$, the induced force is directed away from the interface, and its magnitude increases as α/β decreases. This is believed to be a direct consequence of the increased deformation which occurs as α/β is decreased. In addition, for $l < \sim 3$, the magnitude of the induced force increases

as l decreases, again presumably because the deformation increases. When l is smaller, the magnitude of the induced force appears to *decrease* and even change sign around $l = 1.5$ for all of the cases considered in Figure IX. However, it is *not* expected that the small parameter expansion in l^{-1} which we have adopted from Lee, Chadwick and Leal (1979), will provide meaningful results in this region. We have neglected terms which are $O(l^{-2})$, and it is evident that these higher-order terms will become significant in the region near the interface. Thus, we believe that the peculiar results for $l < \sim 3$ are spurious and no physical explanation is sought here for their existence.

The problem of parallel translation is considered further in Figure X, where we show results for fixed $\alpha/\beta = 1$ and various values of λ. Here, as in the case of normal motion, the deformation at $O(\varepsilon)$ is relatively insensitive to λ and the variations in the induced force are thus a direct consequence of the viscosity difference *rather* than an indirect effect of different degrees of deformation for different λ. It will be noted that the unphysical upturn and sign change for small l is present for $\lambda = 0$ and $2/3$, but not for $\lambda \geq 10$ (from this we might conclude that the higher-order terms in l^{-1}, which have been neglected, decrease in importance with increase in λ).

The qualitative nature of the induced forces at $O(\varepsilon)$ for parallel translation can again be deduced by examining the "equivalent" induced normal velocity at z=0,

$$U_{1z}|_{z=0} = \frac{9l^2}{(\rho^2 + l^2)^3}\left[\frac{3}{2(1+\lambda)} - (\rho^2 + l^2)^{1/2}\right.$$

$$\left. - \frac{3}{1+\lambda}\,\frac{\rho^2\cos^2\varphi}{(\rho^2 + l^2)^2}\,(l^2 + 5\rho^2) + \frac{5\rho^2 l^2}{(\rho^2 + l^2)^{5/2}}\right] \qquad (64)$$

since the discontinuities in the tangential components of velocity and stress are asymptotically smaller than $u_{1z}|_{z=0}$ for large l. This equation indicates an

induced velocity at $O(\varepsilon)$ which is directed toward the sphere (normal to the plane of the undeformed interface) except for very small values of l or very large values of ρ. Thus, the $O(\varepsilon)$ flow between the sphere and the interface is consistent with a normally directed force away from the interface.

Finally, Figures XI and XII present the influence of deformation on a rotating particle, whose axis of rotation is parallel to the interface. The results are very similar in form to those described earlier for motion normal to the interface. The difference is given by the observation that the direction of the force is reversed (i.e. the force is away from the interface) and the magnitude of this force is found to be much smaller for a given distance from the interface (i.e. given value of l). By comparing the magnitudes of deformation in the normal motion problem with the same quantity for the parallel rotation problem for a given magnitude of the deformation, we see that the drag correction for the parallel rotational problem is much less than the drag correction for the normal translational problem. As was noted earlier, we will not discuss the results for $l \leq 2$ due to the neglect of higher-order terms in $1/l$ in the present theory. As in the previous case, the force increases as α/β decreases for $l > 2$ as a consequence of increased deformation. The dependence of the force on λ, as shown in Figure XII, follows quite closely the dependence of the deformation on λ in Figure VI. For example, the case of $\lambda = 0$ yields the largest deformation in Figure VI, which corresponds to the largest force directed away from the interface in Figure XII. In the present case, the "equivalent" induced normal velocity at $O(\varepsilon)$ is given as,

$$U_{1z}|_{z=0} = \frac{24l^2}{(1+\lambda)(\rho^2+l^2)^4}\left[-1 + \frac{8\rho^2\sin^2\varphi}{(\rho^2+l^2)}\right]$$

This yields a velocity directed towards the sphere at the plane z=0 and thus a force on the particle directed away from the interface.

We have determined the corrections to the force and torque, due to $O(\varepsilon)$ deformation, on a body which is translating or rotating either normal or parallel to a deformable interface. This interface has an arbitrary viscosity ratio across it, but has a large interfacial returning force due either to the density difference or interfacial tension. It has been shown by inspection of the symmetry of the terms to be evaluated in the reciprocal theorem that the $O(\varepsilon)$ correction to the torque on a sphere moving relative to the interface is identically zero. The force corrections at $O(\varepsilon)$ have yielded a reduction of the drag for motion normal to and *towards* the interface, while there is an increase in the drag as the sphere moves *away* from the interface. The cases of rotation and translation parallel to the interface both yield a force which is directed normal to and away from the interface. Finally, we have noted that the case of a sphere with its rotational axis directed normal to the interface generates no interfacial deformation and hence no correction to the force or torque on the body.

Acknowledgment

This work was supported by grant CME-8003485 from the National Science Foundation. The authors wish to thank Paul C.-H. Chan and Seong H. Lee for their help in the formulation of this problem.

References

Aderogba, K. and Blake, J. R. 1978 Action of a force near the planar surface between two semi-infinite immiscible liquids at very low Reynolds numbers. Bull. Austral. Math. Soc. **18**, 345.

Brenner, H. 1964 The Stokes resistance of an arbitrary particle -- II. An extension. Chem. Eng. Sci. **19**, 599.

Chaffey, C. H., Brenner, H. and Mason, S. G. 1965 Particle motions in sheared suspensions XVIII: Wall migration (theoretical). Rheol. Acta. **4**, 64, (corrections, 1967, **6**, 100).

Chan, P. C.-H. 1980 PhD Dissertation, California Institute of Technology.

Chan, P. C.-H. and Leal, L. G. 1978 The motion of a deformable drop in a second-order fluid. J. Fluid Mech. **92**, 131.

Happel, J. and Brenner, H. 1973 "Low Reynolds Number Hydrodynamics", Noordhoff International Publishers.

Lee, S. H., Chadwick, R. S. and Leal, L. G. 1979 Motion of a sphere in the presence of a plane interface. Part 1. An approximate solution by generalization of the method of Lorentz. J. Fluid Mech. **93**, 705.

Lee, S. H. and Leal, L. G. 1980 Motion of a sphere in the presence of a plane interface. Part 2. An exact solution in bipolar coordinates. J. Fluid Mech. **98**, 193.

Lorentz, H. A. 1907 A general theory concerning the motion of a viscous fluid. Abhandl. Theoret. Phys. **1**, 23.

Stokes, G. G. 1851 On the effect of the internal friction of fluids on the motion of pendulums. Camb. Phil. Soc. **9**, Pt. II., 8.

Figure Captions

Figure I. Normal translational deformation. The effects of α / β for $l = 6$, $\lambda = 1$ and $\alpha + \beta = 10$.

– – – $\alpha / \beta = .01$, ----- $\alpha / \beta = .1$, ------ $\alpha / \beta = 1$, and _____ $\alpha / \beta = \infty$.

Figure II. Normal translational deformation. The effects of particle distance for $\alpha/\beta = 1$, $\alpha + \beta = 10$ and $\lambda = 1$.

_____ $l = 3$, – – – l and ----- $l = 9$.

Figure III. Normal translational deformation. The effects of viscosity ratio for $\alpha / \beta = 1$, $\alpha + \beta = 10$ and $l = 6$.

_____ $\lambda = \infty$, – – – $\lambda = 1$ and ----- $\lambda = 0$.

Figure IV. Parallel translational deformation. The effects of α / β for $l = 6$, $\lambda = 1$ and $\alpha + \beta = 10$.

_____ $\alpha / \beta = 0$, – - – - – $\alpha / \beta = .01$, ----- $\alpha / \beta = .1$, - - - - - $\alpha / \beta = 1$ and – – – $\alpha / \beta = \infty$.

Figure V. Parallel translational deformation. Contours of displacement in z direction for translation in y direction for $\alpha / \beta = 1$, $\alpha + \beta = 10$, $l = 6$ and $\lambda = 1$.

_____positive displacement, ----- negative displacement.

Figure VI. Parallel rotational deformation vs. parallel translational deformation as plotted against l.

_____ $\lambda = 0$, ----- $\lambda = .1$, - - - - $\lambda = 1$, – – – $\lambda = 10$ and – - – - – $\lambda = \infty$.

Figure VII. Drag ratio for normal translational deformation. The dependence on α/β for $\alpha + \beta = 10$ and $\lambda = 1$ as a function of l.

_____$\alpha / \beta = 0.1$, ----- $\alpha / \beta = .1$, - - - - $\alpha / \beta = 1$ and – – – $\alpha / \beta =$ 10.

Figure VIII. Drag ratio for normal translational deformation. The dependence on λ for $\alpha / \beta = 1$ and $\alpha + \beta = 10$ as a function of l.

_____$\lambda = 0$ and 2/3, ----- $\lambda = 1$, - - - - $\lambda = 10$ and – – – $\lambda = 10000$.

Figure IX. Drag ratio for parallel translational deformation. The dependence on α/β for $\alpha + \beta = 10$ and $\lambda = 2/3$ as a function of l.

_____$\alpha/\beta = .01$, ----- $\alpha/\beta = .1$, - - - - $\alpha/\beta = 1$ and – – – $\alpha/\beta = 10$.

Figure X. Drag ratio for parallel translational deformation. The dependence on λ for $\alpha/\beta = 1$ and $\alpha + \beta = 10$ as a function of l.

_____$\lambda = 0$ and 2/3, ----- $\lambda = 1$, - - - - $\lambda = 10$ and – – – $\lambda = 10000$.

Figure XI. Drag ratio for parallel rotational deformation. The dependence on α/β for $\alpha + \beta = 10$ and $\lambda = 1$ as a function of l.

_____$\alpha/\beta = .01$, ----- $\alpha/\beta = .1$, - - - - $\alpha/\beta = 1$ and – – – $\alpha/\beta = 10$.

Figure XII. Drag ratio for parallel rotational deformation. The dependence on λ for $\alpha/\beta = 1$ and $\alpha + \beta = 10$ as a function of l.

_____$\lambda = 0$ and 2/3, ----- $\lambda = 1$, - - - - $\lambda = 10$ and – – – $\lambda = 10000$.

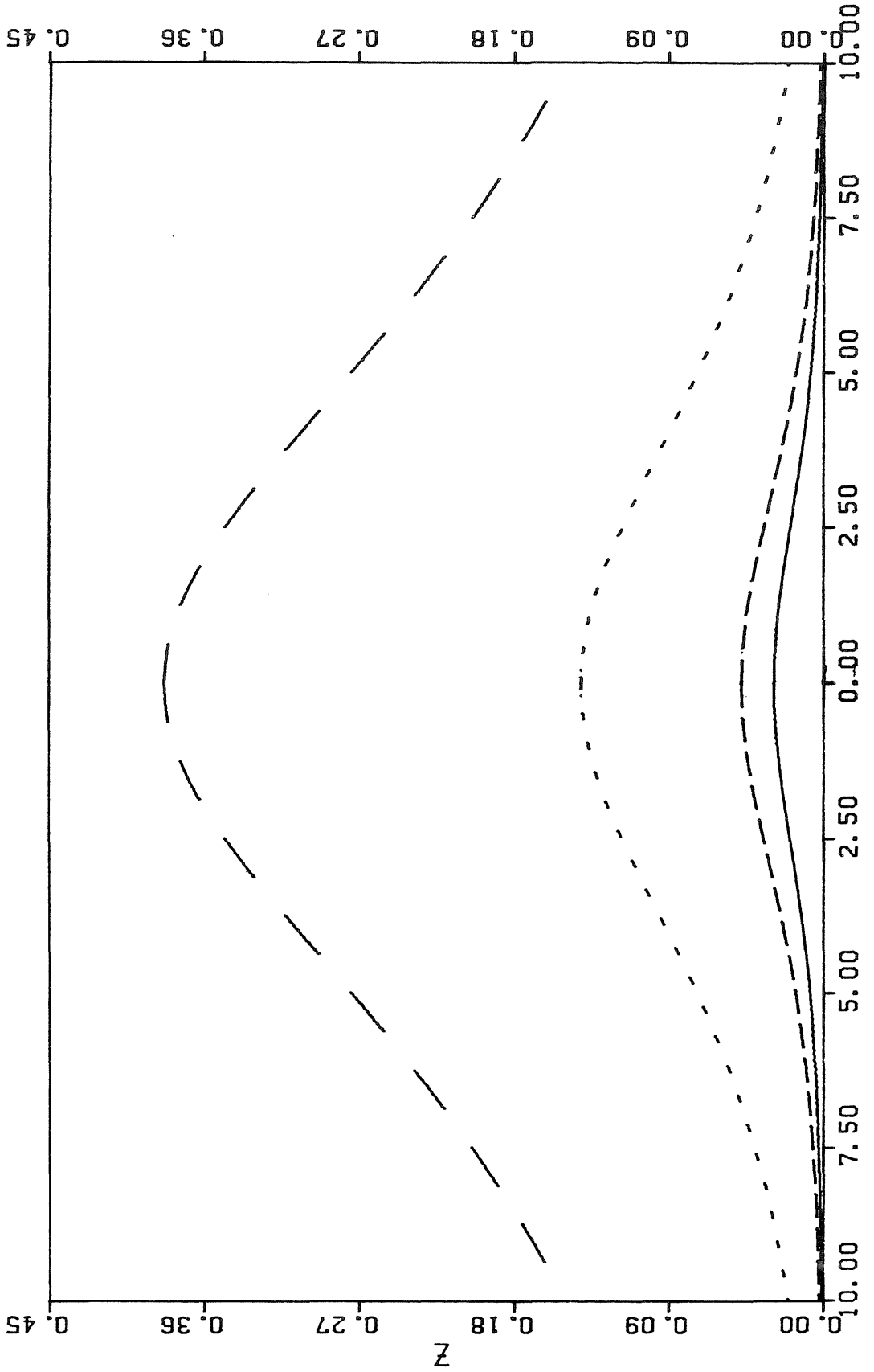

FIGURE I

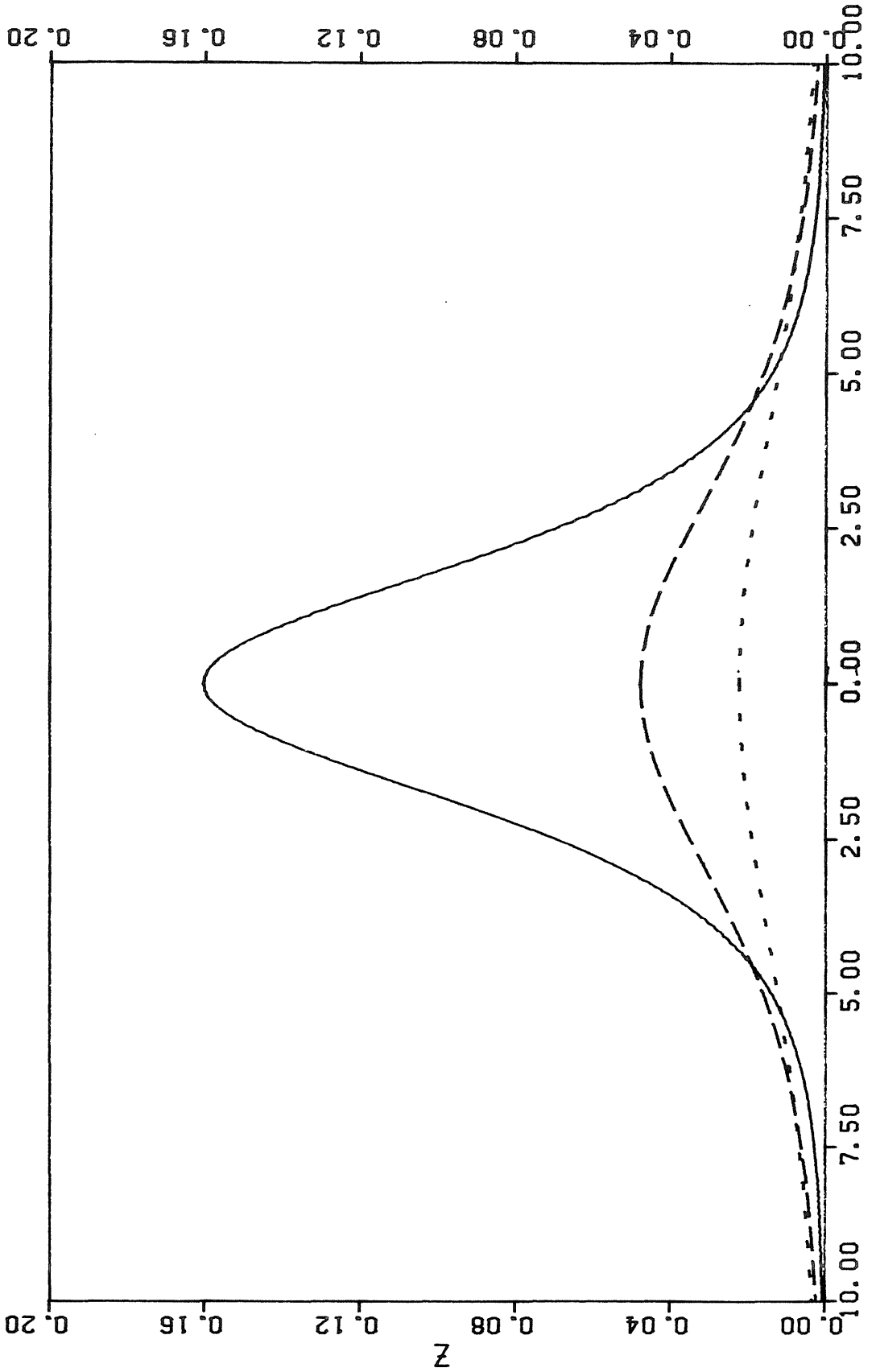

FIGURE II

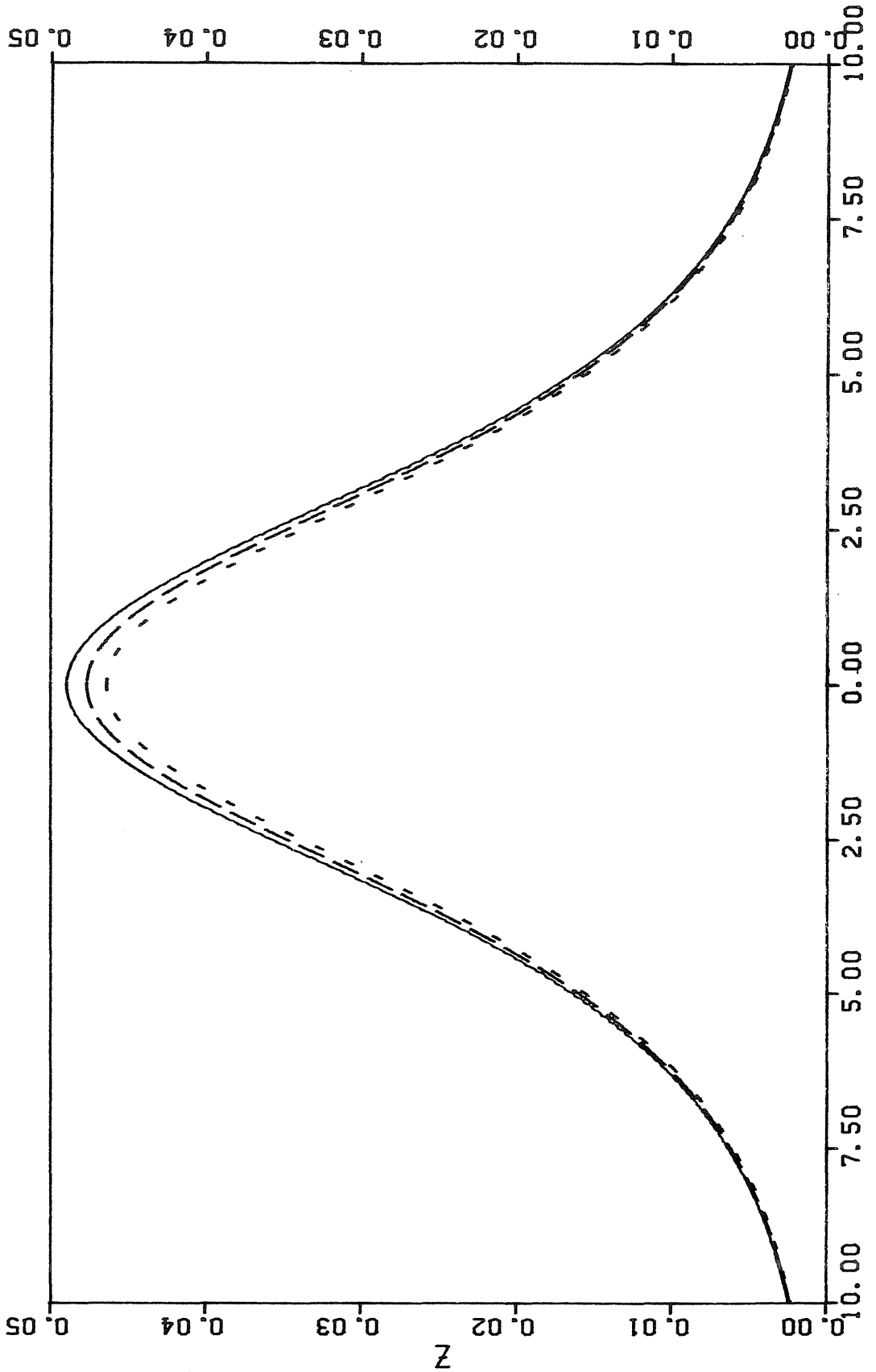

FIGURE III

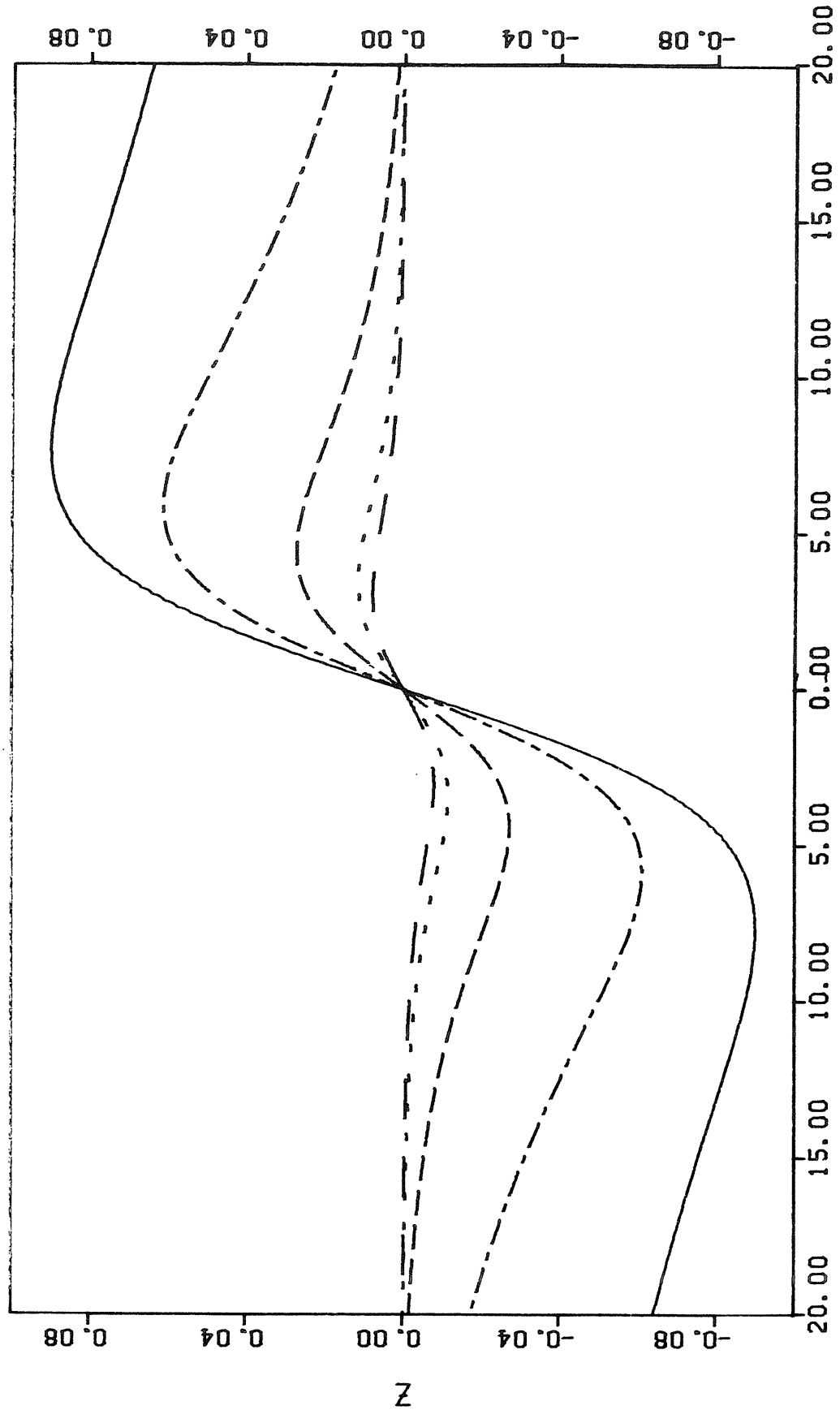
-0.08
-0.04
0.00
0.04
0.08
20.00
15.00
10.00
5.00
0.00
5.00
10.00
15.00
20.00
R
Z

FIGURE IV

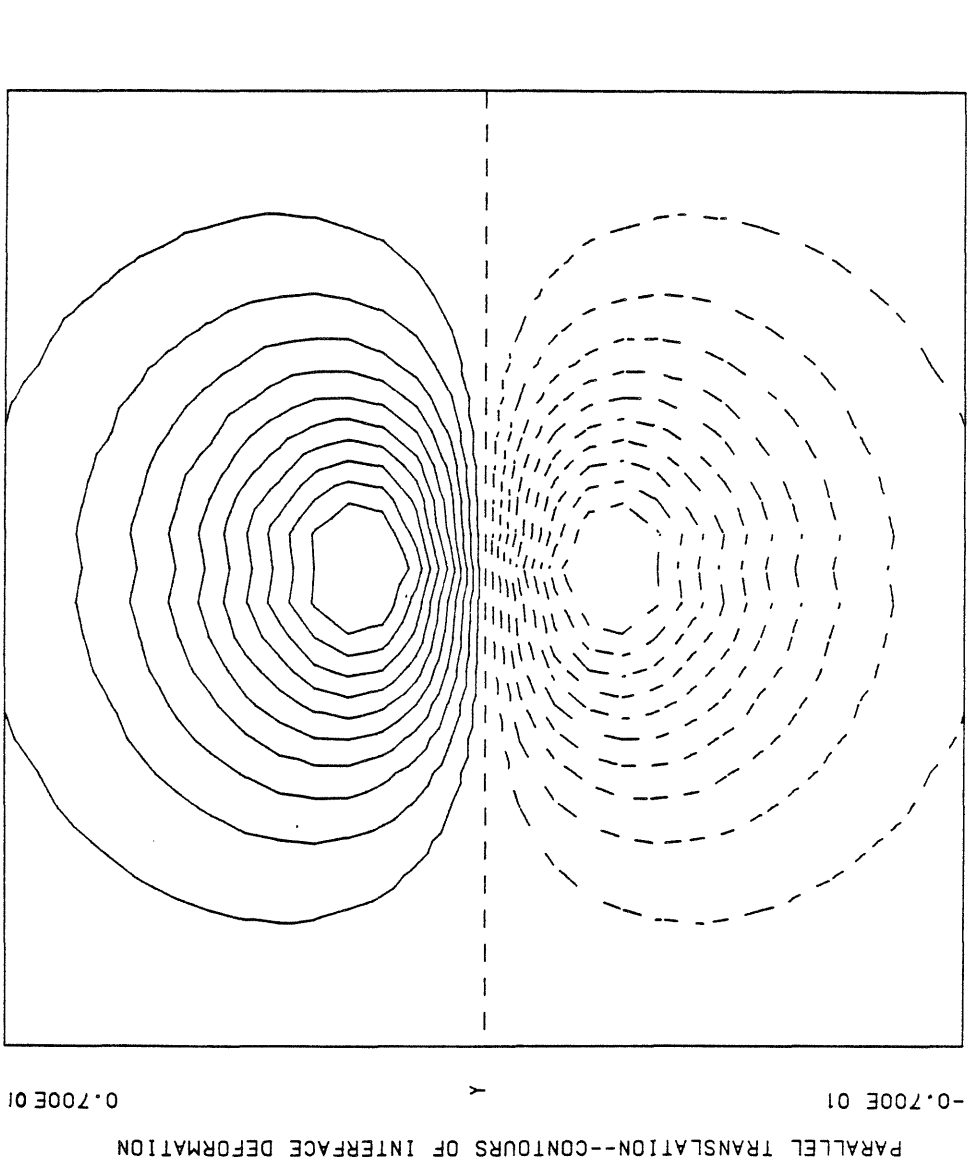
PARALLEL TRANSLATION--CONTOURS OF INTERFACE DEFORMATION
-0.700E 01
0.700E 01
Y
-0.700E 01
0.700E 01
X

FIGURE V

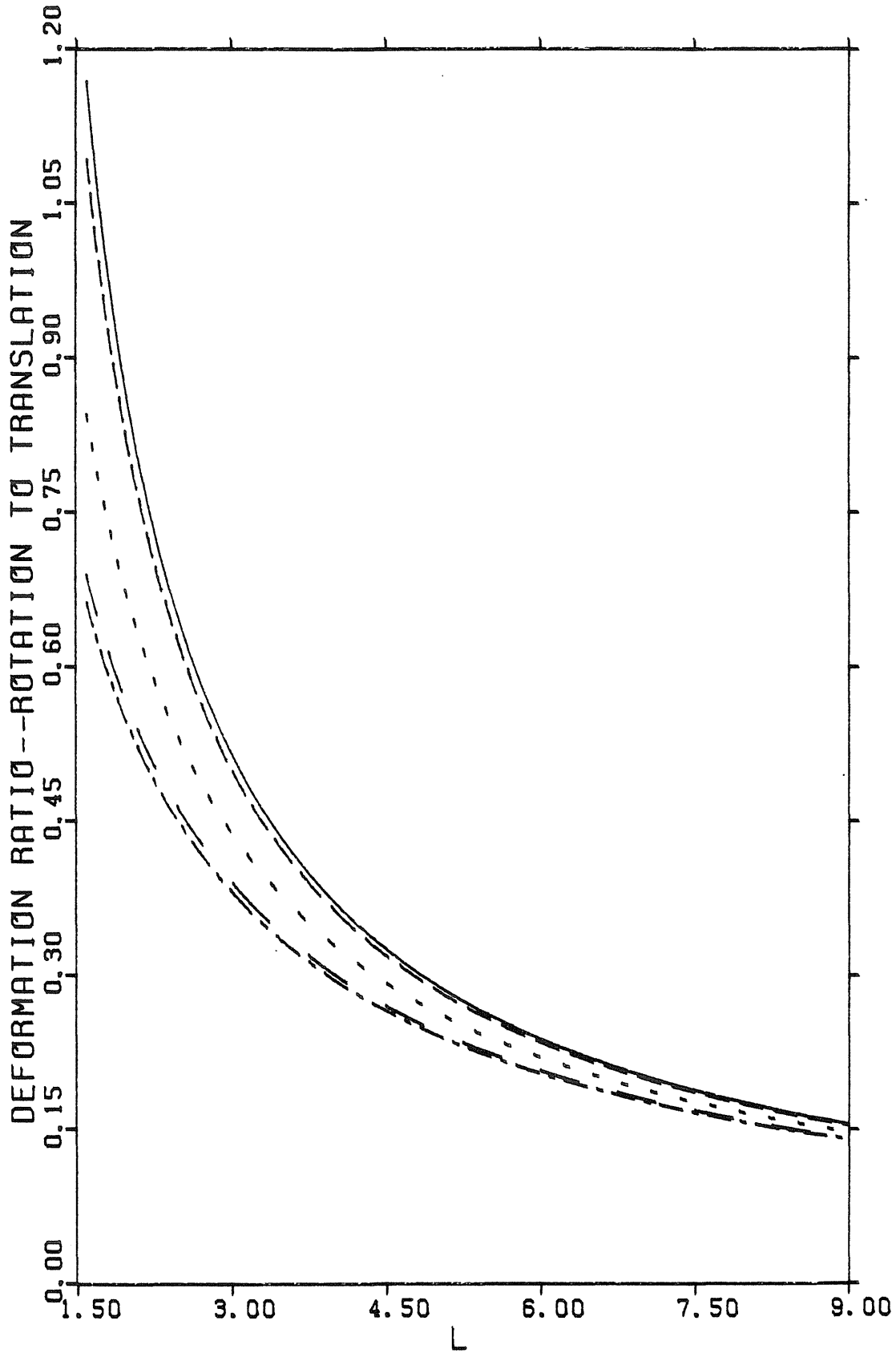
DEFORMATION RATIO--ROTATION TO TRANSLATION
0.00
0.15
0.30
0.45
0.60
0.75
0.90
1.05
1.20
1.50
3.00
4.50
6.00
7.50
9.00
L

FIGURE VI

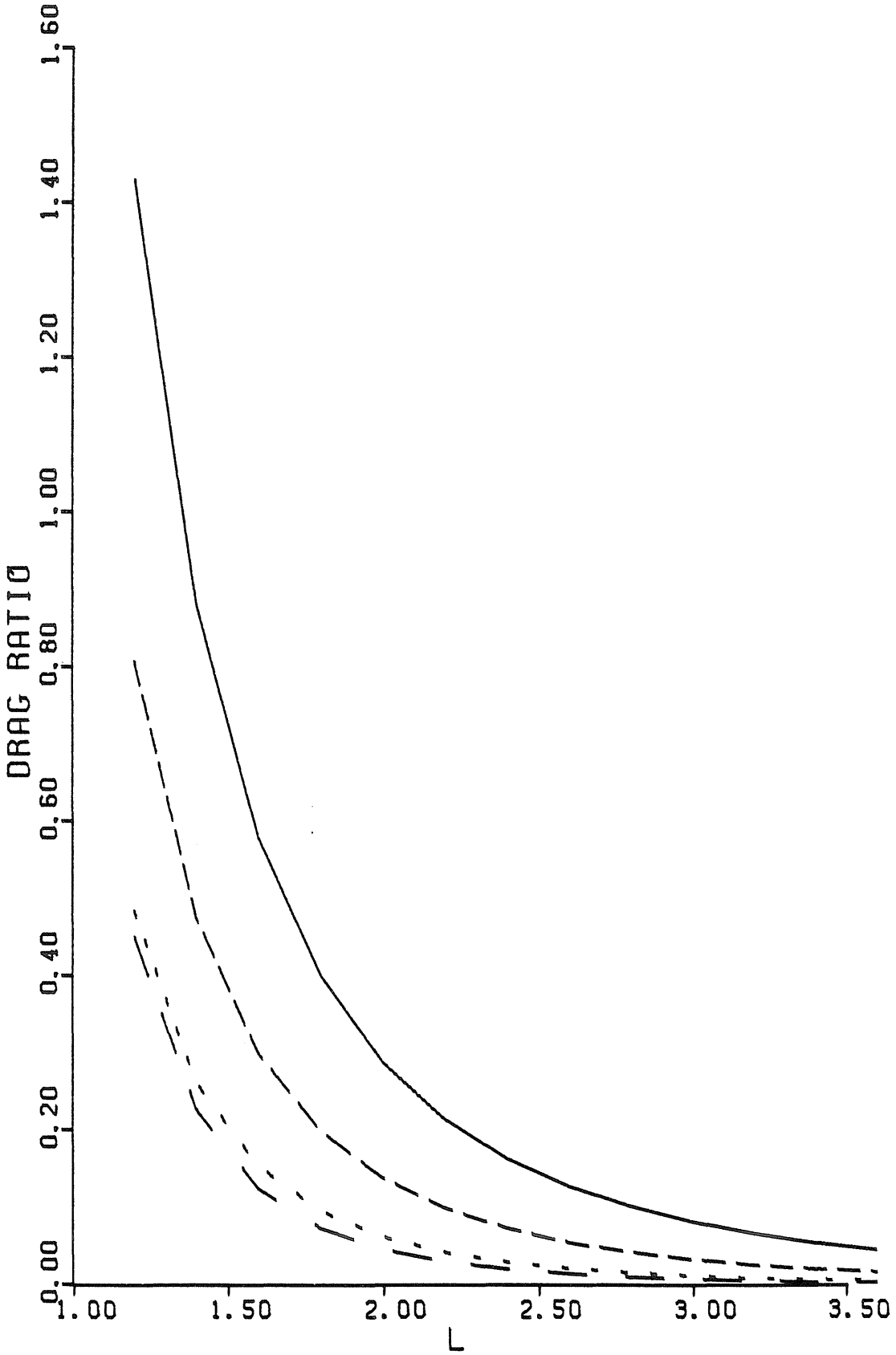
DRAG RATIO
0.00
0.20
0.40
0.60
0.80
1.00
1.20
1.40
1.60
1.00
1.50
2.00
2.50
3.00
3.50
L

FIGURE VII

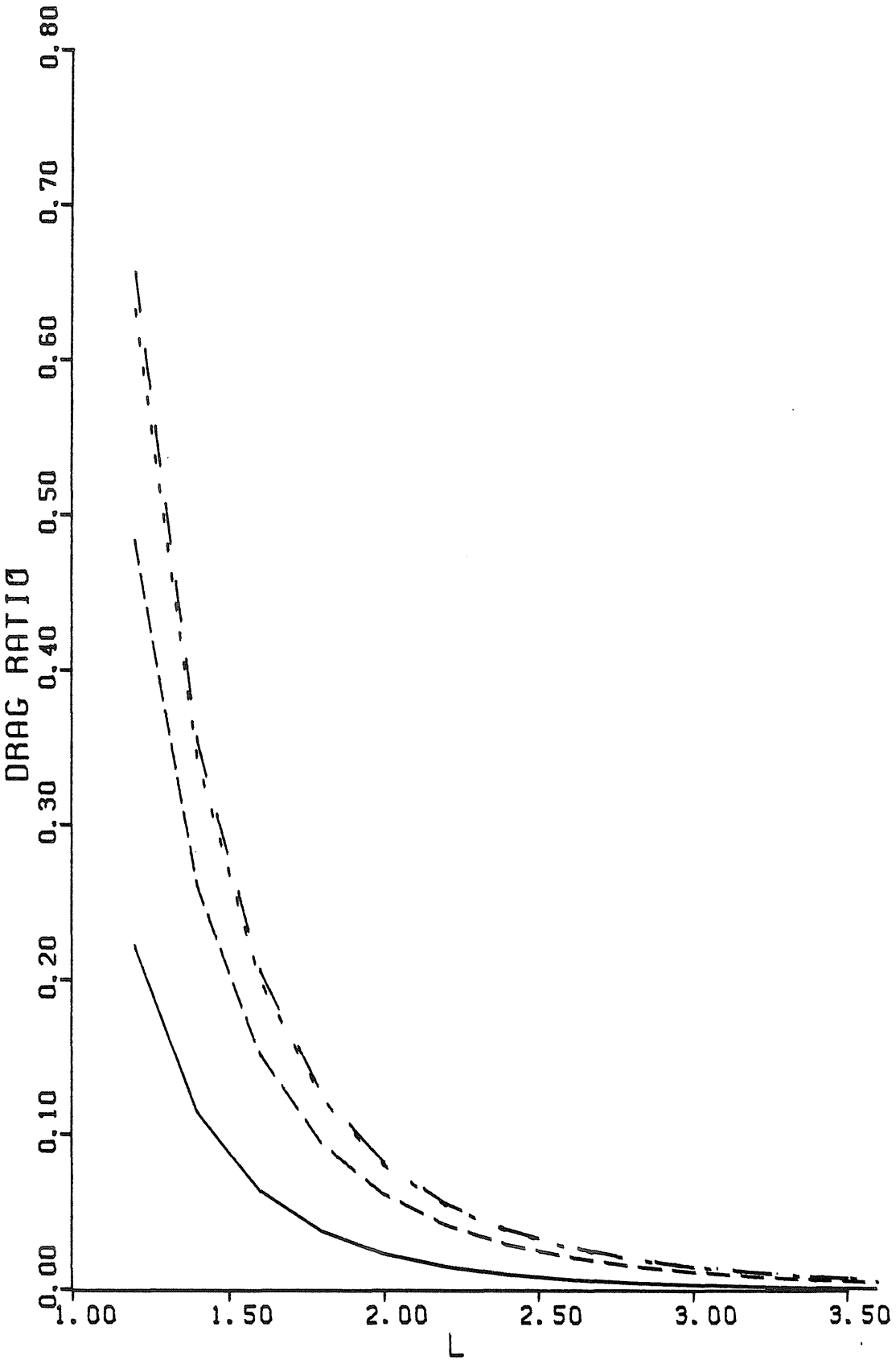
DRAG RATIO
0.00
0.10
0.20
0.30
0.40
0.50
0.60
0.70
0.80
1.00
1.50
2.00
2.50
3.00
3.50
L

FIGURE VIII

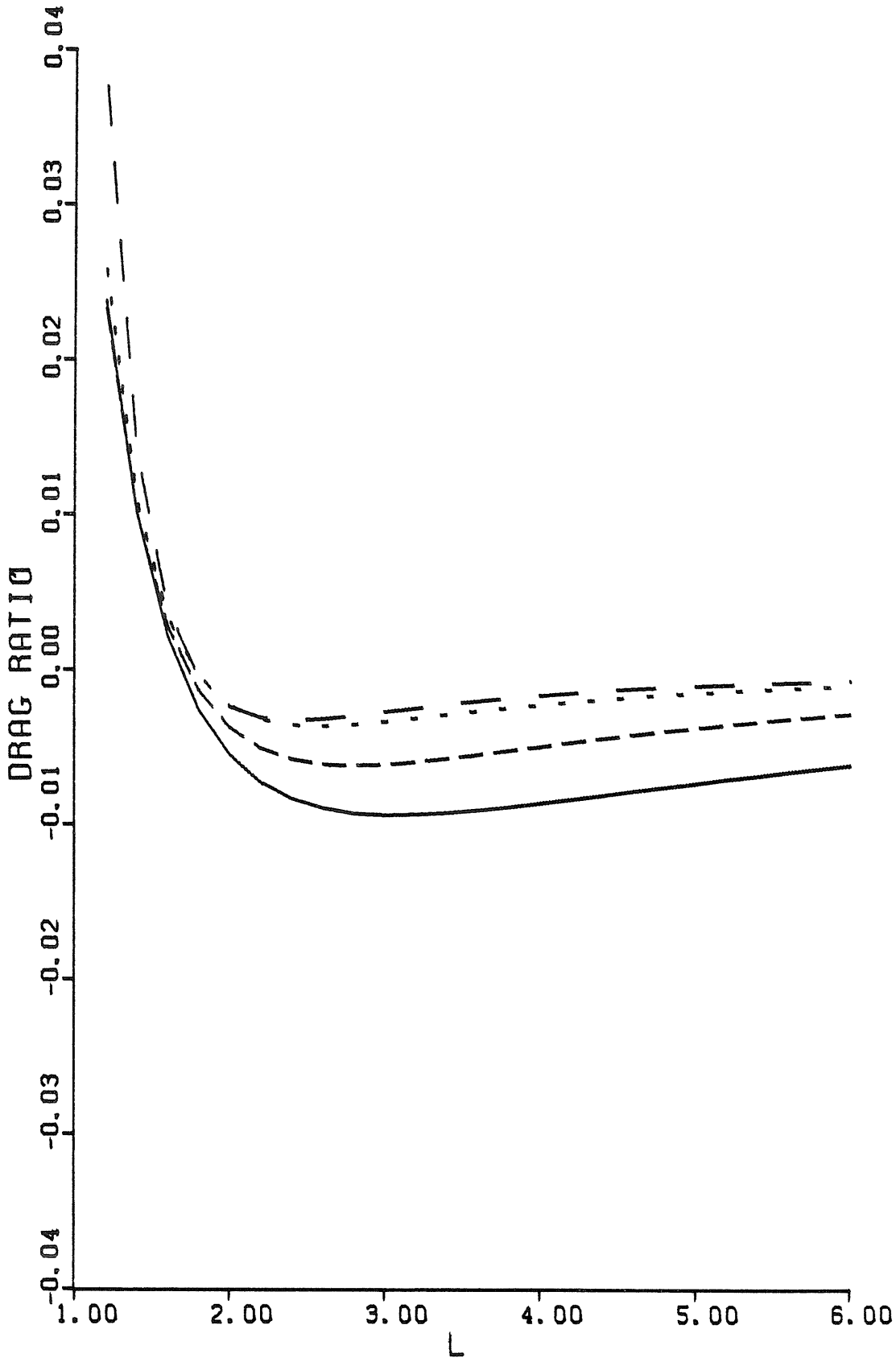
DRAG RATIO
0.04
0.03
0.02
0.01
0.00
-0.01
-0.02
-0.03
-0.04
1.00
2.00
3.00
4.00
5.00
6.00
L

FIGURE IX

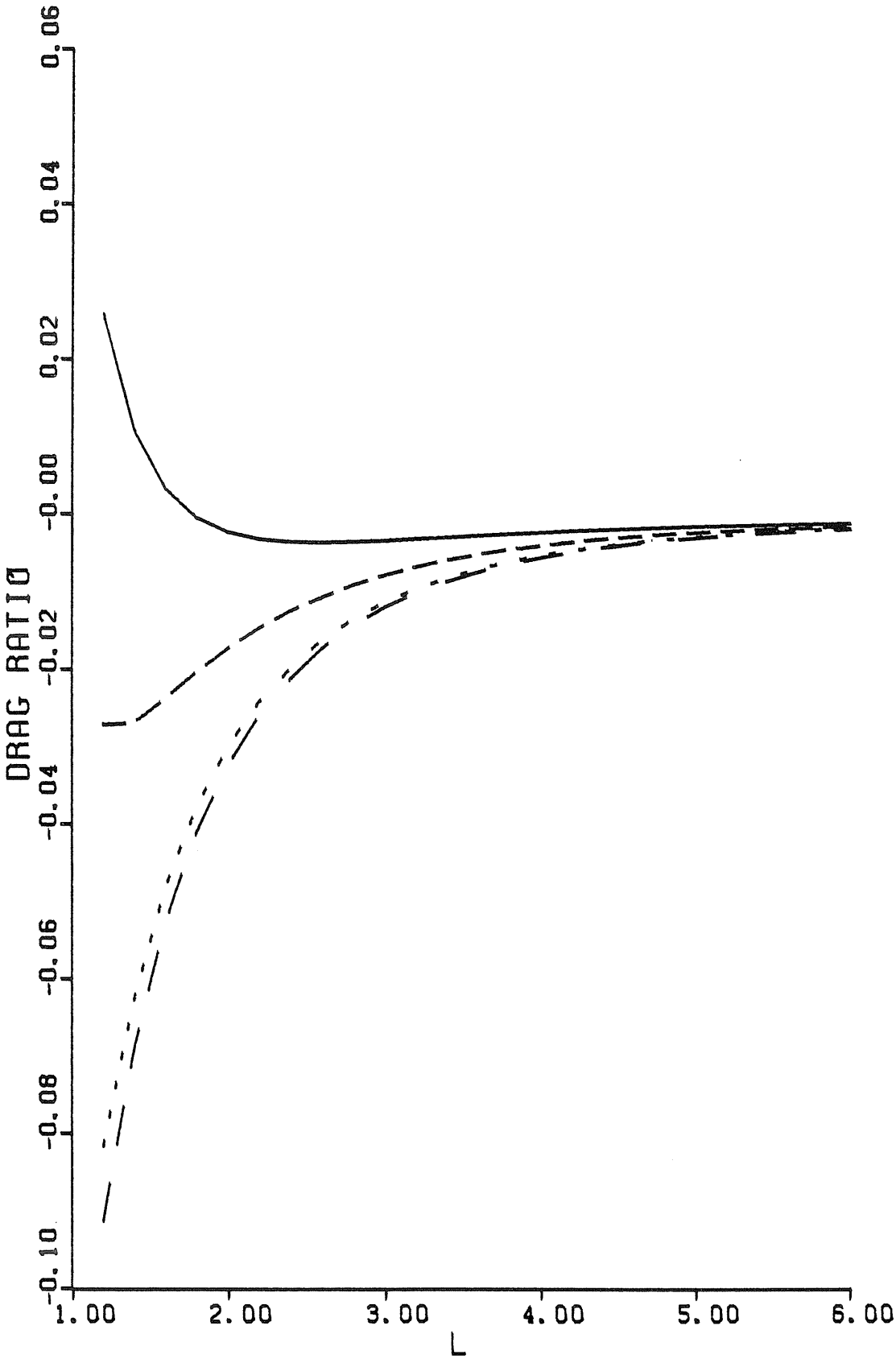
DRAG RATIO
0.06
0.04
0.02
-0.00
-0.02
-0.04
-0.06
-0.08
-0.10
1.00
2.00
3.00
4.00
5.00
6.00
L

FIGURE X

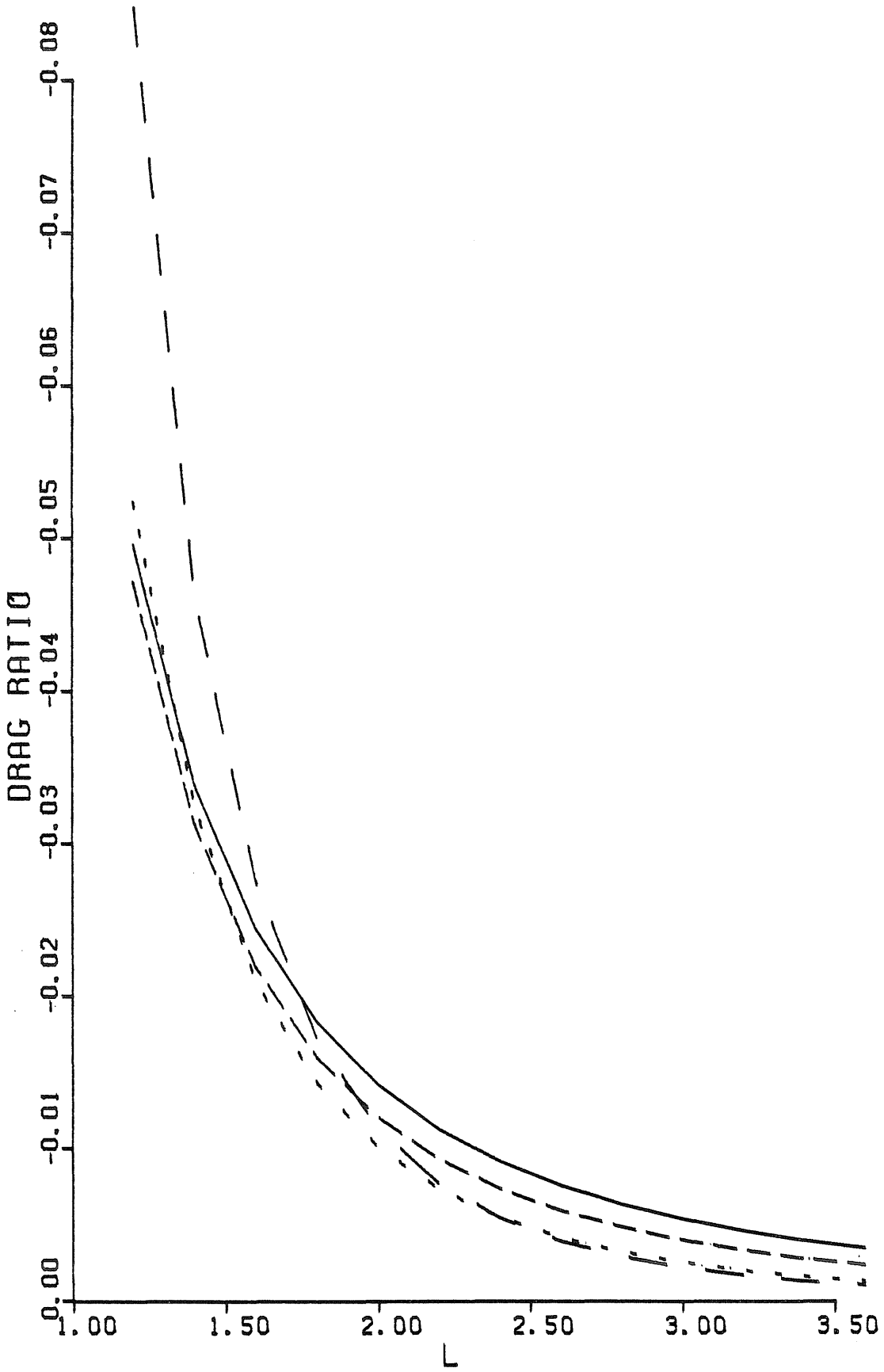
DRAG RATIO
-0.00
-0.01
-0.02
-0.03
-0.04
-0.05
-0.06
-0.07
-0.08
1.00
1.50
2.00
2.50
3.00
3.50
L

FIGURE XI

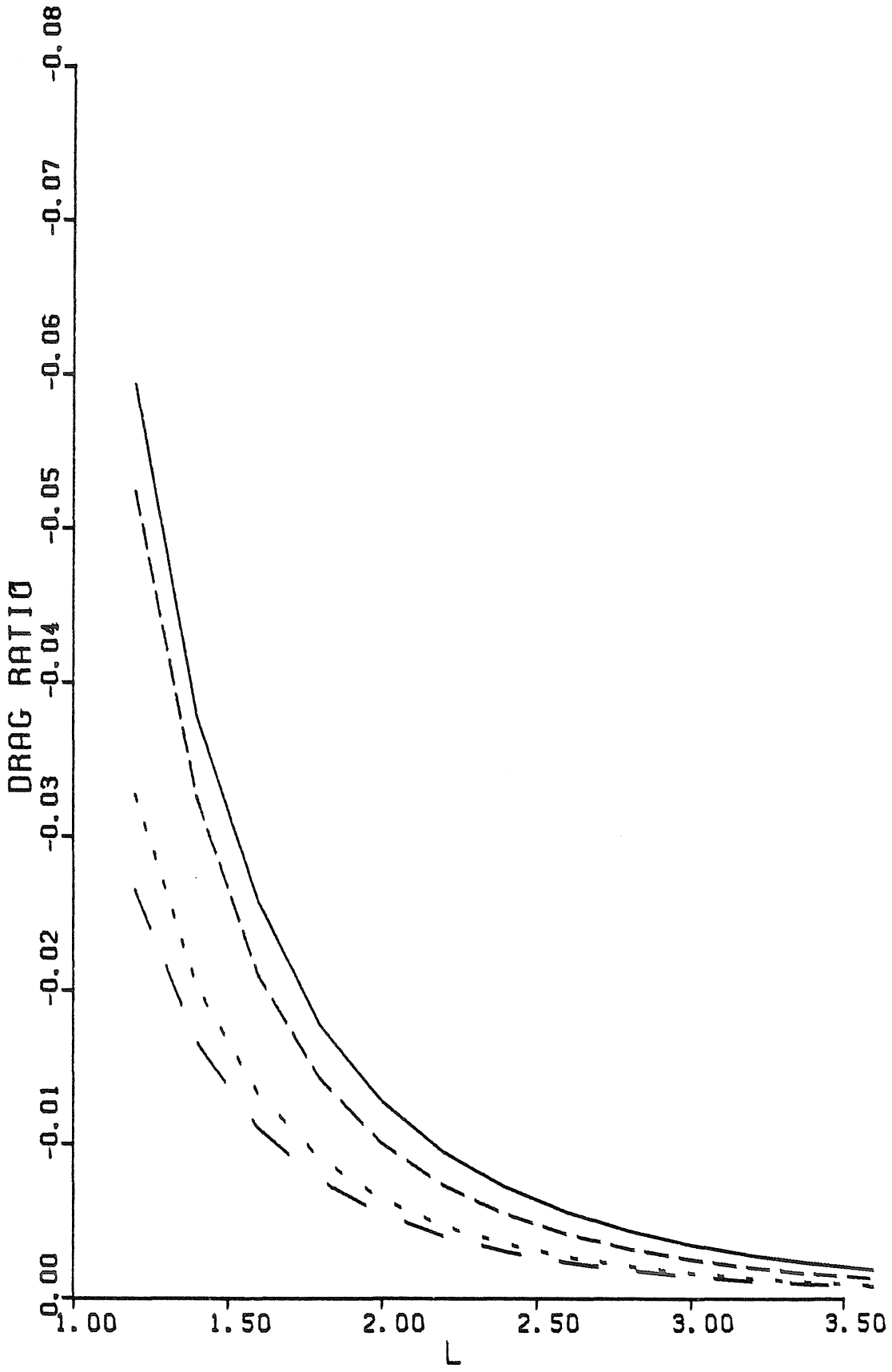
DRAG RATIO
-0.00
-0.01
-0.02
-0.03
-0.04
-0.05
-0.06
-0.07
-0.08
1.00
1.50
2.00
2.50
3.00
3.50
L

FIGURE XII

APPENDIX A: THE COUPLING TENSOR AND CONDITIONS FOR ITS SIMULTANEOUS USE FOR BOTH FORCE AND TORQUE EQUATIONS

Brenner (1964) presented a proof, for the case of a sphere in an infinite fluid, that the coupling tensor, $\mathbf{K}_C$, could be used in both the force and torque equations as shown in equations (3) and (4). The proof uses the reciprocal theorem, discussed in section III, to relate surface stresses, due to translation and rotation, on the sphere. For an infinite fluid, there are no other surfaces to generate contributions to the integrals in the reciprocal theorem as used in Brenner's proof. However, in the work of Lee, Chadwick, and Leal (1979) the problem solved involved a second surface, namely a flat fluid/fluid interface with viscosity ratio λ. Their results showed that the equations for the force and torque were identical in form with those of Brenner (1964), differing only in the elements of the tensors, $\mathbf{K}_C$, $\mathbf{K}_T$ and $\mathbf{K}_R$. In this appendix, we will show, in general, that for equations (3) and (4) to be applicable for a system with surfaces other than the sphere surface, it is sufficient that the fluid motion do no work on the boundaries and have no work done on the fluid by the boundaries. Thus it will be obvious that the results of Lee, Chadwick, and Leal (1979) must fit the form of Brenner (1964), while the work in this paper does not.

Using the governing differential equations for creeping flow with boundary conditions as presented in Lee, Chadwick, and Leal (1979) we can come to some conclusions about the coupling tensor using the reciprocal theorem, as discussed in section II,

$$\int_S \mathbf{v}^T \cdot \boldsymbol{\pi}^R \cdot d\mathbf{s} = \int_S \mathbf{v}^R \cdot \boldsymbol{\pi}^T \cdot d\mathbf{s} \qquad \text{(A-1)}$$

for flows composed of pure translation and pure rotation, where the superscripts T and R respectively distinguish velocities and stresses of the two types of flows, and S includes both the sphere surface and the fluid/fluid interface.

Equation (A-1) applies equally to the second fluid where S now includes only the fluid/fluid interface. Separating S into sphere and interface surfaces, A_S and A_F, we can write equation (A-1) for the lower fluid, containing the sphere, minus λ times (A-1) written for the upper fluid to obtain

$$\int_{A_S}\left[\mathbf{v}^T\cdot\pi^R-\mathbf{v}^R\cdot\pi^T\right]\cdot d\mathbf{s}=\int_{A_F}\left[v_t^R\left(\pi_{tn}^T-\lambda\hat{\pi}_{tn}^T\right)-v_t^T\left(\pi_{tn}^R-\lambda\hat{\pi}_{tn}^R\right)\right]ds$$

$$+\int_{A_F}\left[v_n^R\left(\pi_{nn}^T-\lambda\hat{\pi}_{nn}^T\right)-v_n^T\left(\pi_{nn}^R-\lambda\hat{\pi}_{nn}^R\right)\right]ds \qquad \text{(A-2)}$$

with the $\hat{}$ used to designate the upper fluid. Brenner (1964) has shown that equations (3) and (4) follow when the left hand side of equation (A-2) is equal to zero. The right hand side is precisely zero for any problem formulated with boundary conditions on a fluid/fluid interface of zero normal velocity and matched shear stress as in the problem of Lee, Chadwick, and Leal (1979). In general the right side of equation (A-2) is zero when the boundary conditions on the fluid/fluid interface require the shear stress to be matched and there is either no normal velocity or there is no normal stress jump. These requirements can be restated in terms of the ability of the fluid and boundary to exchange work. For example, if the shear stress experiences a jump at the interface this implies the presence of an external force at the interface, with the consequence that work is performed if the tangential velocity is nonzero. This would result in a nonzero contribution to equation (A-2) by the first integral on the right hand side. In the second integral on the right side it is again obvious that if both the normal velocity and normal stress jump are nonzero on A_F, then the fluid will do work on the interface to displace it. This work is manifest in a nonzero contribution by the second integral on the right hand side of equation (A-2).

As an example, we show that the right hand side of equation (A-2) is nonzero for the problem solved in Chapter I, thus leading to the conclusion that equations (3) and (4) are not applicable in this case. Using the small parameter expansion presented in equations (16) and (18), equation (A-2) can be rewritten in the form

$$\int_{A_S}\left(\mathbf{v}_0^T\cdot\mathbf{T}_0^R-\mathbf{v}_0^R\cdot\mathbf{T}_0^T\right)\cdot d\mathbf{s}+\varepsilon\int_{A_S}\left(\mathbf{v}_0^T\cdot\mathbf{T}_1^R-\mathbf{v}_0^R\cdot\mathbf{T}_1^T+\mathbf{v}_1^T\cdot\mathbf{T}_0^R-\mathbf{v}_1^R\cdot\mathbf{T}_0^T\right)\cdot d\mathbf{s}=$$

$$\int_{A_F}\left[v_{0t}^R\left(T_{0tn}^T-\lambda\hat{T}_{0tn}^T\right)-v_{0t}^T\left(T_{0tn}^R-\lambda\hat{T}_{0tn}^R\right)+v_{0n}^R\left(T_{0nn}^T-\lambda\hat{T}_{0nn}^T\right)-v_{0n}^T\left(T_{0nn}^R-\lambda\hat{T}_{0nn}^R\right)\right]ds+$$

$$\varepsilon\int_{A_F}\left[v_{1t}^R\left(T_{0tn}^T-\lambda\hat{T}_{0tn}^T\right)+v_{0t}^R\left(T_{1tn}^T-\lambda\hat{T}_{1tn}^T\right)-v_{1t}^T\left(T_{0tn}^R-\lambda\hat{T}_{0tn}^R\right)-v_{0t}^T\left(T_{1tn}^R-\lambda\hat{T}_{1tn}^R\right)\right]ds+$$

$$\varepsilon\int_{A_F}\left[v_{1n}^R\left(T_{0nn}^T-\lambda\hat{T}_{0nn}^T\right)+v_{0n}^R\left(T_{1nn}^T-\lambda\hat{T}_{1nn}^T\right)-v_{1n}^T\left(T_{0nn}^R-\lambda\hat{T}_{0nn}^R\right)-v_{0n}^T\left(T_{1nn}^R-\lambda\hat{T}_{1nn}^R\right)\right]ds+O(\varepsilon^2)\quad(A\text{-}3)$$

where we have neglected $O(\varepsilon^2)$ and higher terms. The O(1) terms correspond to the problem of Lee, Chadwick, and Leal (1979) and thus are equal to zero as discussed in the preceeding paragraph. Hence dropping the O(1) terms and cancelling ε from both sides of equation (A-3), we obtain

$$\int_{A_S}\mathbf{v}_0^T\cdot\mathbf{T}_1^R\cdot ds=\int_{A_S}\mathbf{v}_0^R\cdot\mathbf{T}_1^T\cdot ds+$$

$$\int_{A_F}\left[v_{1t}^R\left(T_{0tn}^T-\lambda\hat{T}_{0tn}^T\right)+v_{0t}^R\left(T_{1tn}^T-\lambda\hat{T}_{1tn}^T\right)-v_{1t}^T\left(T_{0tn}^R-\lambda\hat{T}_{0tn}^R\right)-v_{0t}^T\left(T_{1tn}^R-\lambda\hat{T}_{1tn}^R\right)\right]ds+$$

$$\int_{A_F}\left[v_{1n}^R\left(T_{0nn}^T-\lambda\hat{T}_{0nn}^T\right)+v_{0n}^R\left(T_{1nn}^T-\lambda\hat{T}_{1nn}^T\right)-v_{1n}^T\left(T_{0nn}^R-\lambda\hat{T}_{0nn}^R\right)-v_{0n}^T\left(T_{1nn}^R-\lambda\hat{T}_{1nn}^R\right)\right]ds+O(\varepsilon).\quad(A\text{-}4)$$

This can immediately be simplified using the boundary conditions ofmatched shear stress and zero normal velocity for the O(1) terms (cf. Lee, Chadwick, and Leal (1979)) to yield,

$$\int_{A_S} \mathbf{v}_0^T \cdot \mathbf{T}_1^R \cdot ds = \int_{A_S} \mathbf{v}_0^R \cdot \mathbf{T}_1^T \cdot ds + \int_{A_F} \left[v_{0t}^R \left(T_{1tn}^T - \lambda \hat{T}_{1tn}^T \right) - v_{0t}^T \left(T_{1tn}^R - \lambda \hat{T}_{1tn}^R \right) \right] ds$$

$$+ \int_{A_F} \left[v_{1n}^R \left(T_{0nn}^T - \lambda \hat{T}_{0nn}^T \right) - v_{1n}^T \left(T_{0nn}^R - \lambda \hat{T}_{0nn}^R \right) \right] ds + O(\varepsilon). \qquad \text{(A-5)}$$

Now, the first two terms of (A-5) can be expressed in the forms

$$\int_{A_S} \mathbf{v}_0^T \cdot \mathbf{T}_1^R \cdot ds = \mathbf{u}_0 \cdot \int_{A_S} \mathbf{T} \cdot ds \equiv \mathbf{u}_0 \cdot -\mathbf{K}_{D_1} \cdot \omega_0 \qquad \text{(A-6)}$$

and

$$\int_{A_S} \mathbf{v}_0^R \cdot \mathbf{T}_1^T \cdot ds = \omega_0 \cdot \int_{A_S} \mathbf{r}_0 \times \mathbf{T}_1^T \cdot ds \equiv \omega_0 \cdot -\mathbf{K}_{C_1} \cdot \mathbf{u}_0 \qquad \text{(A-7)}$$

where the subscripts 1 denote the $O(\varepsilon)$ terms for each variable. We have used definitions for the $O(\varepsilon)$ contributions, $\mathbf{K}_{C_1}$ and $\mathbf{K}_{D_1}$, which are analogous to the definitions of Brenner (1964) for $\mathbf{K}_C$ and $\mathbf{K}_D$. If we could equate the left hand sides of equations (A-6) and (A-7), we would conclude that $\mathbf{K}_{D_1} = \mathbf{K}_{C_1}^T$ and thus demonstrate the validity of equations (3) and (4) through $O(\varepsilon)$. But we must look at the remaining terms in equation (A-5) and show that they all sum to zero for this to be true. The results of evaluating the remaining terms in equation (A-5) can be obtained by simply noting that these terms are the only terms in (31) and (32) which contribute to the results in equation (43). Thus they are nonzero and represent the difference between the integrals given in equations (A-6) and (A-7). We conclude that $\mathbf{K}_{D_1} \neq \mathbf{K}_{C_1}^T$, and thus, in general, $\mathbf{K}_C \neq \mathbf{K}_D^T$ when the interface is allowed to deform. The equations (3) and (4) clearly do not apply even in the small deformation problem of Chapter I.

APENDIX B: NEXT HIGHER ORDER SHAPE FOR NORMAL MOTION

We notice in the equations for f_1 in the point force solution (i.e. the leading term in each of equations (20a-d)) that the viscosity ratio is conspicuously missing. We hypothesize that this is due to our O(1) calculations being restricted to a flat interface and a point force. Thus one may expect that shapes calculated for higher order flow fields (i.e. flows which take account of the deformation) will include λ. Here we proceed to calculate the $O(\varepsilon)$ flow field and from the normal stress difference at the interface, we calculate f_2 for the case of gravity dominated deformation in the normal motion problem. As the velocity boundary condition on the sphere at $O(\varepsilon)$ is $\mathbf{v}=0$, the only motion in the fluid at $O(\varepsilon)$ is that which is necessary to satisfy the $O(\varepsilon)$ boundary conditions on the fluid/fluid interface. The flow is axisymmetric and can be solved in terms of a stream function, ψ, where ψ satisfies,

$$E^4\psi = 0, \quad E^2 \equiv \frac{\partial^2}{\partial\rho^2} - \frac{1}{\rho}\frac{\partial}{\partial\rho} + \frac{\partial^2}{\partial z^2} \tag{B-1}$$

and is related to the velocity by,

$$\mathbf{u} = -\frac{1}{\rho}\frac{\partial\psi}{\partial z}\mathbf{i}_\rho + \frac{1}{\rho}\frac{\partial\psi}{\partial\rho}\mathbf{i}_\rho. \tag{B-2}$$

For ease in satisfying the boundary conditions in equations (22)–(24) it is convenient to solve equation (B-1) using a Hankel transform. We define the transform, $\bar{\eta}_\nu(\xi, z)$, (see Sneddon (1951)) of any function, $\eta(\rho,z)$, by the equation,

$$\bar{\eta}_\nu(\xi, z) = \int_0^\infty \rho\eta(\rho, z)J_\nu(\xi\rho)d\rho. \tag{B-3}$$

We proceed with the solution of equation (B-1) by introduction of the vorticity, ω, which turns the fourth order equation into a pair of coupled second order equations,

$$E^2\omega = 0 \tag{B-4}$$

and

$$E^2\psi = \omega. \tag{B-5}$$

Applying the Hankel transform (B-3) to the equation (B-4), after first making the substitution $\omega=\rho\chi_1$, we obtain,

$$-\xi^2\bar{\chi}_1(\xi, z) + \frac{\partial^2\bar{\chi}_1(\xi, z)}{\partial z^2} = 0 \tag{B-6}$$

with solution

$$\bar{\chi}_1(\xi, z) = A(\xi)e^{\xi z} + B(\xi)e^{-\xi z}. \tag{B-7}$$

We solve equation (B-5) by again making the substitution $\psi=\rho\vartheta_1$ and transforming to yield,

$$\frac{\partial^2\bar{\vartheta}_1(\xi, z)}{\partial z^2} - \xi^2\bar{\vartheta}_1(\xi, z) = A(\xi)e^{\xi z} + B(\xi)e^{-\xi z}. \tag{B-8}$$

Solving (B-8), we obtain

$$\bar{\vartheta}_1(\xi, z) = \frac{A(\xi)}{2\xi}ze^{\xi z} - \frac{B(\xi)}{2\xi}ze^{-\xi z} + C(\xi)e^{\xi z} + D(\xi)e^{-\xi z}. \tag{B-9}$$

Now we must evaluate the constants $A(\xi)$ through $D(\xi)$ for the upper and lower fluids. It is first required that the flows be well behaved for $z\rightarrow\pm\infty$ in the two fluids. This leads to,

$$\bar{\vartheta}_1^{(1)}(\xi, z) = \left[D(\xi) - \frac{B(\xi)z}{2\xi}\right]e^{-\xi z} \tag{B-10}$$

in the upper fluid, and,

$$\bar{\vartheta}_1^{(2)}(\xi, z) = \left[C(\xi) + \frac{A(\xi)z}{2\xi}\right]e^{\xi z} \tag{B-11}$$

in the lower fluid. Then, applying the matched velocity and shear stress conditions of equations (22)--(24), we obtain,

$$\bar{\vartheta}_1^{(1)}(\xi, z) = \Big[D(\xi) - G(\xi)z\Big]e^{-\xi z} \tag{B-12}$$

$$\bar{\vartheta}_1^{(2)}(\xi, z) = \Big[D(\xi) + H(\xi)z\Big]e^{\xi z} \tag{B-13}$$

for the streamfunctions in the transformed domain, with

$$D(\xi) = \frac{9}{32}\frac{l^2\xi^2}{1+\lambda}K_2(\xi l) \tag{B-14}$$

$$G(\xi) = \frac{9}{64}\frac{l\xi^3}{1+\lambda}\left\{\left[\frac{3}{4}l\xi(1-\lambda) - \frac{3}{8}(3-11\lambda)\right]K_3(\xi l) - 2l\xi K_2(\xi l)\right\} \tag{B-15}$$

$$H(\xi) = \frac{9}{64}\frac{l\xi^3}{1+\lambda}\left\{\left[\frac{3}{4}l\xi(1-\lambda) + \frac{3}{8}(3-11\lambda)\right]K_3(\xi l) - 2l\xi K_2(\xi l)\right\} \tag{B-16}$$

where $K_\nu(x)$ is the modified Bessel's function of order ν. From the transform of the normal stress boundary condition we are led to the equation for the transformed shape,

$$\bar{f}_2(\xi) = \frac{2\lambda}{\xi}\frac{\partial\bar{\vartheta}_1^{(1)}}{\partial z} - \frac{2}{\xi}\frac{\partial\bar{\vartheta}_1^{(2)}}{\partial z}\bigg|_{z=0}. \tag{B-17}$$

Combining equations (B-12)--(B-17) along with the inverse transform,

$$f_2(\rho) = \int_0^\infty \xi\bar{f}_2(\xi)J_0(\xi\rho)d\xi \tag{B-18}$$

we derive

$$f_2(\rho) = -\frac{27}{128}l(1-\lambda)\int_0^\infty\left[l\xi^4 + \frac{1}{2}\frac{3-11\lambda}{1+\lambda}\xi^3\right]K_3(\xi l)J_0(\xi\rho)d\xi \tag{B-19}$$

for the $O(\varepsilon)$ contribution to the interface shape. Equation (B-19) shows that we do indeed get the viscosity ratio in the shape function at higher order. We also have shown in section III that by solving the problem with the added singularities needed for a spherical body, we again obtain the viscosity ratio in the shape function (see equation (36)).

References

Sneddon, I. N. 1951 "Fourier Transforms", 1st. ed. McGraw-Hill.

Watson, G. N. 1966 "A Treatise On The Theory Of Bessel Functions", Cambridge University Press.

APPENDIX C: ADDITIONAL FIGURES

The figures in this appendix are included for completeness as they were discussed in the paper yet left out because of their similarity to other figures or results that were included. The only exception is figure C-III which is a view of the deformation from 30 degrees below the plane of the interface for parallel motion. The sphere is moving in the x direction as indicated by the arrow and the interface deformation is in the z direction. The scale in the z direction has been greatly expanded to allow viewing of the shape as in all the other figures. This figure is simply another view of figure V and of the curves in figures IV and C-II which have the same values for the dimensionless groups.

Figure Captions

Figure C-I. Parallel translational deformation. The effects of particle distance for $\alpha/\beta = 1$, $\alpha + \beta = 10$ and $\lambda = 1$.

_____ $l = 3$, – – – $l = 6$ and ----- $l = 9$.

Figure C-II. Parallel translational deformation. The effects of viscosity ratio for $\alpha / \beta = 1$, $\alpha + \beta = 10$ and $l = 6$.

__ __ __ $\lambda = \infty$, _____ $\lambda = 1$, – – – $\lambda = 2/3$ and ---- $\lambda = 0$.

Figure C-III. Parallel translational deformation. Displacement of the interface as viewed from 30 degrees below the level plane for translation in y direction for $\alpha / \beta = 1$, $\alpha + \beta = 10$, $l = 6$ and $\lambda = 1$.

Figure C-IV. Drag ratio for normal translational deformation. The dependence on α/β for $\alpha + \beta = 10$ and $\lambda = 2/3$ as a function of l.

_____ $\alpha / \beta = 0.1$, ----- $\alpha / \beta = .1$, - - - - $\alpha / \beta = 1$ and – – – $\alpha / \beta = 10$.

Figure C-V. Drag ratio for normal translational deformation. The dependence on α/β for $\alpha + \beta = 10$ and $\lambda = 10$ as a function of l.

_____ $\alpha / \beta = .01$, ----- $\alpha / \beta = .1$, - - - - $\alpha / \beta = 1$ and – – – $\alpha / \beta = 10$.

Figure C-VI. Drag ratio for parallel rotational deformation. The dependence on α/β for $\alpha + \beta = 10$ and $\lambda = 2/3$ as a function of l.

_____ $\alpha/\beta = .01$, ----- $\alpha/\beta = .1$, - - - - $\alpha/\beta = 1$ and – – – $\alpha/\beta = 10$.

Figure C-VII. Drag ratio for parallel rotational deformation. The dependence on α/β for $\alpha + \beta = 10$ and $\lambda = 10$ as a function of l.

_____ $\alpha/\beta = .01$, ----- $\alpha/\beta = .1$, - - - - $\alpha/\beta = 1$ and – – – $\alpha/\beta = 10$.

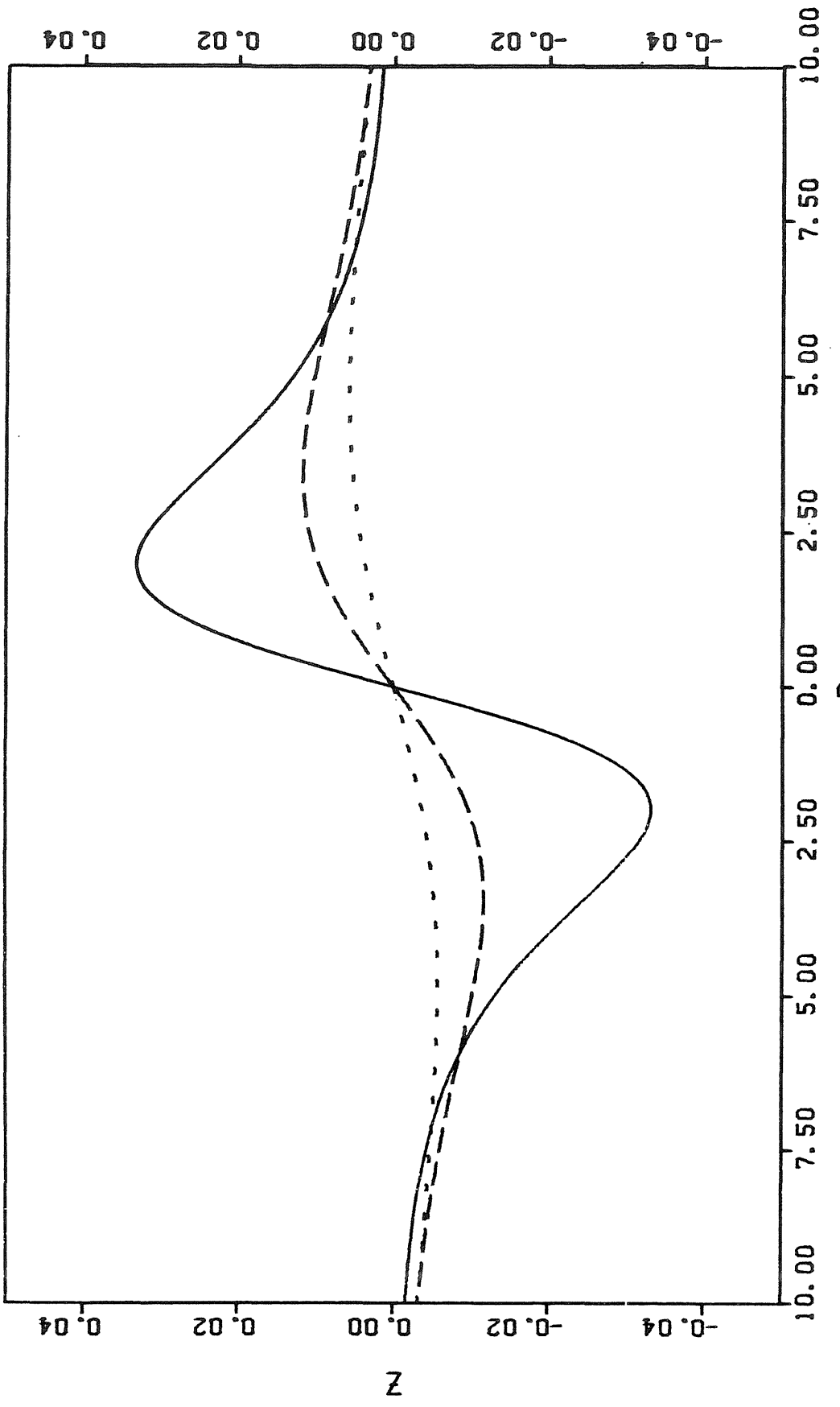

FIGURE C-I

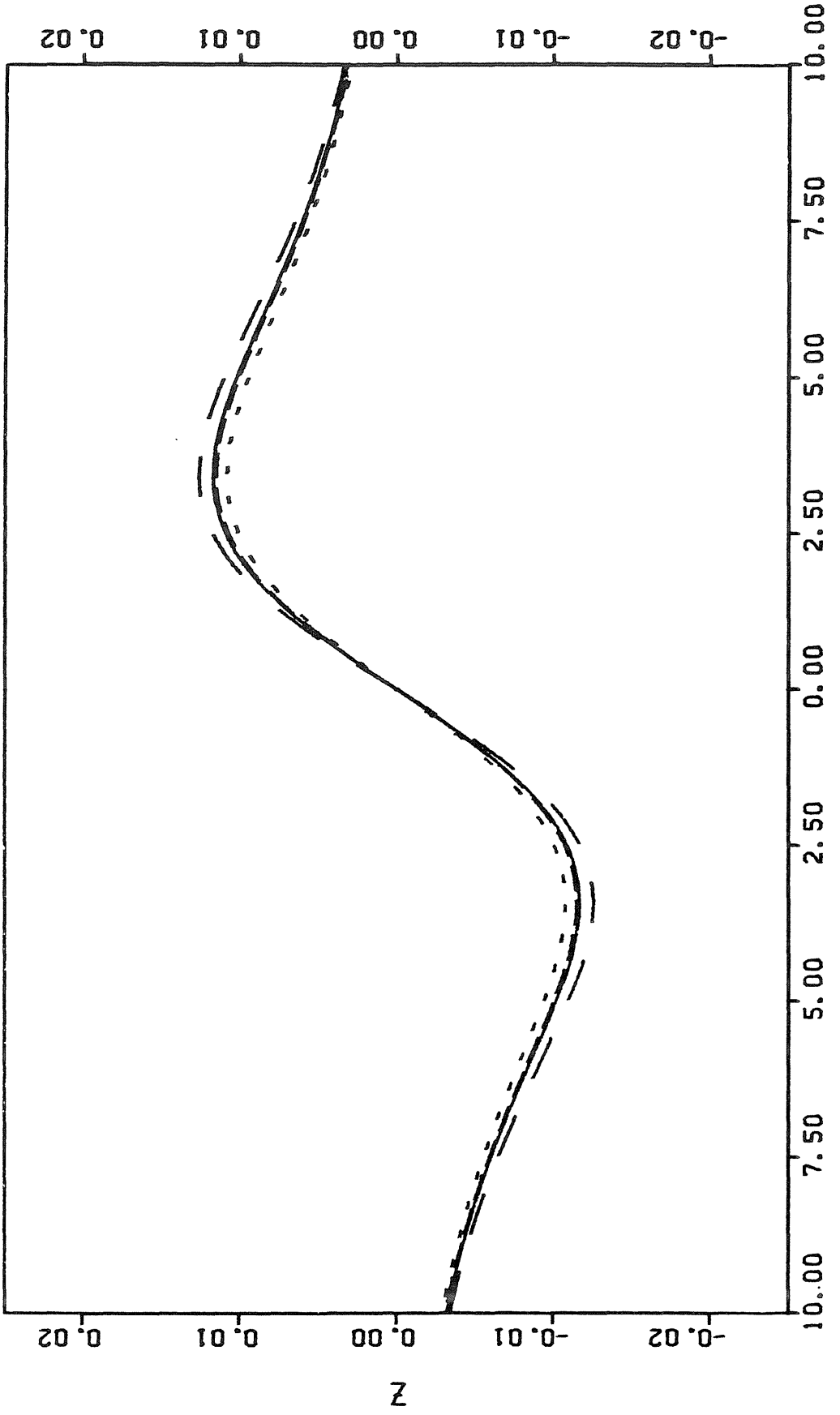

FIGURE c-II

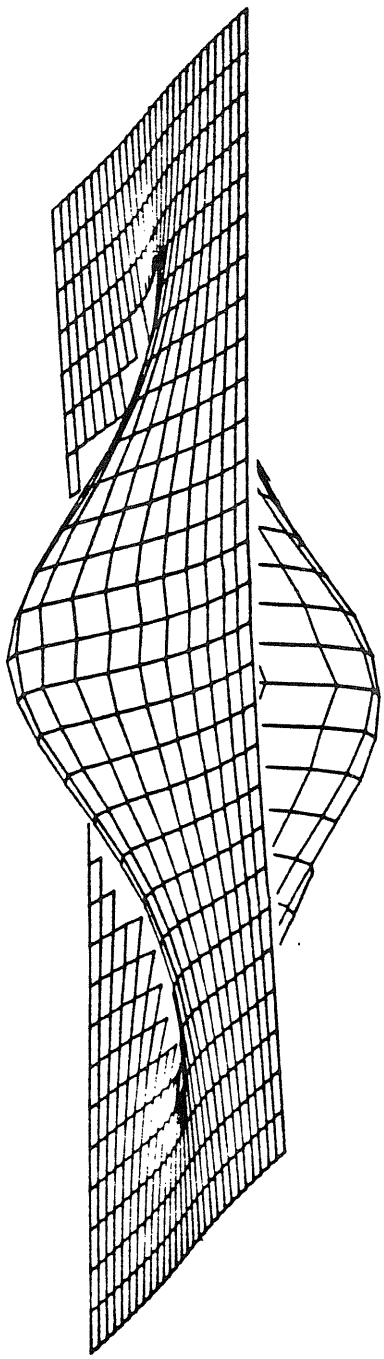

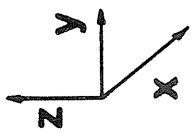

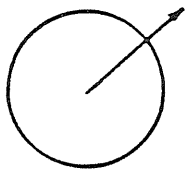

Figure C-III

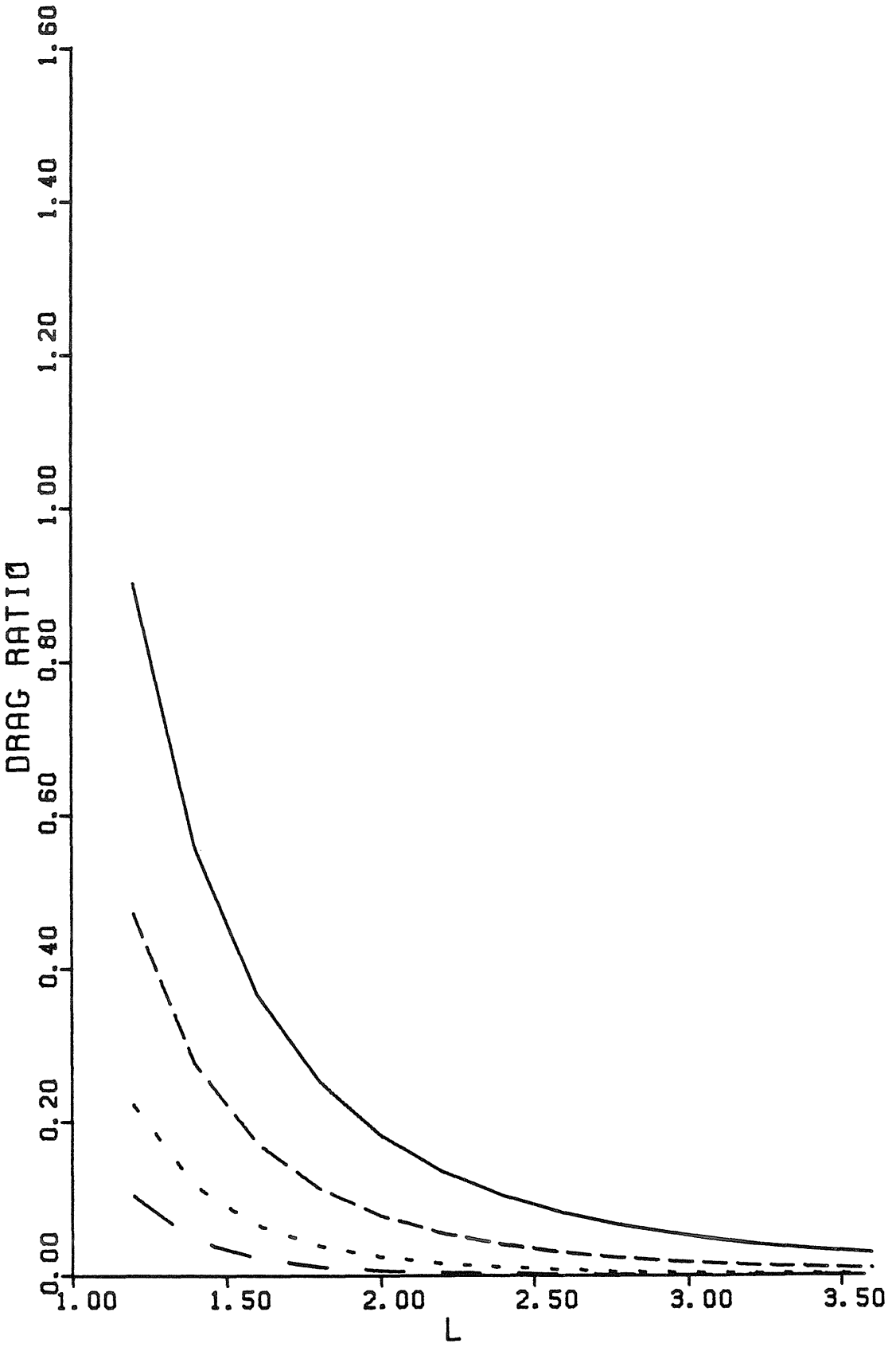
DRAG RATIO
0.00
0.20
0.40
0.60
0.80
1.00
1.20
1.40
1.60
1.00
1.50
2.00
2.50
3.00
3.50
L

FIGURE C-IV

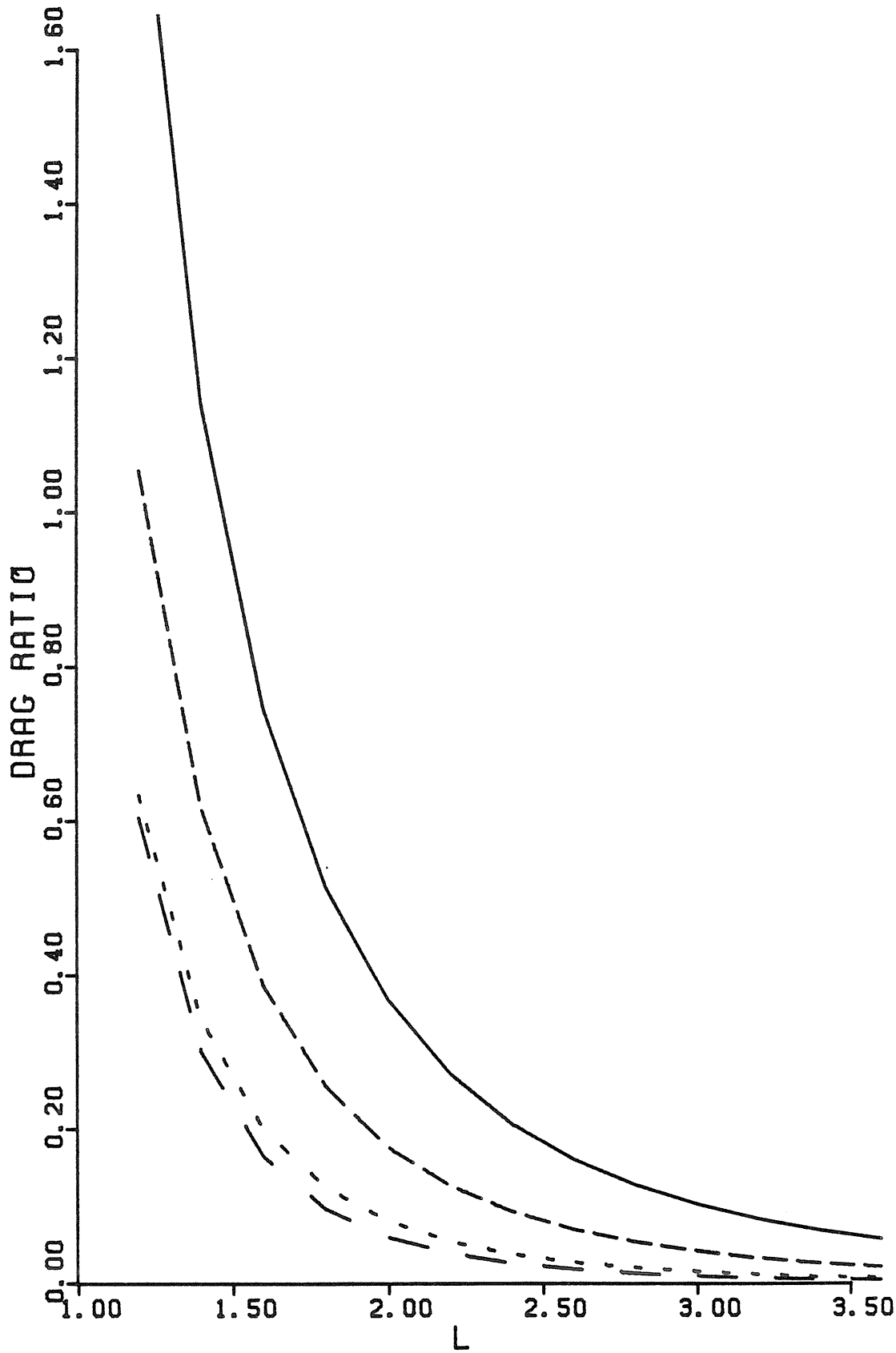
DRAG RATIO
0.00
0.20
0.40
0.60
0.80
1.00
1.20
1.40
1.60
1.00
1.50
2.00
2.50
3.00
3.50
L

FIGURE C-V

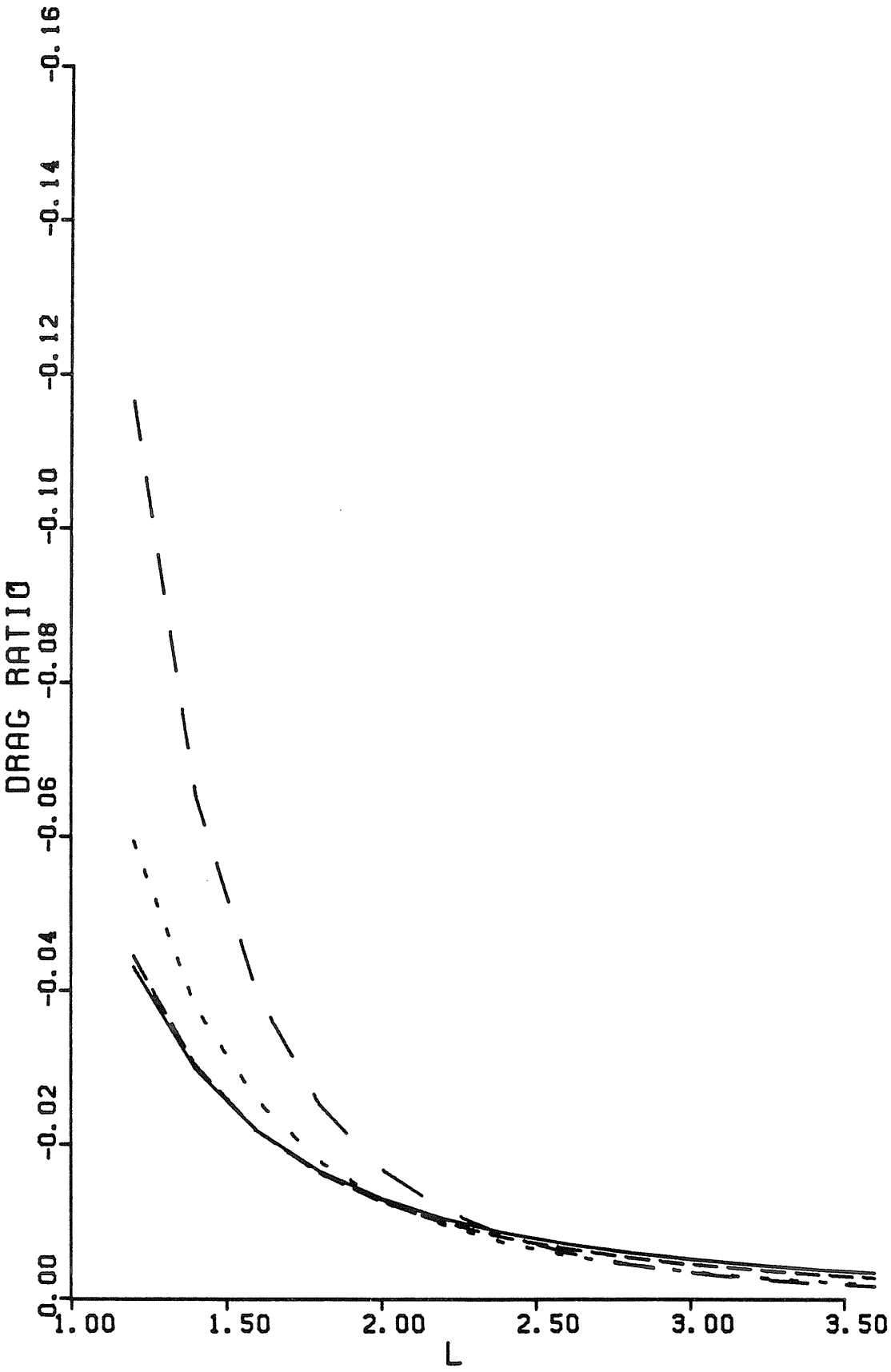
DRAG RATIO
-0.16
-0.14
-0.12
-0.10
-0.08
-0.06
-0.04
-0.02
0.00
1.00
1.50
2.00
2.50
3.00
3.50
L

FIGURE C-VI

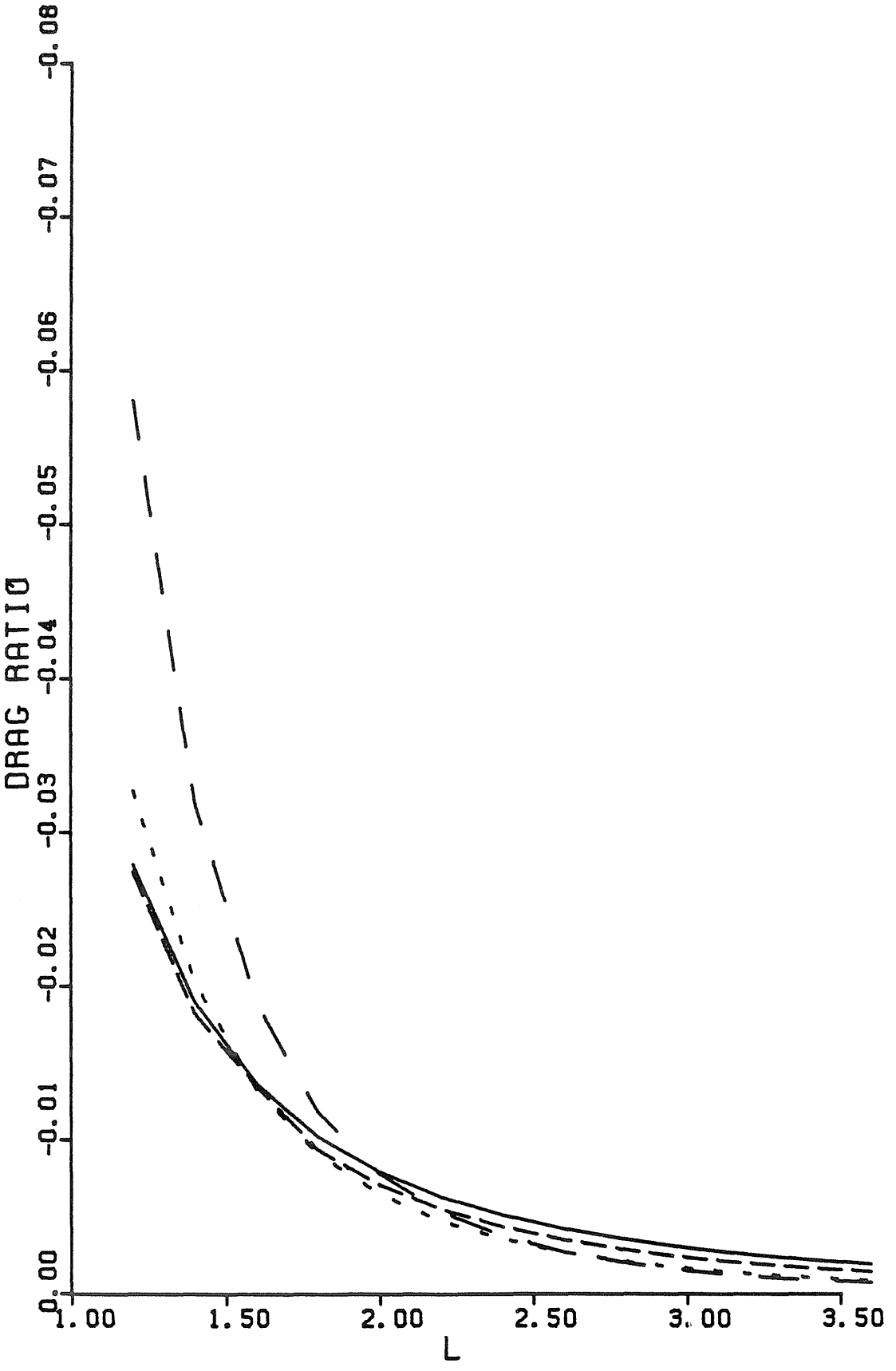
DRAG RATIO
-0.08
-0.07
-0.06
-0.05
-0.04
-0.03
-0.02
-0.01
0.00
1.00
1.50
2.00
2.50
3.00
3.50
L

FIGURE C-VII

CHAPTER III:

Experimental Investigation of the Normal Motion of a Rigid Sphere Near a Deformable Interface

I. INTRODUCTION

This experimental work studies the forces on a spherical particle which moves in the creeping flow regime towards a deformable fluid/fluid interface. This study is designed to investigate some of the cases for normal motion for which Chapter I provides theoretical solutions for small amplitude deformations and the work of Lee and Leal (1981) provides numerical solutions for finite amplitude deformations. The goal of this work is to verify the theoretical and numerical results, as well as to investigate regions of the parameter space which have not previously been studied in the aforementioned works. This work also utilizes a new experimental apparatus which is to be tested for accuracy, as a preliminary to its use in studying the same problem for finite Reynolds numbers, or non-Newtonian suspending fluids, where the existing theoretical and numerical solutions do not apply.

The most common and successful method of evaluating the force on a spherical particle in quasi-steady motion uses the falling-sphere or terminal velocity type experiment, where the velocity of the particle is measured as a function of time. In the case of a sphere settling under the action of gravity, the drag on the sphere equals the net gravitational force on the body. Both Maxworthy (1965) and Pruppacher and Steinberger (1968) used this method with great success for the investigation of deviations from Stokes drag in the low Reynolds number regime (.001-10). Although their results were very reproducible, there was a lack of agreement between the two sets of data as both these researchers made measurements in a bounded system but made no corrections for wall effects. Using the free-fall configuration, Hartland and co-workers [(1968), (1969), and (1970)] studied the *close* approach of a rigid sphere to a fluid/fluid interface, where the interest is in the drainage of the thin film of fluid out from in front of the sphere just before the sphere penetrates the

interface. In these thin film problems, however, the force on the sphere was not determined. Bart (1968), using the same method, tried to evaluate the forces on drops and rigid spheres in their unsteady approach to a fluid/fluid interface. Due to interfacial distortion, the limits of resolution of the experimental procedure, and the unsteady nature of the flow, Bart (1968) found this method of position measurement to be unsuitable when the sphere was within two radii of the interface. Shah, Wasan, and Kintner (1972) studied the mechanism of interface penetration. They were interested in the point at which the interface rutured relative to the position of the sphere.

Other researchers have used a direct force measuring technique which allows the simultaneous measurement of position and force. Jones and Knudsen (1961) used a thin wire and a spring balance to study the force on a sphere in a single "unbounded" fluid for non-zero Reynolds numbers. In the low Reynolds number range, however, their device did not have sufficient sensitivity to accurately measure the small forces they encountered. Kunesh (1971) was able to greatly improve the force measuring system by using a very sensitive two-pan magnetic balance. However, since the balance was bulky it was decided to translate the tank instead of the sphere. The screw-jack used to lift the 1 ton tank could not be machined to close enough tolerance to provide for a smooth translation of the tank and thus no acceptable translation data were obtained. Walker (1965) and Yonas (1967) used strain gauges to measure the forces in their experiments at high Reynolds numbers. A strain gauge is much lighter and easier to translate, thus making it a perfect candidate for force measurements on tethered bodies. Application of a semiconductor bridge to the surface of a thin metal ring, has provided a small deflection ring force transducer which does have the desirable properties of compactness for ease in translating and a large gain with a high signal to noise ratio for measuring small force changes.

Such a device was used in the present study to measure forces on a sphere as it was lowered toward a deformable fluid/fluid interface. The experiments were carried out under conditions where the Reynolds number is very small. In this case, the system is completely characterized by the dimensionless parameters (cf. Chapter I, or Lee and Leal (1981))

$$\lambda \equiv \frac{\mu_1}{\mu_2}$$

$$Ca \equiv \frac{\mu_2 U}{\gamma}$$

$$Cg \equiv \left\{ \frac{\rho_2 g a^2}{\mu_2 U} \left[\frac{\rho_1}{\rho_2} - 1 \right] \right\}^{-1}$$

where the sphere of radius, a, travels at velocity, U, through fluid 2 which lies above fluid 1. Here, γ, μ and ρ represent the interfacial tension, fluid viscosity and fluid density, respectively, while g is the acceleration due to gravity. It is assumed, in the nondimensionalization which leads to this result, that the interface can be completely characterized by the interfacial tension, which is constant independent of time or position on the interface.

In the next section we discuss the fluid systems that were used along with a description of the components of the apparatus, and the errors involved in the measurements. Section III then summarizes the previous theoretical work which is needed to analyze the data to correct for the existence of the wire and the bounding walls. Finally, the last sections include a discussion of the results and a comparison of the results with available theoretical and numerical work.

II. EXPERIMENTAL SYSTEM

The experimental apparatus consists of a large square plexiglas tank containing two immiscible Newtonian liquids. A sphere is lowered at a constant velocity towards the fluid/fluid interface. A wire is attached to the sphere to provide for a constant velocity and to transmit the force on the body to a force transducer. A sketch of the experimental apparatus is shown in figure I. The details of the apparatus will be discussed later in this section.

The decision to use a tethered sphere experiment, instead of the terminal velocity type experiment, was made for the following reasons:

1. A constant velocity could be achieved (and thus constant values for the interfacial parameters, Ca and Cg -- see definitions in section I).
2. The values of Ca and Cg can be varied without changing the fluids or sphere density, by changing the sphere diameter and velocity.
3. The position of the sphere relative to the undeformed interface can be determined to a high degree of accuracy.
4. Forces can be measured close to the interface and even after the sphere has gone past the plane of the undeformed interface.

The drawback to this type of experimental technique is the difficulty in accounting for the disturbance of the flow field created in the neighborhood of the sphere by the wire. Our method of dealing with the wire correction is discussed in section III.

II.A. *FLUID CHARACTERIZATION*

Since we wish to operate in the creeping flow regime, it is necessary that the fluid in which the sphere is located (i.e. the upper fluid in our apparatus) have a large viscosity (greater than 3000 cs in our system). A large viscosity is also necessary to obtain measurable forces (and force changes) on the sphere

using the force transducer in our device. Finally, it is desirable that the upper fluid be hydrophobic so that it can be used with water as a second fluid and more importantly so that fluid properties are not affected by changes in humidity. With these conditions, the experiments consisted of six sets of fluid systems involving three different fluids as shown in table I. Two of the fluids used came in a variety of grades and all three are Newtonian (ref. polybutene [Hardy (1962)] and silicone oil [Olbricht (1981)]). The density data in tables II-VI were obtained with a standard calibrated hydrometer and performed in a temperature bath stable to $\pm 0.06\,^{\circ}C$. The linear equation used to fit the data was sufficient to reproduce the experimental values of the densities in the $19\,^{\circ}C$ to $24\,^{\circ}C$ range to within $\pm 0.2\%$. The viscosity data were also measured in the temperature bath using a Cannon-Fenske viscometer calibrated to ASTM Std. (D-445) and incorporating the density data. The viscosity data were fit quite well ($\pm 0.2\%$) by the three constant exponential equation indicated in table II and the results for the fluids are shown in tables II-VI. Finally the interfacial tension for the two-fluid systems was measured using a du Nouy balance following ASTM Std. (D-971), with results which are presented in table I.

II.B. *EXPERIMENTAL SET-UP*

To study the influences of interfacial deformation on a body moving normal to the interface at a constant velocity, one must be able to obtain accurate measurements of the force on the body, its position relative to the undeformed interface, and the shape of the deformed interface. One way of achieving this goal is to use a tether system which requires the sphere to move at a known velocity and is also able to transfer the force on the sphere to a force measuring device. As noted above, a successful tether system will either have to introduce an insignificant disturbance to the fluid or (at least) produce a *known* contribution to the experimental measurements as in the case of the present

experiments. In addition to a tether, the other components of our system are a force transducer with sufficient sensitivity to detect the force changes to be investigated, a translation device to provide a constant velocity and a measurable sphere position, and finally, a video system to monitor the shape of the interface. In the remainder of this section, these components will be discussed separately and in detail. This is followed by a discussion of the apparatus as a whole in section II.C.

TANK, BODY AND TETHER

The tank containing the fluids is constructed of 1/2" thick plexiglas which is 15" on a side in cross section and 36" deep (interior dimensions). Tank sizing involves consideration of the wall effects and our ability to evaluate them. Any contribution to the drag by the walls tends to diminish our ability to resolve interfacial forces by decreasing the percentage of the total force signal which is due to the interface. We require the ratio of the forces,

$$\frac{F_{interface}}{F_{wall}} \gtrsim O(1) \qquad (1)$$

so that the interface will produce a measurable contribution to the force relative to the wall effects. The spheres were made of bronze, polished smooth and spherical to $\pm$ 0.0002 inches. The sphere diameters ranged from 3/8 inch to 1 inch. The maximum and minimum sphere sizes were determined empirically, from equation (1) and the limits of resolution of our ring force transducer. The tether is made from stainless steel wire, 32 inches long by 0.0041 inch diameter. Sizing of the tether represents a competition between the desire to minimize the disturbance to the flow field caused by the wire, and the need for a wire which will not experience a change in length sufficient to decrease the accuracy of the position measurement (or break). Combining the maximum forces with the elastic modulus of the wire, it can be shown that the maximum change in total

wire length is less than 0.02 inches for our 32 inch wire. It is also important that the wire does not act as a spring by coiling up rather than hanging straight. This is an especially important consideration in the present experiments. These experiments are commonly run close to the terminal velocity of the sphere (when the sphere is close to the interface), and this results in a very small tension in the wire. To eliminate this potential problem, each piece of wire was mechanically straightened so it would hang vertically under its own weight. The equations and data which quantify this discussion are presented in section III after the force measuring system and the method for introducing wall and wire corrections have been discussed.

FORCE MEASUREMENT

The tension in the wire is measured with a ring force transducer that has been fitted with a semiconductor bridge. This bridge is stimulated by a constant 5 ± 0.001 volt power supply and its output is measured with a strip chart recorder. The transducer gain was found on calibration to be $620 \pm 2\mu V$ per gram and in operation the transducer output could be read to $\pm 2\mu V$ for a period of 60 seconds (or the length of the longest experiment). This was the most accurate small deflection force transducer available, that could give sufficient output for small forces and force changes. The ring was affixed rigidly with a thermally isolating coupling to the guide bar of the translation system and housed inside a box. This isolation of the force transducer was necessary to insure there would be no fluctuations in the heat transfer from the ring which would greatly affect its output. To produce stable thermal surroundings, the force transducer was allowed to heat up under load conditions for a period of at least one hour.

The strain in the ring causes a change in the resistances of the individual

legs of the bridge and thus a change in the voltage drop across the measured leg of the bridge. This voltage is continuously recorded on an Omni-Scribe (Model A-5141-5) multi-span (0.001 to 10 volts full scale) strip chart recorder which came equipped with an event marker feature which allowed correlation of the force data with the independently determined sphere position as will be discussed in more detail later.

TRANSLATION SYSTEM

The translation system consists of a rigid guide bar, cable, take-up spool and motor as depicted in figure I. The rigid guide is a 3/4 in. square by 42 in. long aluminum bar. At one end there is a thermal isolation housing in which the ring force transducer is inserted. The bar then passes through a 6 in. centering guide which allows only vertical movement of the bar and centers the bar over the tank. Finally the bar is attached by ball and socket to a 1/16 in. flexible stainless steel cable. The cable is wound around a 6 in. take-up spool. The large diameter spool with its small thread pitch is necessary to maintain a constant velocity within a desired accuracy of 2% as the cable is unwound from the spool. The spool is attached to the gearbox of a 1/50 h.p. Bodine motor which is rated at 38 in.lbs. maximum torque. The motor has a continuous setting feedback controller to insure constant r.p.m. of the motor during operation. The controller allowed the selection of constant velocities in the range of 0.25 cps to 1.4 cps. The lower bound is the limit of smooth and constant rotation of the motor while the upper bound is restricted by the use of a manual event marker. This upper bound on the velocity is obtained by assuming a reaction time of 1/20 sec to actuate the event marker and requiring the position to be known to 0.03 inches.

VIDEO SYSTEM

The video system is designed to serve two purposes; first, to monitor the position and velocity of the sphere and second, to record the interface shape as a function of sphere position. Figure I shows that one camera can simultaneously view a real time clock and a ruler attached to the guide bar. The position of the sphere can be related to the position of the pointer on the ruler and thus the video images of the clock and ruler give the change in position with time or simply the average sphere velocity over an element of distance. By checking the video image all along the experimental run we are able to verify that the system ran at a velocity which did not vary by more than 2%.

The second camera is placed to view along the interface and thus record the interface shape as a function of time. The information from the second camera is related to the position of the sphere by combining the images of the two cameras using a screen splitter and recording both on one tape as depicted in figure I.

II.C. *METHOD OF OPERATION*

Once the system parameters for a given experimental run have been set (i.e. $\lambda, a, \rho_1, \rho_2$ etc.) there are five pieces of data that must be recorded during an individual run. First there is the force from the transducer as a function of time. These data, as collected on the strip chart recorder, must be converted to drag on the sphere as a function of its position relative to the interface and the method by which this is done is discussed in section III. Next there is the measurement of sphere position as a function of time. The first video camera records this information on video tape by monitoring the tape measure attached to the guide bar while simultaneously recording a digital clock as is shown in figure I. The second video camera records the time history of the interface shape. The force is related to the sphere position by use of the

manual event marker which puts a mark next to the force read on the chart paper when *actuated*. This event marker is triggered manually when the sphere passes a set point in the tank as represented by a reading of the ruler on the guide bar. Finally the average of the temperature in the center of the tank is recorded and the run is accepted if the readings at beginning and end of run agree to within 0.02 °C. This criterion was easily met as the room temperature varied by less than 2 °C during any given day. It may be noted, that a temperature change of 0.02 °C in the center of the tank over a fifteen minute period corresponds to an approximate temperature gradient of 0.8 °C between the wall and the tank center, based upon a conservative value for the heat capacity of $0.6 \frac{cal}{g\,°K}$ and a thermal conductivity of $0.0007 \frac{cal}{sec\,cm\,°K}$, values which were assumed by Kunesh (1971). 75% of this temperature gradient takes place in the outer half of the tank (Carslaw and Jaeger (1959)) and thus the viscosity for the most temperature sensitive fluid (polybutene) would change by less than 2% in the central region of the tank.

III. EXPERIMENT CALIBRATION AND DATA EVALUATION FOR THEORETICAL COMPARISONS

We have pointed out in the first section that the experiments measure the drag on a tethered sphere translating normal to a deformable fluid/fluid interface in a bounded system. In order to compare our experimental results with previous theoretical work and also to evaluate the accuracy of the experimental method, it is necessary to relate these experimental results to the analogous case of an untethered sphere moving normal to a fluid/fluid interface with no other bounding surfaces (cf. Chapter I and Lee and Leal (1971)). To make these comparisons it is necessary to account for wire/sphere interactions, wire/wall interactions, wire/fluid interactions, and sphere/wall interactions in the data. The known theoretical work concerning these interactions will be summarized here, as well as the data reduction procedure used to actually make comparisons with theory. Also discussed is the work of Brenner (1961) for the drag on a sphere approaching an infinite solid wall. Measurements taken in a single fluid as the sphere approaches the bottom of the tank can be (and are) compared to Brenner's theoretical predictions. This comparison yields an independent measure of the accuracy of the assumptions that were made in transforming the data from a bounded, tethered system to an unbounded, untethered system.

It is also possible to run the experiments sufficiently far from the bottom of the tank and the upper free surface that the most important corrections will be due to the container walls and to the wire attached to the sphere. As anticipated in the discussion on equipment sizing, both of these contributions to the drag will be significant.

Ho and Leal (1974) discuss the correction to the drag on a sphere in proximity to two parallel plane infinite walls, while Brenner's (1961) discussion gives some motivation for extrapolation to four bounding walls by simply summing two two-wall corrections without accounting for the interactions between the

two pairs of walls. It is, of course, evident that this "extrapolation" is not rigorously correct. On the other hand, the error introduced by the assumption of independent two-wall interactions will be small compared to the deviations from Stokes' law as the sphere approaches the interface and it is this latter quantity which we desire to determine experimentally. The problem of a sphere moving axially through a circular cylinder has also been solved (cf. Happel and Brenner (1973)) for translation parallel to the walls. The various predicted corrections due to "wall effects" may be summarized in terms of the coefficient, k, in the equation

$$\text{Drag Ratio} \equiv \frac{F}{F_\infty} = \frac{1}{1 - k\left(\frac{a}{h}\right) + O\left(\frac{a}{h}\right)^3} \tag{2}$$

where the sphere radius is denoted as, a, and the distance to (all) bounding walls as, h. F_∞ is simply Stokes law for an unbounded fluid

$$F_\infty = 6\pi\mu aU \tag{3}$$

with the velocity of the sphere denoted as U and the viscosity of the fluid as μ. The predicted values of k corresponding to different wall "geometries" are

infinite fluid	k=0	
1 wall	k=0.5625	(ref. Happel and Brenner (1973))
2 walls	k=1.0040	(ref. Ho and Leal (1973))
4 walls	k=2.0080	(summation of two wall corrections)
cylindrical wall	k=2.1044	(ref. Happel and Brenner (1973))

It is useful, at this point, to return to our discussion of multiple wall corrections in order to try to obtain some measure of the possible error in estimating wall corrections to the drag on the sphere using equation (2). By doubling the single wall correction and choosing h/a=15 (the smallest value used in these

experiments), we can compare the predicted drag ratio for two walls using the simple additivity assumption, with the exact theoretical value for the drag ratio calculated from the two correct wall correction factor. The difference in these two calculations represents less than a 1% change in the correction to the drag on a sphere. Thus, we would anticipate the four wall correction obtained by using twice the two wall correction to be in error by less than 2%. We may also note that doubling the two wall correction does quite correctly lead to a value for k which is less than the value for an "inscribed" cylindrical wall as expected based on the fact that the average distance of the sphere to the cylindrical wall is smaller for the same a/h, thus leading to stronger interactions. Since no rigorous theoretical results are available for the 4-wall, square cross-section tank, some arbitrariness and uncertainty must necessarily be associated with any choice of a particular wall-correction factor k for use in estimating the drag on a sphere in an unbounded fluid from measurements in the tank. Fortunately, the largest value of a/h in our experiments was only 1/15, and the differences in F' resulting from use of the approximate 4-wall value, or the "inscribed" circular cylinder (i.e. for the same a/h values) are very small (less than 2% for the 1 inch sphere where a/h=1/15). Thus, the data in our experiments were reduced using the wall correction factor for an inscribed cylinder. This choice was made, in part, because of the existence of exact theoretical results for the axial motion of two concentric circular cylinders (this will be used to estimate the drag on the wire tether), and the lack of any solution for axial motion of a circular cylinder inside a square cylinder.

The problem of a circular cylinder moving axially through a second circular cylinder is discussed in Happel and Brenner (1973). The resulting formula for the force per unit length on an inner cylinder which is moving at a relative velocity U, is

$$F^* = \frac{2\pi\mu U}{\ln\left(\frac{h}{b}\right) - 1}$$

for $b/h << 1$, where b is the radius of the inner cylinder and h the radius of the outer one. With certain additional assumptions, this result can be used to estimate the drag on the wire *alone* (i.e. without the sphere) as it moves along the centerline of the tank. First, it is again necessary to "replace" the square cross-section, 4-wall tank with a circular cylinder which, it is hoped, will be equivalent in some sense. Unfortunately, though it is evident that the drag on a wire in a circular cylinder will be larger than that in a tank of square cross-section for the same b/h (since the "wall" is, on average, further from the wire), there is no way without a full theory of the square tank problem to quantitatively account for this fact in "predicting" the wire drag for our experimental set-up.[1] In addition, the theory of axial motion of two concentric circular cylinders presumes that the cylinders are both infinite in length. In the case of the tether wire, however, the length of wire immersed at any moment is *finite* and of the same order as the cross-sectional dimension of the tank. Furthermore, the wire penetrates the air-liquid interface at the top of the tank. Apart from any attempt to correct for the finite length of the immersed wire, we know of no method to account for the effect on the wire drag of the local flow conditions at the air-liquid interface. In spite of these considerable uncertainties, we have adopted the formula for F^* to estimate the drag on the length L of wire tether which is in the liquid at any instant, i.e.

1. A lower bound on the drag in a square tank is, however, clearly given by the drag on a wire in a circular cylinder whose diameter is equal to the *diagonal* dimension of the square cross-section. This suggests that the drag on the wire in the square tank will be within 5% of that estimated from equation (5).

$$F_{wire} = \frac{2\pi\mu LU}{\ln\left(\frac{h}{b}\right) - 1}. \qquad (5)$$

Here b is now interpreted as the wire radius, and h is the half-width of the tank (i.e. the radius of the "inscribed" cylinder).

In the earlier discussion of the multi-wall corrections for a sphere, we alluded to the fact that boundary/boundary interactions are not taken into account when a simple summation is used to obtain values of k, equation (2), for many walls (2 or 4) from the solutions for one and two walls. For this same reason, we would not expect a simple summation to apply when *any* two (or more) boundaries are located in close physical proximity to one another. In particular, we expect the presence of the wire to greatly influence the stress on the sphere at and near the point of attachment so that the drag on the composite wire/sphere body is different from the sum of the drags which would act on the individual components taken separately. Thus, it is necessary to either theoretically or experimentally evaluate the wire-sphere interaction if the data for the tethered sphere is to provide any useful information on the motion of an untethered sphere. This problem is addressed for an unbounded fluid by DE Mestre and Katz (1974), who showed that the drag on a sphere with a long slender body attached is significantly lower (O(10%)) than the sum of the forces on the sphere and tail when calculated separately. It is important to note that the results of DE Mestre and Katz (1974) apply only in the limit of an infinite surrounding fluid and that the exact degree of interaction is a function both of b/a and L/a. To date, no-one has considered the DE Mestre and Katz (1974) problem in a bounded domain and it is not at all evident that the error in using their wire/sphere interaction equations in a bounded domain will be small even with walls located at a large distance as in the present experiments. As a consequence of this, and of the additional uncertainties in the use of equation (5) for

the wire drag, we adopt what is essentially an empirical scheme for estimating the wire/sphere interaction coefficient in our bounded system. That is, we introduce an empirical factor, α, defined by

$$\alpha+\beta \equiv \frac{\text{Actual Drag on Sphere + Wire in Tank}}{\text{Sum of Drag on Sphere in Tank + Drag on Wire in Tank}} \qquad (6)$$

which has the effect of modifying the DE Mestre and Katz interaction factor, β, to account for hydrodynamic effects of the tank walls and the interface. As the boundary interactions are expected to yield only modest corrections to the DE Mestre and Katz interaction factor when the sphere is far from the gas/liquid interface, the liquid/liquid interface and the walls, a single α is determined for all the runs. This value of α is determined by simply adjusting α starting from some initial guess, until an optimal match is achieved between theory and experiment for the drag on a sphere which is far ($l> > 10$) from either the fluid/fluid interface in the case of the two fluid experiments or the tank bottom in the single fluid experiments. This correction factor α may need further modification on close approach of the sphere to the interface, but there is no way to evaluate this change and we will simply *assume* there is no change at all. A partial test of this hypothesis is to use the value of α, determined for $l> > 10$, to reduce the data for close approach of the sphere to a plane solid wall where there is an exact analytic result available (cf. Brenner (1961)) for comparison.

The actual data analysis was performed in a two-step fashion. The data were first reduced to a form sufficient for the determination of α from the far-field drag measurements, and then the remaining data was analyzed, incorporating the empirically obtained value for α, to obtain "corrected" experimental data for comparison with available fluid/fluid interface theories. To determine α, the total force versus position was first obtained for each experimental run for $l> > 1$ (actually $l> 10$). The DE Mestre and Katz (1974) correction β (which is a

function of l and varies between .88 and .94 for our experimental conditions) was then applied to the raw force data to obtain a set of values which would correspond to the sum of the forces on the wire and sphere taken separately provided the actual value of α is zero as assumed in this first step. The drag on the wire alone was then calculated from equation (5) and subtracted from the "corrected" sum to yield an estimate for the drag on the sphere alone in a bounded domain, far from the interface (since $l> > 1$). Finally, this drag estimate was corrected for "wall effects" using equations (2) and (3), and the resulting "measurements" for the drag on a sphere far from an interface ($l> > 1$) were compared with theoretical values from Brenner (1961). In all cases, the reduced experimental data obtained with α equal to zero, yielded too large values for the corrected drag. Thus, a new "guess" for α was made and a "best value" of α for each run was determined by iteration. Finally, a best single overall value of α was adopted based on the smallest average deviation of the "measured" drag from the results of Brenner (1961) over all of the experimental runs. This process resulted in a predicted value of α=0.03 which decreases the DE Mestre and Katz (1974) correction in this region from roughly a 10% change to a 7% change in the total force. After incorporating α, we were able to experimentally reproduce the theoretically predicted drag ratios for normal motion of an isolated sphere far from an interface to within $\pm$ 4% for *all* runs. This entire method of data reduction, once α has been chosen, is presented in the appendix to this chapter. The appendix shows the force transducer output and the steps which followed to reduce the data for comparison with theory.

Any uncertainty associated particularly with the use of equation (5) to estimate the wire drag may, of course, be compensated for in the case of a sphere far from either an interface or bounding walls by the choice of α. The key problem is that comparisons for this "far-field" data alone cannot distinguish

between errors in (5) compensated by a change in α, and genuine changes in the wire/sphere interaction factor due to the presence of the bounding walls. Furthermore, we have no way to determine whether additional changes in α are required when the sphere approaches the interface. (If such changes in α were necessary, it would be impossible to determine what fraction of measured changes in the total drag are due to these (unknown) changes in the relative level of the wire/sphere interaction as the sphere approaches the interface, and which represent a meaningful change in the drag on the sphere alone.) Fortunately, an answer to both of these uncertainties in the choice of α is available. In particular, in figure III, we compare experimental data for a sphere approaching a solid wall, "corrected" in the manner outlined above using the value α=0.03, with theoretical predictions for a sphere approaching an infinite solid wall due to Brenner (1961). Evidently, the corrected experimental data and the theoretical predictions agree to within approximately ($\pm$ 5%). This provides a strong indication that the changes in the wire/sphere interaction coefficient associated with a nonzero value of α are a physically relevant reflection of the presence of side (wall) boundaries (rather than inaccuracy in equation (5)), and further that the value of α can be considered as constant even when the sphere is in close proximity to an interface (or solid end wall) without significant loss of accuracy. Further comparisons of the corrected experimental results with α=0.03 will be made with the numerical results of Lee and Leal (1981) for approach to a deformed interface in section IV. However, it is evident that our experimental apparatus can be expected to yield values for the drag on a sphere in normal motion towards a fluid/fluid interface which should lie within approximately $\pm$ 5% of the "expected" values for motion of an isolated sphere toward the interface in an unbounded fluid system.

Now that the method for wire correction has been discussed, we can

present our consideration of the restraint on sphere sizes due to the presence of the wire. For our experiment to yield accurate information about the sphere, we must have

$$\frac{F_{sphere}}{F_{wire}} \gtrsim O(1) \tag{7}$$

so as not to mask the forces on the sphere. Upon substituting equation (5) and equation (3) for F_{sphere} we see that we require

$$R_0 \equiv \frac{\ln\frac{h}{b} - 1}{\frac{L}{a}} \gtrsim O(1). \tag{8}$$

If we constrain the wire length to a maximum of 10 inches and choose the smallest sphere to be 3/8 inch, we have that $R_0 \sim O(0.3)$ and thus the limit taken for the smallest sphere size to be investigated.

We have shown that we must rely on our ability to make wire and wall corrections to be able to obtain meaningful comparisons between experiment and theory. The results of Lee and Leal (1981)predict the existence of a column of fluid which trails behind the sphere for very large interfacial deformations ($l << -1$). They were able to show for the cases which they studied, that a long tail of the upper fluid travels behind the sphere instead of breaking off and completing the penetration of the interface. In our experiment, for $l < -1$, the wire is moving through this column of liquid which is trailing behind the sphere. Thus the wire does not 'see' the tank surrounding it in this region, but instead it 'sees' a much closer interface consisting of the fluid which makes up this trailing column. For large values of λ ($\lambda \geq O(1)$) the "corrected" data from the experiment may thus be expected to yield too large a value for the drag due to the proximity of more viscous fluid not accounted for in the wire correction when $l < -1$. For the case of small λ, on the other hand we would expect the "corrected"

experimental values to be too small since the wire correction is based on the surrounding fluid being more viscous. Due to the lack of relevant corrections for the wire/wall and wire/sphere interactions in this region, the experiments do not generally study cases where $l < -1$. However, one experimental run (B4) is compared with numerical results for $l << 1$ in figure XIV which illustrates the problems of data evaluation discussed above.

IV. EXPERIMENTAL RESULTS

The values of the dimensionless groups for the individual experiments that will be discussed are contained in table VII. The same information is also shown in figure II where Cg is plotted as a function of Ca with the approximate value of λ indicated by the marker type. It is quite apparent from this figure that there were only a limited number of experiments in the small Ca regime. This is a consequence of the real difficulty of finding fluids which will yield small values of Ca in our experimental apparatus, while simultaneously yielding measurably large drag forces. The drag on the sphere must be large enough to be measured accurately on the force transducer, as explained in the previous section. Since the drag and Ca are both linearly proportional to μU, any increase in the drag associated with μU, tends to lead to large values of Ca. The alternative to larger μU is an increase in the particle size, a, which allows for a large force for a smaller μU and thus a smaller value for Ca. However, beyond a $\sim \frac{1}{2}$ in., this leads to an undesirable increase in the wall correction which tends to 'wash out' the interfacial phenomena even though we have included corrections for wall effects in the data analysis. Thus to obtain small values of Ca in our experimental apparatus, the fluid system was required to have a large interfacial tension, O(30 dynes/cm), which we found to be difficult to achieve with the added constraints of immiscibility, and large viscosity for the less dense fluid, O(3000 cs).

It may be noted that interfacial tension and a density difference across the interface both act to resist interface deformation. Thus, in order for either to exhibit a dominating influence on the degree of deformation, it is necessary that either $Ca << Cg$ in which case the degree of deformation will depend primarily on the magnitude of Ca, or $Cg << Ca$ in which case the dominant influence will be due to Cg. It can be seen from either table VII or figure II, that the only cases which afford an opportunity to examine the dependence of deformation or drag

on interfacial tension are C11 compared with A6 (or possibly B8), and C4 compared with E2 or E4. In the latter case there is a large change in λ as well as Ca and this will complicate the comparison. However, in the first case, λ is very small except for case B8 and thus the variation in λ between case C11 and case A6 should not be very important. The changes in Cg are relatively small in all of these cases compared to the changes in Ca. Cases which allow investigation of the effects of Cg are more numerous since $Ca >> Cg$ in the majority of experiments as can be seen from figure II. Likewise investigation of the effects of λ is also facilitated by the large number of runs where Cg is approximately constant and Ca is unimportant.

IV.A. *EXPERIMENTAL COMPARISONS*

In figures IV--XI, we present comparisons of the experimental runs which relate to the effects of Ca, Cg and λ after the method of data reduction of section III has been applied. These comparisons are made to illustrate the experimentally measured effects of Ca, Cg, and λ on the interface shape and the forces on the sphere. Conclusions from the experimental data were qualitatively checked against results from Chapter I to determine if there are any obvious disagreements with the theory for normal motion of a sphere towards a fluid/fluid interface.

EFFECT OF Ca

Figures IV and V present comparisons of the runs which were previously identified as providing the best data sets for determining the effects of variation in Ca for "fixed" values of Cg and λ. It is evident that the drag for both runs C11 and C4 lies above that for A6 and E4, respectively, presumably as a consequence of the much smaller values for Ca in the former runs. It is also evident in figure IX that the small value of Ca in C11 results in a much smaller deformation along

the centerline but a broadening of the region of interface deformation to larger values of R. Finally it is apparent that the drag curves of C4 and E4 will cross at $l \approx -2$, a result of the significantly larger value for λ in the latter case. These conclusions are in complete qualitative agreement with the results of the work in Chapter I.

EFFECT OF Cg

The influence of Cg on drag and interface shape can be determined from the results shown in figures V--VIII and X. In figure VI, the drag for run B4 is larger than the drag experienced by the sphere in run B8 due to the smaller value of Cg for B4. The same result is shown in figure VII where run D10 has a larger drag ratio than run D8, due again to the smaller value of Cg for D10. Smaller values for Cg correspond to decreased deformation of the interface, as is evident when the results for run B4 are compared with those for B8 in figure X. Figures V and VIII show the same qualitative dependence on Cg by comparison between runs E1 and E4 and runs E2 and E3 for $l < 3$. For $l > 3$ in figures V and VIII, the drag ratio appears slightly larger in the runs with the larger values for Cg, but this is presumably a manifestation of experimental error. The dependence of the drag ratio and interface deformation on Cg is again in good qualitative agreement with the results of Chapter I.

EFFECT OF λ

Figures IV, VI--VIII, and XI compare runs where the influence on the drag ratio and the interface shape due to λ can be studied. In figures VI and VIII we observe very weak dependence of the drag ratio on λ. The comparison of runs D2 and E2 in figure VIII shows almost no difference in the drag ratio even though there is a ten fold change in λ. Figure VI compares runs D8, D10, and E3, and it is again evident that the drag ratio for run E3 is largest for all l, due to the larger value of λ. Even though the differences in the drag ratio, shown in figure

VI, are relatively small, however, it should be noted that the increased drag due to increased λ is partially compensated by the fact that Cg is slightly smaller for run D10 than it is for run E3. Likewise, the dependence of λ indicated in figure VII is weaker than might be anticipated, because of the competition between increased λ and increased Cg. In particular, all that we can conclude from figure VII is that the increased drag due to the tenfold increase in λ from case D2 to E2 is almost exactly balanced by the decreased drag associated with the increase in Cg. In figure IV, a competition between λ and Cg is evident where the effects of λ on drag ratio apparently dominate for $l < -2$ and the effects of Cg dominate for $l > 2$. It is interesting to now observe in figure XI how the interface shape fits into this picture of a competition between λ and Cg in runs A6 and B8. Run A6 experiences smaller deformations and larger drag ratios for $l > 2$ when compared with run B8, while the opposite is true when $l < 2$. This is not to say that the whole story of drag ratio can be told by simply observing the interface shape. It is quite obvious that the shapes for runs A6 and B8 are not equal between $l=-2$ and $l=2$ where the drag ratios are equal. But it does appear that the proximity of the sphere to the interface plays an important role. Finally figure VII compares the drag ratio for runs B4 and D8 where it is obvious from comparisons at large l that experimental error has accentuated differences in the drag for small l. Still we can conclude, that for values of Cg and λ near 1, differences in Cg are more important than differences in λ in determining the drag ratio. This result would be expected as it has already been shown that λ only has a small influence on the drag for $l > 0$. These conclusions are again verification of those obtained in Chapter I.

IV.B. *QUANTITATIVE COMPARISONS WITH THEORY*

Essentially the comparisons of the preceding sub-sections have demonstrated good qualitative agreement with the theoretical predictions of Chapter I.

It is also of great interest to verify the quantitative accuracy of the experimental techniques, not only to better understand the particular results obtained in this investigation, but as a preliminary to future investigation of problems which cannot easily be studied theoretically. The theories available for quantitative comparisons are the small deformation results of Chapter I and the large deformation numerical results of Lee and Leal (1981).

Our objective, then, is to compare the present experimental results (after applying wire and wall corrections which were presented in section III) with these analytical and numerical results. As discussed in Chapter I, the small deformation theory is expected to apply when $1/Ca + 1/Cg$ is large and $l > > 1$. The condition on the interfacial parameters is required in order that the interface remain near flat, while the requirement $l > 1$, is a result of the solutions for the flow field being obtained as a series solution in the small parameter l^{-1}. The numerical solutions for the force and interface shape by Lee and Leal (1981) are expected to apply for all values of l (except as noted in the comparison with run B4), Ca, Cg and λ. However, only one numerical run ($\lambda=1$, $Cg=1$, and $Ca=\infty$) in the paper of Lee and Leal (1981) corresponded closely to the experimental runs which were performed (run B4 $\lambda=0.965$, $Cg=0.934$, and $Ca=65.8$). Thus, additional numerical results were obtained here, using the numerical scheme developed by Lee and Leal (1981), for values of λ, Cg, and Ca which were obtained experimentally.

We will first make quantitative comparisons of the experimental work with the results of Chapter I to determine the values of l and $1/Ca + 1/Cg$ (and the resultant degree of interface deformation) that are associated with the failure of the small deformation expansion. This is followed by comparisons of the experimental data with the numerical results mentioned above, primarily as a test of the accuracy of the experiment. Finally comparison is made with an

experimental run where it is anticipated that theoretical results may not agree due to an interfacial phenomena associated with large interfacial tensions.

Figure XII shows the experimental data for the drag ratio for run E1 ($1/Ca + 1/Cg = 9.2$) and the corresponding theoretical prediction from Chapter I for motion of a sphere towards a slightly deformed interface. It is evident that the agreement is good down to $\ell \sim 3$ where, presumably, the assumption $\ell^{-1} << 1$ starts to break down. Since the interface deformation also starts to become significant at about the same point (e.g. for $\ell=3$ the centerline deformation is found to be ~ 0.2 for run E1 -- note that the deformation has been nondimensionalized with respect to the sphere radius), we would expect the predicted results to diverge rather rapidly from the experiments with decrease in ℓ, as is in fact observed in figure XII.

A similar comparison of drag ratio data for run E2 ($1/Ca + 1/Cg = 5.56$) with both the small deformation theory and the numerical results, is shown in figure XIII. In this case, the small deformation theory and the experiments diverge for larger values of ℓ, as a consequence of the larger deformation which occurs for the smaller value of $1/Ca + 1/Cg$. Much better comparison is apparent between the numerical results and the experiments (as expected), thus tending to confirm the accuracy of the experimental methods.

Finally, in figure XIV, we compare numerical, small deformation and experimental results for run B4, where $1/Ca + 1/Cg = 1.08$. In this case, the deviation between the latter two results is particularly severe, as would be expected since $1/Ca + 1/Cg \sim O(1)$. It may be noted, in this regard, that the interface deformation already yields a centerline displacement of ~ 0.2 for $\ell=5.5$. Comparison between the numerical results and experiment, on the other hand, is much better. Indeed, from $\ell=1.5$ to $\ell=-1.5$ the drag ratios agree exceptionally well. The agreement is poor at $\ell=3$ but this is due to the fact that in the work of Lee and

Leal (1981) this case was started with a flat interface at ℓ=3, and it takes some distance before the interface shape and velocity fields are not influenced by the fact that the sphere has not come from some large value of ℓ. The departure of the two curves for ℓ< -1.5 is a consequence of the presence of the tether in the experiments. The numerical work of Lee and Leal (1981) is able to accurately predict the force on a sphere which is located even at "large" negative values of ℓ, provided that the sphere is still surrounded by the upper fluid. As discussed in section III, the experimental results are not expected to accurately handle the case for large deformations of the interface where a long tail of fluid trails behind the sphere. Figure XVII also shows good agreement between the measured and calculated interface shapes in the region ℓ=-1.

Finally, figure XV compares run C4 (1/Ca + 1/Cg = 6.21) with predictions from both the small deformation theory of Chapter I and with numerical predictions for the same values of Ca, Cg and λ. Evidently, in this case, the theoretical and experimental results are in only modest agreement, and the "large" deformation, "exact" numerical results appear worse relative to the data rather than better as expected. In addition, it can be seen by comparing the experimentally observed interface shapes for run C4 with the numerically calculated results in figure XVIII that the observed deformation is much larger than predicted numerically. A possible rationalization of the rather poor agreement in this case, relative to those cases considered earlier, arises from the observation that run C4 involves a large interfacial tension. Thus, relatively smaller amounts of surfactant contamination can lead to interfacial gradients of sufficient magnitude to significantly retard the tangential velocity at the interface. This would naturally lead to the observed larger drag forces, and the smaller mean values of the interfacial tension relative to those of the uncontaminated interface would tend to allow more deformation for the same nominal values of Ca, Cg, and λ (note

that the value of Ca based upon γ for the uncontaminated interface will be lower than the effective value based on γ at the contaminated interface). A partial test of this hypothesized explanation for the relatively poor comparisons cited earlier, is shown in figure XVI, in which the experimental results are compared with theoretical results for a *solid wall* from figure III. It is evident that the experimental results show much better agreement with these drag ratio predictions for a solid wall, thus lending support to the hypothesis of reduced tangential velocity on the interface due to contamination in this case of "large" γ.

We have thus found good agreement ($\sim 5\%$) for $l > 3$ between the experiments and the small deformation results of Chapter I when $1/Ca + 1/Cg = O(10)$. For smaller interfacial returning forces and thus larger interfacial deformations, the comparisons of experiment with the numerical predictions from Lee and Leal (1981) provide agreement to within 10% for $l > -1$. One significant exception which was found not to agree with the numerical results involved run C4 with its large interfacial tension. It has been hypothesized here, that interfacial contamination was responsible for the discrepancies between experiment and theory in this case by producing gradients in the interfacial tension under flow circumstances.

V. CONCLUSIONS

In the observations of the dependence of drag ratio on Ca, Cg, and λ in section IV.A., we found good qualitative agreement with the predictions from Chapter I. Section IV.B. provided the quantitative comparisons with the results in Chapter I from which some conclusions can be drawn about the range of validity of the small deformation theory. A correlation was found indicating when deviation of the small deformation theory from the experimental results would occur. For $1/Ca + 1/Cg \approx 10$ this deviation occurred at $l \approx 3$ and corresponded to an interfacial deformation of $\sim .2$. As the value of $1/Ca + 1/Cg$ decreased, the value of l for which deviation became significant appeared to increase. Finally for $1/Ca + 1/Cg \approx 1$, the point of deviation of the small deformation theory for the drag ratio and the drag ratio from experimental measurement had moved out to $l \approx 5.5$, where again this deviation corresponded to an interfacial deformation of $\sim .2$. These results correspond to values of $Ca/Cg > 1$ and no conclusions can be drawn for the case of $Ca/Cg < 1$.

Furthermore, in section IV.B., the error between the experimental results and the numerical prediction was less than $\sim 10\%$ of the total drag for $l > -1$. The exception to this level of agreement was concerned with a system where the interfacial tension was large and expected to dominate and thus presumably be subject to the effects of interface contaminants. The case of large interfacial tension proved to be quite interesting. The results indicate care is necessary in applications of theories when interfacial phenomena dominated by surface tension are studied in the possible presence of surfactant contaminants.

ACKNOWLEDGMENT

The author is greatly indebted to the work of Joe Stoot of SCS Company. He developed a method to straighten the wire tether from its originally coiled state.

References

Bart, E. 1968 The slow unsteady settling of a (fluid, solid) sphere toward a flat interface. Chem. Eng. Sci. **23**, 193.

Brenner, H. 1961 The slow motion of a sphere through a viscous fluid towards a plane surface. Chem. Eng. Sci. **16**, 242.

Carslaw, H. C. and Jaeger, J. C. 1959 "Conduction of Heat in Solids", Oxford University Press, pg. 200.

Happel, J. and Brenner, H. 1973 "Low Reynolds Number Hydrodynamics", Noordhoff International Publishing, 2nd. ed.

Hardy, R. C. 1962 U.S. Nat Bur. Stds. Monograph 55, pg. 5.

Hartland, S. 1968 The approach of a rigid sphere to a deformable liquid/liquid interface. J. Coll. and Interface Sci. **26**, 383.

Hartland, S. 1969 The profile of the draining film between a rigid sphere and a deformable fluid-liquid interface. Chem. Eng. Sci. **24**, 987.

Hartland, S. and Robinson J. D. 1970 Unsymmetrical drainage beneath a rigid sphere approaching a deformable liquid-liquid interface. Chem. Eng. Sci. **25**, 277.

Ho, B. P. and Leal, L. G. 1974 Inertial migration of rigid spheres in two-dimensional unidirectional flows. J. Fluid Mech. **65**, 365.

Jones, A. M. and Knudsen, J. G. 1961 Drag coefficients at low Reynolds numbers for flow past immersed bodies. A. I. Ch. E. Jour. **7**, 20.

Kunesh, J. G. 1971 PhD Dissertation, Carnegie-Mellon University.

Lee, S. H., Chadwick, R. S. & Leal, L. G. 1979 Motion of a sphere in the presence of a plane interface. Part 1: An approximate solution by generaliza-

tion of the method of Lorentz. J. Fluid Mech. **93**, 705.

Lee, S. H. and L. G. Leal 1981 The Motion of a Sphere in the Presence of a Deformable Interface Part 2: A Numerical Study of the Translation of a Sphere Normal to an Interface, Submitted **JCIS**.

Maxworthy, T. 1965 Accurate measurement of sphere drag at low Reynolds numbers. Jour. Fluid Mech. **23**, 369.

Mestre, N. J. DE and Katz, D. F. 1974 Stokes flow about a sphere attached to a slender body. Jour. Fluid Mech. **64**, 817.

Olbricht, W. L. 1981 PhD Dissertation, California Institute of Technology.

Pruppacher, H. R. and Steinberger E. H. 1968 An experimental determination of the drag on a sphere at low Reynolds numbers. Jour. Applied Physics **39**, 4129.

Stokes, G. G. 1851 On the effect of the internal friction of fluids on the motion of pendulums. Trans. Camb. Phil. Soc. **9**, pt. II, 8.

Shah, S. T., Wasan, D. T. and Kintner, R. C. 1972 Passage of a liquid drop through a liquid-liquid interface. Chem. Eng. Sci. **27**, 881.

Walker, R. E. 1965 "Symposium on Rheology", Marris, A. W. and Wang, J. T. S., eds., Cath. Univ. Press.

Yonas, G. 1967 Measurements of drag in a conducting fluid with an aligned field and large interaction parameter. Jour. Fluid Mech. **30**, 813.

TABLE I			
Experimental Systems			
System	Lower Phase	Upper Phase	Interfacial Tension (dynes/cm)
#	Solid Wall	Polybutene # 24	--
A	Water	Polybutene # 24	34.1 ± 0.4
B	Silicone Oil 30,000	Polybutene # 24	1.9 ± 0.2
C	Water	Silicone Oil Blend	37.1 ± 0.4
D	Silicone Oil Blend	Polybutene # 16	1.9 ± 0.2
E	Silicone Oil 30,000	Polybutene # 16	1.9 ± 0.2

Silicone Oil 30,000 is Dow Corning Silicone Oil 200 Fluid grade 30,000 cs; Silicone Oil Blend is Dow Corning Silicone Oil 200 Fluid 28.9% grade 30,000 cs and 71.1% grade 1,000 cs; Polybutene is Chevron Polybutene w/ grade code

TABLE II

Fluid Parameters

Viscosity- - - -19°C--24°C

Fluid	A	B	C
Silicone Oil 30,000	-75.1993	45798.4	-6465589.
Silicone Oil Blend	-188.302	110957.	-16040387.
Polybutene # 16	90.9942	-59131.8	9861929.
Polybutene # 24	52.9987	-36094.8	6531496.
Water	0.229832	-4944.93	1034272.

$\mu = e^{\left[A + \frac{B}{T} + \frac{C}{T^2}\right]}$, T in °K, μ in poise; $\frac{gm}{cm\ sec}$

--

Density- - - -19°C--24°C

Fluid	ρ	$\Delta\rho$	TEMP
Silicone Oil 30,000	0.972533	-1.00449×10^{-3}	21.00
Silicone Oil Blend	0.971046	-8.97484×10^{-4}	20.95
Polybutene # 16	0.872236	-4.91887×10^{-4}	19.92
Polybutene # 24	0.886373	-5.17835×10^{-4}	20.65
Water	0.998405	-2.1167×10^{-4}	19.00

$\rho = RHO + (T - TEMP) \times \Delta\rho$, T in °C, ρ in g/cc

TABLE III

Polybutene #16 Viscosity and Density Data

Temp. (°C)	Time (sec)	Specific Gravity
19.71 ± 0.06	292.1	
	291.1	
	292.0	
	291.9	
	$\bar{x}$ = 291.775	
19.92 ± 0.06		0.8738
20.56 ± 0.06	269.8	
	269.1	
	270.0	
	269.7	
	$\bar{x}$ = 269.65	
21.30 ± 0.02	252.1	
	252.5	
	252.2	
	252.1	
	$\bar{x}$ = 252.225	
22.03 ± 0.03	236.1	
	236.2	
	236.4	
	236.6	
	$\bar{x}$ = 236.325	
23.17 ± 0.03		0.8728

Viscometer #600 J964

TABLE IV

Polybutene #24 Viscosity and Density Data

Temp. (°C)	Time (sec)	Specific Gravity
19.44 ± 0.03	2015.3	0.8891
	2014.0	
	2011.8	
	2008.2	
	$\bar{x}$ = 2012.325	
20.65 ± 0.03	1786.4	0.8881
	1784.3	
	2--1787.3	
	1788.6	
	$\bar{x}$ = 1786.78	
21.86 ± 0.03	1590.5	0.8877
	1589.7	
	1595.7	
	2--1596.0	
	1597.2	
	$\bar{x}$ = 1594.12	
22.94 ± 0.04	2--1446.1	0.8871
	1436.1	
	1444.2	
	1446.6	
	1441.9	
	1441.3	
	$\bar{x}$ = 1443.186	

Viscometer #600 J964

TABLE V

Silicone Oil Blend Viscosity and Density Data

Temp. (°C)	Time (sec)	Specific Gravity
19.86 ± 0.04		0.9738
19.94 ± 0.04	2--443.3	
	443.6	
	443.5	
	$\bar{x}$ = 443.425	
20.55 ± 0.04	2--438.5	
	438.9	
	438.6	
	$\bar{x}$ = 438.625	
20.95 ± 0.04		0.9730
21.30 ± 0.04	432.1	
	431.8	
	431.9	
	431.7	
	$\bar{x}$ = 431.875	
21.96 ± 0.04		0.9723
22.09 ± 0.04	2--425.4	
	2--425.3	
	$\bar{x}$ = 425.35	
23.17 ± 0.04		0.9714

Viscometer #500 E483

TABLE VI

Silicone Oil 30,000 Viscosity and Density Data

Temp. (°C)	Time (sec)	Specific Gravity
19.94 ± 0.04	1599.8	0.9755
	1599.5	
	1599.2	
	$\bar{x}$ = 1599.5	
21.00 ± 0.03	1566.6	0.9745
	1566.1	
	1568.0	
	1568.0	
	$\bar{x}$ = 1567.175	
22.00 ± 0.03	1534.6	0.9737
	1535.4	
	1534.4	
	1534.7	
	$\bar{x}$ = 1534.775	
22.95 ± 0.03	1506.9	0.9729
	1507.8	
	1506.5	
	1507.4	
	$\bar{x}$ = 1507.15	

Viscometer #600 J964

TABLE VII

Run Parameters

Run	Particle Radius (cm)	Velocity (cm/sec)	Temperture (°C)	Ca	Cg	λ
9	0.9521	0.396	21.18	--	--	--
A6	0.6286	0.355	20.56	3.506	2.720	$3.\times 10^{-5}$
B4	1.2697	0.380	20.60	65.790	0.934	0.965
B8	0.6286	0.470	21.55	74.158	4.247	1.036
C4	1.2697	0.382	21.13	0.347	0.301	$3.\times 10^{-4}$
C11	0.4747	0.372	20.93	0.339	2.107	$3.\times 10^{-4}$
D2	1.2697	0.380	20.31	9.924	0.122	0.631
D8	0.6286	0.681	20.98	16.742	0.831	0.662
D10	0.6286	0.550	20.98	13.517	0.671	0.662
E1	1.2697	0.397	21.84	9.029	0.110	7.146
E2	1.2697	0.655	21.84	14.894	0.182	7.146
E3	0.6286	0.651	21.90	14.738	0.724	7.175
E4	0.6286	0.387	21.90	8.762	0.430	7.175

Figure Captions

Figure I: Schematic view of experimental apparatus. a: variable speed motor; b: low pitch 6 in. aluminum take-up wheel; c: 1/16 in. stainless steel cable w/ swivel fitting at lower connection; d: ruler; e: 3/4 in. square by 42 in. aluminum guide bar; f: 6 in. guide affixed rigidly to wall w/ 8 screw adjustments for vertical alignment of guide bar; g: mark for ruler readings, attached to f; h: digital clock; i: ring force transducer w/ thermal isolation mounting to guide bar; j: thermal isolation housing for force transducer; k: .004 in. straightened stainless steel wire; l: polished bronze sphere; m: fluid 1, lower phase; n: fluid 2, upper phase; o: 16 in. square by 36 in. plexiglas tank, 1/2 in. thick; p: video camera with 6:1 zoom and 2 diopter close-up lens; q: video camera with 6:1 zoom and 4 diopter close-up lens; r: screen splitter and recorder to combine images from cameras p and q and record results; s: video monitor with interface from camera p in upper section and clock and ruler from camera q in lower section.

Figure II: Log/Log plot of parameter space for experimental runs.
+ λ=0., * λ=0.6, o λ=1., and o λ=7.

Figure III: Approach of solid sphere normal to infinite plane solid wall. Drag ratio versus distance to the interface.
_____experimental results __ __ __ __theoretical results

Figure IV: Drag ratio versus distance to the interface.
_____C11, __ __ __ __A6, and - - - - - - - B8

Figure V: Drag ratio versus distance to the interface.
_____C4, __ __ __ __E4, and - - - - - - - E1

Figure VI: Drag ratio versus distance to the interface.

_____D8, __ __ __ __D10, and - - - - - - - E3

Figure VII: Drag ratio versus distance to the interface.

_____B4, __ __ __ __B8, and - - - - - - - D8

Figure VIII: Drag ratio versus distance to the interface.

_____D2, __ __ __ __E2, and - - - - - - - E3

Figure IX: Interface shape comparison for the variation of distance to the interface, l, with $\lambda=1$, $Cg=1$, and $Ca=\infty$.

_____C11 and __ __ __ __A6

Figure X: Interface shape comparison for the variation of distance to the interface, l, with $\lambda=1$, $Cg=1$, and $Ca=\infty$.

_____B4 and __ __ __ __B8

Figure XI: Interface shape comparison for the variation of distance to the interface, l, with $\lambda=1$, $Cg=1$, and $Ca=\infty$.

_____A6 and __ __ __ __B8

Figure XII: Drag ratio versus distance to the interface.

_____E1 and __ __ __ __small deformation results

Figure XIII: Drag ratio versus distance to the interface.

_____E2, __ __ __ __small deformation results,

and - - - - - - - numerical results

Figure XIV: Drag ratio versus distance to the interface.

_____B4, __ __ __ __small deformation results,

and - - - - - - - numerical results

Figure XV: Drag ratio versus distance to the interface.

_____C4, __ __ __ __small deformation results,

and - - - - - - - numerical results

Figure XVI: Drag ratio versus distance to the interface.

_____C4, __ __ __ __solid wall theoretical results,

and - - - - - - - numerical results

Figure XVII: Interface shape comparison for the variation of distance to the interface, l, with λ=0.965, Cg=0.934, and Ca=65.790 for B4 and λ=1., Cg=1., and Ca=∞ for the numerical results.

_____B4 and __ __ __ __numerical results

Figure XVIII: Interface shape comparison for the variation of distance to the interface, l, with λ=0.0003, Cg=0.301, and Ca=0.347.

_____C4 and __ __ __ __numerical results

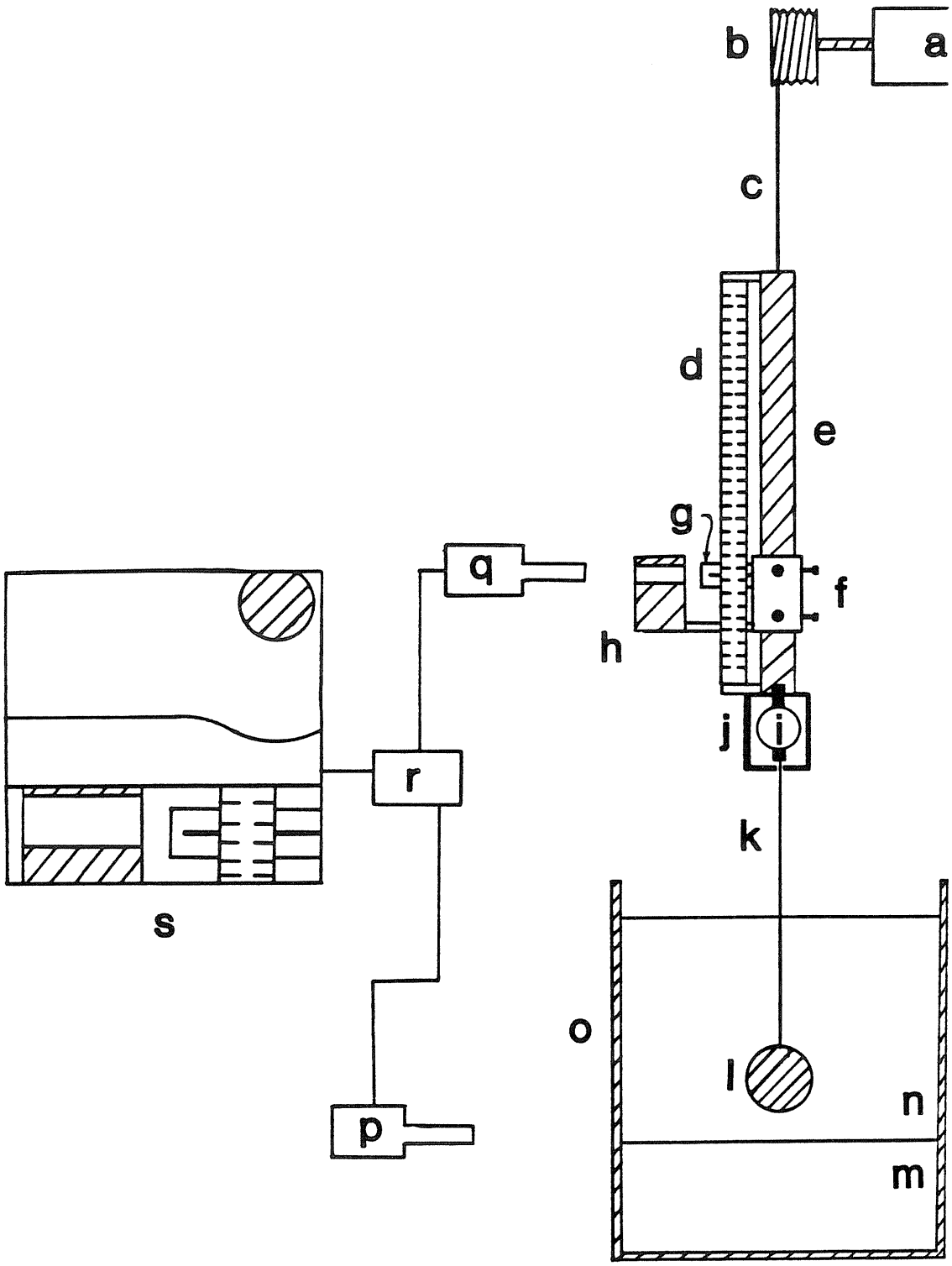

Figure I

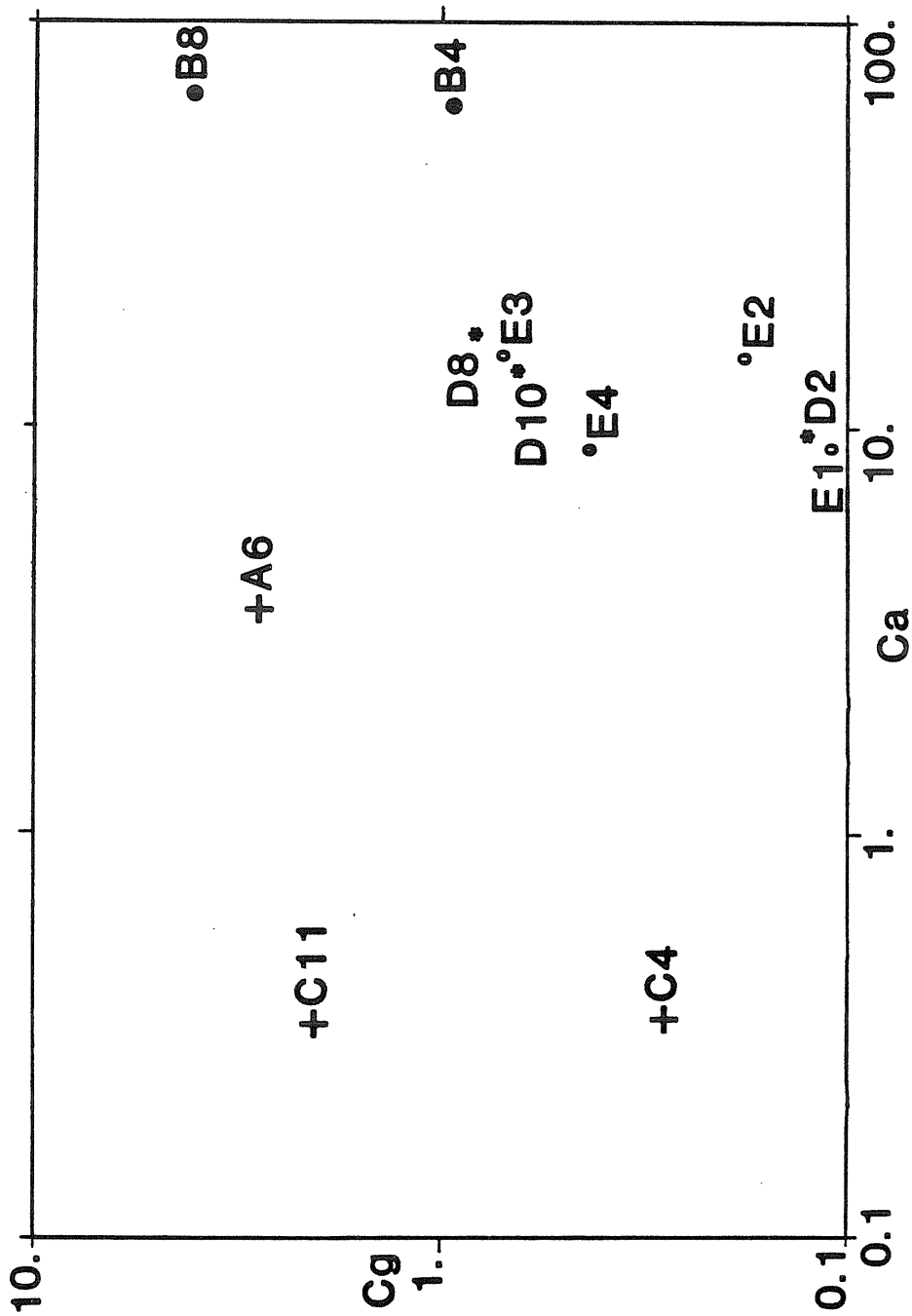

Figure II

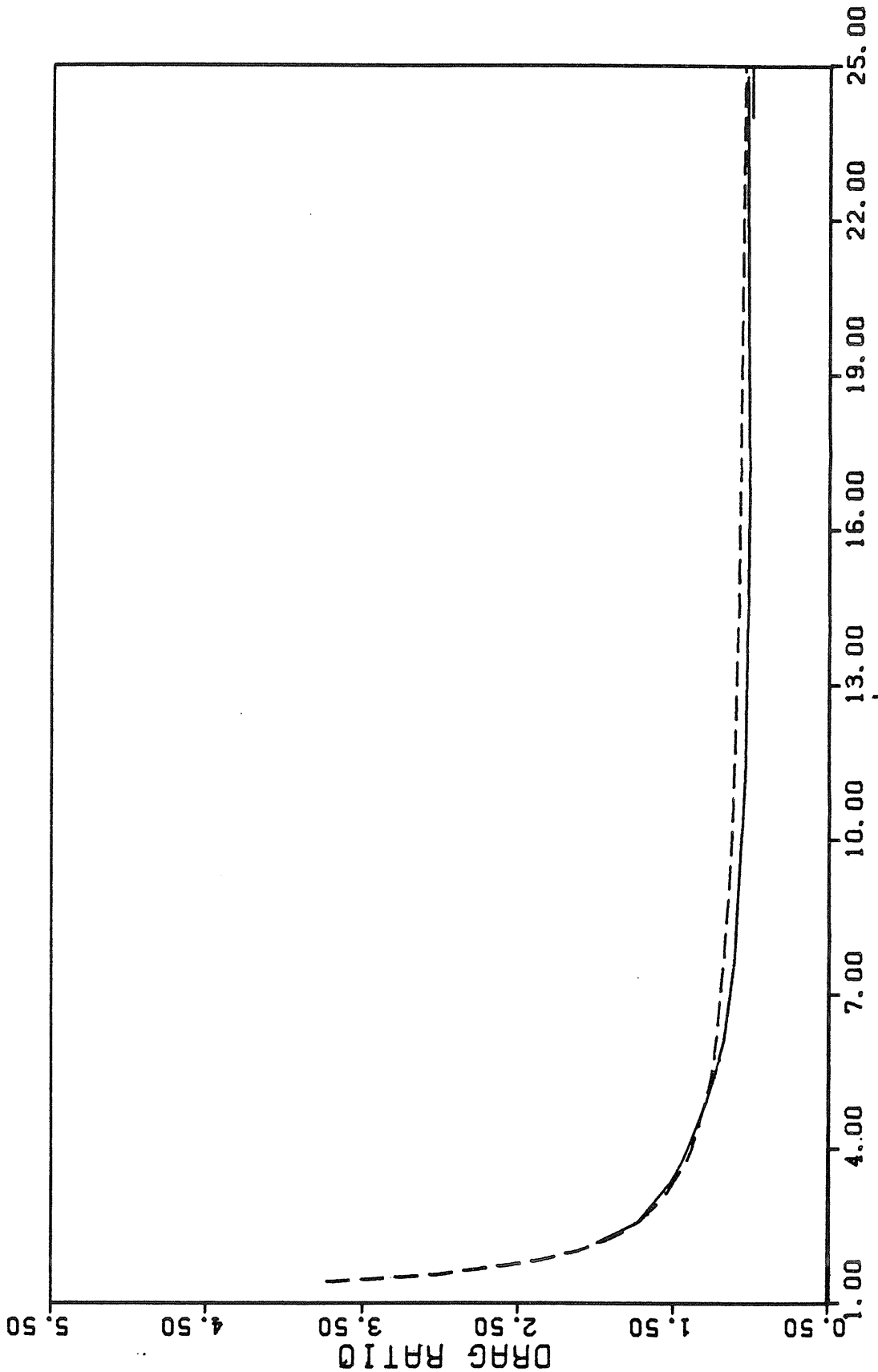
DRAG RATIO
0.50
1.50
2.50
3.50
4.50
5.50
1.00
4.00
7.00
10.00
13.00
16.00
19.00
22.00
25.00
L

FIGURE III

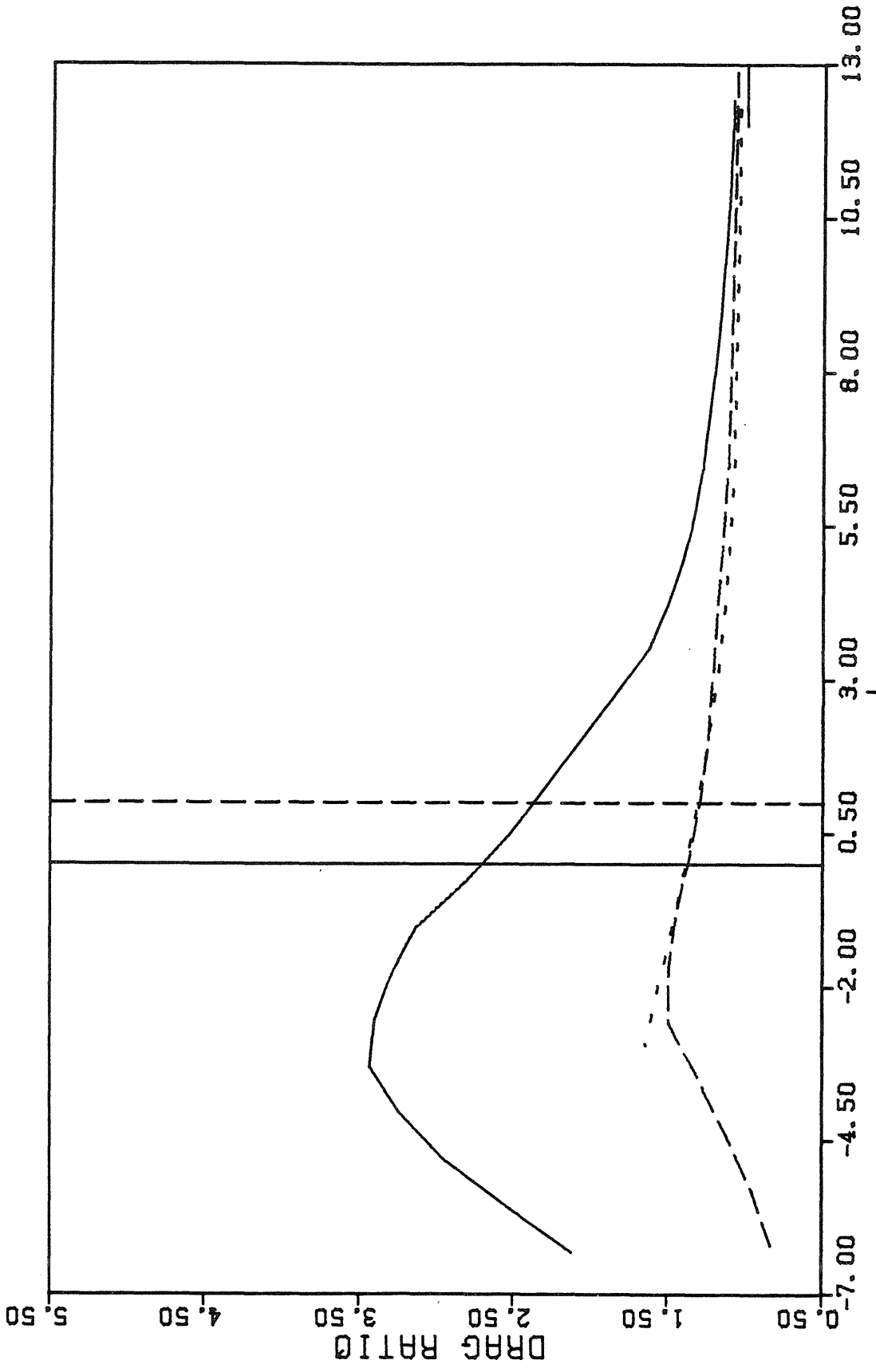
DRAG RATIO
0.50
1.50
2.50
3.50
4.50
5.50
-7.00
-4.50
-2.00
0.50
3.00
5.50
8.00
10.50
13.00
L

FIGURE IV

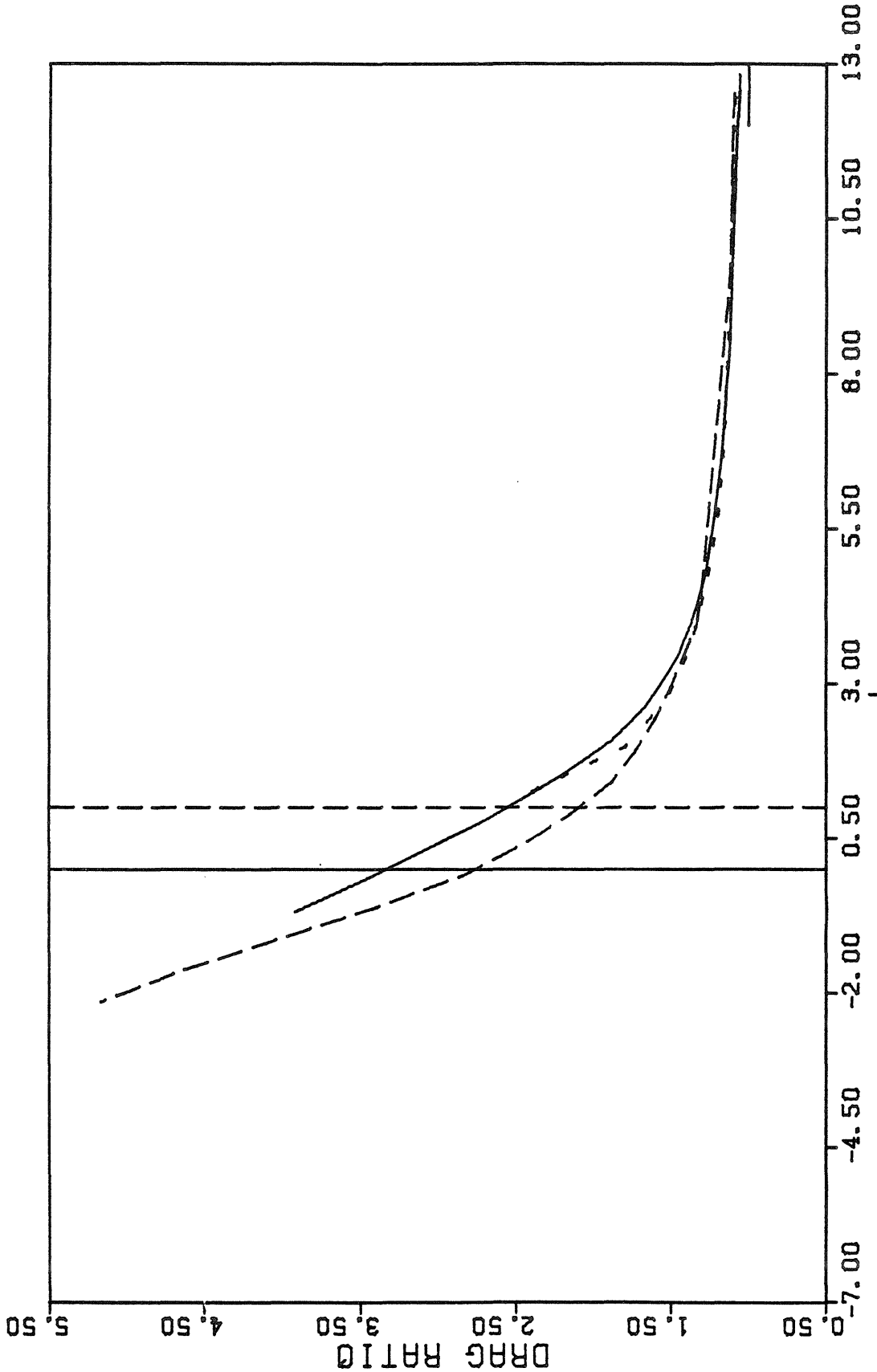
DRAG RATIO
0.50
1.50
2.50
3.50
4.50
5.50
L
-7.00
-4.50
-2.00
0.50
3.00
5.50
8.00
10.50
13.00

FIGURE V

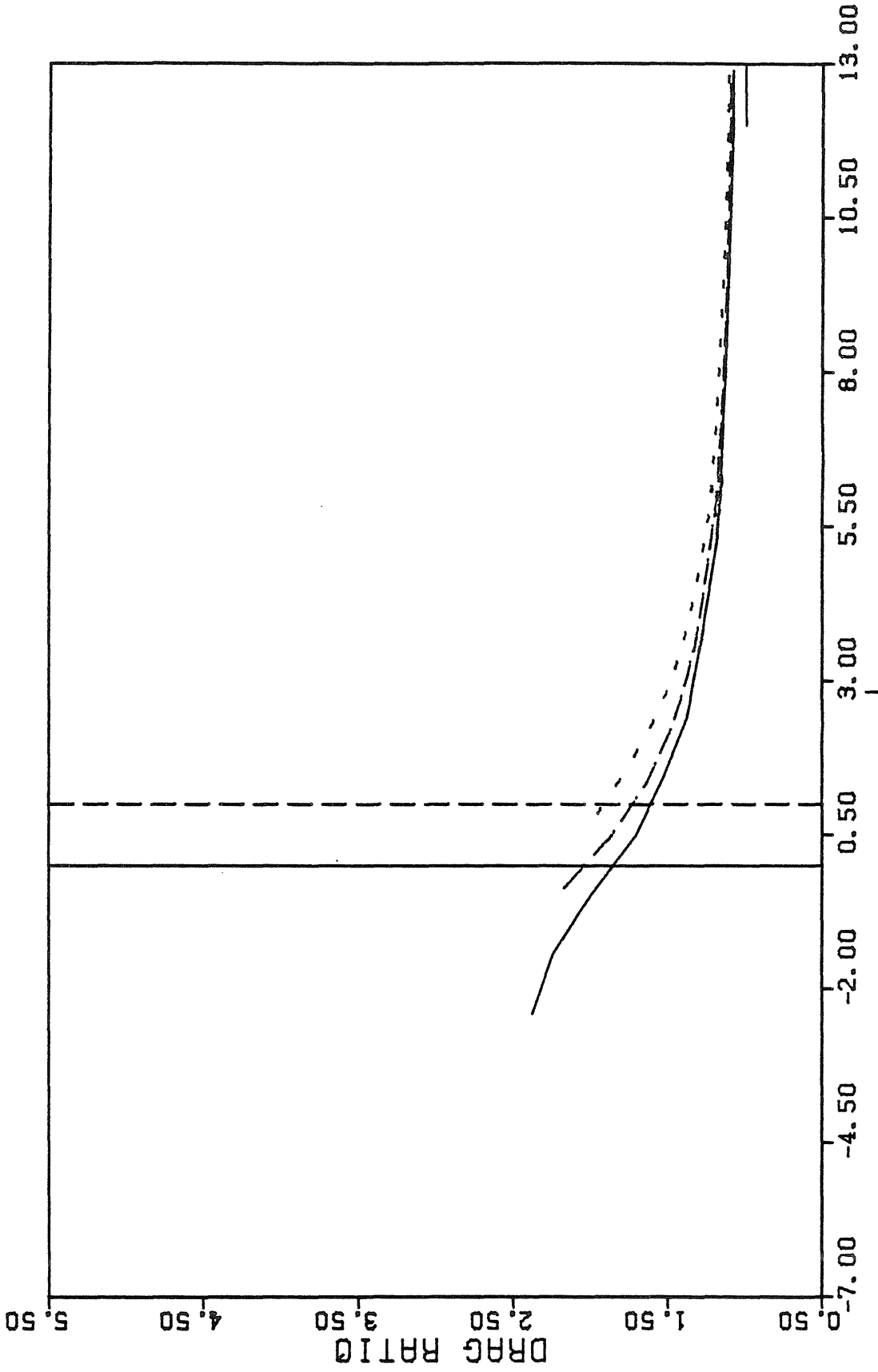
DRAG RATIO
0.50
1.50
2.50
3.50
4.50
5.50
-7.00
-4.50
-2.00
0.50
3.00
5.50
8.00
10.50
13.00
L

FIGURE VI

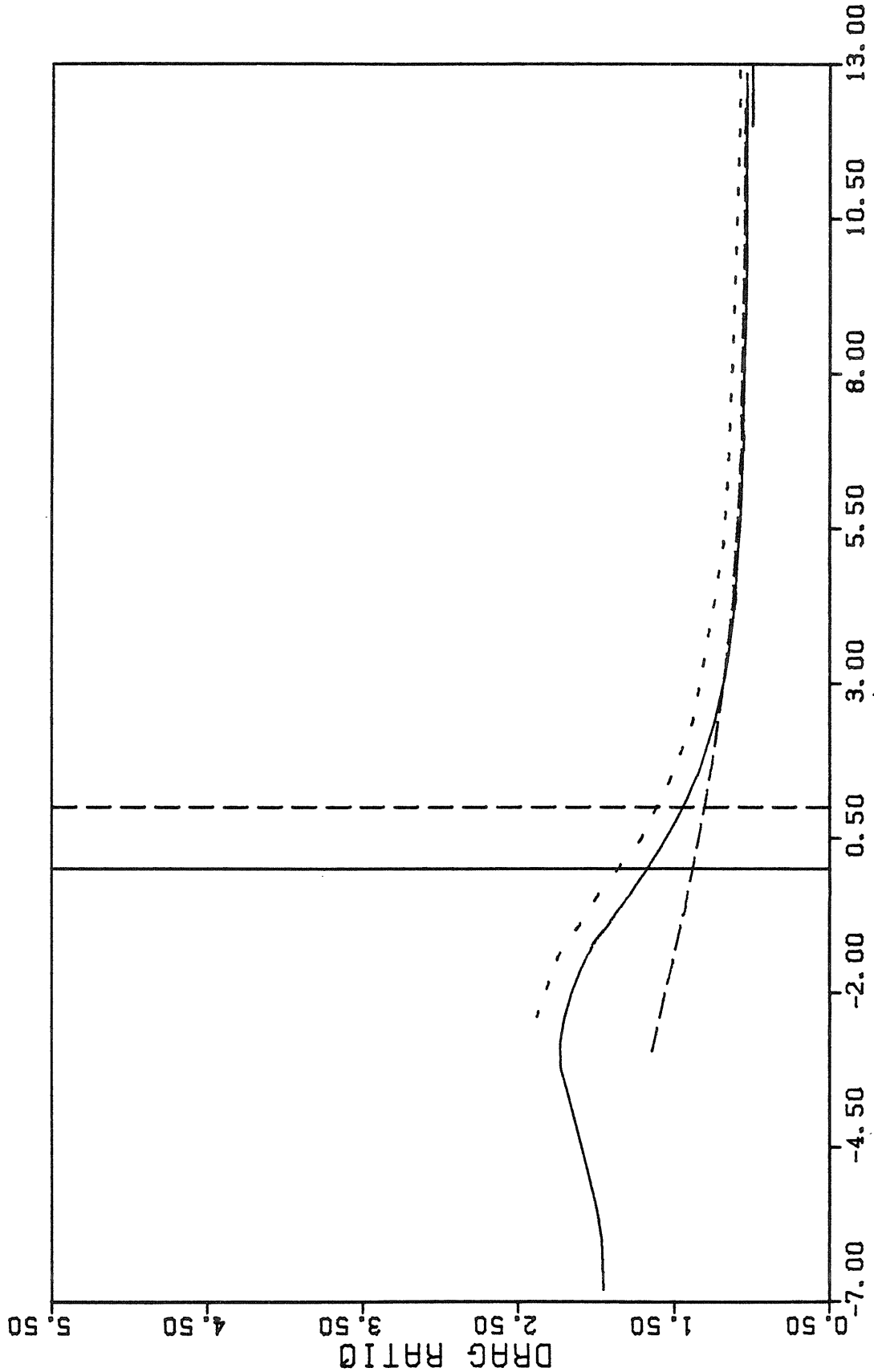
DRAG RATIO
0.50
1.50
2.50
3.50
4.50
5.50
-7.00
-4.50
-2.00
0.50
3.00
5.50
8.00
10.50
13.00
L

FIGURE VII

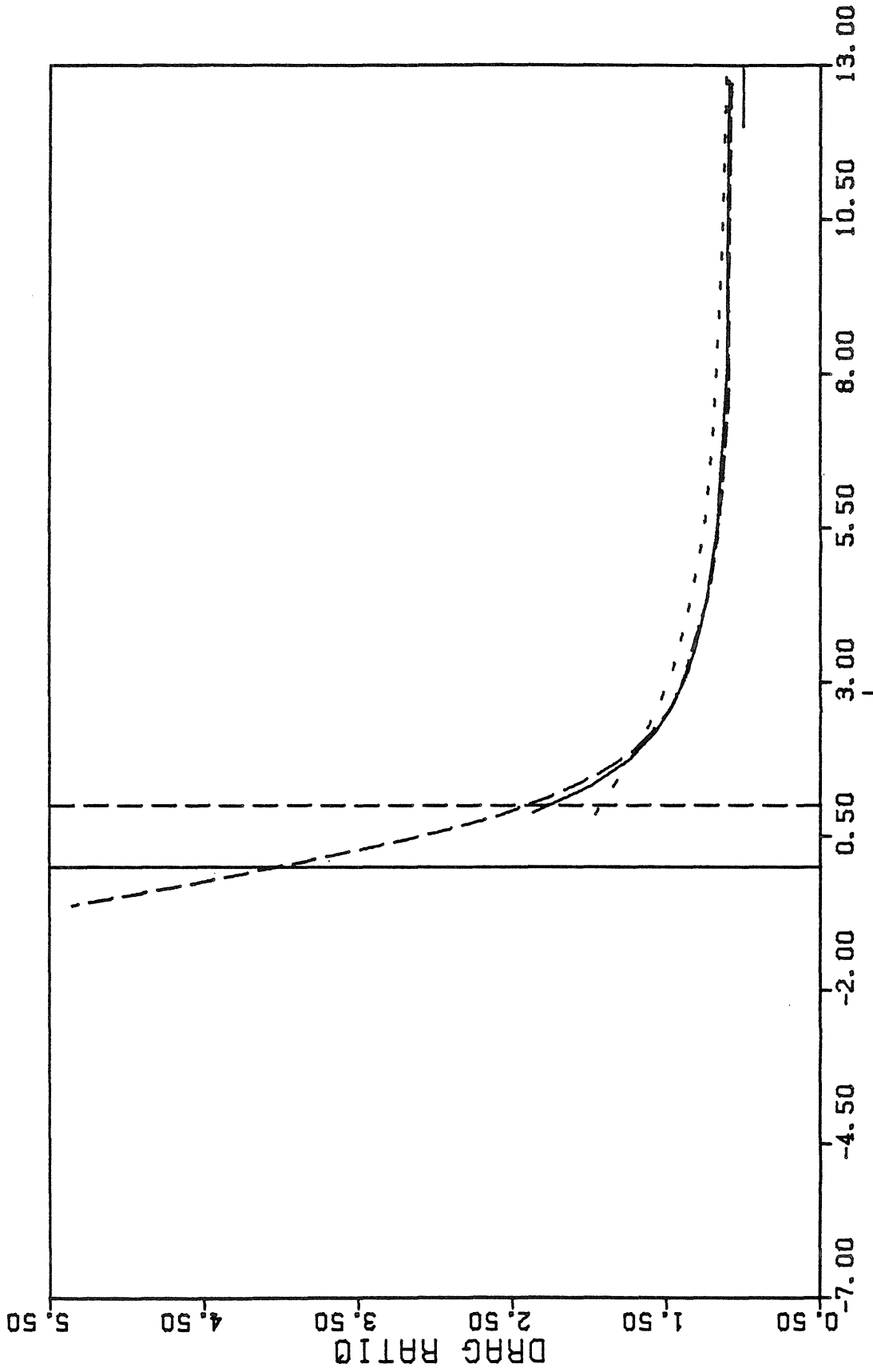
13.00
10.50
8.00
5.50
3.00
0.50
-2.00
-4.50
-7.00
L
0.50
1.50
2.50
3.50
4.50
5.50
DRAG RATIO

FIGURE VIII

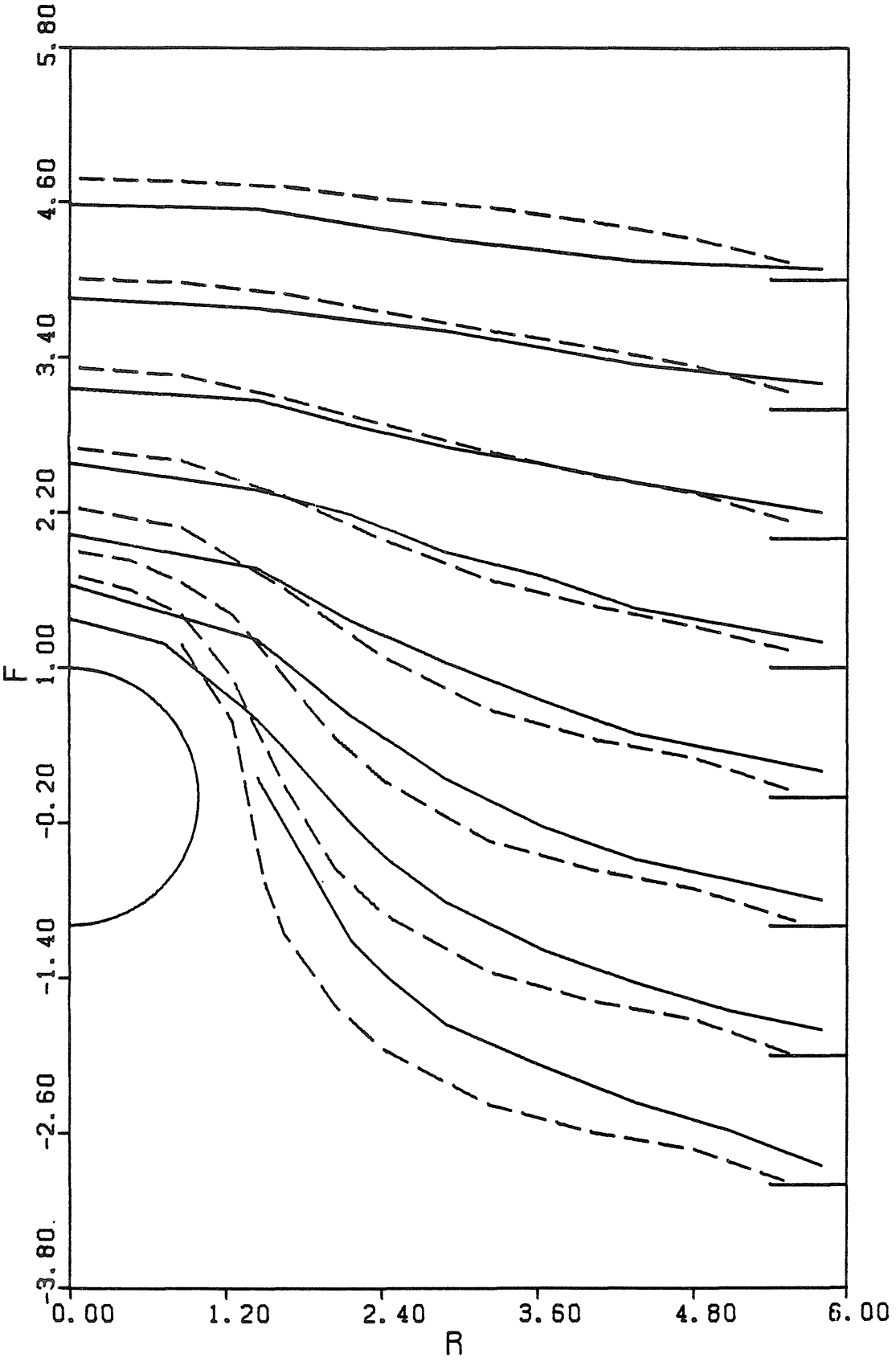

FIGURE IX

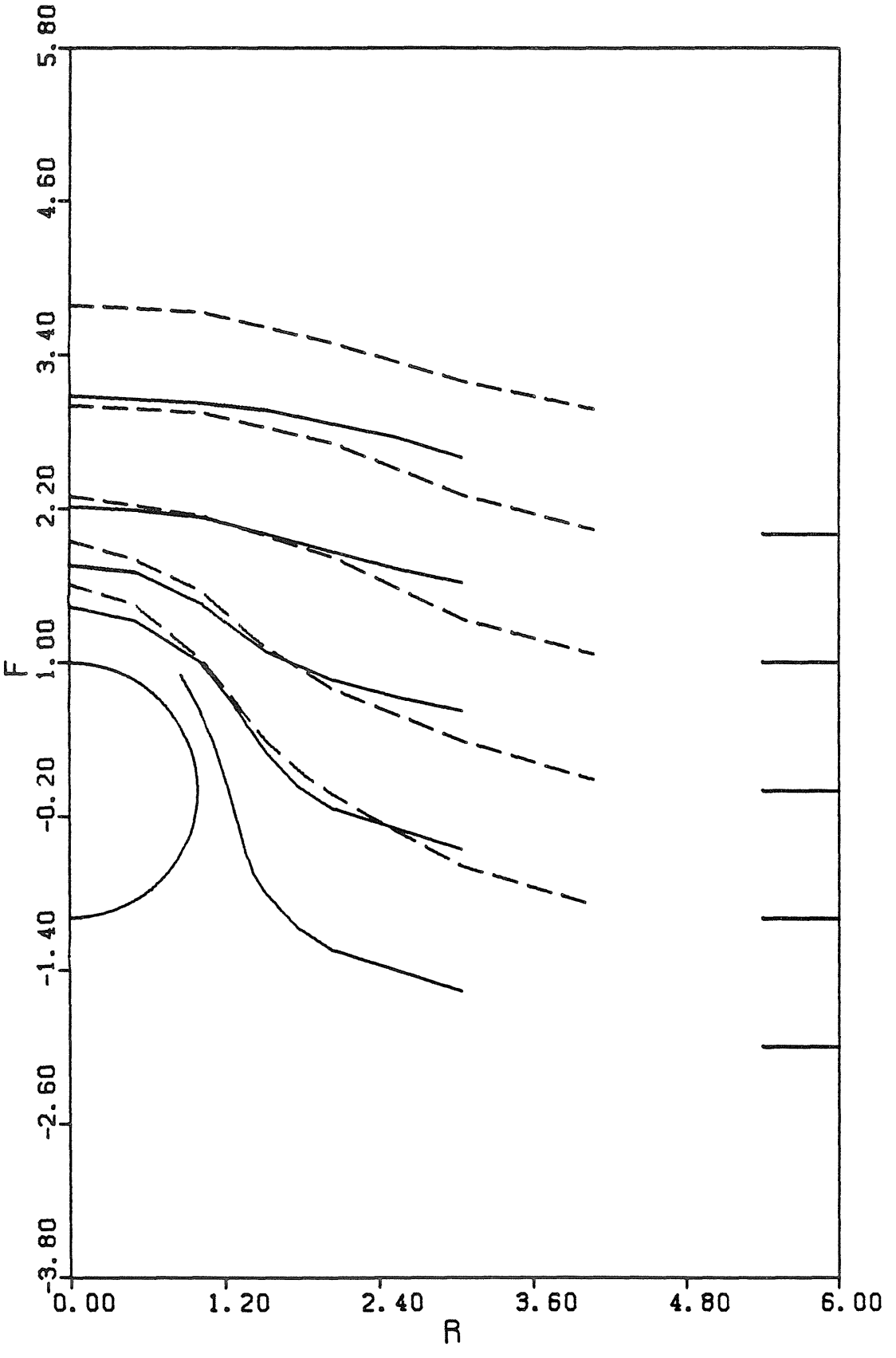

FIGURE X

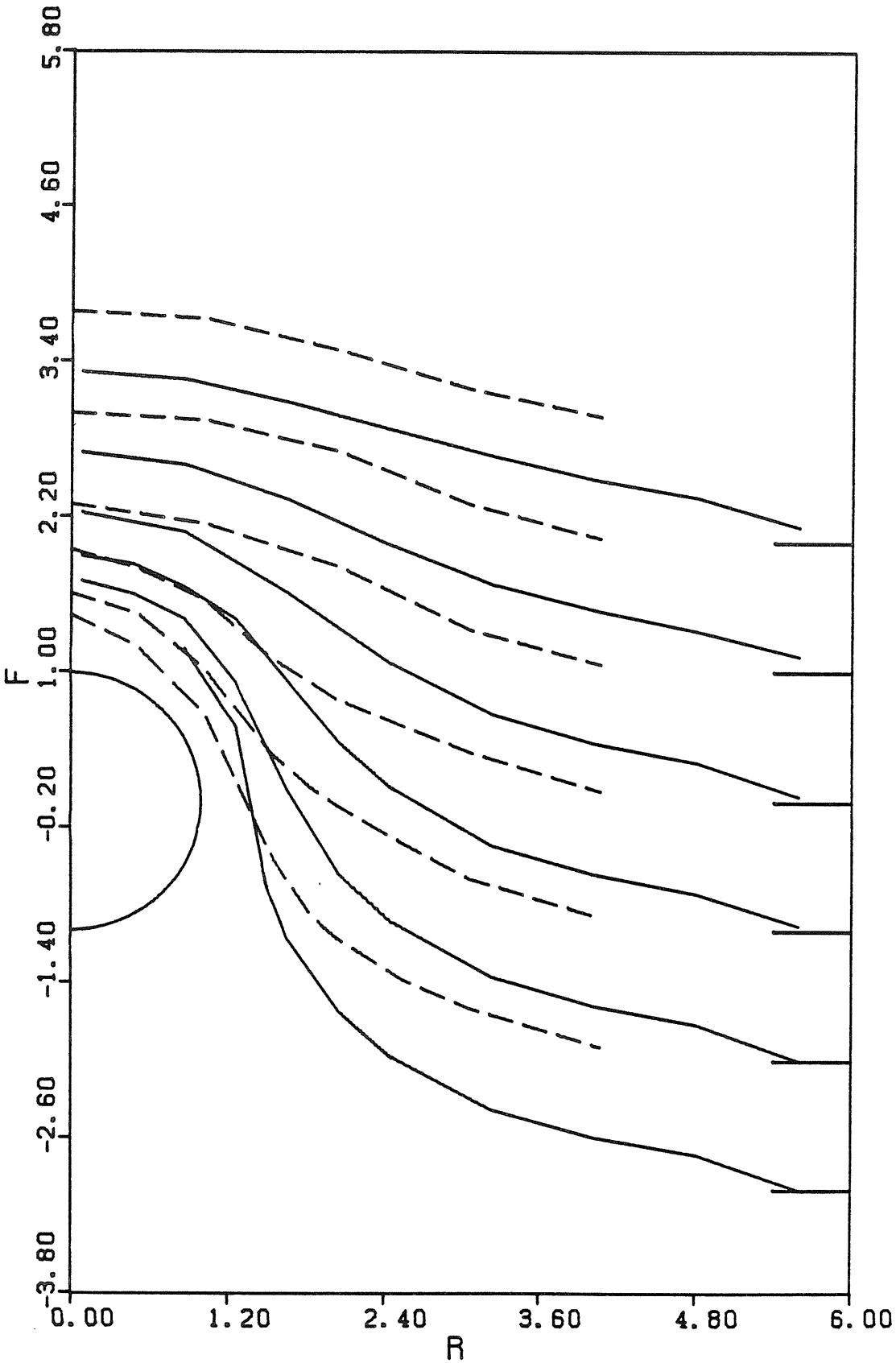

FIGURE XI

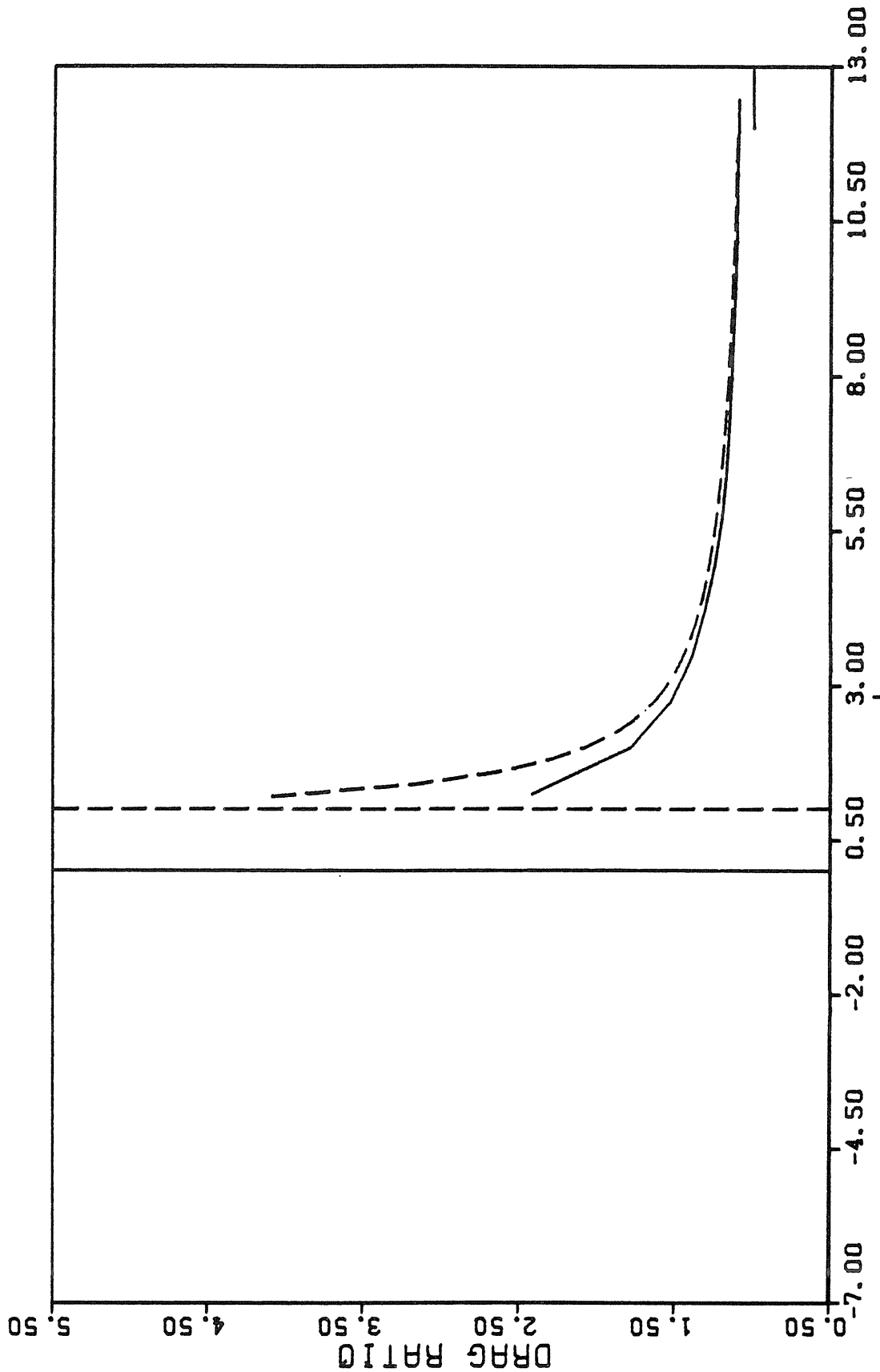
DRAG RATIO
0.50
1.50
2.50
3.50
4.50
5.50
-7.00
-4.50
-2.00
0.50
3.00
5.50
8.00
10.50
13.00
L

FIGURE XII

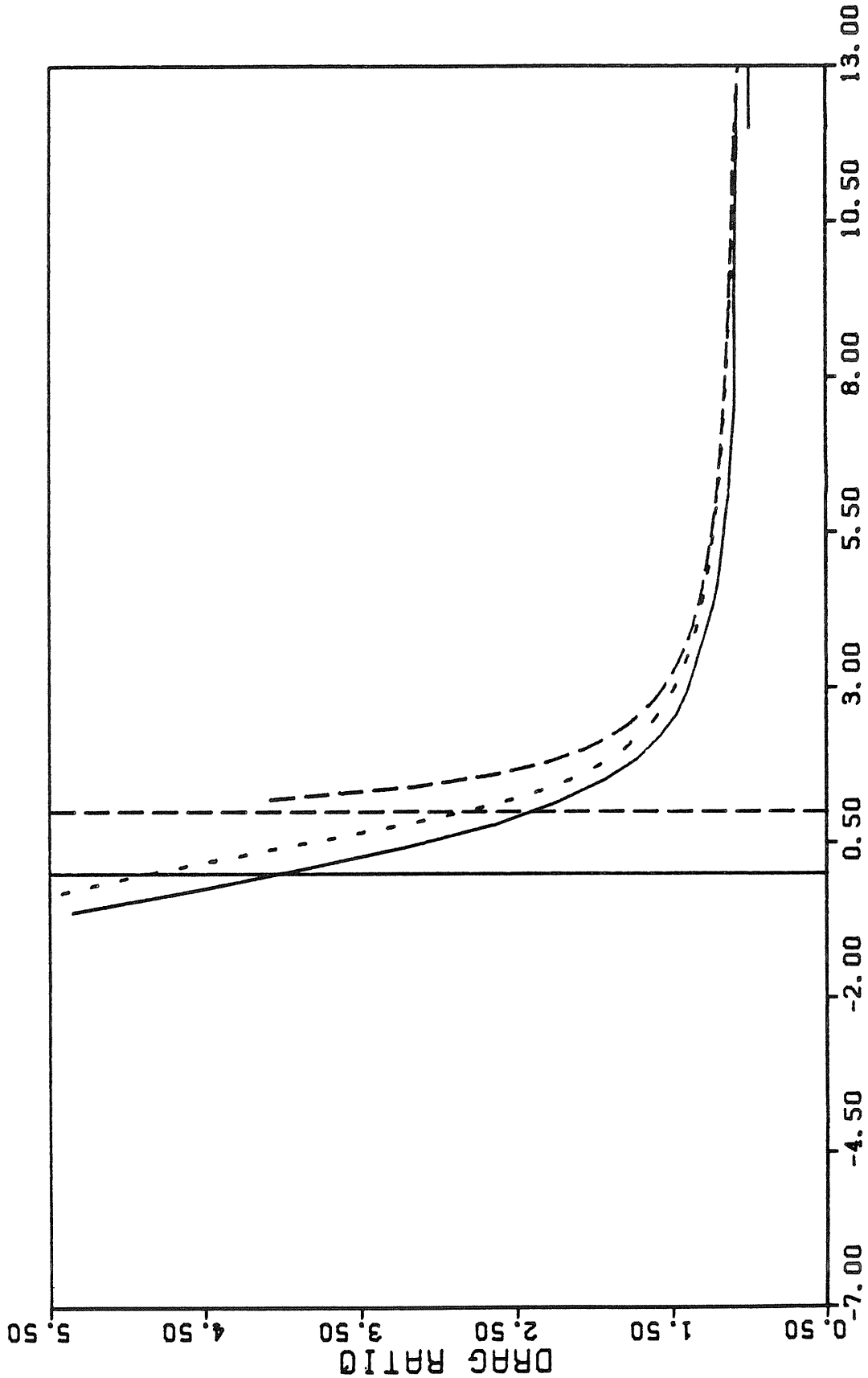
13.00
10.50
8.00
5.50
3.00
0.50
-2.00
-4.50
-7.00
L
0.50
1.50
2.50
3.50
4.50
5.50
DRAG RATIO

FIGURE XIII

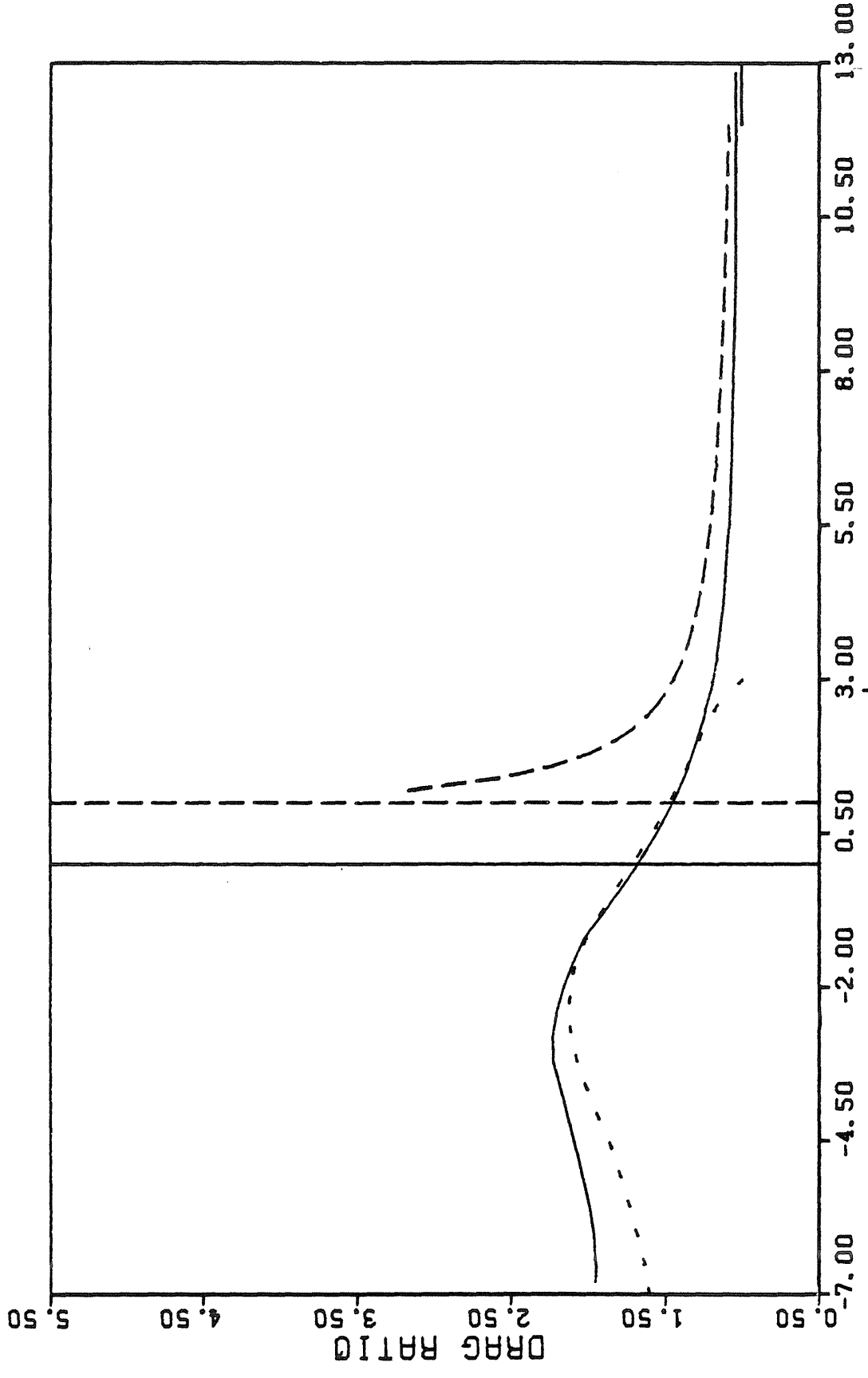
DRAG RATIO
0.50
1.50
2.50
3.50
4.50
5.50
-7.00
-4.50
-2.00
0.50
3.00
5.50
8.00
10.50
13.00
L

FIGURE XIV

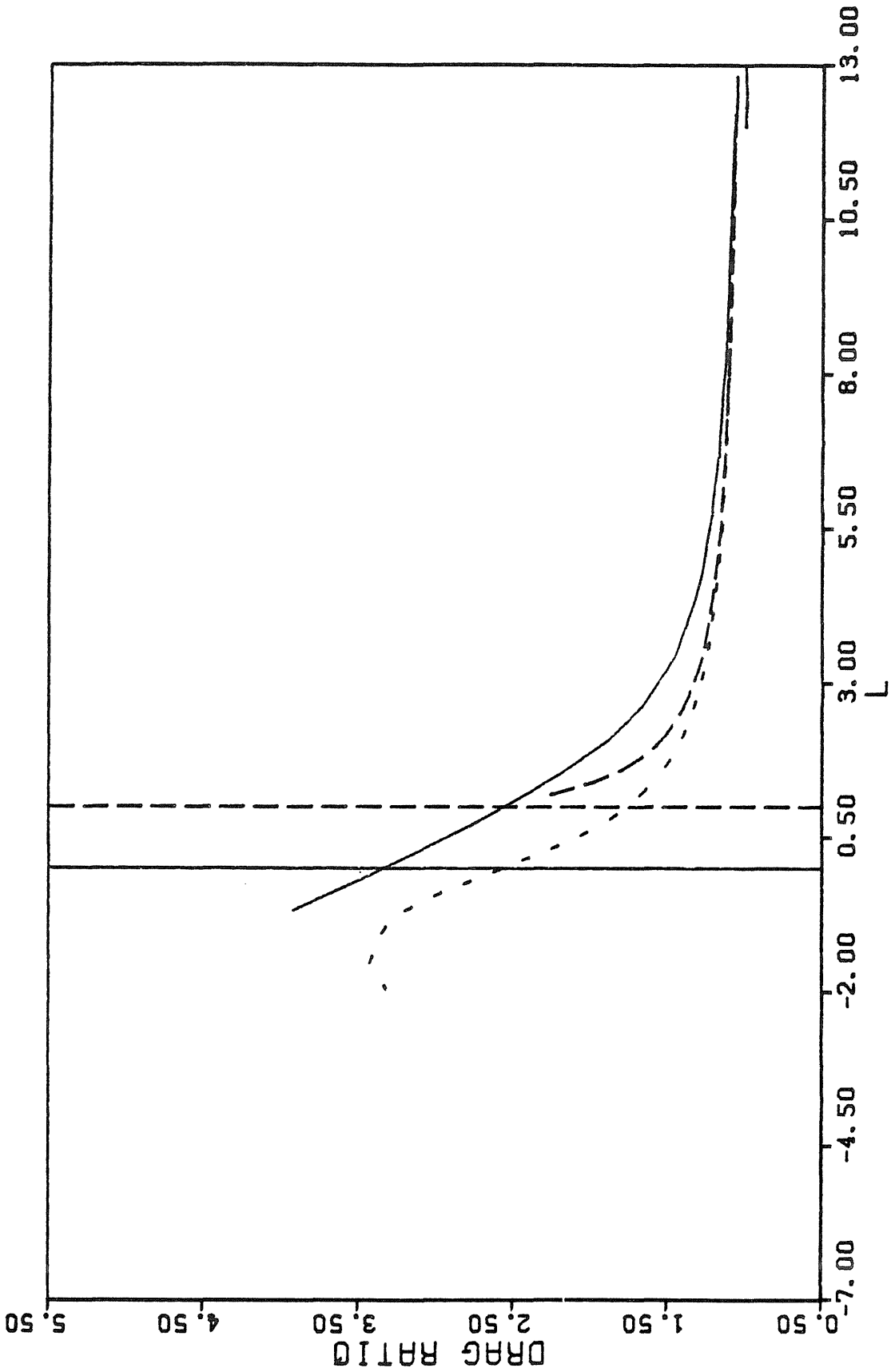
DRAG RATIO
0.50
1.50
2.50
3.50
4.50
5.50
-7.00
-4.50
-2.00
0.50
3.00
5.50
8.00
10.50
13.00
L

FIGURE XV

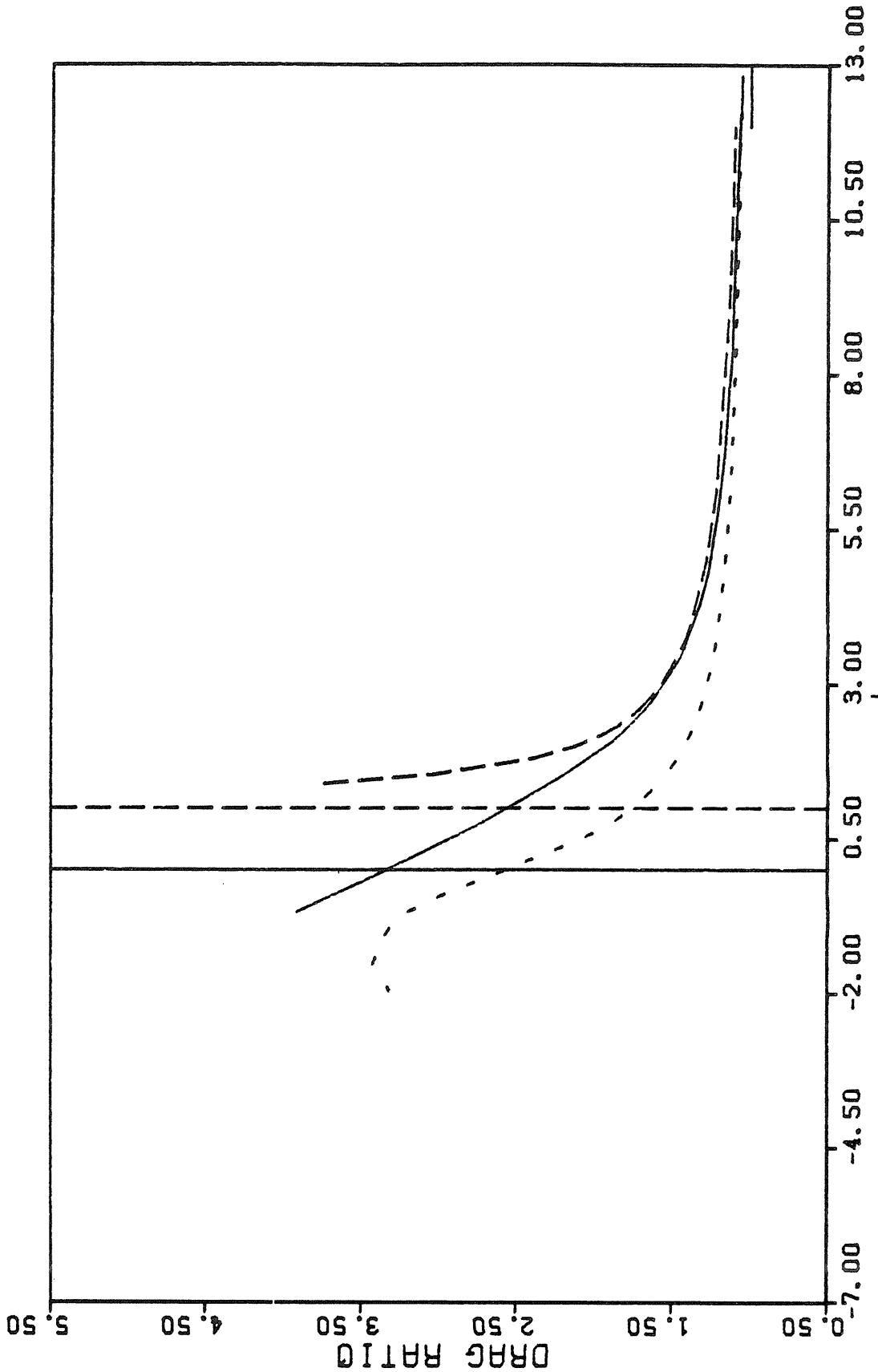
DRAG RATIO
0.50
1.50
2.50
3.50
4.50
5.50
L
13.00
10.50
8.00
5.50
3.00
0.50
-2.00
-4.50
-7.00

FIGURE XVI

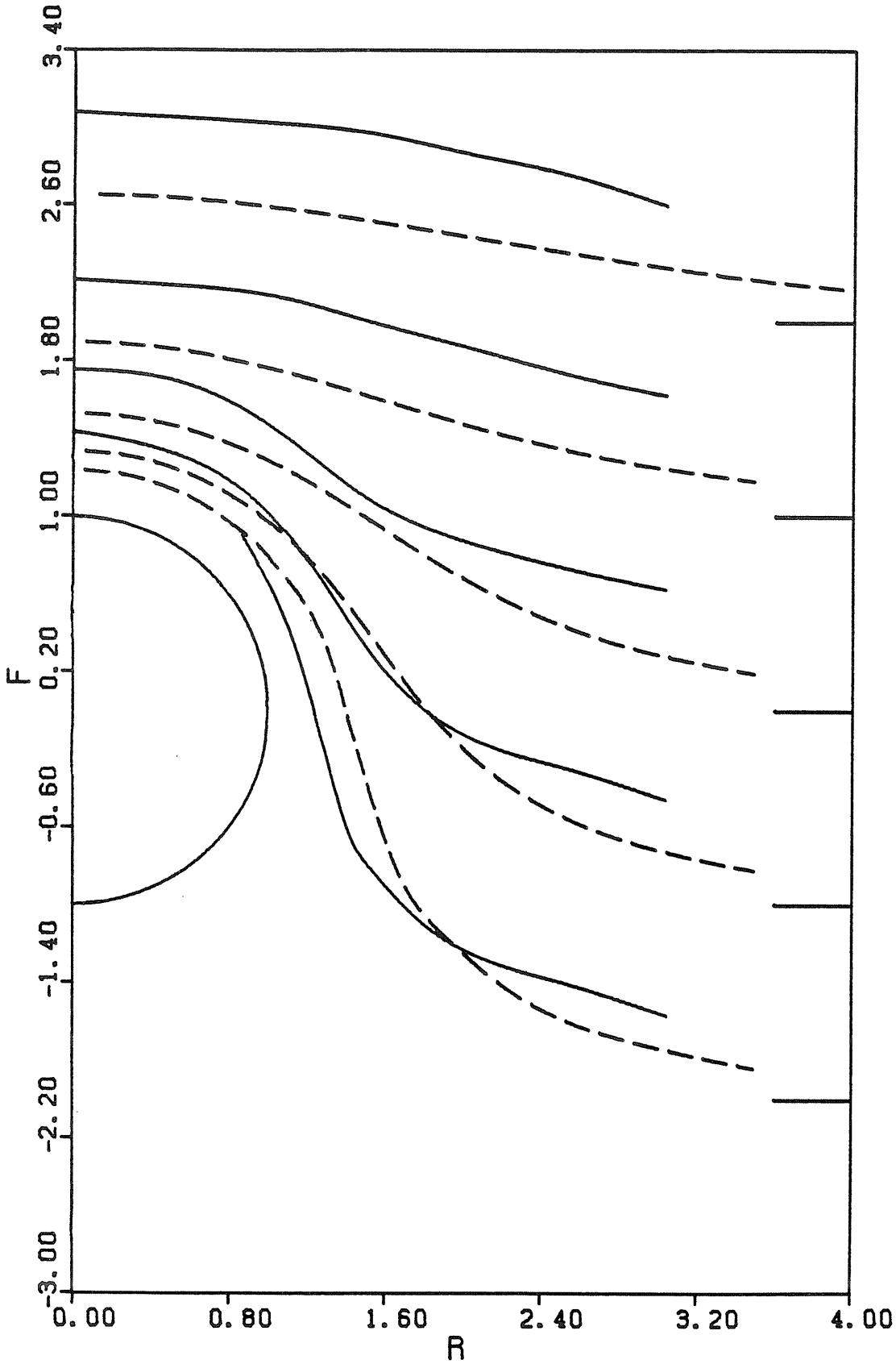

FIGURE XVII

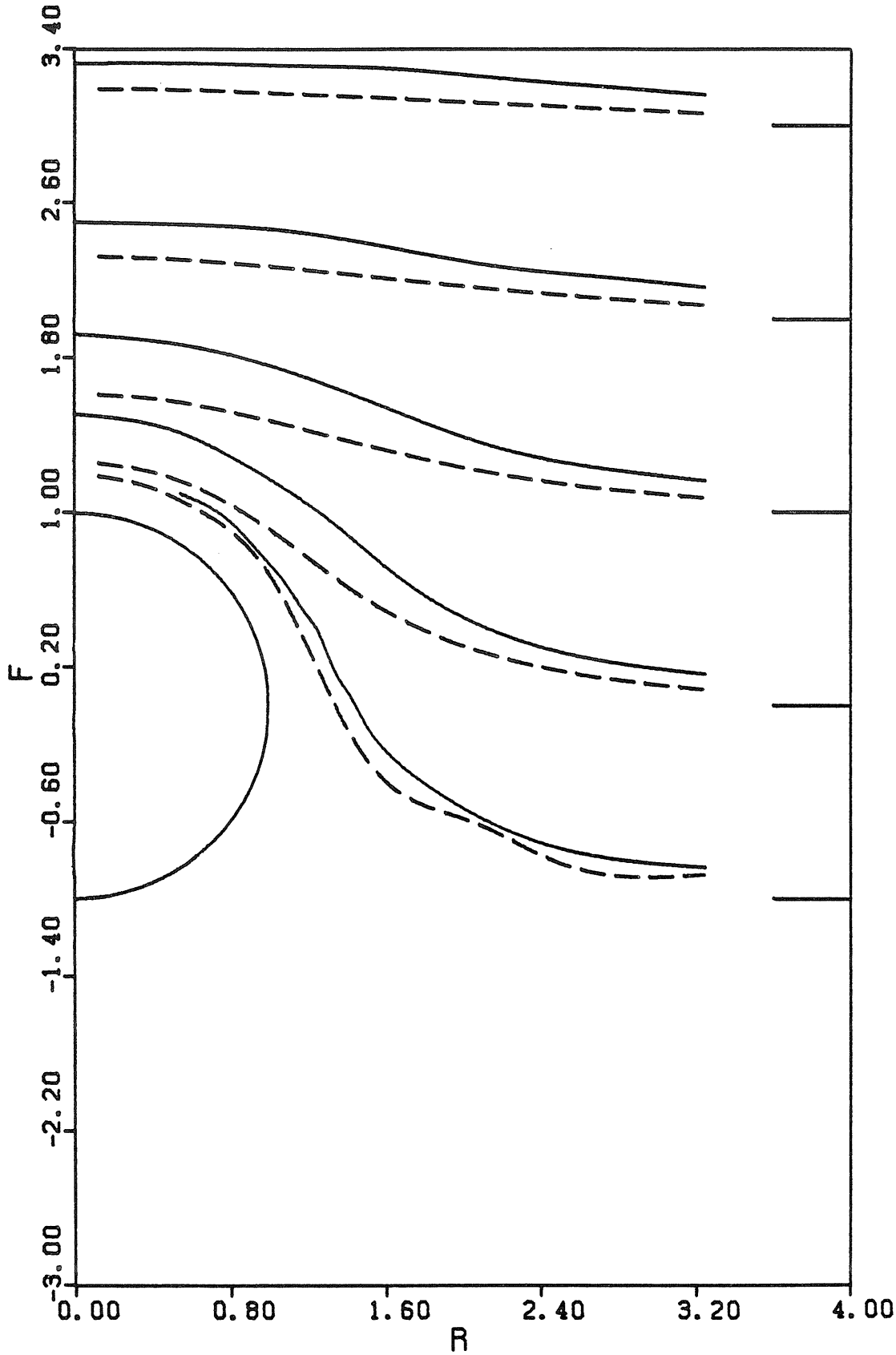

FIGURE XVIII

APPENDIX

For completeness, the force transducer output voltage as a function of sphere position is presented for each experimental run in figures I -- XIII. While photographs of the sphere and interface for selected runs and values for l are presented in figures XIV--XXIII. These are accompanied by the corresponding computer outputs which relate to the analysis of the wire and wall corrections, in tables I -- XIII. We present here a discussion for the data of run B4 to point to the important aspects in the force plot and also to illustrate the method used to "correct" these data for the presence of the wire and walls.

Figure III and table III present the force data and the corrected drag ratio results, respectively, for run B4. The force data in figure III have four distinct regions relating to the interaction of the sphere with the interface. The force in region 1 represents the the weight of a stationary sphere immersed in the fluid. The sphere is set impulsively into motion by lowering the wire in region 2. Here the force on the sphere remains relatively constant while the force on the wire increases "linearly" (only an approximation as boundary/boundary interactions complicate the problem) with increasing length immersed in the fluid. In region 3 we see the interaction of the sphere with the interface which accelerates the decrease in measured force on the wire and sphere. Finally the sphere center passes the plane of the undeformed interface and enters region 4 where the force on the sphere is associated with local stretching of the deformable interface.

These same data are analyzed in table III where the wire and wall corrections are calculated to obtain a value for the drag ratio to be used in comparisons with theory. The top half of the table is concerned with the physical data for the experimental run and the headings for each number are intended to be descriptive of the listed quantity. For example, some of the more useful

quantities are; sphere diameter (SPH D IN), wire diameter (WIRE D IN), fluid temperature (FL TEMP °C), sphere nominal velocity (VEL CPS) and self explanatory fluid properties and dimensionless groups. The first two columns of numbers are the data from the strip chart recorder (figure III). Next is the dimensionless distance of the sphere center to the undeformed interface. Column four has the total force data ($\frac{g\,cm}{sec^2}$) as measured by the force tranducer. The following column records the total length of immersed wire. The sixth column has the corrected value for the ratio of DE Mestre and Katz (1974) and the empirical correlation ($\alpha+\beta$). The next column has the wire drag as calculated in equation (5). this is followed by the drag on the sphere which is obtained by dividing 'RATIO" into the 'TOTAL FORCE" and then subtracting the wire drag and the drag due to the wall correction (not shown). Finally the drag ratio (SCALED DRAG) is obtained by dividing the drag on the sphere by Stokes' drag (note that the velocity does change during the course of the experimental run).

INTER IN	SPH D IN	WIRE D IN	EL TEMP C	DEPTH IN	HT ST CM	SOR	UPDN	VEL CPS	DATA CALC CM SP	CPM E	MARK CM E	TANK IN
0.00000	0.74970	0.00805	21.18000	26.13750	18.73000	1.00000	1.00000	0.39626	10	60	0.33333	10.48000	16.15937

R1	R2	DYNES P VOLT	CH FULL SCALE	CH WIDTH CM	WALL FACTOR	TANK D IN	CH VEL FACTOR
0.300000E-01	0.625000E+01	0.159800E+07	0.100000E-01	0.252000E+02	0.210440E+01	0.150000E+02	0.101500E+01

Z1	Z2	Z3	VISCOSITY	DENSITY	LAMDA
0.529987E+02	-0.360548E+05	0.653150E+07	0.317412E+03	0.886099E+00	0.306750E-04

Y1	Y2	Y3	VIS LOWER	RHO LOWER	GAMMA
0.229832E+00	-0.494493E+04	0.103477E+07	0.973662E-02	0.997944E+00	0.341000E+02

REYNOLDS NO.	1/CAPILLARY NO.	BOND NO./CAP NO.	STOKES DRAG
0.104324731E-02	0.271113311E+00	0.789988227E+00	0.233932711E+04

POSITION	HEIGHT	DIST TO INTER	TOTAL FORCE	WIRE LEN IN	RATIO	WIRE DRAG	SPHERE DRAG	SCALED DRAG
25.0000000	7.4200001	25.9586335	7171.9755859	16.1826717	0.9496861	9054.9409180	2361.2873535	1.0293571
32.0000000	5.6999998	25.1720123	7218.7197266	16.3269215	0.9500393	9101.8706055	2368.2028809	1.0326318
36.0000000	4.5700002	24.7884655	7269.4443359	16.4716187	0.9503893	9148.8452148	2367.9895020	1.0315984
38.0000000	3.8499999	24.3987904	7312.2084961	16.5687561	0.9507359	9195.8642578	2367.3315430	1.0309721
39.0000000	3.5000000	24.0119858	7358.9526367	16.7617588	0.9510792	9242.9291992	2366.5979004	1.0303131
40.0000000	3.0200000	23.6280556	7405.6967773	16.9067993	0.9514193	9290.0380859	2365.8127441	1.0296323
41.0000000	2.3099999	23.2380009	7452.4406297	17.0518856	0.9517757	9337.1909180	2364.8149414	1.0288594
42.0000000	1.6000000	22.8459129	7499.1850586	17.1970234	0.9521061	9384.3896484	2363.9533691	1.0281461
42.9000015	0.0000000	22.4635010	7545.9296875	17.3422070	0.9524328	9431.6333008	2363.0451660	1.0274132
43.0000000	-0.7000000	22.0760612	7592.6743164	17.4874401	0.9527485	9478.9218750	2362.1513672	1.0268869
85.7000000	8.4899998	21.6884918	7639.4179688	17.6327190	0.9530735	9526.2553711	2361.1035156	1.0259942
143.5000000	8.2100000	21.3007965	7686.1625977	17.7780476	0.9533963	9573.6337891	2360.0076801	1.0250809
0.0000000	0.0000000	20.9129772	7732.9062500	17.9234219	0.9537143	9621.0571289	2358.8569336	1.0242448
0.0000000	0.0000000	20.5250282	7779.6500000	18.0688438	0.9540304	9668.5244141	2357.6586914	1.0233884
0.0000000	0.0000000	20.1369514	7826.3945313	18.2143154	0.9543437	9716.0375977	2356.4060059	1.0225090
0.0000000	0.0000000	19.7487469	7873.1391602	18.3596328	0.9546641	9763.5942383	2355.0192871	1.0215719
0.0000000	0.0000000	19.3604126	7919.8828125	18.5053997	0.9549716	9811.1972656	2353.6669922	1.0206504
0.0000000	0.0000000	18.9719543	7966.6274414	18.6510143	0.9553035	9858.8461914	2352.0258789	1.0196043
0.0000000	0.0000000	18.5833772	8013.3720703	18.7966747	0.9556069	9906.5375977	2350.5598145	1.0186348
0.0000000	0.0000000	18.1946754	8060.1157227	18.9423847	0.9559070	9954.2768555	2349.0458984	1.0176451
0.0000000	0.0000000	17.8058128	8106.8598633	19.0881424	0.9562047	6002.0595703	2347.4809570	1.0166340
0.0000000	0.0000000	17.4168453	8153.6035156	19.2339458	0.9564990	6049.8867188	2346.0723145	1.0156047
0.0000000	0.0000000	17.0277519	8200.3466797	19.3797989	0.9567916	6097.7592773	2344.2077637	1.0145519
0.0000000	0.0000000	16.6385250	8247.0927734	19.5256996	0.9570817	6145.6777344	2342.4892578	1.0134764
0.0000000	0.0000000	16.2491760	8293.8359375	19.6716480	0.9573693	6193.6406250	2340.5947266	1.0144880
0.0000000	0.0000000	15.8597012	8352.2451172	19.8176422	0.9576544	6241.6489258	2351.0832520	1.0165292
0.0000000	0.0000000	15.4700956	8405.9863281	19.9636860	0.9579373	6289.7021484	2356.5122070	1.0185434
0.0000000	0.0000000	15.0803528	8459.7294922	20.1097794	0.9582177	6337.8012695	2361.8956250	1.0205344
0.0000000	0.0000000	14.6904974	8513.4716797	20.2559185	0.9584968	6385.9448242	2367.2529297	1.0224958
0.0000000	0.0000000	14.3005123	8567.2138672	20.4021034	0.9587692	6434.1328125	2373.0988770	1.0245276
25.5588335	7171.9755859	13.9103947	8620.9550781	20.5483398	0.9590786	6482.3676758	2378.3149414	1.0266244
16.1826717	0.9496861	13.5201530	8674.6972656	20.6946220	0.9592499	6530.6476609	2383.4753418	1.0285162
9054.9409180	2361.2873535	13.1297836	8728.4414063	20.8409519	0.9595190	6578.9711914	2388.5842285	1.0303845
1.0293571	25.1720123	12.7392845	8782.1826172	20.9873295	0.9597861	6627.3417969	2393.6342773	1.0322261
7218.7197266	16.3269215	12.3486614	8835.9257813	21.1337547	0.9600507	6675.7553711	2398.6357422	1.0340457
0.9500393	0.9500393	11.9579105	8889.6679688	21.2802277	0.9603396	6724.2163086	2403.3269043	1.0357112
2368.2028809	1.0320316	11.5670328	8943.4082031	21.4267483	0.9606026	6772.7207031	2408.1887207	1.0374874
24.7884655	7269.4443359	11.1760168	9001.1435547	21.5733204	0.9608808	6821.2714844	2417.4814453	1.0411516
16.4716187	0.9503893	10.7848877	9068.8154297	21.7199364	0.9609222	6869.8676758	2437.5354004	1.0494665
9148.8452148	2367.9895020	10.3936283	9134.4931641	21.8666000	0.9613717	6918.5092773	2453.6975098	1.0566038
1.0315984	24.3987904	10.0022354	9201.1826172	22.0133133	0.9614990	6967.1943359	2473.3608398	1.0641776
7312.2084961	16.5617561	9.6107216	9267.7656250	22.1600723	0.9617102	7015.9272461	2491.3212891	1.0715963
0.9507359	0.9507359	9.2190933	9334.3476563	22.3068810	0.9619494	7064.7055664	2509.2185059	1.0789232
2367.3315430	1.0309721	8.8273468	9400.9316406	22.4537354	0.9621781	7113.5278320	2527.3036133	1.0863916
24.0119858	7358.9526367	8.4355803	9467.5117188	22.6006393	0.9624221	7162.3955078	2547.7822266	1.0947726
16.7617588	0.9510792	8.0437907	9534.4404297	22.7475891	0.9628519	7211.3090820	2567.5373535	1.1029 28
9242.9291992	2366.5979004	7.6519756	9601.2851563	22.8945885	0.9630933	7260.2685547	2589.1374512	1.1118200
1.0303131	24.6280556	7.2600436	9668.1914063	23.0416355	0.9633323	7309.2724609	2617.9243164	1.1238165
7405.6967773	16.9067993	6.8679929	9735.1503906	23.1887283	0.9635887	7358.3212891	2661.1323242	1.1419961
0.9514193	0.9514193	6.4758224	9802.1933594	23.3358707	0.9638046	7407.4178809	2704.2556152	1.1611233
2365.8127441	1.0296323	6.0835304	9869.3144531	23.4830608	0.9640379	7456.5576172	2747.3146973	1.1792334
23.2380009	7452.4406297	5.6911159	10097.2031250	23.6302967	0.9642701	7505.7431641	2835.6718750	1.2157118
17.0518856	0.9517757	5.2986285	10232.2734375	23.7775841	0.9645001	7554.9755859	2923.9411621	1.2531482
5337.1909180	2364.8149414	4.9059670	10367.3417969	23.9249153	0.9647285	7604.2539063	3012.1159668	1.2905200
1.0288594	22.8459129	4.5131941	10527.7773437	24.0722961	0.9649553	7653.5742188	3126.4887695	1.3390884
7499.1850586	17.1970234	4.1201172	10700.8925781	24.2197247	0.9651804	7702.9448242	3253.8935547	1.3932048
0.9521061	5384.3896484	3.7268066	10874.0107422	24.3672028	0.9654043	7752.3579102	3381.1892090	1.4472398
2363.9533691	1.0281461	3.3331299	11084.0263672	24.5147266	0.9656259	7801.8173828	3550.7744141	1.5193352
23.4635010	7545.9296875	2.9391479	11383.6982422	24.6622963	0.9658462	7851.3222656	3804.9980469	1.6275876
17.3422070	0.9524328	2.5448608	11670.9130859	24.8099174	0.9660647	7900.8720703	4059.5593262	1.7357008
5431.6333008	2363.0451660	2.1502686	12321.6806641	24.9575825	0.9662717	7950.4677734	4670.3862305	1.9964656

Run 9

Table I

INTER IN	SPH D IN	WIRE D IN	EL TEMP C	DEPTH IN	HT ST CM	SOR	UPON	VEL CPS	DATA CALC	CM SP	CPM E	MARK CM	TANK IN
10.98750	0.49900	0.00410	20.56000	26.21250	1.74000	-1.00000	1.00000	0.35475	17	60	0.33333	17.09000	11.84690

P1	P2	DYNES P VOLT	CM FULL SCALE	CM WIDTH CM	WALL FACTOR	TANK D IN	CM VEL FACTOR
0.300000E-01	0.160000E+02	0.159800E+07	0.100000E-01	0.252000E+02	0.210440E+01	0.150000E+02	0.101500E+01

Z1	Z2	Z3	VISCOSITY	DENSITY	LAMDA
0.529987E+02	-0.360948E+05	0.653150E+07	0.336962E+03	0.886420E+00	0.293318E-04

Y1	Y2	Y3	VIS LOWER	RHO LOWER	GAMMA
0.229832E+00	-0.494493E+04	0.103427E+07	0.988368E-02	0.998075E+00	0.341000E+02

REYNOLDS NO.	L/CAPILLARY NO.	BOND NO./CAP NO.	STOKES DRAG
0.591405 90E-03	0.285266 94E+00	0.367628 81E+00	0.146613 99E+04

POSITION	HEIGHT	DIST TO INTER	TOTAL FORCE	WIRE LEN IN	RATIO	WIRE DRAG	SPHERE DRAG	SCALED DRAG
2.0000000	6.1999998	29.8590870	3145.2697754	7.5256672	0.9208803	1949.1046143	1416.5093994	1.0162629
11.0000000	8.3400002	28.9713154	3211.0649414	7.7471561	0.9225961	2004.0852051	1426.4556885	1.0225147
14.0000000	8.7900000	28.0427170	3276.8603516	7.9688463	0.9242799	2063.2138672	1432.4620361	1.0259361
16.0000000	9.0299997	27.1093750	3342.6560059	8.1907291	0.9259842	2122.4914551	1438.2598877	1.0291984
17.0000000	9.1299999	26.1733398	3408.4516602	8.4128017	0.9277893	2181.9177246	1443.8884277	1.0323360
18.0000000	9.2300001	25.2412109	3474.2470703	8.6350670	0.9297170	2241.4934082	1449.3847656	1.0353736
18.5000000	9.2700005	24.5209484	3540.0427246	8.8575230	0.9301335	2301.2172852	1454.7392578	1.0383048
19.0000000	9.9600000	23.6285744	3605.8378906	9.0801706	0.9315027	2361.0915527	1459.8610840	1.0410650
19.5000000	10.1800003	22.7354336	3671.6331787	9.3030090	0.9327860	2421.1137695	1465.0072021	1.0438380
20.0000000	10.4700003	21.8415260	3737.4289551	9.5260391	0.9340476	2481.2856445	1469.9168701	1.0464380
20.5000000	10.6999998	20.9468498	3803.2246094	9.7492609	0.9352685	2541.6083984	1474.6771240	1.0489268
21.1499996	10.8800001	20.0514069	3869.0200195	9.9726734	0.9364521	2602.2793457	1479.2838135	1.0513024
22.0000000	10.3800001	19.1551952	3934.8156738	10.1962786	0.9376001	2662.7011719	1483.7351074	1.0535637
23.0000000	9.8999996	18.2582188	4000.6110840	10.4200735	0.9387142	2723.4719238	1488.0312500	1.0557110
24.0000000	9.6800003	17.3604736	4066.4067383	10.6440611	0.9397965	2784.3930664	1492.1696777	1.0577430
26.0000000	9.6499996	16.4619217	4132.2021484	10.8682404	0.9408485	2845.4650879	1496.1489258	1.0596585
34.0000000	9.6499996	15.5626831	4197.9975586	11.0926094	0.9418718	2906.6870117	1499.9680176	1.0614576
98.0000000	7.3000002	14.6636963	4263.7934570	11.3171721	0.9428682	2968.0598145	1503.6254883	1.0630472
137.6999969	7.1500001	13.7818298	4329.5888672	11.5419245	0.9438480	3029.5817871	1507.0745850	1.0644709
0.0000000	0.0000000	12.8802490	4395.3837891	11.7668686	0.9447807	3091.2561035	1510.4696045	1.0661616
0.0000000	0.0000000	11.9578972	4461.1801758	11.9920044	0.9457013	3153.0808105	1513.6473389	1.0674967
0.0000000	0.0000000	11.0347919	4530.8374023	12.2173309	0.9465994	3215.0556641	1520.7402344	1.0715884
0.0000000	0.0000000	10.1109018	4606.9326172	12.4428482	0.9475111	3277.1823730	1534.2756348	1.0802088
0.0000000	0.0000000	9.1862430	4683.0278320	12.6685581	0.9483664	3339.4602051	1547.8078613	1.0888126
0.0000000	0.0000000	8.2607956	4759.1230469	12.8944607	0.9492004	3401.8896484	1561.1650391	1.0972786
0.0000000	0.0000000	7.3346558	4835.2182617	13.1205530	0.9500164	3464.4709473	1577.6765322	1.1079412
0.0000000	0.0000000	6.4077272	4919.4572754	13.3468380	0.9508139	3527.2031250	1595.9906006	1.1198590
0.0000000	0.0000000	5.4799805	5015.9448242	13.5733137	0.9516968	3590.0871582	1630.6514893	1.1432130
0.0000000	0.0000000	4.5515137	5117.4047852	13.7999802	0.9525592	3653.1228027	1669.8985596	1.1697402
0.0000000	0.0000000	3.6222496	5218.8652344	14.0268383	0.9533956	3716.3110352	1708.9221191	1.1960660
29.8590870	3145.2697754	2.6922119	5320.3256836	14.2538872	0.9542078	3779.6503906	1747.3635254	1.2214405
7.5256672	0.9208803	1.7614440	5417.1357422	14.4811287	0.9549882	3843.1433105	1783.6020508	1.2462322
1945.1046143	1416.5093994	1.0298817	5518.5957031	14.7085619	0.9558559	3906.7883301	1852.5976563	1.2933515
1.0162629	29.9713154	0.1457732	5705.8754883	14.9361849	0.9558805	3970.5849609	1949.9938965	1.3602026
3211.0649414	7.7471561	-0.7355139	5891.8852539	15.1640015	0.9565703	4034.5354004	2073.7163086	1.4452893
0.0225961	2004.0852051	-1.6693210	6028.1083984	15.3920078	0.9572203	4098.6381836	2147.6350098	1.4955512
1424.4556885	1.0225147	-2.5983920	6094.3330078	15.6202059	0.9578629	4162.8940430	2148.2485352	1.4947263
28.0427170	3276.8603516	-3.5093994	6095.3911133	15.8485947	0.9584951	4227.3022461	1872.0445557	1.3014539
7.9688463	0.9242799	-4.4155273	5714.2607422	16.0771770	0.9591153	4291.8627930	1615.1215820	1.1219000
2063.2138672	1432.4620361	-4.1324463	5552.4155273	16.3059082	0.9597244	4356.5786133	1377.4355469	0.9559975
1.0259361	27.1934700	-6.2501493	5445.0371094	16.5349121	0.9603208	4421.4477539	1197.1142578	0.8321530
3342.6560059	8.1907291	-7.1886902	5370.6328125	16.7640667	0.9608856	4486.4692383	1051.2846680	0.7281171
0.0291984	2122.4914551	-8.0878325	5348.2265625	16.9934139	0.9614615	4551.6450195	949.4135132	0.6642066
1438.2598877	1.0291984	-9.0078430	5343.1538086	17.2229519	0.9620280	4616.9746094	885.4921265	0.6145196
26.3033981	3408.4516602	-9.9288712	5338.0807617	17.4526806	0.9625826	4682.4580078	811.3867313	0.5627872
8.4128017	0.9323898	-10.8551941	5333.0073242	17.6826019	0.9631476	4748.0961914	737.2932739	0.5091574
2181.9177246	1443.8884277	-11.7774048	5342.3081055	17.9127140	0.9636859	4813.8867188	678.6183716	0.4678343
1.0323360	25.4125557	-12.6994629	5351.6083984	18.1430168	0.9641454	4879.8330078	619.0335083	0.4267798
3474.2470703	8.8350670	-13.6192932	5360.9086914	18.3735123	0.9647195	4945.9331055	549.2272949	0.3852276
0.0353736	2241.4934082	-14.5408936	5370.2089844	18.6041985	0.9652286	5012.1884766	499.6344910	0.3438913
1449.3847656	1.0353736	-15.4602661	5379.5107422	18.8350754	0.9657732	5078.5986328	439.9649683	0.3025293
24.5209484	3540.0427246	-16.3903503	5388.8117065	19.0661469	0.9662252	5145.1625977	380.3871460	0.2611752
8.8575230	0.9301335	-17.3222713	5398.1113281	19.2974072	0.9667096	5211.8928125	320.1495667	0.2198074
2301.2172852	1454.7392578	-18.2469482	5407.4121094	19.5288582	0.9671873	5278.7568359	260.0909424	0.1784249
1.0383048	23.6285744	-19.1783638	5416.7124023	19.7605019	0.9676552	5345.7866211	199.9263458	0.1371382
3605.8378906	9.0801706	-20.1075592	5426.0126953	19.9923363	0.9681181	5412.9711914	139.6284790	0.0956284
0.9315027	2361.0915527	-21.0375290	5435.3139648	20.2243633	0.9685723	5480.3125000	79.2187729	0.0542104
1459.8610840	1.0410650	-21.9682579	5444.6147461	20.4565792	0.9690196	5547.8090820	18.6874924	0.0127756
22.7354336	3671.6331787	-22.8997574	5453.9145508	20.6889896	0.9694595	5615.4404492	-41.9638977	-0.0286692
9.3030090	0.9327860	-23.8320465	5463.2133789	20.9215908	0.9698932	5683.2690430	-102.7412796	-0.0701337
2421.1137695	1465.0072021	-24.7650528	5472.5156250	21.1543808	0.9703202	5751.2319336	-163.6412048	-0.1116136

Run A6

Table II

INTER IN	SPH D IN	WIRE D IN	EL TEMP C	DEPTH IN	HT ST CM	SOR	UPON	VEL CPS	DATA CALC CH	SP CPM	E MARK CM	E TANK IN
5.56250	0.99980	0.00410	20.65000	17.48750	20.15000	1.00000	1.00000	0.38024	22 60	0.33333	19.67000	5.48750

R1	R2	DYNES P VOLT	CH FULL SCALE	CH WIDTH CM	WALL FACTOR	TANK D IN	CH VEL FACTOR
0.300000E-01	0.100000E+01	0.159800E+07	0.100000E-01	0.252000E+02	0.210440E+01	0.150000E+02	0.101500E+01

Z1	Z2	Z3	VISCOSITY	DENSITY	LAMDA
0.529987E+02	-0.360594E+05	0.653150E+07	0.335656E+03	0.886399E+00	0.965123E+00

Y1	Y2	Y3	VIS LOWER	RHO LOWER	GAMMA
-0.791993E+02	0.457984E+05	-0.646999E+07	0.323949E+03	0.972935E+00	0.194000E+01

REYNOLDS NO.	1/CAPILLARY NO.	BOND NO./CAP NO.	STOKES DRAG
0.12749999E-02	0.15200223E-01	0.10712806E+01	0.31064700E+04

POSITION	HEIGHT	DIST TO INTER	TOTAL FORCE	WIRE LEN IN	RATIO	WIRE DRAG	SPHERE DRAG	SCALED DRAG
2.0000000	14.2200003	16.6731724	3760.3723145	3.0902052	0.9171643	842.2322998	3020.7382813	1.0257488
10.0000000	12.6099997	16.2920094	3815.6735840	3.2807236	0.9174863	894.9755859	3039.1037598	1.0296853
14.0000000	11.6159999	15.9185444	3870.9743652	3.4714174	0.9174014	947.8615112	3043.3308105	1.0315343
16.0000000	10.9799995	15.5278333	3926.2761230	3.6622849	0.9175846	1000.8901367	3049.5710449	1.0327067
17.0000000	10.5600002	15.1445731	3981.5769043	3.8533268	0.9178065	1054.0615234	3055.4140625	1.0337429
18.0000000	9.9700003	14.7640667	4036.8781738	4.0445423	0.9180635	1107.3757324	3060.9147949	1.0346613
19.0000000	9.2200003	14.3812103	4092.1799316	4.2359319	0.9183522	1160.8327637	3066.0849609	1.0354666
19.5000000	8.7399998	13.9980469	4147.4804688	4.4274960	0.9186698	1214.4329834	3070.9328613	1.0361615
20.0000000	8.1899996	13.6144543	4202.7822266	4.6192331	0.9190126	1268.1763916	3075.4721680	1.0367513
20.5000000	7.5900002	13.2305117	4258.0825195	4.8111463	0.9193783	1322.0638428	3079.7065430	1.0372370
21.0000000	6.9700003	12.8461838	4313.3842773	5.0032320	0.9197640	1376.0942383	3083.6518555	1.0376247
21.5000000	6.1999998	12.4617052	4368.6855469	5.1954927	0.9201676	1430.2683105	3087.3112793	1.0379159
22.0000000	5.4459998	12.0767593	4423.9863281	5.3879271	0.9205872	1484.5864258	3090.7971191	1.0381479
22.5000000	5.0000000	11.6914663	4479.2879639	5.5805349	0.9210095	1539.0483398	3093.9165039	1.0382566
23.0000000	4.6700002	11.3058224	4534.5883789	5.7733183	0.9214451	1593.6546631	3096.6577148	1.0382384
23.5000000	4.2800002	10.9198322	4589.8896484	5.9662747	0.9219208	1648.4045410	3099.2519531	1.0381709
24.0000000	4.0999998	10.5334930	4645.1914063	6.1594052	0.9223854	1703.2987061	3101.5969238	1.0380203
24.5000000	4.2100000	10.1468750	4700.4921875	6.3527107	0.9229590	1758.3380127	3103.6882324	1.0377849
25.0000000	4.3000002	9.7601709	4755.7934570	6.5461898	0.9233381	1813.5216064	3105.5661426	1.0374720
26.0000000	4.4800000	9.3723860	4811.0939941	6.7398434	0.9238731	1868.8497756	3114.5744629	1.0395530
27.0000000	4.6100001	8.9846535	4866.3945312	6.9336710	0.9245256	1924.3231201	3128.4926758	1.0432608
28.0000000	4.4200001	8.5965738	4921.6958008	7.1276717	0.9248860	1979.9412842	3134.6037598	1.0476925
21.4500008	6.8499999	8.2081442	5021.9882812	7.3218479	0.9253024	2035.7043457	3159.2580566	1.0516317
58.5000000	6.6799998	7.8193665	5089.9785156	7.5161982	0.9258013	2091.6127930	3173.6774902	1.0554855
0.0000000	0.0000000	7.4302397	5157.9882813	7.7107224	0.9263020	2147.6669922	3187.8662578	1.0592550
0.0000000	0.0000000	7.0407777	5225.9985352	7.9054193	0.9268036	2203.8657227	3201.8247070	1.0629427
0.0000000	0.0000000	6.6509447	5294.0087891	8.1002922	0.9273062	2260.2106934	3215.5571289	1.0665482
0.0000000	0.0000000	6.2607756	5362.0185547	8.2953377	0.9278092	2316.7011719	3229.0649414	1.0700729
0.0000000	0.0000000	5.8702660	5430.1586914	8.4905586	0.9285072	2373.3381348	3247.7236328	1.0752966
0.0000000	0.0000000	5.4793882	5524.0000203	8.6859531	0.9288143	2430.1206055	3283.4685059	1.0861632
16.6731224	3760.3723145	5.0881724	5617.0234375	8.8815222	0.9293170	2487.0493164	3317.7348633	1.0965217
0.0000000	0.9171643	4.6966598	5690.9858604	9.0772638	0.9298160	2544.1237793	3351.7867617	1.1067891
842.2322998	3020.7382813	4.3048946	5787.0881836	9.2731819	0.9303148	2601.3461914	3385.5825195	1.1169574
1.0257488	16.2920094	3.9124358	5896.7465820	9.4692776	0.9308121	2658.7138672	3418.1362305	1.1269816
3815.6735840	3.0807236	3.5198774	6014.0057617	9.6655388	0.9313078	2716.2280273	3450.4453066	1.1369095
0.9174863	894.9755859	3.1272807	6148.9179688	9.8619776	0.9318010	2773.8896484	3480.9453125	1.1812321
3039.1037598	1.0296853	2.7335681	6308.2949219	10.0585899	0.9322921	2831.6977539	3499.4038086	1.2161705
15.9105444	3870.9743652	2.3399122	6471.2646484	10.2553768	0.9327808	2889.6530762	3817.4091797	1.2522124
3.4714174	0.9174014	1.9454093	6637.3564453	10.4523392	0.9332671	2947.7553711	3971.3120117	1.3032526
947.8615112	3043.3308105	1.5501106	6843.4462891	10.6494751	0.9337501	3006.0053711	4129.8012695	1.3560670
1.0315343	15.9287333	1.1558605	7133.9287109	10.8467865	0.9342286	3064.4025879	4336.6093359	1.42.2796
3926.2761230	3.6622849	0.7618144	7521.3994141	11.0442686	0.9347031	3122.9475098	4586.3940039	1.4991457
0.9175846	1000.8901367	0.3664182	7736.3491211	11.2419271	0.9351690	3181.6398926	4852.6821289	1.5868801
3049.5710449	1.0327067	-0.0393744	8077.9316406	11.4397583	0.9356263	3240.4807129	5156.1665039	1.6846391
15.1465731	3981.5769043	-0.4252172	8450.3789063	11.6377649	0.9361253	3299.4689941	5490.5019531	1.7922976
3.4533268	0.9178065	-0.8110448	8846.0703125	11.8359451	0.9366911	3358.6056885	5849.1499023	1.9076964
1054.0615234	3055.4140625	-1.1971440	9258.2548828	12.0343008	0.9370536	3417.8933105	6224.8691406	2.0286555
1.0337429	14.7640667	-1.5857315	9630.9277344	12.2328281	0.9376405	3477.3232422	6557.9345703	2.1002791
4036.8781738	4.0445423	-2.0013428	9770.6289063	12.4315319	0.9379971	3536.9047852	6641.7416992	2.1605077
0.9180635	1107.3757324	-2.4113098	9955.5166016	12.6304083	0.9384644	3596.6350098	6784.9624023	2.2051647
3060.9147949	1.0346613	-2.8203430	10161.6425781	12.8294592	0.9388841	3656.5136719	6864.7802734	2.2291553
14.3812103	4092.1799316	-3.2278137	10163.7871094	13.0286846	0.9392993	3716.5419922	6885.6044922	2.2274752
4.2359319	0.9183522	-3.6344910	10164.1787109	13.2280836	0.9397597	3776.7185059	6736.4892578	2.1836777
1160.8327637	3066.0849609	-4.0405273	10164.9169922	13.4276571	0.9401990	3837.0419443	6618.3232422	2.1435025
8.8384668	18.9980059	-4.4456914	10165.5 883	13.6274414	0.9407844	3897.8195801	6898.0101563	2.1028316
4147.4804688	4.4274960	-4.8494156	9955.7929688	13.8273268	0.9412155	3958.1445313	6340.1538086	2.0627675
0.9186698	1214.4329834	-5.2556641	9914.2861328	14.0274220	0.9416433	4018.9189453	6270.8173828	2.0256546
3070.9328613	1.0361615	-5.6602173	9879.6435547	14.2276926	0.9420668	4079.8425293	6167.0336914	1.9833984
13.6144543	4202.7822266	-6.0627747	9870.9074707	14.4281359	0.9424878	4140.9160156	6001.8715820	1.9644325
4.6192331	0.9190126	-6.4648437	9922.6074219	14.6287546	0.9429055	4202.1396484	6001.1723633	1.9592811
1268.1763916	3075.4721680	-6.8702941	9974.8164063	14.8295460	0.9431875	4263.5126953	6071.7988281	1.9565654

Run B4

Table III

INTER IN	SPH D IN	WIRE D IN	EL TEMP C	DEPTH IN	HT ST CM	SOR	UPDN	VEL CPS	DATA CALC CH	SP CPM	E - ARK CM	E TANK IN
9.96250	0.49900	0.00410	21.55000	17.48750	2.93000	-1.00000	1.00000	0.46950	10	40	0.33333	17.82000	9.80625

R1	R2	DYNES P VOLT	CH FULL SCALE	CH WIDTH CM	WALL FACTOR	TANK D IN	CH VEL FACTOR
0.300000E-01	0.160000E+02	0.159800E+07	0.100000E-01	0.252000E+02	0.210440E+01	0.150000E+02	0.101500E+01

Z1	Z2	Z3	VISCOSITY	DENSITY	LAMDA
0.529987E+02	-0.360548E+05	0.653150E+07	0.306423E+03	0.885907E+00	0.103597E+01

Y1	Y2	Y3	VIS LOWER	RHO LOWER	GAMMA
-0.751993E+02	0.457984E+05	-0.646559E+07	0.317446E+03	0.971981E+00	0.194000E+01

REYNOLDS NO.	1/CAPILLARY NO.	BOND NO./CAP NO.	STOKES DRAG
0.86021324E-03	0.13484789E-01	0.23547523E+00	0.17217531E+04

POSITION	HEIGHT	DIST TO INTER	TOTAL FORCE	WIRE LEN IN	RATIO	WIRE DRAG	SPHERE DRAG	SCALED DRAG
2.0000000	6.5100002	32.4244499	2282.8571777	2.3380985	0.8002161	735.0267334	2052.3095703	1.2105638
14.0000000	8.4499998	34.4227905	2367.2666016	2.5880079	0.8184359	813.9075928	2007.8551025	1.1838808
14.0000000	9.8499999	34.4227764	2437.6630859	2.8380156	0.8333747	892.8806152	1971.6217041	1.1620642
16.0000000	10.5500002	34.4182540	2515.0466309	3.0881195	0.8450761	971.9451294	1943.6314697	1.1451211
17.0000000	11.0000000	33.4155426	2592.4697266	3.3383207	0.8547250	1051.1014404	1921.4134521	1.1315907
18.0000000	11.6099997	32.4123421	2669.8728027	3.5886192	0.8628544	1130.3497314	1903.2207520	1.1204699
18.5000000	11.9700003	31.4087505	2747.2741699	3.8390150	0.8698266	1209.6900635	1888.6919189	1.1111021
19.0000000	12.3500004	30.4047489	2824.6780090	4.0895090	0.8758978	1289.1228027	1875.1129150	1.1030354
19.5000000	12.7749996	29.4004002	2902.0822754	4.3400993	0.8812556	1368.6470947	1863.7916260	1.0959499
20.0000000	13.1700001	28.3956337	2979.4865417	4.5907884	0.8860368	1448.2637939	1853.7412109	1.0896169
33.2799988	5.4600000	27.3904800	3056.8884277	4.8415742	0.8903443	1527.9726563	1844.6748047	1.0838667
64.9300003	8.4099998	26.3849373	3134.2912598	5.0924573	0.8942592	1607.7736816	1836.3745117	1.0785713
0.0000000	0.0000000	25.3790035	3211.6945801	5.3434377	0.8978423	1687.6667480	1828.6810303	1.0736362
0.0000000	0.0000000	24.3726788	3289.0979004	5.5945158	0.9011596	1767.6520996	1821.3969727	1.0689453
0.0000000	0.0000000	23.3659687	3366.5007324	5.8456898	0.9042622	1847.7296143	1814.6181641	1.0645541
0.0000000	0.0000000	22.3588867	3443.9038086	6.0969620	0.9070255	1927.8995361	1808.1729736	1.0603621
0.0000000	0.0000000	21.3513489	3521.3071289	6.3483324	0.9096380	2008.1619873	1802.0742188	1.0563765
0.0000000	0.0000000	20.3434448	3598.7099609	6.5997992	0.9122136	2088.5166016	1796.6176758	1.0526843
0.0000000	0.0000000	19.3352127	3677.4609375	6.8513637	0.9152395	2168.9636230	1788.1485596	1.0474023
0.0000000	0.0000000	18.3265476	3760.9277344	7.1030254	0.9174445	2249.5031738	1788.9062500	1.0474469
0.0000000	0.0000000	17.3174934	3844.3955078	7.3547845	0.9189288	2330.1352539	1792.4600830	1.0491159
0.0000000	0.0000000	16.3080521	3927.8613281	7.6066403	0.9215603	2410.8593750	1798.3364258	1.0474681
0.0000000	0.0000000	15.2982168	4011.3283691	7.8585939	0.9234206	2491.6762695	1791.2987061	1.0476263
0.0000000	0.0000000	14.2879915	4094.7966309	8.1106453	0.9252781	2572.5864258	1792.0915527	1.0476851
0.0000000	0.0000000	13.2773743	4178.2626953	8.3627939	0.9269560	2653.5886230	1792.8601074	1.0477330
0.0000000	0.0000000	12.2663708	4261.7294922	8.6150398	0.9286085	2734.6833496	1793.6041260	1.0477804
0.0000000	0.0000000	11.2549753	4345.1958008	8.8673830	0.9301942	2815.8708496	1794.2998047	1.0477626
0.0000000	0.0000000	10.2431908	4428.6611328	9.1198235	0.9317380	2897.1518555	1794.9866455	1.0505028
0.0000000	0.0000000	9.2310162	4530.2026367	9.3723612	0.9331828	2978.5246582	1814.8923340	1.0589705
0.0000000	0.0000000	8.2184458	4627.2260742	9.6249962	0.9345839	3059.9904785	1829.8858643	1.0673077
37.4244499	2282.8571777	7.2054539	4724.2490234	9.8777285	0.9358537	3141.5490723	1844.7709961	1.0755750
2.3380985	0.8002161	6.1921477	4821.2675781	10.1305580	0.9372663	3223.2009277	1849.5408936	1.0837693
734.0267334	2052.3095703	5.1784174	4946.1899414	10.3834858	0.9385343	3304.9455566	1903.9270020	1.1092113
1.2105638	36.4228096	4.1642842	5074.6010742	10.6365099	0.9397605	3386.7832031	1951.8319092	1.1366829
2360.2666016	2.5880079	3.1497757	5233.4492188	10.8896313	0.9409473	3468.7133789	2031.8845215	1.1828480
0.8184359	813.9075928	2.1348122	5407.5170898	11.1428509	0.9420971	3550.7370605	2127.8156738	1.2382176
2007.8551025	1.1838808	1.1195480	5598.5356445	11.3961668	0.9432219	3632.8537598	2238.1667480	1.3019325
35.4227764	2437.6630859	0.1038794	5804.2978516	11.6495810	0.9442915	3715.0629883	2370.8225098	1.3785683
2.8380156	0.8333747	-0.9121993	6027.3769531	11.9030933	0.9453406	3797.3662109	2517.1223145	1.4630758
892.8806152	1971.6217041	-1.9286636	6268.0263672	12.1567011	0.9463597	3879.7619629	2682.1262207	1.5583860
1.3620642	34.4183540	-2.9455230	6493.4599609	12.4104071	0.9473847	3962.2514648	2830.4008789	1.6439064

Run B8

Table IV

INTER IN	SPH D IN	WIRE D IN	EL TEMP C	DEPTH IN	HT ST CM	SOR	UPDN	VEL CPS	DATA CALC	CH SP	CPM E	MARK CM	F	TANK IN
7.72500	0.99970	0.00410	21.13000	21.76880	24.97000	1.00000	1.00000	0.38195	17	60	0.33333	16.52000		8.48750

R1	R2	DYNES P VOLT	CH FULL SCALE	CH WIDTH CM	WALL FACTOR	TANK D IN	CH VEL FACTOR
0.300000E-01	0.100000E+01	0.199800E+07	0.100000E-02	0.252000E+02	0.210440E+01	0.150000E+02	0.301500E+01

Z1	Z2	Z3	VISCOSITY	DENSITY	LAMDA
-0.188397E+03	0.110557E+04	-0.160404E+08	0.336611E+02	0.970885E+00	0.289602E-03

Y1	Y2	Y3	VIS LOWER	RHO LOWER	GAMMA
0.229832E+00	-0.494493E+04	0.103427E+07	0.974832E-02	0.997954E+00	0.371100E+02

REYNOLDS NO.	1/CAPILLARY NO.	BOND NO./CAP NO.	STOKES DRAG
0.139870288E-01	0.288636721E+01	0.332588655E+01	0.312270028+03

POSITION	HEIGHT	DIST TO INTER	TOTAL FORCE	WIRE LEN IN	RATIO	WIRE DRAG	SPHERE DRAG	SCALED DRAG
2.0000000	18.1499996	15.4178881	432.4744483	5.8393211	0.9216189	155.9741364	290.0962134	1.0050969
10.0000000	15.9200001	15.1459496	437.7775269	6.9682493	0.9219244	159.6360168	292.7914649	1.0131083
12.0000000	15.2200003	14.8976612	443.0803223	6.0973554	0.9222343	163.3120575	294.7397461	1.0185397
13.0000000	14.7799997	14.6540247	448.3833008	6.2263345	0.9225492	167.0021820	296.6082458	1.0236005
14.0000000	14.2900000	14.4100323	453.6861267	6.3553066	0.9228665	170.7065277	298.4526978	1.0285645
14.8000000	13.9600000	14.1706494	458.9890137	6.4843744	0.9231872	174.4250641	300.2769775	1.0334496
15.0000000	13.5800002	13.9269924	464.2918701	6.6155343	0.9235106	178.1578522	302.0815735	1.0382450
14.5000000	13.1099997	13.6859436	469.5948181	6.7455196	0.9238369	181.9048309	303.8666687	1.0429661
16.0000000	12.4899998	13.3005409	474.8976746	6.8756819	0.9243789	185.6661072	305.5134583	1.0471996
16.5000000	11.7799997	13.0797863	480.2005615	7.0060201	0.9247081	189.4416504	307.2591248	1.0517601
17.0000000	10.7400002	12.8184938	485.5034790	7.1363337	0.9248284	193.2314606	309.1052551	1.0566917
17.5000000	9.4499998	12.5677204	490.8063354	7.2672248	0.9251624	197.0356445	310.8127441	1.0610569
18.0000000	7.9299998	12.2984497	496.1092529	7.3980908	0.9254979	200.8541107	312.5912170	1.0653852
18.5000000	6.2700000	12.0332451	501.4120483	7.5291338	0.9258347	204.6869507	314.1704407	1.0696365
19.0000000	4.4399998	11.7707272	506.7149963	7.6603532	0.9261723	208.5341492	315.8209534	1.0738127
19.5000000	2.5200000	11.5078583	512.0179443	7.7917485	0.9265107	212.3957520	317.4524757	1.0779136
20.0000000	0.5000000	11.2446346	517.3207397	7.9233208	0.9268499	216.2717743	319.0650635	1.0819386
22.0000000	7.0500002	10.9815698	522.6237183	8.0550690	0.9271897	220.1622162	320.6589966	1.0858902
112.4000015	6.4499998	10.7171335	527.9264526	8.1869926	0.9275302	224.0671082	322.2336731	1.0897659
0.0000000	0.0000000	10.4528427	533.2294312	8.3190937	0.9278706	227.9864807	323.7901001	1.0935696
0.0000000	0.0000000	10.1882200	538.5324097	8.4513693	0.9282072	231.9203339	325.2055054	1.0968877
0.0000000	0.0000000	9.9232340	543.8351440	8.5838232	0.9285523	235.8687134	326.8467407	1.1009575
0.0000000	0.0000000	9.6578570	549.1381226	8.7164516	0.9288930	239.8315735	328.3474426	1.1045439
0.0000000	0.0000000	9.3923662	554.4410400	8.8492575	0.9292347	243.8090363	329.8286438	1.1080541
0.0000000	0.0000000	9.1261625	559.7438354	8.9822388	0.9295738	247.8010712	331.2930603	1.1115007
0.0000000	0.0000000	8.8607479	565.0466919	9.1153965	0.9301094	251.8076324	332.6164736	1.1144449
0.0000000	0.0000000	8.5930204	570.3496094	9.2487307	0.9302533	255.8288269	334.1653442	1.1181757
0.0000000	0.0000000	8.3259192	575.6523682	9.3822412	0.9305924	259.8646545	335.6595093	1.1220305
0.0000000	0.0000000	8.0584460	580.7626953	9.5159273	0.9309309	263.9151001	338.9058838	1.1310503
0.0000000	0.0000000	7.7906494	589.4209595	9.6497898	0.9312685	267.9802246	341.7328796	1.1389846
15.4178848	432.4744873	7.5225019	596.6793823	9.7838287	0.9316058	272.0600586	344.5466919	1.1468338
6.8393211	0.9216189	7.2539911	602.7376099	9.9180441	0.9319423	276.1545715	347.3290100	1.1545981
155.9741364	290.0962134	6.9852734	609.0958557	10.0524368	0.9322774	280.2638550	350.0986023	1.1622796
1.0050969	15.1459496	6.7159100	616.0543213	10.1870041	0.9326122	284.3878479	352.8489990	1.1698774
437.7775269	5.9682493	6.4463470	623.8560669	10.3217478	0.9329460	288.5265198	356.8038635	1.1814437
0.9219244	159.6360168	6.1764712	632.2246094	10.4566669	0.9333787	292.6800232	361.3501723	1.1949362
292.7915649	1.0131083	5.9061475	640.5950317	10.5917635	0.9336104	296.8483582	365.8764648	1.2083261
14.8976612	443.0803223	5.6355705	649.2825928	10.7270365	0.9339411	301.0314636	370.7218933	1.2227343
6.0973554	0.9222343	5.3646611	658.6043091	10.8624859	0.9342715	305.2294617	376.2256671	1.2392715
163.3120575	294.7397461	5.0932293	667.9259644	10.9981108	0.9346003	309.4423218	381.7085266	1.2557011
1.0185397	14.6360247	4.8215251	677.2476196	11.1339121	0.9349473	313.6699524	387.1544800	1.2719694
448.3833008	6.2266345	4.5494890	689.8032837	11.2698889	0.9352525	317.9125366	396.0697632	1.2995700
0.9225492	167.0021820	4.2770996	703.3736877	11.4060431	0.9355774	322.1700439	406.0304260	1.3305292
296.6082458	1.0236005	4.0043373	718.9731445	11.5423737	0.9359010	326.4425049	418.1353455	1.3684260
14.3940125	453.6861267	3.7312629	735.3336182	11.6788797	0.9362234	330.7299194	431.6278320	1.4087981
6.3553066	0.9228665	3.4578156	752.0744629	11.8155622	0.9365445	335.0322876	444.3009644	1.4503106
170.7065277	298.4526978	3.1840164	768.8144836	11.9524202	0.9368644	339.3495789	456.8960022	1.5196613
1.0285645	14.1706494	2.9098842	800.3950806	12.0894556	0.9371828	343.6819763	486.6025085	1.5843125
454.9890137	6.4843744	2.6353583	827.4080505	12.2266674	0.9375278	348.0293884	510.7242432	1.6607132
0.9231872	174.4250641	2.3605018	862.2858887	12.3640547	0.9378440	352.3918457	543.2221680	1.7641318
300.2769775	1.0334496	2.0852909	901.0946655	12.5016184	0.9381588	356.7694092	579.8724976	1.880733
13.8609924	464.2918701	1.8097290	940.9309937	12.6393585	0.9384263	361.1619568	628.2882080	2.0351570
6.4155343	0.9234106	1.5338145	1003.4435059	12.7772741	0.9387387	365.5694611	679.4453735	2.198 555
178.1578522	302.0815735	1.2575458	1061.2751465	12.9153671	0.9390483	369.9922523	736.2256638	2.378 7453
1.0382458	11.6009436	0.9809262	1122.6885986	13.0536356	0.9393779	374.4305420	796.7054171	2.57.8327
469.5948181	6.7455196	0.7039539	1185.8173828	13.1920795	0.9396817	378.8836060	859.0480957	2.7684767
0.9238369	181.9048309	0.4266274	1255.8254395	13.3307018	0.9399877	383.3519897	928.6159058	2.9888725
303.8666687	1.0429661	0.1489864	1326.7208811	13.4694986	0.9402924	387.8355408	999.0659790	3.2115450
13.3855400	474.8976746	-0.1200811	1399.3917236	13.6084728	0.9407451	392.3343506	1071.1066791	3.4387574
6.8756819	0.9243789	-0.4074635	1474.8527832	13.7476215	0.9410458	396.8482971	1146.2747803	3.6754270
185.6661072	305.5134583	-0.6861084	1551.7087402	13.8869476	0.9413451	401.3775940	1222.8615723	3.9160390

Run C4

Table V

INTER IN	SPH C IN	WIRE D IN	EL TEMP C	TDEPTH IN	HT ST CM	SOR	UPDN	VEL CPS	DATA CALC CH S	CPM E	MARK CM E	TANK IN
7.72500	0.37460	0.00410	20.93000	21.76880	19.32000	1.00000	1.00000	0.37235	15 30	0.33333	17.57000	7.07500

R1	R2	DYNES P VOLT	CH FULL SCALE	CH WIDTH CM	WALL FACTOR	TANK D IN	CH VEL FACTOR
0.300000E-01	0.250000E+02	0.159800E+07	0.100000E-02	0.252000E+02	0.210440E+01	0.150000E+02	0.101500E+01

Z1	Z2	Z3	VISCOSITY	DENSITY	LAMDA
-0.188307E+03	0.110957E+06	-0.160404E+08	0.338098E+02	0.971064E+00	0.289722E-03

V1	V2	V3	VIS LOWER	RHO LOWER	GAMMA
0.229832E+00	-0.494493E+04	0.103427E+07	0.979544E-02	0.997996E+00	0.371100E+02

REYNOLDS NO.	1/CAPILLARY NO.	BOND NO./CAP NO.	STOKES DRAG
0.508770538E-02	0.294782908E+01	0.474514078E+00	0.113559818E+03

POSITION	HEIGHT DIST TO INTER	TOTAL FORCE	WIRE LEN IN	RATIO	WIRE DRAG	SPHERE DRAG	SCALED DRAG
10.0000000	13.1199999	15.3612204	393.1587219	10.9793444	0.9419500	299.0561218	115.1659698	1.0443979
12.0000000	12.0799999	14.6234887	398.5804444	11.1174850	0.9427051	303.1199341	116.7746735	1.0579342
14.0000000	12.1599998	13.8854266	404.0022583	11.2557611	0.9433264	307.1949463	118.1725769	1.0695301
14.0000000	11.4455997	13.1464772	409.4240723	11.3941765	0.9448000	311.2811890	119.1542511	1.0773518
14.5000000	11.5200005	12.4068944	414.8459167	11.5327272	0.9455110	315.3786926	120.4622803	1.0880996
15.0000000	10.8499999	11.6663302	420.2676697	11.6714163	0.9462006	319.4874573	121.7669100	1.0987417
15.5000000	9.4300003	10.9250345	425.6894226	11.8102427	0.9468819	323.6074829	123.0443115	1.1092252
16.0000000	8.7100000	10.1831007	432.0729675	11.9492064	0.9475508	327.7388611	124.3296051	1.1207109
16.5000000	7.9999995	9.4404373	438.9004517	12.0883074	0.9482077	331.8814697	128.0686035	1.1522404
17.0000000	6.2199998	8.6970466	445.7278748	12.2275457	0.9488543	336.0354004	130.7918243	1.1755816
17.5000000	5.8200000	7.9529128	453.4007874	12.3669205	0.9494873	340.2006531	134.3416016	1.2067478
18.0000000	7.2000002	7.2080498	461.0736063	12.5064335	0.9500707	344.3771973	138.7960663	1.2450711
18.5000000	6.6999998	6.4624534	470.2686157	12.6460838	0.9506442	348.5651550	143.1629639	1.2829823
19.0000000	8.1999997	5.7161255	480.0341187	12.7858715	0.9512074	352.7644653	148.9126740	1.3331993
19.5000000	9.5500002	4.9690633	492.0824890	12.9257956	0.9518824	356.9751282	157.0411072	1.4045935
97.8000031	7.1399999	4.2212691	507.3015137	13.0658579	0.9525009	361.1971741	168.4585114	1.5052357
139.3999939	6.8400002	3.4727423	525.8181152	13.2060566	0.9530742	365.4304810	183.3302307	1.6365165
0.0000000	0.0000000	2.7234812	543.5294189	13.3463936	0.9536381	369.6753845	207.8146820	1.8532652
0.0000000	0.0000000	1.9734879	562.0017090	13.4868670	0.9541973	373.9315491	233.0544739	2.0763254
0.0000000	0.0000000	1.2227615	610.9340820	13.6274776	0.9546193	378.1991577	258.8273621	2.3036847
0.0000000	0.0000000	0.4712993	660.2568970	13.7682266	0.9551538	382.4782410	284.8815918	2.5331073
0.0000000	0.0000000	-0.2808911	674.5208130	13.9091120	0.9557920	386.7687683	315.9893494	2.8069739
0.0000000	0.0000000	-1.0338192	714.2807007	14.0501356	0.9563282	391.0707092	352.8643494	3.1314895
0.0000000	0.0000000	-1.7874747	736.7921143	14.1912956	0.9568749	395.3841248	371.6795044	3.2952576
0.0000000	0.0000000	-2.5418496	753.3428955	14.3325939	0.9573409	399.7091064	384.2329407	3.4032457
0.0000000	0.0000000	-3.2970023	761.3751221	14.4740276	0.9578397	404.0453796	387.8697205	3.4321246
0.0000000	0.0000000	-4.0529827	744.4331970	14.6156006	0.9583336	408.3933105	366.4786377	3.2396989
0.0000000	0.0000000	-4.8094459	718.6560059	14.7573109	0.9588177	412.7527771	339.7918701	2.9478879
0.0000000	0.0000000	-5.5667672	679.6995239	14.8991566	0.9592928	417.1236877	288.4372559	2.5448732
0.0000000	0.0000000	-6.3248262	638.1853027	15.0411415	0.9597651	421.5060425	240.4487305	2.1194217
15.3612204	393.1587219	-7.0836148	594.8111572	15.1832628	0.9602304	425.9000549	190.5591583	1.6780510

Run C11

Table VI

INTER IN	SPH D IN	WIRE D IN	FL TEMP C	TDEPTH IN	HT ST CM	SOR	UPDN	VEL CPS	DATA CALC	CM SP	CPM E	MARK CM E	TANK IN
13.03125	0.99970	0.00410	20.31000	30.01875	25.58000	1.00000	1.00000	0.37967	13	40	0.33333	21.90000	13.94688

P1	P2	DYNES P VOLT	CM FULL SCALE	CM WIDTH CM	WALL FACTOR	TANK D IN	CM VEL FACTOR
0.300000E-01	0.100000E+01	0.198800E+07	0.100000E-02	0.252000E+02	0.210440E+01	0.150000E+02	0.101500E+01

Z1	Z2	Z3	VISCOSITY	DENSITY	LAMDA
0.141693E+02	-0.139222E+00	0.320347E+07	0.907083E+02	0.872044E+00	0.831239E+00

Y1	Y2	Y3	VIS LOWER	RHO LOWER	GAMMA
-0.716203E+02	0.424111E+00	-0.597960E+07	0.320088E+02	0.971621E+00	0.194000E+01

REYNOLDS NO.	1/CAPILLARY NO.	BOND NO./CAP NO.	STOKES DRAG
0.828977277E-02	0.100766222E+00	0.817040546E+01	0.460085396E+03

POSITION	HEIGHT	DIST TO INTER	TOTAL FORCE	WIRE LEN IN	RATIO	WIRE DRAG	SPHERE DRAG	SCALED DRAG
2.0000000	14.7400002	17.6914387	712.7587280	6.8445845	0.9243006	279.5779114	460.5475769	1.0587494
3.0000000	10.5799999	17.2827892	723.0546875	7.0488482	0.9346048	284.2113342	464.0002747	1.0651506
4.0000000	9.6000004	16.8734436	733.3505840	7.2534075	0.9351270	292.8404016	466.0674438	1.0683575
16.0000000	9.0699997	16.4637203	743.6464844	7.4582596	0.9256523	301.5550220	467.9948730	1.0712353
17.0000000	8.4200001	16.0533447	753.9424438	7.6634054	0.9261802	310.3253479	469.8692954	1.0739744
17.5000000	7.9899998	15.6422949	764.2382813	7.8688468	0.9267095	319.1015930	471.6857300	1.0765916
18.0000000	7.8100002	15.2305714	774.5342407	8.0744840	0.9272401	327.9134827	473.4572144	1.0790899
18.5000000	6.9499998	14.8185148	784.8302002	8.2806158	0.9277715	336.7613831	475.1798401	1.0814698
19.0000000	6.7399998	14.4057436	795.1260376	8.4869394	0.9284983	345.6450500	476.8742249	1.0833262
19.5000000	5.7399999	13.9923401	805.4219360	8.6935587	0.9288342	354.5647888	478.4810181	1.0858822
20.0000000	4.0500002	13.5784292	815.7178955	8.9004726	0.9293647	363.5205078	480.0662842	1.0879173
20.5000000	2.0999999	13.1638908	826.0138550	9.1076794	0.9300903	372.5122986	481.4953995	1.0894167
21.0000000	-0.8000000	12.7487412	836.3096924	9.3151817	0.9304222	381.5402527	483.0775452	1.0916511
60.2400017	6.9600000	12.3330431	846.6056519	9.5229788	0.9309486	390.6043396	484.5163269	1.0933524
101.4499969	6.6900001	11.9167366	856.9016724	9.7310696	0.9314732	399.7045898	485.9088440	1.0949448
0.0000000	6.0000000	11.4998407	867.1975098	9.9394550	0.9319943	408.8411865	487.2550354	1.0964284
0.0000000	0.0000000	11.0823574	877.4934082	10.1481342	0.9325157	418.0140991	488.5556946	1.0978055
0.0000000	0.0000000	10.6642838	887.7893066	10.3571081	0.9330332	427.2233582	489.8119736	1.0992767
0.0000000	0.0000000	10.2456207	898.0852661	10.5663767	0.9337284	436.4691467	490.8348999	1.0998261
0.0000000	0.0000000	9.8263693	908.3811646	10.7759399	0.9340603	445.7512817	492.1851807	1.1013037
0.0000000	0.0000000	9.4065285	918.6770020	10.9857969	0.9345693	455.0699768	493.3049927	1.1022621
0.0000000	0.0000000	8.9861012	928.9730225	11.1959476	0.9350896	464.4252625	494.3649902	1.1030843
0.0000000	0.0000000	8.5650816	939.2689209	11.4063940	0.9355782	473.8172302	495.4104614	1.1038719
0.0000000	0.0000000	8.1434765	949.5647583	11.6171341	0.9360779	483.2458191	496.3963318	1.1045247
0.0000000	0.0000000	7.7212796	959.8606567	11.8281679	0.9365742	492.7110901	501.3514099	1.1139953
0.0000000	0.0000000	7.2984848	970.1566162	12.0394974	0.9370670	502.2133179	507.4099792	1.1250004
0.0000000	0.0000000	6.8751211	980.4525146	12.2511206	0.9375842	511.7523193	512.5883179	1.1357970
0.0000000	0.0000000	6.4511580	990.7484131	12.4630384	0.9380707	521.3281860	518.1484985	1.1465236
0.0000000	0.0000000	6.0266061	1001.0443115	12.6752510	0.9385081	530.9410400	524.5233765	1.1590207
0.0000000	0.0000000	5.6014557	1011.3403320	12.8877573	0.9389865	540.5906982	531.2712402	1.1723062
17.6914387	712.7587280	5.1757150	1021.6362915	13.1005583	0.9394822	550.2775879	539.9691772	1.1898320
6.8445845	0.9243006	4.7494173	1031.9321289	13.3136539	0.9399502	560.0017090	550.4457703	1.2113073
279.5779114	460.5475769	4.3225098	1042.2280273	13.5270433	0.9404182	569.7626343	563.7371826	1.2388011
1.0587494	17.2827892	3.8950133	1052.5239258	13.7407274	0.9410310	579.5609741	581.8358765	1.2768124
723.0546875	7.0488482	3.4669094	1062.8198242	13.9547052	0.9414901	589.3964844	603.6980591	1.3229668
0.9346048	284.2113342	3.0382080	1073.1157227	14.1689787	0.9419445	599.2692871	631.5235596	1.3820447
464.0002747	1.0651506	2.6089091	1083.4116211	14.3835449	0.9423963	609.1794434	669.6358276	1.4621303
16.8735657	733.3505840	2.1790125	1093.7075195	14.5984058	0.9428445	619.1269531	720.2911377	1.5719900
7.2534075	0.9351270	1.7485201	1104.0034180	14.8135620	0.9431519	629.1120605	796.3684814	1.7349937
292.8804016	466.0674438	1.3174202	1114.2993164	15.0290127	0.9437299	639.1345825	912.7741699	1.9866321
1.0683575	16.4637203	0.8856511	1124.5952148	15.2447577	0.9441746	649.1947021	1086.9492188	2.3624945

Run D2

Table VII

INTER IN	SPH D IN	WIRE D IN	FL TEMP C	TDEPTH IN	HT ST CM	SOR	UPON	VEL CPS	DATA CALC CH	SP CPM E	MARK CM E	TANK IN
13.83125	0.49900	0.00410	20.98000	30.01875	14.09000	1.00000	1.00000	0.68097	10	40	0.33333	10.13000	14.02500

P1	P2	DYNES P VOLT	CH FULL SCALE	CH WIDTH CM	WALL FACTOR	TANK D IN	CH VEL FACTOR
0.300000E-01	0.160000E+02	0.199800E+07	0.100000E-01	0.252000E+02	0.210440E+01	0.150000E+02	0.101500E+01

Z1	Z2	Z3	VISCOSITY	DENSITY	LAMDA
0.141693E+02	-0.139222E+05	0.320347E+07	0.476975E+02	0.871715E+00	0.662259E+00

Y1	Y2	Y3	VIS LOWER	RHO LOWER	GAMMA
-0.716203E+02	0.424111E+05	-0.597960E+07	0.315881E+02	0.971020E+00	0.194000E+01

REYNOLDS NO.	1/CAPILLARY NO.	BOND NO./CAP NO.	STOKES DRAG
0.78869220E-02	0.59728429E-01	0.12033294E+01	0.38940945E+03

POSITION	HEIGHT	DIST TO INTER	TOTAL FORCE	WIRE LEN IN	RATIO	WIRE DRAG	SPHERE DRAG	SCALED DRAG
1.0000000	12.7600002	34.6605186	843.3887939	7.2902002	0.9190114	517.6331787	385.2939758	1.0062240
8.0000000	12.0500002	33.7122274	862.1536255	7.5253019	0.9208955	534.5531006	387.9497681	1.0127301
9.0000000	11.9400003	33.5244141	886.0184570	7.7600047	0.9224969	551.4942017	384.5516663	1.0164808
10.0000000	11.8000002	31.8324375	899.6883179	7.9958057	0.9244232	568.4566040	391.1005859	1.0200900
10.5000000	11.6899996	30.8888427	918.4486694	8.2312088	0.9260628	585.4404297	392.6508789	1.0236996
11.0000000	11.5699997	29.9450474	937.2133789	8.4667110	0.9276459	602.4454956	394.1758423	1.0272404
11.5000000	11.3400002	29.0007572	955.9782104	8.7023115	0.9291645	619.4717407	395.6878052	1.0307403
12.0000000	11.0000000	28.0560627	974.7431134	8.9380121	0.9305848	636.5192261	397.7927246	1.0357891
12.3299999	10.8899999	27.1109695	993.5084229	9.1738129	0.9320363	653.5882568	398.6564941	1.0375993
13.6700001	10.7900000	26.1654778	1012.2731934	9.4097137	0.9333947	670.6785889	400.1129761	1.0409498
13.5000000	9.7700000	25.2198877	1031.0379639	9.6457129	0.9347071	687.7898560	401.5486450	1.0442437
40.0999985	3.7300000	24.2737966	1048.8034668	9.8818130	0.9359753	704.9228516	402.9644165	1.0474828
0.0000000	0.0000000	23.3286018	1068.5682373	10.1180134	0.9372022	722.0770264	404.3582764	1.0506625
0.0000000	0.0000000	22.3795109	1087.3330078	10.3543119	0.9383904	739.2525024	405.7301025	1.0537821
0.0000000	0.0000000	21.4320221	1106.0980225	10.5907106	0.9395416	756.4494629	407.0800781	1.0568423
0.0000000	0.0000000	20.4841328	1124.8632813	10.8272085	0.9406582	773.6676636	408.4079590	1.0598418
0.0000000	0.0000000	19.5358429	1143.6280518	11.0638075	0.9417422	790.9073486	409.7113037	1.0627768
0.0000000	0.0000000	18.5871525	1162.3929443	11.3005066	0.9427811	808.1683960	410.9708252	1.0655949
0.0000000	0.0000000	17.6380634	1181.1577148	11.5373030	0.9438283	825.4508057	412.2353516	1.0684236
0.0000000	0.0000000	16.6885738	1199.9230957	11.7742046	0.9448113	842.7546387	413.4852295	1.0712121
0.0000000	0.0000000	15.7386827	1218.6878662	12.0111990	0.9457787	860.0800781	414.6955566	1.0738955
0.0000000	0.0000000	14.7883930	1237.4527588	12.2482958	0.9467412	877.4266968	415.8536377	1.0764415
0.0000000	0.0000000	13.8377056	1256.2175293	12.4854927	0.9476744	894.7947998	416.9934082	1.0789381
0.0000000	0.0000000	12.8866177	1274.9822998	12.7227888	0.9485689	912.1844482	418.1301880	1.0814248
0.0000000	0.0000000	11.9351273	1293.7712402	12.9601860	0.9494396	929.5955200	419.2762146	1.0839179
0.0000000	0.0000000	10.9832401	1315.9718018	13.1976814	0.9502904	947.0279541	423.9736938	1.0956174
0.0000000	0.0000000	10.0309534	1338.1727295	13.4352770	0.9510831	964.4819336	428.7025146	1.1073725
0.0000000	0.0000000	9.0782623	1360.3737793	13.6729727	0.9518342	981.9572754	433.4357605	1.1191292
0.0000000	0.0000000	8.1251793	1383.6457520	13.9107676	0.9526258	999.4542847	439.1746521	1.1334714
0.0000000	0.0000000	7.1716024	1407.6906433	14.1486626	0.9534560	1016.9727783	445.6104431	1.1495996
34.6605186	843.3887939	6.2176063	1431.7476807	14.3866577	0.9542173	1034.5125732	452.0920715	1.1658325
7.2902002	0.9190114	5.2631207	1458.3239746	14.6247520	0.9549984	1052.0740967	461.7659607	1.1902803
517.6331787	385.2939758	4.3088341	1499.0255127	14.8629456	0.9557249	1069.6569824	485.6205139	1.2512456
1.0062240	53.7122274	3.3537490	1541.3471680	15.1012392	0.9563769	1087.2614746	514.5363464	1.3148929
862.1536255	7.5253019	2.3982617	1585.7491455	15.3396330	0.9570493	1104.8875732	538.1319580	1.3853860
0.9208955	534.5531006	1.4423791	1659.4212158	15.5781260	0.9577449	1122.5349121	596.4413452	1.5348580
387.9497681	1.0127301	0.4860939	1745.1425781	15.8167200	0.9584078	1140.2043457	666.8004150	1.7151998
32.7755318	880.9184570	-0.4709898	1870.9470215	16.0554123	0.9590568	1157.8968975	779.0469360	2.0035928
7.7605547	0.9226559	-1.4276748	1981.0606689	16.2942047	0.9596934	1175.6072998	874.7730713	2.2482853
551.4942017	389.5516663	-2.3841598	2049.0878906	16.5331963	0.9603162	1193.3410645	926.5330200	2.3813215
1.0164808	31.8324375	-3.3430440	6544.1904297	16.7720890	0.9609059	1211.0965576	5585.4462891	14.3433762

Run D8

Table VIII

INTER IN	SPH D IN	WIRE D IN	FL TEMP C	TDEPTH IN	HT ST CM	SOR	UPDN	VEL CPS	DATA CALC	CH SP CPN	E MARK C	E TANK IN
13.83125	0.49900	0.00410	20.98000	30.01875	24.01000	1.00000	1.00000	0.54978	12	40	0.33333	13.14000	14.82500

P1	P2	DYNES P VOLT	CH FULL SCALE	CH WIDTH CM	WALL FACTOR	TANK D IN	CH VEL FACTOR
0.3000000E-01	0.1600000E+02	0.1498800E+07	0.1000000E-02	0.2520000E+02	0.2104440E+01	0.1900000E+02	0.1801500E+01

Z1	Z2	Z3	VISCOSITY	DENSITY	LAMDA
0.1416935+02	-0.1392225+05	0.3203675+07	0.6769755+02	0.8717155+00	0.6622595+00

Y1	Y2	Y3	VIS LOWER	RHO LOWER	GAMMA
-0.7162035+02	0.4241115+05	-0.5979605+07	0.3158815+02	0.9710205+00	0.1940005+01

REYNOLDS NO.	1/CAPILLARY NO.	BOND NO./CAP NO.	STOKES DRAG
0.6367586615-02	0.7397999075-01	0.1490449335+01	0.3134023465+03

POSITION	HEIGHT	DIST TO INTER	TOTAL FORCE	WIRE LEN IN	RATIO	WIRE DRAG	SPHERE DRAG	SCALED DRAG
2.0000000	17.9300003	34.3723984	702.6126709	7.3620863	0.9189882	426.5124817	325.9736023	1.0433601
10.0000000	7.7500000	33.5048866	716.1315918	7.5785303	0.9213099	439.0862427	327.0290527	1.0466624
11.0000000	7.0700002	32.6373100	729.6505737	7.7949905	0.9229528	451.6628418	327.7470398	1.0488784
12.0000000	6.3000002	31.7696629	743.1694946	8.0114689	0.9244350	464.2424927	328.4371033	1.0510045
12.5000000	5.9400002	30.9019566	756.6883545	8.2279634	0.9260414	476.8250122	329.1447144	1.0531867
13.0000000	5.3099998	30.0341702	770.2072754	8.4444742	0.9274992	489.4105530	329.8496094	1.0553594
13.5000000	4.6399999	29.1663189	783.7261963	8.6610031	0.9289024	501.9989014	330.5596008	1.0575486
14.0000000	3.7700000	28.2984028	797.2451172	8.8775482	0.9302567	514.5902710	331.2714844	1.0597434
14.3799999	2.9600000	27.4304199	810.7640381	9.0941105	0.9315856	527.1846313	331.9655762	1.0618806
14.6599998	1.8900000	26.5623627	824.2830200	9.3106909	0.9328302	539.7819214	332.6987000	1.0641426
15.0000000	0.3800000	25.6942444	837.8019790	9.5272865	0.9340544	552.3820801	333.4128723	1.0663435
15.1799991	-0.6000000	24.8260536	851.3206787	9.7438993	0.9352397	564.9852295	334.1268921	1.0685437
14.2000008	4.6300001	23.9577961	864.8397217	9.9605303	0.9363886	577.5913696	334.8404236	1.0707418
85.9599991	4.6199999	23.0894756	878.3585205	10.1771755	0.9374933	590.2003174	335.5525208	1.0729351
0.0000000	0.0000000	22.2210827	891.8775635	10.3938398	0.9385853	602.8123169	336.2631836	1.0751235
0.0000000	0.0000000	21.3526211	905.3964233	10.6105213	0.9396364	615.4273071	336.9716797	1.0773046
0.0000000	0.0000000	20.4840946	918.9152222	10.8272181	0.9406582	628.0451660	337.6779480	1.0794783
0.0000000	0.0000000	19.6154995	932.4342651	11.0439329	0.9416523	640.6660156	338.3816833	1.0816433
0.0000000	0.0000000	18.7468357	945.9531860	11.2606649	0.9426194	653.2897949	339.0833130	1.0838015
0.0000000	0.0000000	17.8781013	959.4721069	11.4774141	0.9435609	665.9165039	339.7599792	1.0858794
0.0000000	0.0000000	17.0093040	972.9909058	11.6941786	0.9444783	678.5460205	340.4269592	1.0880860
0.0000000	0.0000000	16.1404362	986.5099487	11.9109612	0.9453727	691.1787720	341.1688843	1.0902120
0.0000000	0.0000000	15.2715015	1000.0288696	12.1277609	0.9462448	703.8142090	341.8577881	1.0923283
0.0000000	0.0000000	14.4025011	1013.5476685	12.3445759	0.9471163	716.4527588	342.5196228	1.0943579
0.0000000	0.0000000	13.5334291	1027.0667725	12.5614090	0.9479631	729.0941772	343.1825256	1.0963899
0.0000000	0.0000000	12.6642933	1040.5856934	12.7782593	0.9487731	741.7385864	344.3632813	1.1000762
0.0000000	0.0000000	11.7950869	1054.1047363	12.9951258	0.9496659	754.3858643	345.7505188	1.1044217
0.0000000	0.0000000	10.9258108	1067.6237793	13.2120104	0.9503410	767.0362549	347.1322327	1.1087486
0.0000000	0.0000000	10.0564709	1081.1427002	13.4289103	0.9510611	779.6895531	348.5081661	1.1174091
0.0000000	0.0000000	9.1870594	1094.6616211	13.6458292	0.9517425	792.3456421	349.8861938	1.1262295
34.3723984	702.6126709	8.3175812	1108.1806641	13.8627634	0.9524676	805.0048218	351.2661743	1.1350004
7.3620863	0.9189882	7.4480376	1121.6995850	14.0797148	0.9531770	817.6668701	352.6481628	1.1437317
426.5124817	325.9736023	6.5784235	1135.2185059	14.2966833	0.9539339	830.3319092	354.0321655	1.1524948
1.0433601	33.5048866	5.7087417	1148.7375488	14.5136690	0.9546159	842.9998169	355.4181824	1.1612877
716.1315918	7.5785303	4.8390040	1162.2565918	14.7306709	0.9552238	855.6707764	356.8062134	1.1701107
0.9213099	439.0862427	3.9691785	1175.7756348	14.9476900	0.9558148	868.3446655	358.1961670	1.1789637
327.0290527	1.0466624	3.0992808	1189.2946777	15.1647272	0.9565624	881.0216064	359.5880737	1.1878467
32.6373100	729.6505737	2.2293403	1202.8137207	15.3817797	0.9571911	893.7012329	360.9819336	1.1967590
7.7949905	0.9229528	1.3593186	1216.3327637	15.5988503	0.9578030	906.3840942	362.3777466	1.2057018
451.6628418	327.7470398	0.4892296	1229.8518066	15.8159370	0.9584057	919.0697632	363.7755127	1.2146738
1.0488784	31.7696629	-0.3809246	1243.3708496	16.0330410	0.9589965	931.7583008	365.1752319	1.2236753

Run D10

Table IX

INTER IN	SPH D IN	WIRE D IN	FL TEMP C	TDEPTH IN	HT ST CH	SOR	UPDN	VEL CPS	DATA CALC CH	SP CPM E	MARK CH E	TANK IN
5.37500	0.99970	0.00410	21.84000	21.41875	24.92000	1.00000	1.00000	0.39687	21	38	0.33333	32.84000	5.48750

R1	R2	DYNES P VOLT	CH FULL SCALE	CH WIDTH CM	WALL FACTOR	TANK D IN	CH VEL FACTOR
0.300000E-01	0.100000E+01	0.159800E+07	0.100000E-02	0.252000E+02	0.210440E+01	0.150000E+02	0.101500E+01

Z1	Z2	Z3	VISCOSITY	DENSITY	LAMDA
0.141493E+02	-0.139222E+05	0.320347E+07	0.441366E+02	0.871292E+00	0.714588E+01

Y1	Y2	Y3	VIS LOWER	RHO LOWER	GAMMA
-0.791993E+02	0.457984E+05	-0.646559E+07	0.315394E+03	0.971689E+00	0.194000E+01

REYNOLDS NO.	1/CAPILLARY NO.	BOND NO./CAP NO.	STOKES DRAG
0.994700 10E-02	0.110751445E+00	0.90540676E+01	0.41920038E+03

POSITION	HEIGHT DIST TO INTER	TOTAL FORCE	WIRE LEN IN	RATIO	WIRE DRAG	SPHERE DRAG	SCALED DRAG
2.0000000	15.4799994	29.3465623	527.1433716	0.8750515	0.9946954	32.7267456	518.6836717	1.2036577
3.0000000	16.1800003	28.6199570	513.5898606	1.2382154	0.9156637	46.3466524	483.6170284	1.1956972
4.0000000	16.3799999	27.8026926	509.8253174	1.6017380	0.9171782	60.0227547	464.5212708	1.1473533
6.0000000	16.2099991	27.1647186	507.6777258	1.9656162	0.9173954	73.7310181	448.2660217	1.1061151
8.0000000	15.7700005	26.4360218	513.6607056	2.3298550	0.9172311	87.4796371	441.1521301	1.0874926
10.0000000	15.0899998	25.7066135	524.1890259	2.6944494	0.9171116	101.2684631	438.8854065	1.0808438
14.0000000	16.9899998	24.9764862	535.2310181	3.0594044	0.9171496	115.0977402	437.0410767	1.0752473
27.0000000	9.7900000	24.2456474	547.3525391	3.4247141	0.9173908	128.9673157	436.2204590	1.0721776
28.0000000	9.2799997	23.5140915	561.3047791	3.7903824	0.9177267	142.8772888	437.2452087	1.0736455
29.0000000	8.6300001	22.7818222	574.2588501	4.1564064	0.9182265	156.8276672	438.1268616	1.0747594
30.0000000	7.7900000	22.0488338	589.2119751	4.5227909	0.9188353	170.8186188	438.8757019	1.0755455
30.5000000	7.2700000	21.3151264	603.1651611	4.8895350	0.9195118	184.8502197	439.5017395	1.0760295
31.0000000	6.6100001	20.5807495	617.1182251	5.2566328	0.9202788	198.9221802	440.0283203	1.0762695
31.3799999	6.0500002	19.8455353	631.0714111	5.6240902	0.9211185	213.0348816	440.4216003	1.0761831
31.6700001	5.3699999	19.1097260	645.0245972	5.9919043	0.9219810	227.1881714	440.7304993	1.0758909
32.0000000	4.4499998	18.3731384	658.9777222	6.3600769	0.9228745	241.3822021	440.9460144	1.0753715
32.3300018	3.2500000	17.6358337	672.9308472	6.7286081	0.9237943	255.6170197	441.0751343	1.0746427
32.4499969	1.3800000	16.8978786	686.8839722	7.0974960	0.9247288	269.8925171	441.1215820	1.0737140
32.4300018	0.1500000	16.1591644	700.8371582	7.4667425	0.9256742	284.2088623	441.0893250	1.0725958
30.2000007	6.5000000	15.4197330	714.7902832	7.8363476	0.9266255	298.5661621	440.9818420	1.0712968
69.1999969	6.4000001	14.6795902	730.7899628	8.2063074	0.9275800	312.9641418	443.0072327	1.0751771
0.0000000	0.0000000	13.9387283	747.5195313	8.5766277	0.9285338	327.4031982	445.7462158	1.0807800
0.0000000	0.0000000	13.1971512	764.2498779	8.9473047	0.9294846	341.8832397	448.4113464	1.0861933
0.0000000	0.0000000	12.4548378	780.9801636	9.3183403	0.9304302	356.4042969	451.0051575	1.0914232
0.0000000	0.0000000	11.7118502	797.7106323	9.6897326	0.9313693	370.9663086	453.5293579	1.0964750
0.0000000	0.0000000	10.9681263	814.4410400	10.0614834	0.9323003	385.5694580	455.9854126	1.1013525
0.0000000	0.0000000	10.2236872	831.1713257	10.4335909	0.9332219	400.2136841	458.3751526	1.1060606
0.0000000	0.0000000	9.4785318	848.9238892	10.8060570	0.9341336	414.8991089	461.2586365	1.1119499
30.1974472	658.8379102	8.7326607	868.5003662	11.1788807	0.9350488	429.6258240	467.0834656	1.1249117
0.1497985	-0.3413247	7.9860740	888.5776978	11.5522720	0.9359241	444.3937378	472.8866992	1.1377846
5.5913148	-1968.3426514	7.2387714	908.6552582	11.9256010	0.9368019	459.2028809	478.9680847	1.1503643
-4.8809800	30.0723305	6.4907627	930.7490845	12.2994986	0.9376955	474.0534668	486.3262634	1.1678951
564.7679138	0.5122461	5.7420187	957.0656738	12.6737528	0.9385046	488.9453430	498.5888062	1.1961991
0.8447273	19.1306305	4.9925494	989.6899414	13.0483666	0.9393661	503.8785706	517.4196777	1.2401925
617.7261719	1.4292804	4.2424035	1030.3147888	13.4233351	0.9401912	518.8533936	544.6981591	1.3043323
29.3466797	527.1433716	3.4915226	1078.2518311	13.7986631	0.9411567	533.8695679	579.4627686	1.3862559
0.8750515	0.9946954	2.7399256	1149.6186523	14.1743488	0.9419559	548.9272461	639.1655273	1.5276282
32.7267456	518.6836717	1.9876128	1268.8885498	14.5503922	0.9427447	564.0266113	749.5276489	1.7896938
1.2036577	28.6199570	1.2345845	1532.6849365	14.9267941	0.9435213	579.1674805	1012.8353271	2.4161127

Run E1

Table X

INTER IN	SPH D IN	WIRE D IN	FL TEMP C	DEPTH IN	HT ST CM	SOR	UPDN	VEL CPS	DATA CALC	CH SP CPM	E MARK CM	E TANK IN
5.37500	0.99970	0.00410	21.84000	21.41875	14.63000	1.00000	1.00000	0.65464	16	60	0.33333	13.10000	5.48750

P1	P2	DYNES P VOLT	CH FULL SCALE	CH WIDTH CM	WALL FACTOR	TANK D IN	CH VEL FACTOR
0.300000E-01	0.100000E+01	0.199800E+07	0.100000E-01	0.252000E+02	0.210440E+01	0.150000E+02	0.101500E+01

Z1	Z2	Z3	VISCOSITY	DENSITY	LAMDA
0.161693E+02	-0.139222E+05	0.320347E+07	0.641366E+02	0.871292E+00	0.714586E+01

Y1	Y2	Y3	VIS LOWER	RHO LOWER	GAMMA
-0.791993E+02	0.457984E+05	-0.646559E+07	0.315394E+03	0.971689E+00	0.194000E+01

REYNOLDS NO.	1/CAPILLARY NO.	BOND NO./CAP NO.	STOKES DRAG
0.16407421E-01	0.67143083E-01	0.54890299E+01	0.69400244E+03

POSITION	HEIGHT	DIST TO INTER	TOTAL FORCE	WIRE LEN IN	RATIO	WIRE DRAG	SPHERE DRAG	SCALED DRAG
1.0000000	13.0600004	19.9226017	995.5790405	5.5855885	0.9210097	346.1829529	680.8927612	1.0168529
8.0000000	12.4300003	19.5804643	1008.4203491	5.7566357	0.9214250	357.0007324	685.9212036	1.0229042
9.0000000	12.2600004	19.3379971	1021.2613474	5.9277878	0.9217842	367.8379211	688.1529541	1.0264485
10.0000000	12.2200003	19.0953819	1034.1022949	6.0990438	0.9222385	379.6943665	690.7076416	1.0296347
11.0000000	12.0600004	18.8526670	1046.9434814	6.2704048	0.9226563	389.5702515	693.2115596	1.0327407
11.5000000	11.9200001	18.7298761	1059.7844238	6.4418688	0.9230785	400.4654846	695.6765137	1.0357863
12.0000000	11.7799997	17.8662891	1072.6254883	6.6134357	0.9235065	411.3799438	698.1044922	1.0387725
12.3799999	11.6499994	17.6224456	1085.4667969	6.7851086	0.9239167	422.3140564	700.4952393	1.0416995
12.6700001	11.4200001	17.1791859	1098.3074951	6.9568844	0.9245839	433.2673950	702.5762329	1.0441629
13.0000000	11.0600004	16.8353271	1111.1486816	7.1287622	0.9248085	444.2400208	705.1688843	1.0473832
13.3299999	10.8100002	16.4913448	1123.9899902	7.3007469	0.9252403	455.2322388	707.4528198	1.0501413
13.6700001	9.6599997	14.7469893	1136.8308105	7.4728327	0.9256898	466.2436523	709.2702026	1.0528848
14.0000000	8.5200005	13.0026321	1149.6719971	7.6450243	0.9261329	477.2747803	711.9174194	1.0554945
14.1700001	7.9200001	12.1579599	1162.5131836	7.8173199	0.9266765	488.3251953	714.0999756	1.0580928
14.3299999	7.2800002	11.3120117	1175.3540039	7.9897165	0.9270213	498.3950500	716.2484131	1.0606371
14.5000000	6.7700005	10.7677994	1188.1951904	8.1622210	0.9274662	510.4845276	718.3646851	1.0631309
14.6400017	5.9600000	9.4224758	1201.0364990	8.3348265	0.9279113	521.5933838	720.4488525	1.0655740
66.7799988	3.8800001	4.9726510	1213.8770752	8.5075369	0.9285506	532.7217407	722.2265015	1.0676613
0.0000000	0.0000000	13.7312222	1226.7183838	8.6803493	0.9288003	543.8694458	724.5214844	1.0703105
0.0000000	0.0000000	13.3852825	1239.5596924	8.8532677	0.9292451	555.0368652	726.5095215	1.0726031
0.0000000	0.0000000	13.0391359	1252.4009399	9.0262890	0.9296900	566.2236938	728.4519043	1.0748258
0.0000000	0.0000000	12.6929016	1265.2416992	9.1994143	0.9301288	577.4301758	730.3983765	1.0770515
0.0000000	0.0000000	12.3462191	1278.0828857	9.3726435	0.9305688	588.6561279	732.2969971	1.0792042
0.0000000	0.0000000	11.9998407	1290.9238281	9.5459757	0.9310068	599.9017944	734.1649170	1.0813091
0.0000000	0.0000000	11.6524715	1303.7648926	9.7194128	0.9314438	611.1668701	736.0063324	1.0833694
0.0000000	0.0000000	11.3052864	1316.6060791	9.8929539	0.9318795	622.4515381	737.8135986	1.0853832
0.0000000	0.0000000	10.9578934	1329.4467773	10.0665979	0.9323130	633.7558594	739.5938110	1.0873516
0.0000000	0.0000000	10.6107044	1342.2880859	10.2403460	0.9327444	645.0797119	741.3461914	1.0892770
0.0000000	0.0000000	10.2634945	1355.1292725	10.4141979	0.9331741	656.4231567	743.0693970	1.0911571
0.0000000	0.0000000	9.9164467	1367.9702759	10.5881529	0.9337819	667.7863159	744.4814453	1.0925783
19.9226017	995.5790405	9.5662441	1380.8112793	10.7622137	0.9340268	679.1693115	746.4306641	1.0949856
9.8888884	0.9210097	9.2178135	1393.6525879	10.9363766	0.9344499	690.5716553	748.0695801	1.0965356
346.1829529	680.8927612	8.8691740	1406.2250977	11.1106443	0.9348913	701.9937744	748.2904663	1.0962059
1.9168529	19.5804643	8.5203266	1416.6339722	11.2850161	0.9352887	713.4356689	748.3829346	1.0956889
1008.4203491	5.7566357	8.1717232	1428.0538330	11.4594898	0.9357044	724.8970337	748.4155273	1.0950848
0.9214250	357.0007324	7.8229100	1439.4638062	11.6340694	0.9361179	736.3782959	748.4215698	1.0944425
685.9212036	0.9214250	7.4729409	1454.0524231	11.8087511	0.9366266	747.8791504	751.7886719	1.0987122
19.2379971	1021.2613474	7.1229823	1472.6009521	11.9835377	0.9369769	759.3998413	759.3563232	1.1091138
5.9277878	0.9218282	6.7730759	1491.1402930	12.1584291	0.9373864	770.9402466	766.8178711	1.1193476
367.8379211	688.1529541	6.4228840	1509.6796008	12.3334227	0.9377736	782.5003052	774.3486938	1.1294701
1.9168488	18.8953819	6.0728622	1528.2449707	12.5085211	0.9381744	794.0803833	781.8201904	1.1398938
1034.1022949	6.0990438	5.7227745	1551.0745850	12.6837215	0.9385272	805.6799316	793.9065737	1.1568213
0.9223385	379.6943665	5.3713674	1573.9025879	12.8590279	0.9389220	817.2994385	805.8676758	1.1736636
690.7076416	1.0296347	5.0204329	1596.7311230	13.0344372	0.9393351	828.9386597	817.7629395	1.1901819
19.5525879	1046.9434814	4.6693025	1619.5611877	13.2099504	0.9397212	840.5977173	829.6672974	1.2067935
6.2704048	0.9226563	4.3179932	1651.9003906	13.3855677	0.9401844	852.2766113	851.6477051	1.2380331
389.5702515	693.2115479	3.9664459	1691.8850098	13.5612879	0.9406427	863.9752808	881.3964844	1.2805136
1.9227407	18.2089691	3.6146545	1731.8705444	13.7371130	0.9410232	875.6938477	911.3670654	1.3232822
1059.7844238	6.4418688	3.2628078	1771.7561035	13.9130421	0.9414011	887.4323120	941.2957153	1.3659316
0.9230785	400.4654846	2.9109232	1811.6427002	14.0890741	0.9417751	899.1906738	973.0962524	1.4112452
695.6765137	1.0357863	2.5581484	1851.5313721	14.2652102	0.9421477	910.9686890	1002.1836777	1.4786623
17.8662891	1072.6254883	2.2055664	1891.4208984	14.4415501	0.9425174	922.7666626	1094.7723389	1.5858376
6.2734357	0.9235058	1.8527896	2056.3007813	14.6177940	0.9428848	934.5847778	1192.8427734	1.7268801
411.3799438	698.1044922	1.4997693	2211.9492188	14.7942410	0.9431141	946.4224854	1345.4861328	1.9467084
1.9187775	17.9238052	1.1466908	2422.3742676	14.9707928	0.9436113	958.2803345	1555.3436279	2.2490263
1089.4667969	6.7881088	0.7931426	2688.1389160	15.1474485	0.9439705	970.1580811	1824.0073242	2.6359646
0.9239367	422.3140564	0.4395101	3065.8164063	15.3242073	0.9443271	982.0559082	2210.9658203	3.1932721
700.4962769	1.0414886	0.0866868	3567.9777832	15.5010700	0.9446818	993.9732666	2668.8244629	3.8479950
17.1791859	1098.3074951	-0.2663323	4084.4104614	15.6780367	0.9450332	1005.9109497	3158.7514893	4.5568366
6.9568844	0.9245839	-0.6192007	4621.3242798	15.8551071	0.9453818	1017.8686523	3711.0156250	5.3504600
433.2673950	702.4762329	-0.9722844	4984.2377930	16.0322819	0.9457300	1029.8461914	4186.7226563	6.0327206

Run E2

Table XI

INTER IN	SPH D IN	WIRE D IN	EL TEMP C	TDEPTH IN	HT ST CM	SOR	UPDN	VEL CPS	DATA CALC	CM SP CPM	E MARK CM	E TANK IN
5.37500	0.49900	0.00410	21.90000	21.41875	24.42000	1.00000	1.00000	0.69128	9 40	0.33333	9.45000	9.76875

P1	P2	DYNES P VOLT	CM FULL SCALE	CM WIDTH CM	WALL FACTOR	TANK D IN	CM VEL FACTOR
0.300000E-01	0.160000E+02	0.159800E+07	0.100000E-02	0.252000E+02	0.210440E+01	0.150000E+02	0.101500E+01

Z1	Z2	Z3	VISCOSITY	DENSITY	LAMDA
0.141693E+02	-0.139222E+05	0.320347E+07	0.438998E+02	0.871262E+00	0.717665E+01

Y1	Y2	Y3	VIS LOWER	RHO LOWER	GAMMA
-0.791993E+02	0.457984E+05	-0.646559E+07	0.314966E+03	0.971629E+00	0.194000E+01

REYNOLDS NO.	1/CAPILLARY NO.	BOND NO./CAP NO.	STOKES DRAG
0.819142B1E-02	0.67853153E-01	0.13816330E+01	0.34178339E+03

POSITION	HEIGHT	DIST TO INTER	TOTAL FORCE	WIRE LEN IN	RATIO	WIRE DRAG	SPHERE DRAG	SCALED DRAG
1.0000000	11.1999998	28.8744402	838.9499512	8.5900726	0.9284496	537.9831543	352.5782166	1.0439237
6.0000000	6.8699999	28.1700682	851.2775269	8.7636226	0.9295517	549.0289917	354.6739502	1.0498149
7.0000000	5.9200001	27.4814682	863.6044922	8.9376249	0.9300829	560.0845947	356.3802795	1.0545503
8.0000000	4.7900000	26.7946584	875.9327393	9.1114788	0.9316887	571.1499023	346.9436847	1.0559001
8.5000000	4.0999999	26.4528446	888.2598267	9.2853432	0.9326850	582.2249756	358.0273315	1.0589391
9.0000000	3.0999999	25.3004171	900.5872192	9.4593420	0.9336745	593.3100586	349.1024951	1.0618900
9.3299999	2.1900001	24.6029855	912.9144116	9.6333513	0.9346395	604.4046631	360.2778320	1.0648104
9.6700001	1.2800000	23.9053461	925.2420654	9.8074121	0.9355804	615.5090332	361.3637695	1.0677012
10.0000000	-0.0500000	23.2074907	937.5694580	9.9815265	0.9364983	626.6232300	362.4600024	1.0705615
10.6500015	3.9400001	22.5094415	949.8964844	10.1556902	0.9373942	637.7472534	363.5062256	1.0733936
74.1499985	3.9000001	21.8011765	962.2242432	10.3299074	0.9382694	648.8809814	364.3621033	1.0761877
0.0000000	0.0000000	21.2026997	974.5516968	10.5041771	0.9391428	660.0246582	365.5874329	1.0788927
0.0000000	0.0000000	20.5040188	986.8792114	10.6784983	0.9399601	671.1780396	366.6430969	1.0816857
0.0000000	0.0000000	19.8051300	999.2066040	10.8528709	0.9407772	682.3412476	367.6676941	1.0843854
0.0000000	0.0000000	19.1060276	1011.5339966	11.0272970	0.9414772	693.5142822	368.6809998	1.0870501
0.0000000	0.0000000	18.4067249	1023.8614502	11.2017727	0.9423588	704.6968384	369.6852722	1.0896869
0.0000000	0.0000000	17.7072105	1036.1888428	11.3763018	0.9431359	715.8895264	370.6643982	1.0922476
0.0000000	0.0000000	17.0074844	1048.5163574	11.5508833	0.9438860	727.0919800	371.6457214	1.0948135
0.0000000	0.0000000	16.3075542	1060.8438721	11.7255163	0.9446090	738.3041382	372.6300354	1.0973866
0.0000000	0.0000000	15.6074142	1073.1712646	11.9002008	0.9453288	749.5261841	373.5895691	1.0998852
0.0000000	0.0000000	14.9070663	1085.4986572	12.0749378	0.9460344	760.7579956	374.5379639	1.1023495
0.0000000	0.0000000	14.2065115	1097.8260498	12.2497263	0.9467466	771.9996338	375.4953174	1.1047865
0.0000000	0.0000000	13.5057459	1110.1533203	12.4245672	0.9474393	783.2510986	376.3587036	1.1070533
0.0000000	0.0000000	12.8047747	1123.4351807	12.5994596	0.9481069	794.5124512	378.2774658	1.1123637
0.0000000	0.0000000	12.1035519	1135.9897461	12.7744045	0.9487580	805.7835693	380.4751587	1.1164942
0.0000000	0.0000000	11.4022736	1150.5441895	12.9494009	0.9494005	817.0645142	382.6575317	1.1245757
0.0000000	0.0000000	10.7006473	1164.0986328	13.1244497	0.9500303	828.3554688	384.8269653	1.1346157
0.0000000	0.0000000	9.9988812	1178.5900332	13.2995501	0.9506488	839.6560059	387.8864332	1.1392593
0.0000000	0.0000000	9.2967892	1194.6319580	13.4747019	0.9512186	850.9664307	392.7772827	1.1532893
0.0000000	0.0000000	8.5945663	1210.7548828	13.6499062	0.9517564	862.2867432	397.6835632	1.1673490
28.8744402	838.9499512	7.8921951	1226.8771973	13.8251629	0.9523429	873.6168823	402.4958191	1.1811246
8.5000726	0.9284496	7.1894979	1242.9997559	14.0004711	0.9529197	884.9570313	407.2913513	1.1948429
537.9831543	352.5782166	6.4866614	1262.2932129	14.1758308	0.9535432	896.3067627	415.3185120	1.2180308
1.0439237	28.1700682	5.7835951	1281.5869202	14.3512440	0.9541060	907.6665039	423.8111267	1.2425697
85.2775269	8.7636226	5.0803337	1307.5697021	14.5267076	0.9546564	919.0361328	438.4653625	1.2851536
0.9295517	549.0289917	4.3768616	1336.1054688	14.7022238	0.9548365	930.4154663	456.7095032	1.3382316
354.6739502	1.0498149	3.6731830	1369.4441004	14.8777914	0.9553696	941.8048706	479.4329529	1.4043992
27.4814682	863.6049194	2.9693960	1408.7891174	15.0534115	0.9558296	953.2039185	508.5033264	1.4891143
8.9376249	0.9300829	2.2651680	1463.4189911	15.2290840	0.9562484	964.6130371	552.7689209	1.6182642
560.0845947	356.3802795	1.5608853	1526.6317139	15.4048071	0.9572568	976.0318604	606.5742798	1.7752576
1.0545503	26.7946584	0.8563820	1499.2683105	15.5805836	0.9577519	987.4606323	670.1582642	1.9607689

Run E3

Table XII

INTER IN	SPH D IN	WIRE D IN	EL TEMP C	DEPTH IN	HT ST CM	SOR	UPDN	VEL CPS	DATA CALC	CH SP	CP E	MARK CM	E TANK IN
5.37500	0.49900	0.00410	21.90000	21.41875	10.20000	1.00000	1.00000	0.38719	12	60	0.33333	15.80000	5.76875

P1	P2	DYNES P VOLT	CH FULL SCALE	CH WIDTH CM	WALL FACTOR	TANK D IN	CH VEL FACTOR
0.300000E-01	0.160000E+02	0.149800E+07	0.100000E-01	0.252000E+02	0.210440E+01	0.190000E+02	0.101500E+01

Z1	Z2	Z3	VISCOSITY	DENSITY	LAMDA
0.141693E+02	-0.139222E+01	0.320347E+07	0.438998E+02	0.871262E+00	0.717465E+01

Y1	Y2	Y3	VIS LOWER	RHO LOWER	GAMMA
-0.751993E+02	0.457984E+01	-0.646559E+07	0.314966E+03	0.971629E+00	0.194000E+01

REYNOLDS NO.	1/CAPILLARY NO.	BOND NO./CAP NO.	STOKES DRAG
0.498899?8E-02	0.114137?2E+00	0.232397?2E+01	0.20386984E+03

POSITION	HEIGHT DIST TO INTER		TOTAL FORCE	WIRE LEN IN	RATIO	WIRE DRAG	SPHERE DRAG	SCALED DRAG
2.0000000	9.4300003	27.9687481	488.2774658	8.8160486	0.9298773	324.6055603	192.8258667	0.9711100
12.0000000	9.1000004	27.4734726	493.9729919	8.9396191	0.9300943	329.3020630	194.6883240	0.9800531
14.0000000	9.0000000	26.9779720	499.6685486	9.0632467	0.9313836	334.0047302	195.3826123	0.9831113
15.0000000	8.9499998	26.4827940	505.3634949	9.1868287	0.9321131	338.7134399	196.3614807	0.9875960
16.0000000	8.8900003	25.9863167	511.0588989	9.3106651	0.9328300	343.4282227	197.3324585	0.9920382
16.0000000	8.8199997	25.4901581	516.7549133	9.4344568	0.9335344	348.1491089	198.2960968	0.9964396
16.0000000	8.7200003	24.9937763	522.4500732	9.5583038	0.9342265	352.8760376	199.2524872	1.0008007
17.0000000	8.5299997	24.4971771	528.1450195	9.6822052	0.9349059	357.6090088	200.2014160	1.0051204
17.3799999	8.3699999	24.0003986	533.8405762	9.8061609	0.9355718	362.3482056	201.1435089	1.0094018
17.6700001	8.1199999	23.5033169	539.5361328	9.9301729	0.9362298	367.0934753	202.0787964	1.0136454
18.0000000	7.8699999	23.0064458	545.2314453	10.0542402	0.9368750	371.8448486	203.0066986	1.0178483
18.3799999	7.6599998	22.5085735	550.9271851	10.1783619	0.9375094	376.6022949	203.9273682	1.0220112
18.6000015	6.6999998	22.0108700	556.6220703	10.3025389	0.9381331	381.3658447	204.8414694	1.0261323
108.1500015	6.5599999	21.5129452	562.3176270	10.4267712	0.9387472	386.1355286	205.7488403	1.0302162
0.0000000	6.0000000	21.0148010	568.0131836	10.5510578	0.9393527	390.9113464	206.6496582	1.0341905
0.0000000	6.0000000	20.5164356	573.7087402	10.6753998	0.9399455	395.6932373	207.5379791	1.0382651
0.0000000	6.0000000	20.0178509	579.4042969	10.7997971	0.9405305	400.4813232	208.4227600	1.0422301
0.0000000	0.0000000	19.5190430	585.0992432	10.9242496	0.9411067	405.2755127	209.2994843	1.0461515
0.0000000	0.0000000	19.0200157	590.7947998	11.0487566	0.9416742	410.0757446	210.1697998	1.0500373
0.0000000	0.0000000	18.5207710	596.4902954	11.1733189	0.9422328	414.8822327	211.0328827	1.0538836
0.0000000	0.0000000	18.0213013	602.1858521	11.2979364	0.9427999	419.6947632	211.8877563	1.0576946
0.0000000	0.0000000	17.5216160	607.8807373	11.4226074	0.9433439	424.5133667	212.7243042	1.0613929
0.0000000	0.0000000	17.0217037	613.5762939	11.5473356	0.9438708	429.3382263	213.5708466	1.0651466
0.0000000	0.0000000	16.5215759	619.2718506	11.6721172	0.9443860	434.1691589	214.4136659	1.0688754
0.0000000	0.0000000	16.0212231	624.9674072	11.7969561	0.9449053	439.0062866	215.2400360	1.0725269
0.0000000	0.0000000	15.5206547	630.6629639	11.9218473	0.9454149	443.8495178	216.0601501	1.0761372
0.0000000	0.0000000	15.0198612	636.3579102	12.0467958	0.9459217	448.6989441	216.8721161	1.0797056
0.0000000	0.0000000	14.5188484	642.0534058	12.1717978	0.9464194	453.5544128	217.6776886	1.0832393
0.0000000	0.0000000	14.0176163	647.7489624	12.2968559	0.9469307	458.4161682	218.4617233	1.0866599
0.0000000	0.0000000	13.5161619	653.4445190	12.4219685	0.9474293	463.2839966	219.2418365	1.0900632
27.9687481	488.2774658	13.0144901	659.1394043	12.5471354	0.9479068	468.1580200	220.0234680	1.0934684
8.8160486	0.9298773	12.5125933	664.8349609	12.6723585	0.9483807	473.0382385	220.7907509	1.0968443
324.6055603	192.8258667	12.0104799	670.5305176	12.7976360	0.9488449	477.9246605	221.5700073	1.1001871
0.9711100	27.4734726	11.5081453	676.2260742	12.9229689	0.9493043	482.8169861	222.3320770	1.1034965
493.9729919	8.9396191	11.0055866	681.9216309	13.0483570	0.9497579	487.7156372	223.0888855	1.1067694
0.9800947	329.3020630	10.5028124	687.6165161	13.1737995	0.9502047	492.6205139	223.8338318	1.1099654
194.6883240	0.9800531	9.9998140	693.3120728	13.2992973	0.9506480	497.5315247	224.5742645	1.1131488
26.9779720	499.6685486	9.4965973	699.7641602	13.4248495	0.9510471	502.4487000	226.1320801	1.1203792
9.0632467	0.9313836	8.9931874	708.3971710	13.5504580	0.9514180	507.3720398	229.9876099	1.1389835
334.0047302	195.3826123	8.4894981	717.0231323	13.6761208	0.9517548	512.3015747	233.7883301	1.1572980
0.9831113	26.4822940	7.9856176	725.6522827	13.8018389	0.9522644	517.2373047	237.5784454	1.1755451
505.3634949	9.1869287	7.4815173	734.2814941	13.9276123	0.9526811	522.1792603	241.3586121	1.1937603
0.9321131	338.7134399	6.9771967	742.9111328	14.0534401	0.9530921	527.1273804	245.1295776	1.2118474
196.3614807	0.9875960	6.4726548	751.5404663	14.1793232	0.9535544	532.0816650	248.8937042	1.2296711
25.9863167	511.0588989	5.9678936	760.1702271	14.3052616	0.9539610	537.0422363	252.5903015	1.2476398
9.3106651	0.9328300	5.4629097	768.7994385	14.4312544	0.9539328	542.0089111	256.2899109	1.2673355
343.4282227	197.3324585	4.9577069	777.4292603	14.5573025	0.9547502	546.9817505	260.0627441	1.2834274
0.9920382	25.4901581	4.4522820	786.0584717	14.6834068	0.9547789	551.9609375	264.0939026	1.3027527
516.7549133	9.4344568	3.9466381	797.5288086	14.8095666	0.9551635	556.9462280	270.7826843	1.3351654
0.9335344	348.1491089	3.4407737	818.2390747	14.9357777	0.9554793	561.9376831	287.1873779	1.4154357
198.2960968	0.9964396	2.9346860	840.9239136	15.0620461	0.9562616	566.9354858	304.5807495	1.5005 68
26.9937763	522.4500732	2.4284812	864.4861450	15.1883698	0.9566313	571.9393921	324.4917297	1.5979011
9.4583038	0.9342265	1.9221816	894.4571533	15.3147488	0.9569978	576.9495850	350.4514099	1.7249786
352.8760376	199.2524872	1.4157067	928.9743042	15.4411812	0.9573580	581.9659424	381.1134338	1.8751895
1.0008007	24.4971771	0.9081374	985.9786987	15.5676708	0.9577155	586.9885864	415.2606321	2.1495950
528.1450195	9.6822052	0.4009479	1051.5627441	15.6942139	0.9580691	592.0173950	498.3091125	2.4495656
0.9349059	357.6090088	-0.1064625	1133.1918945	15.8208132	0.9584188	597.0524902	578.6410156	2.8402729
200.2014160	1.0051204	-0.6149900	1246.0136719	15.9474659	0.9587649	602.0938110	690.2432251	3.3911179
24.0003986	331.8465576	-1.1219412	1374.5502930	16.0741749	0.9591073	607.1413574	818.7466736	4.0195112
9.3961609	0.9355758	-1.6300100	1500.8632812	16.2009392	0.9594466	612.1951294	944.8238525	4.6364594
362.3482056	201.1435089	-2.1383030	1610.6823730	16.3277569	0.9597817	617.2550659	1053.6461182	5.1682296

Run E4

Table XIII

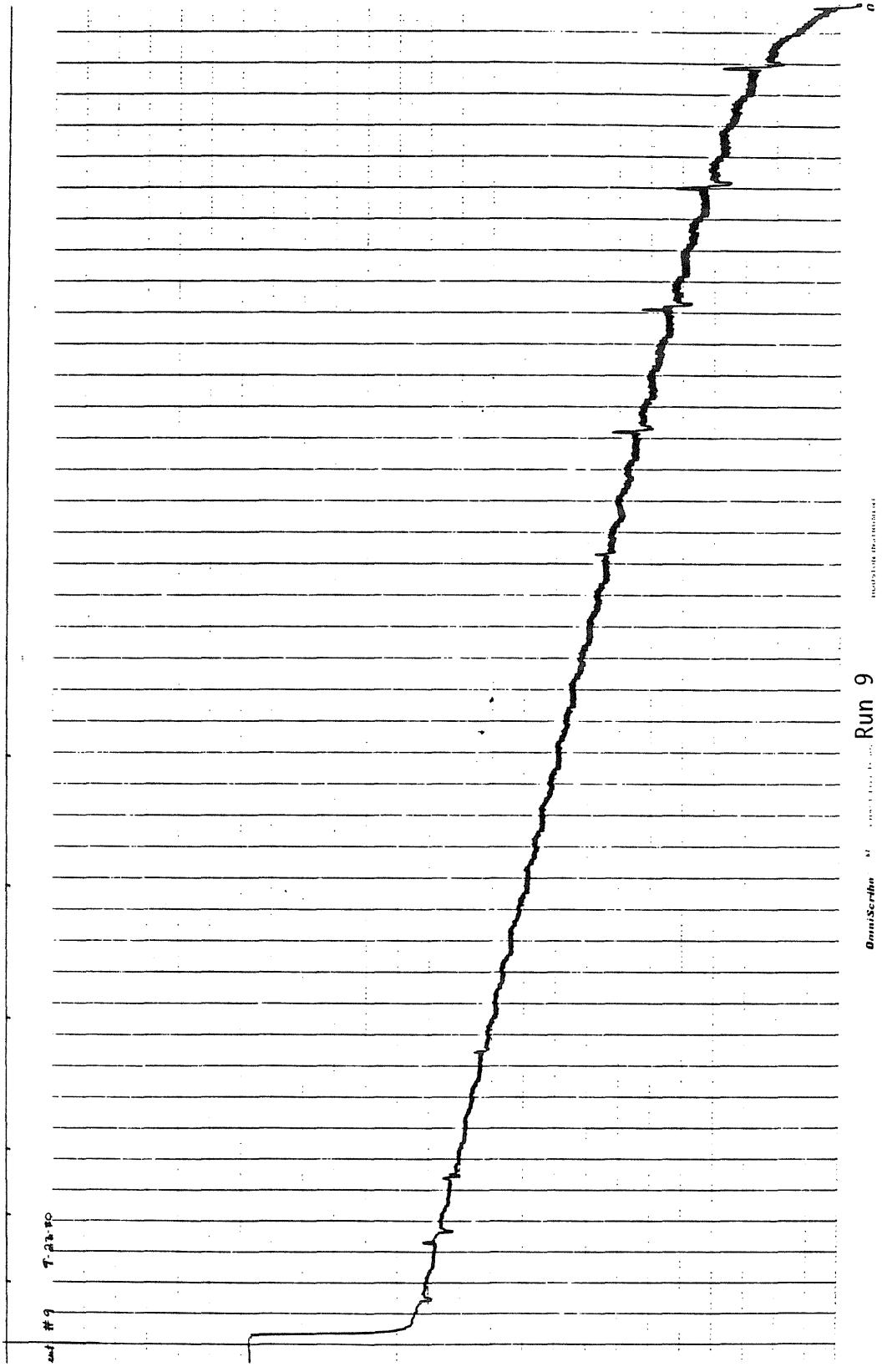

Figure I

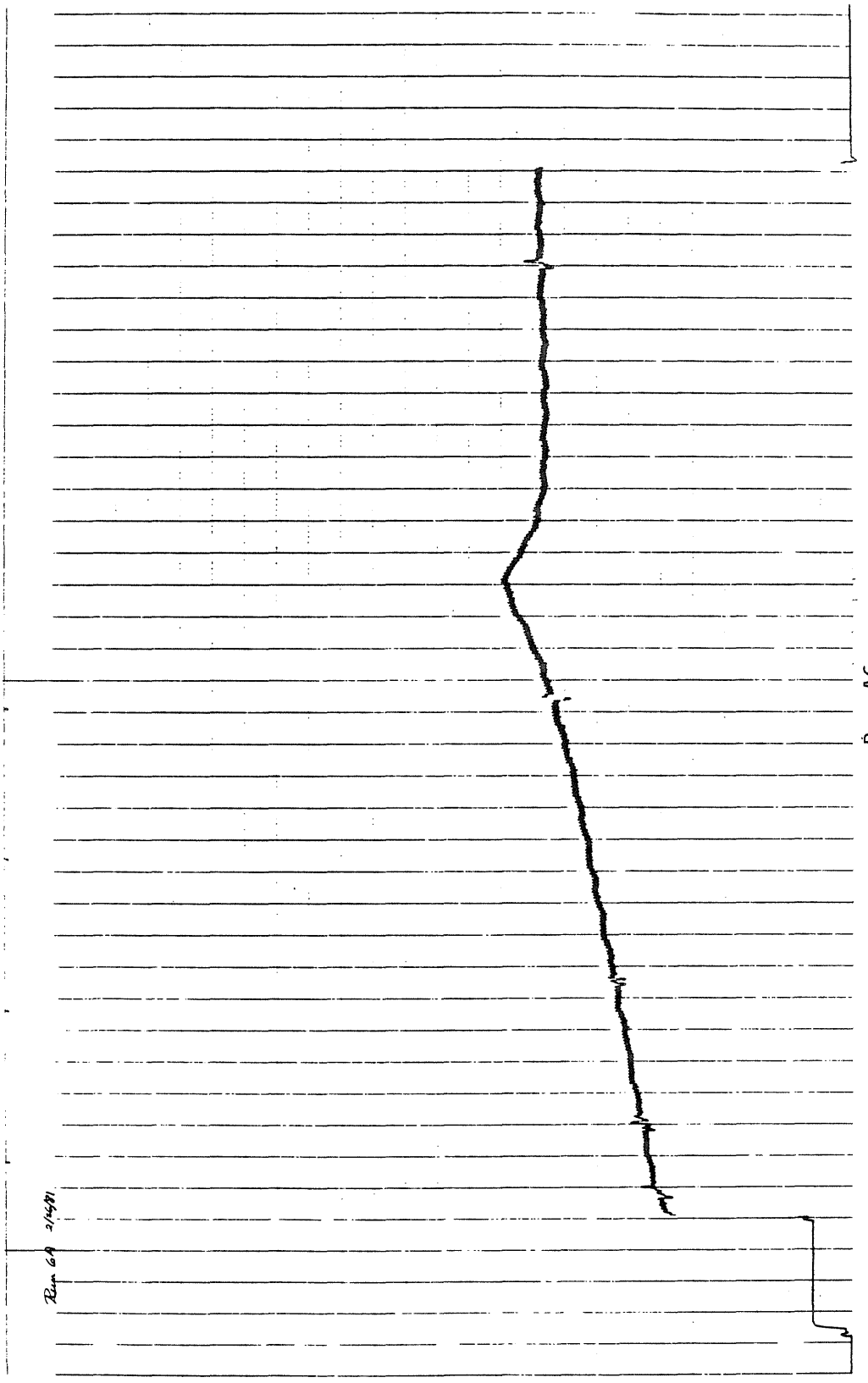

Figure II
Run A6

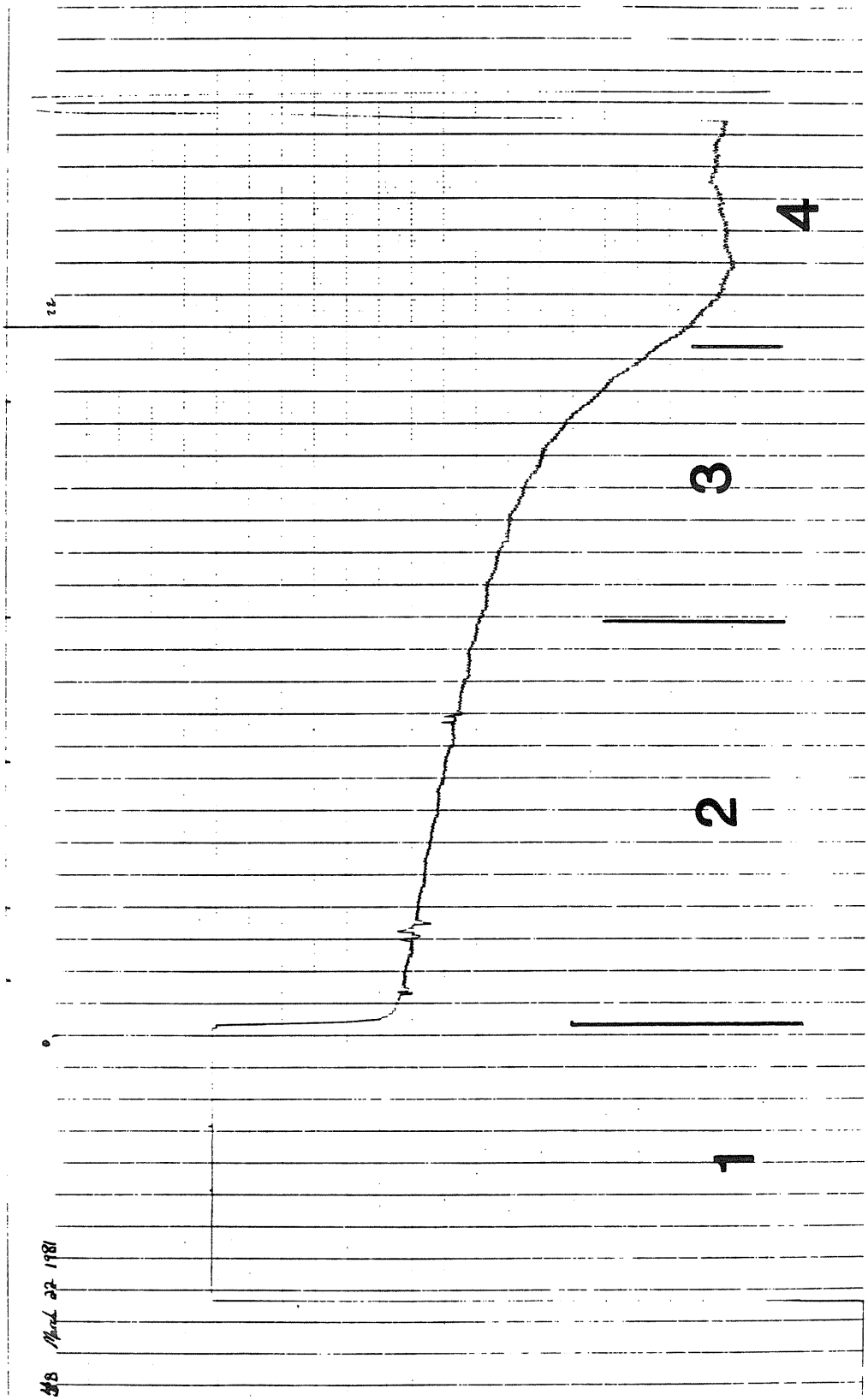

Run B4
Figure III

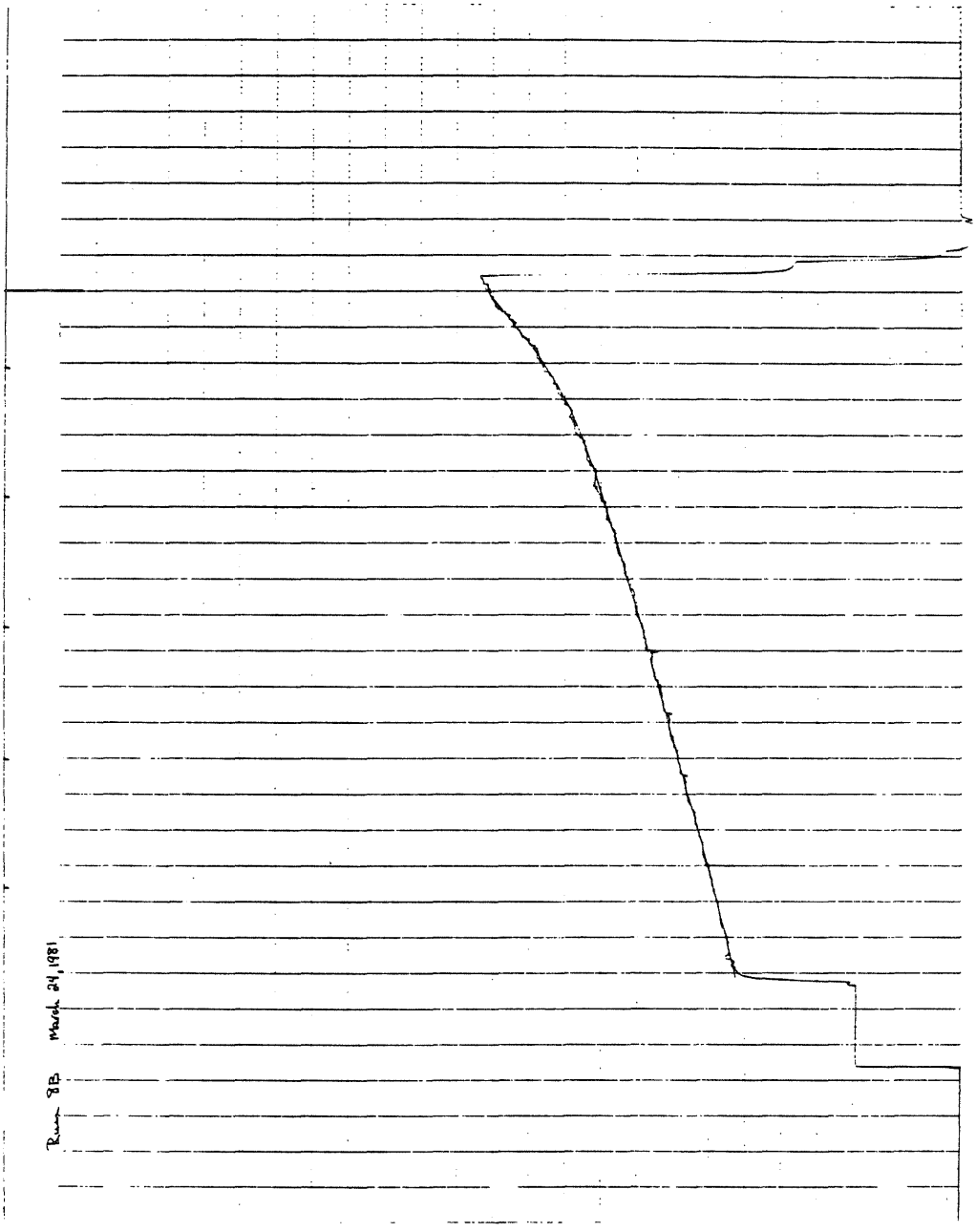

Run B8
Figure IV

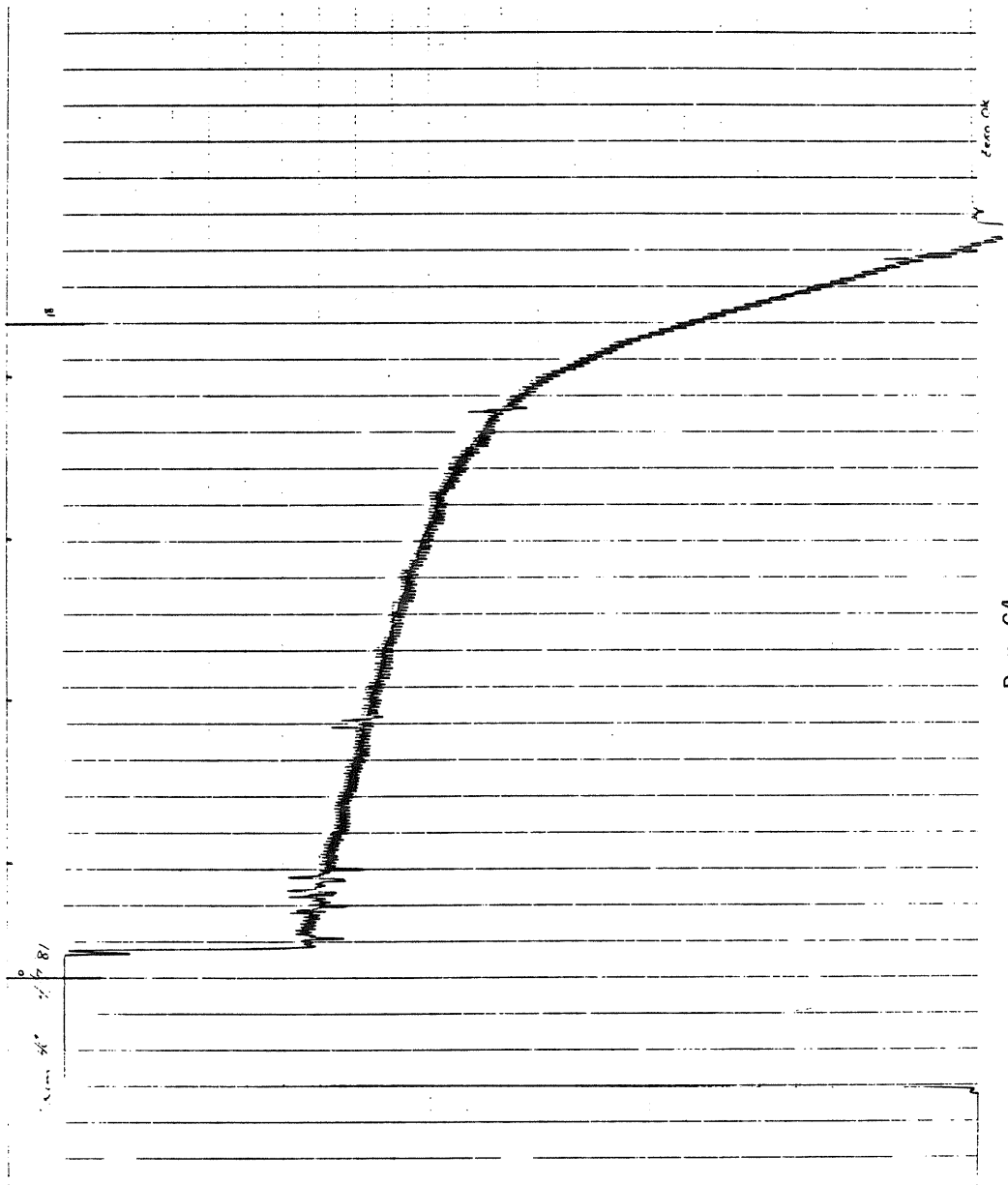

Run C4
Figure V

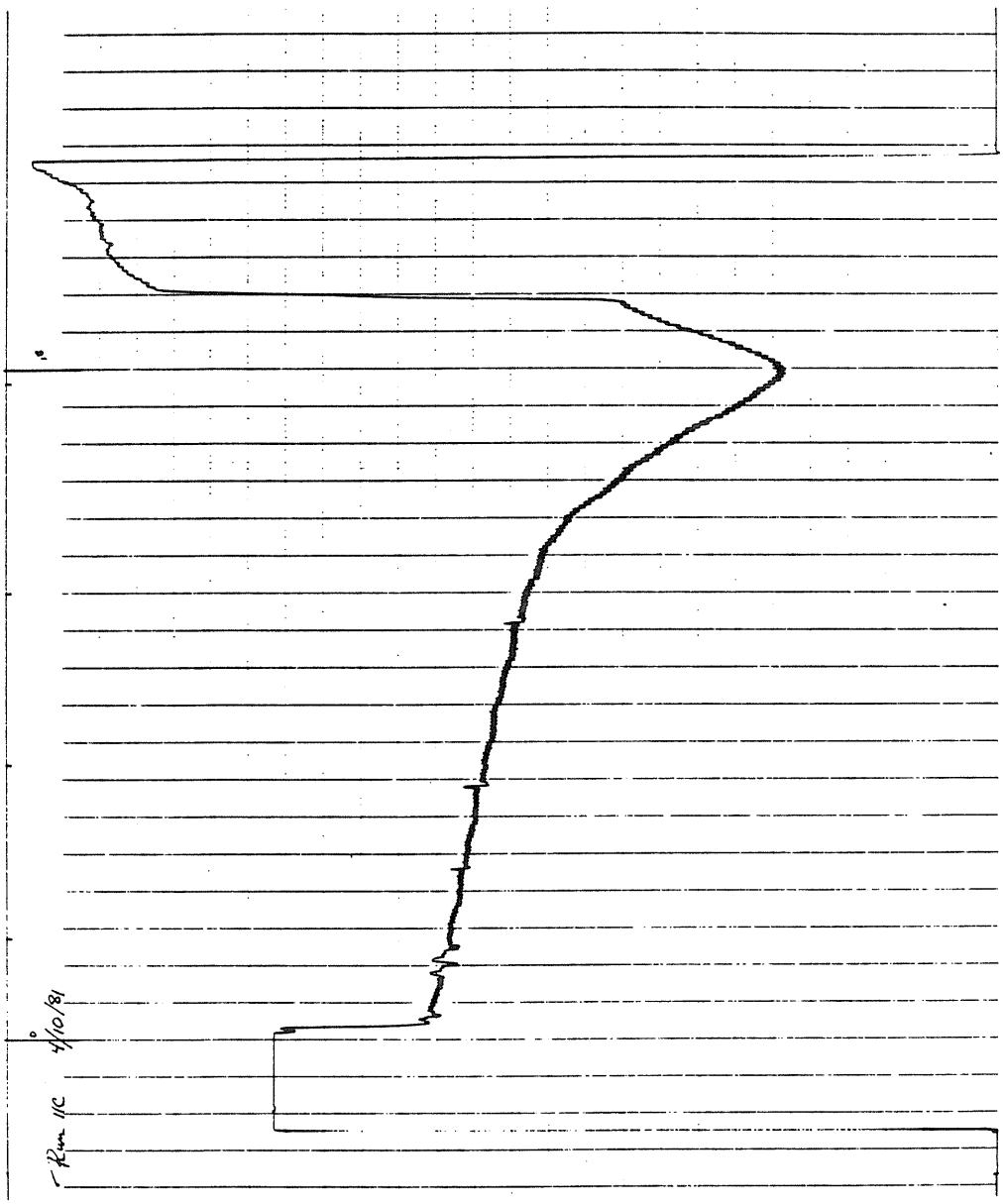

Run C11

Figure VI

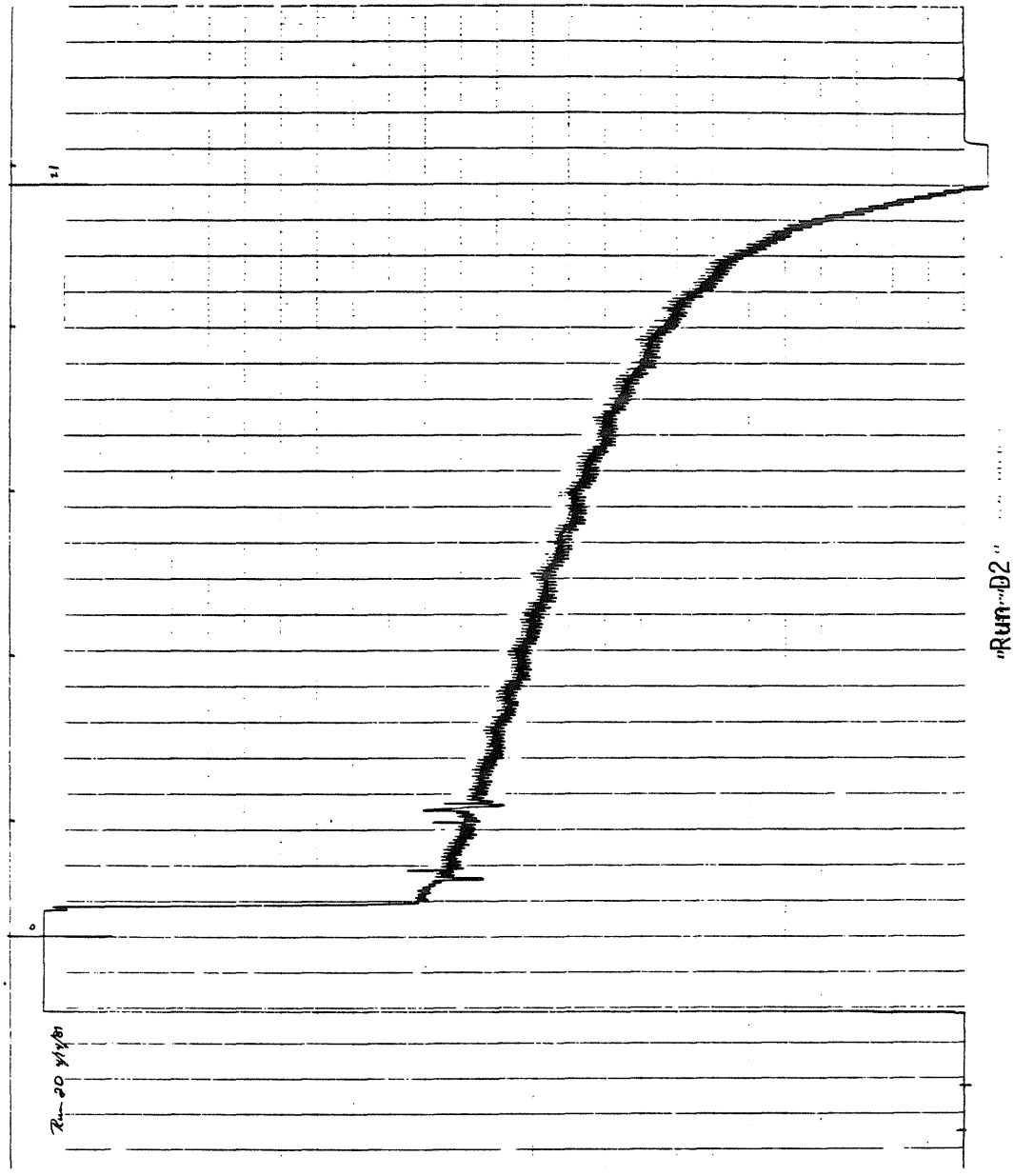

Figure VII

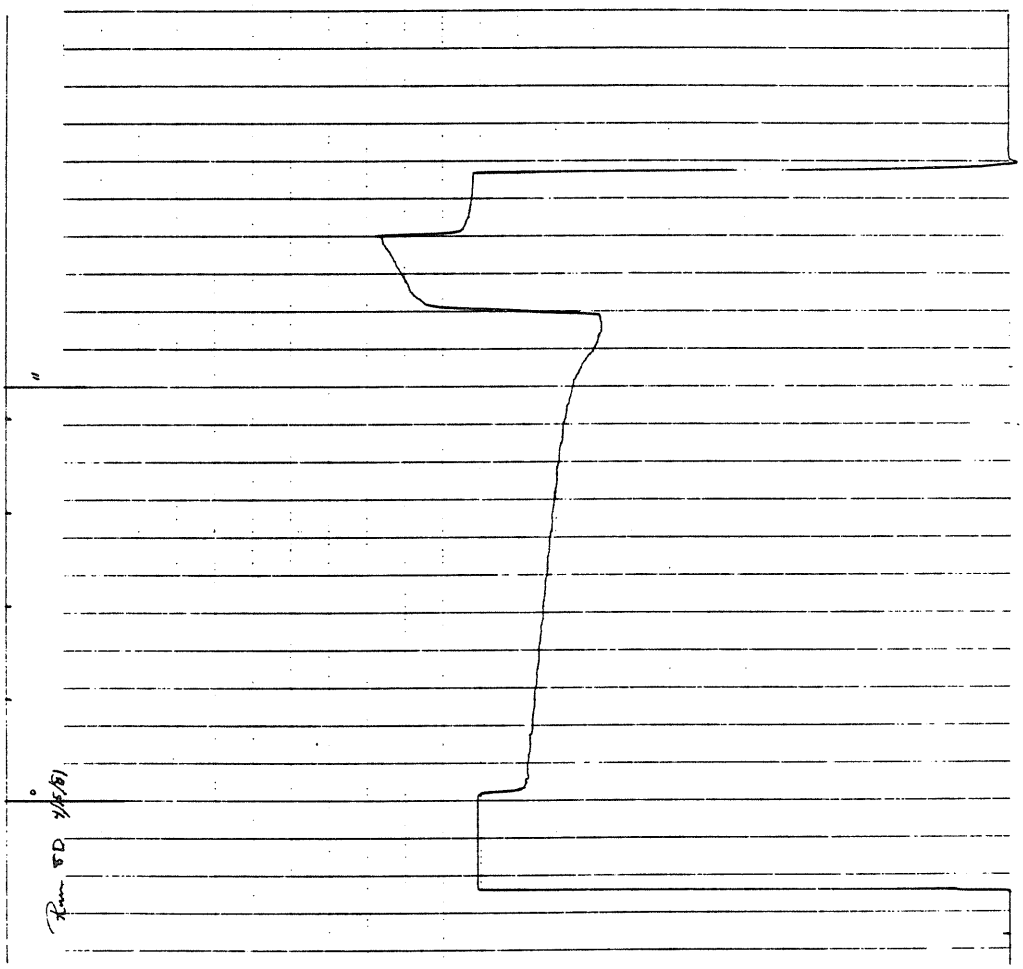

Run D8

Figure VIII

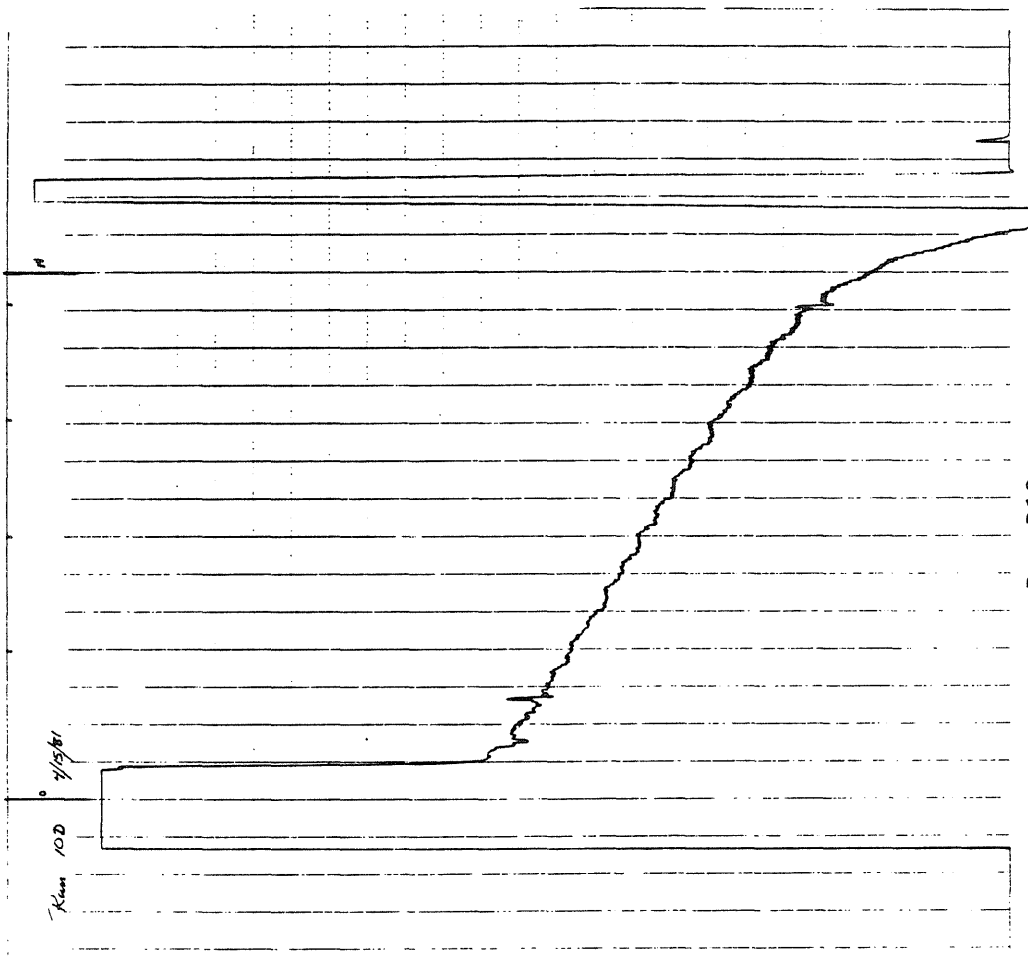

Figure IX

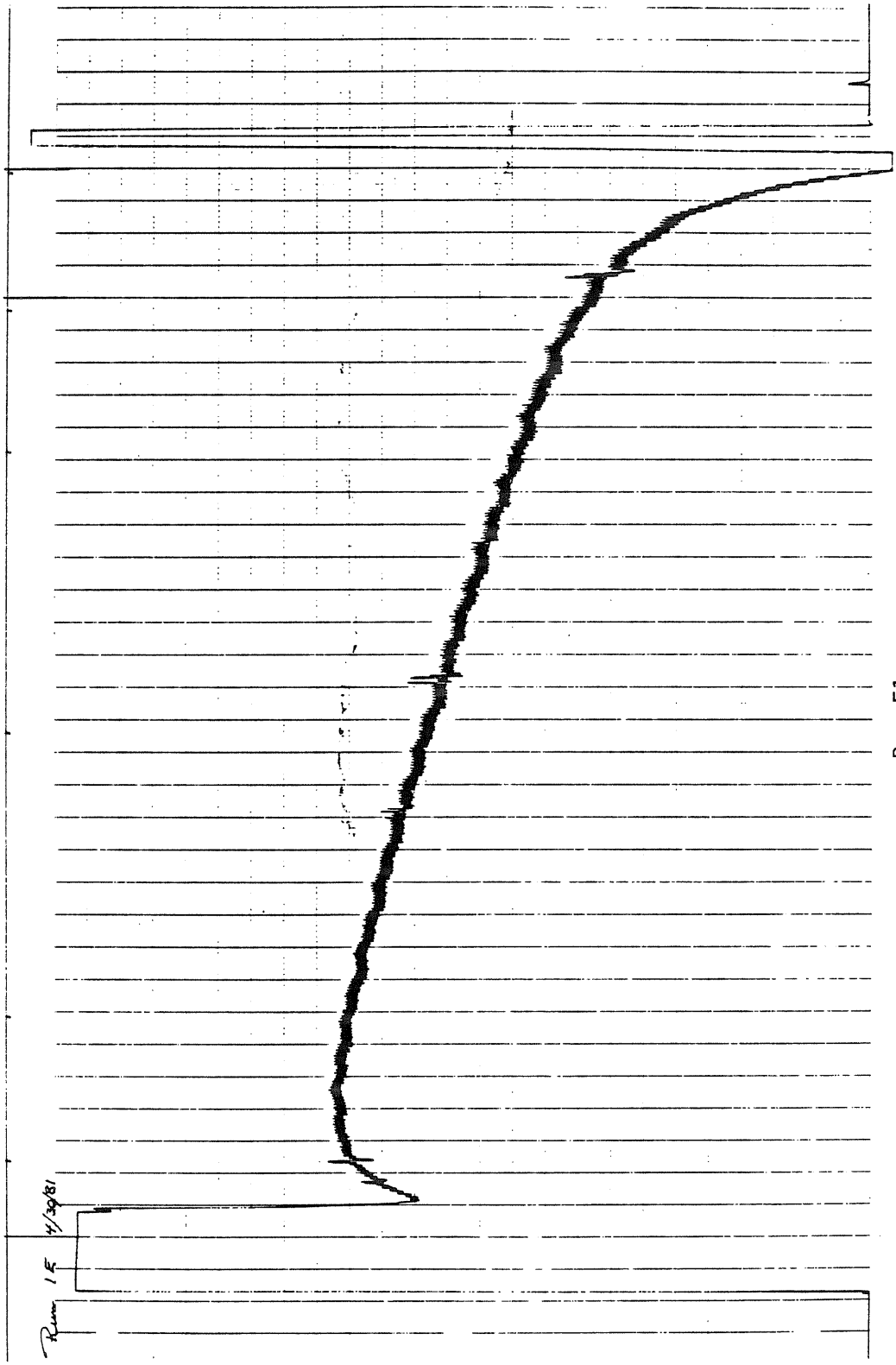

Run E1

Figure X

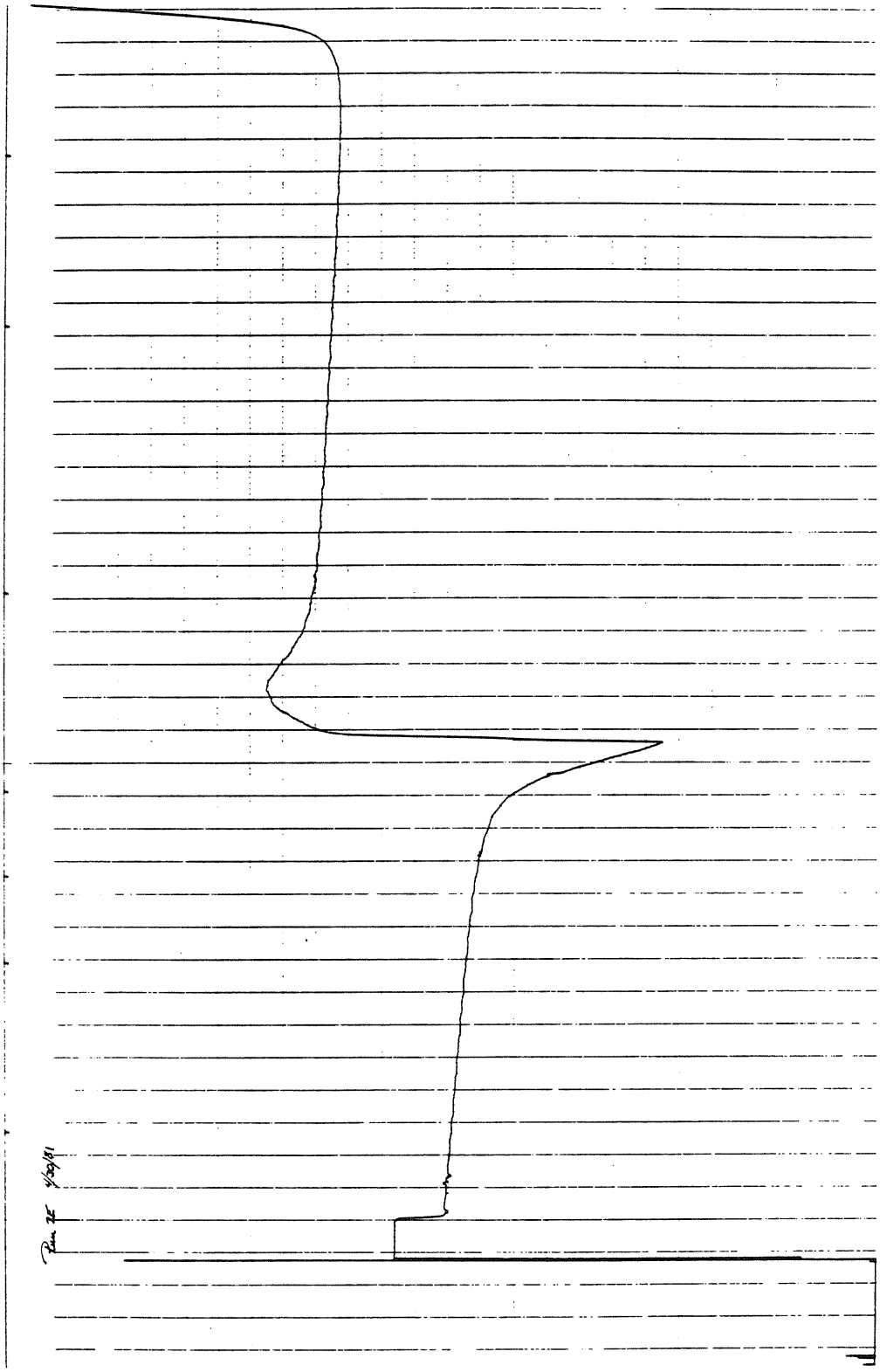

Run E2
Figure XI

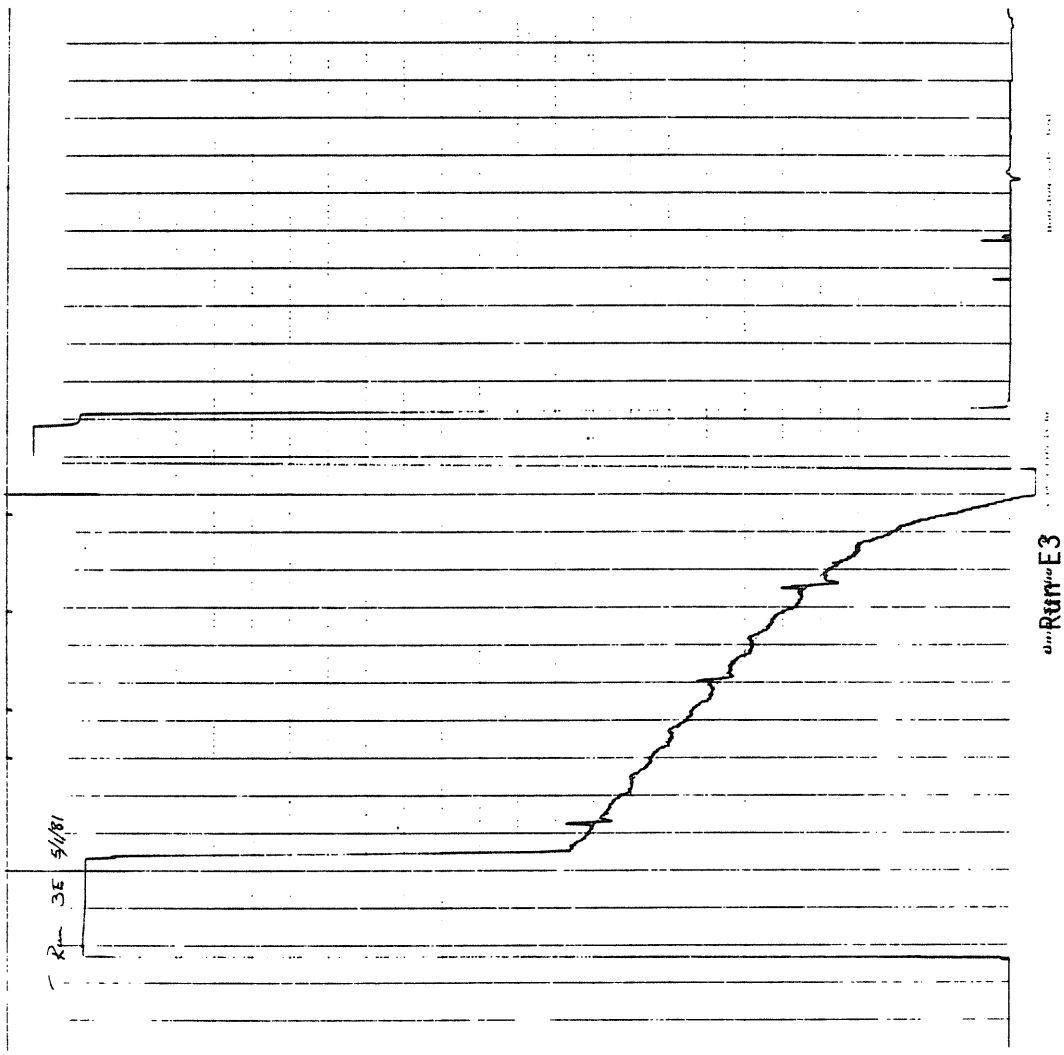

Figure XII

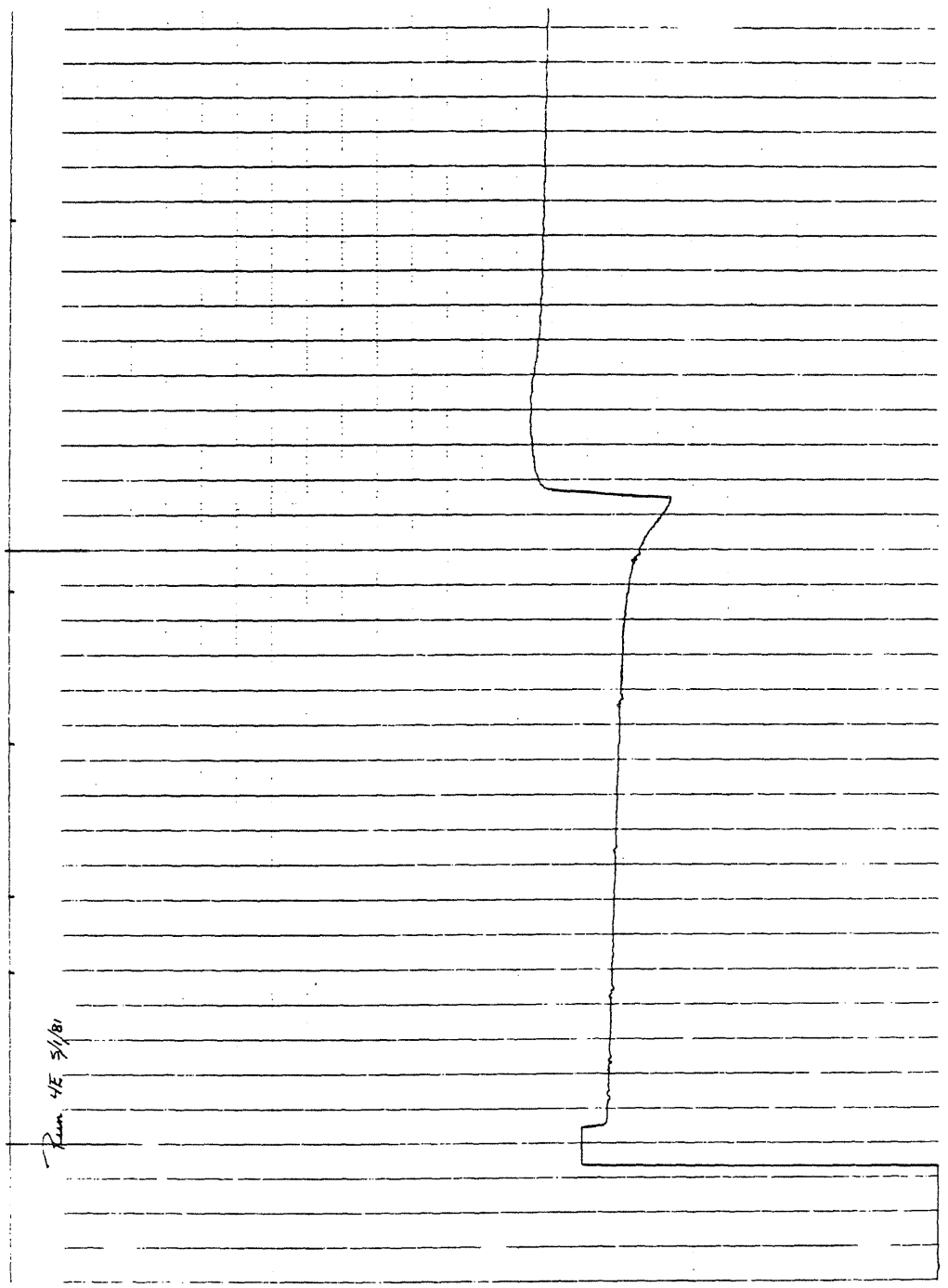

Run E4

Figure XIII

(a)

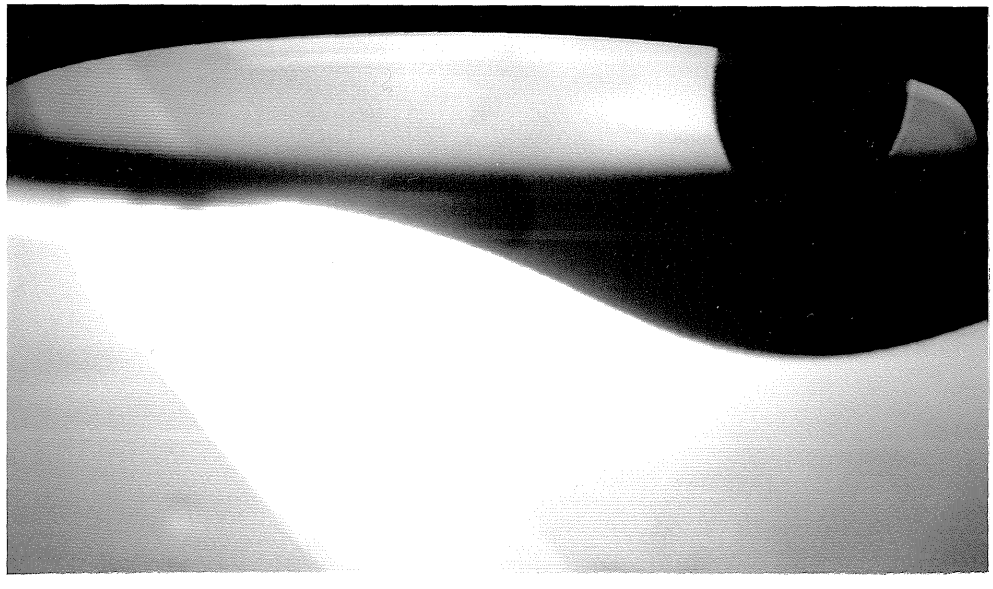

(b)

(c)

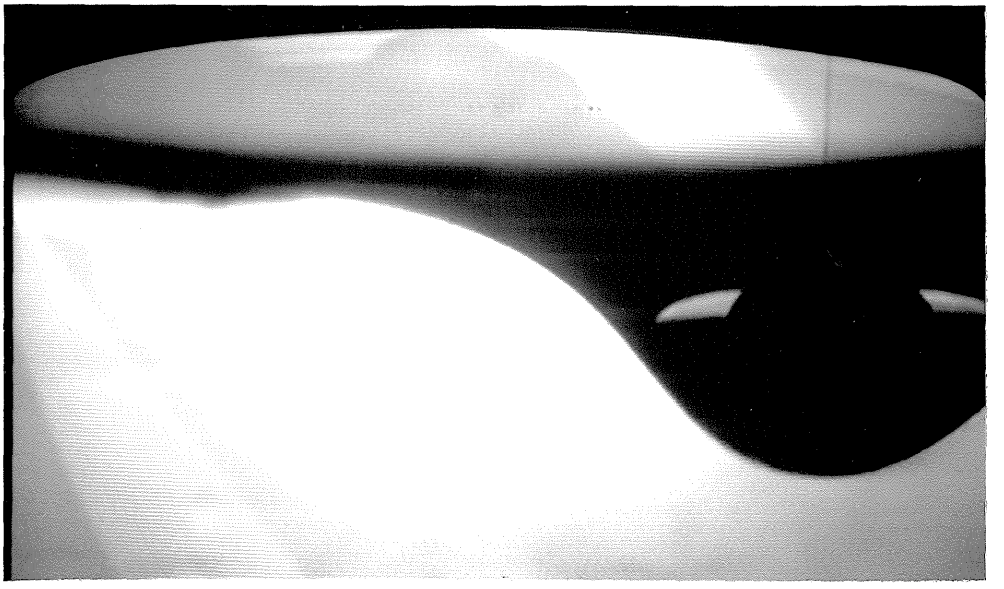

(d)

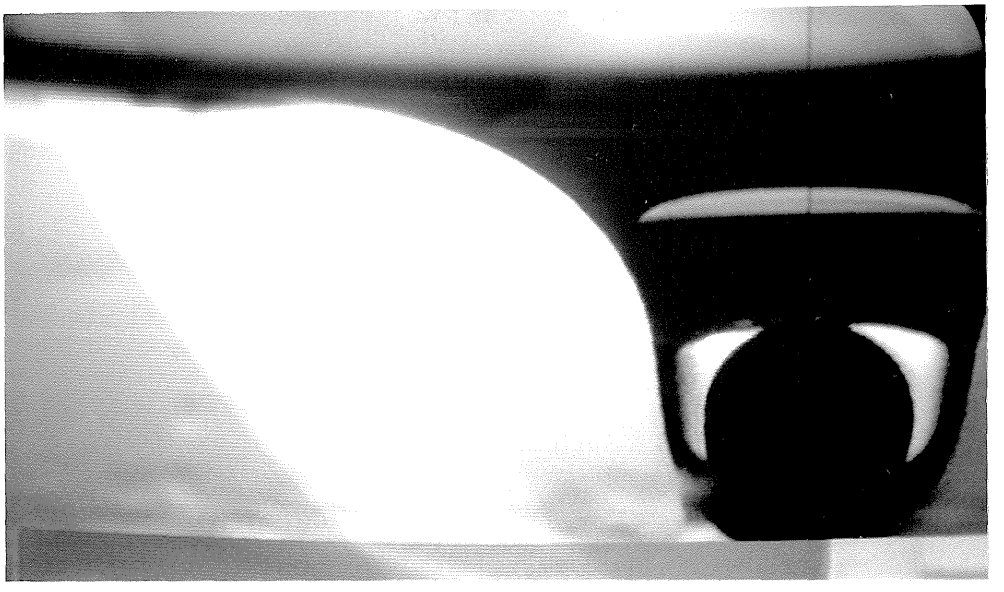

(e)

Figure XIV: Photographs for Run A6. a.) l=3, b.) l=1, c.) l=0, d.) l=-1, e.) l=-3.

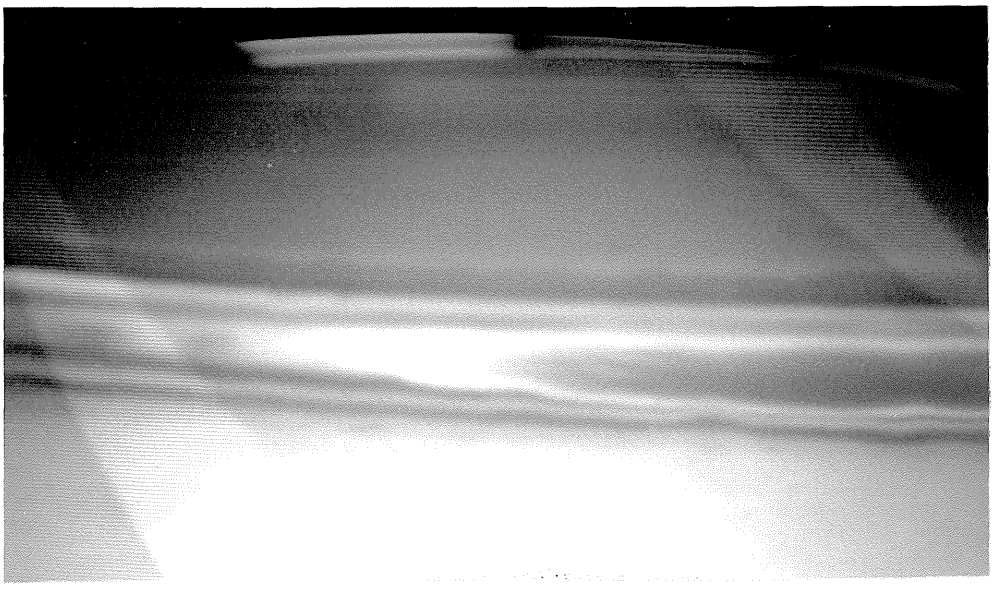

(a)

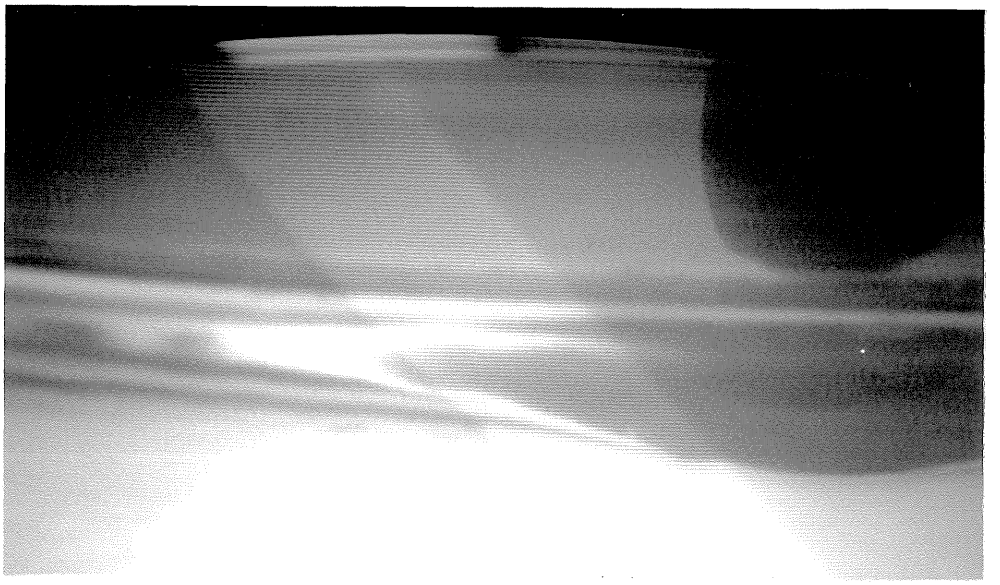

(b)

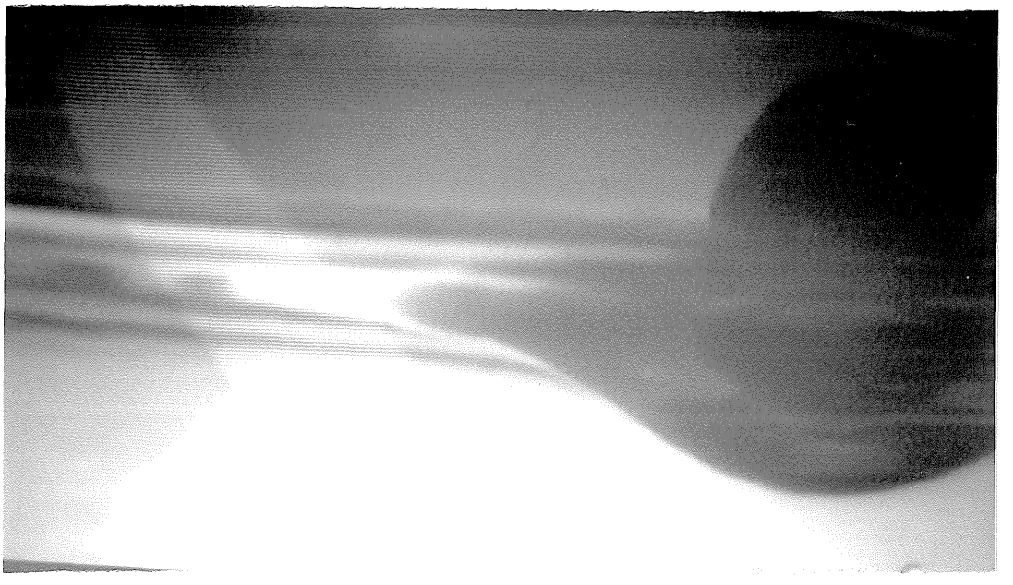

(c)

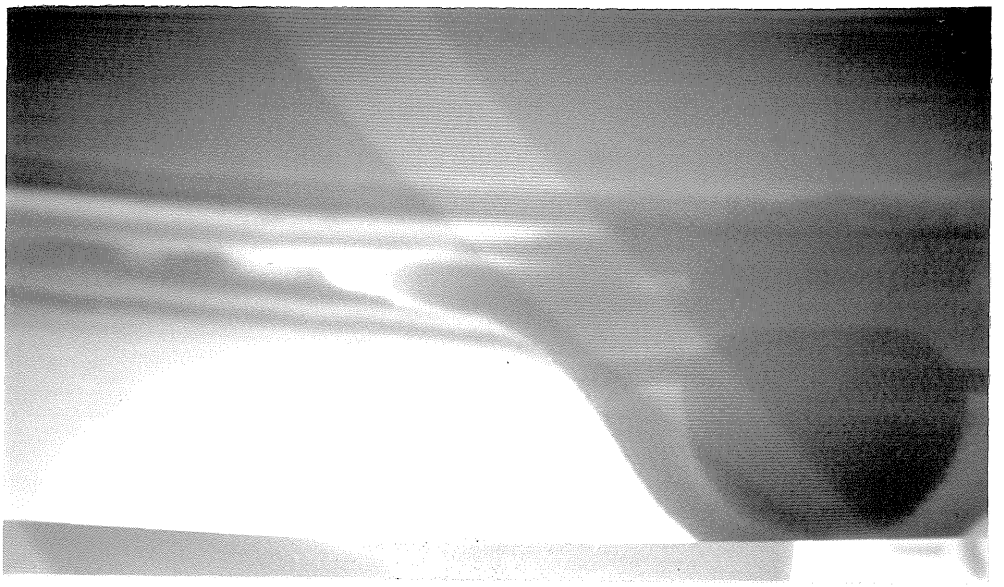

(d)

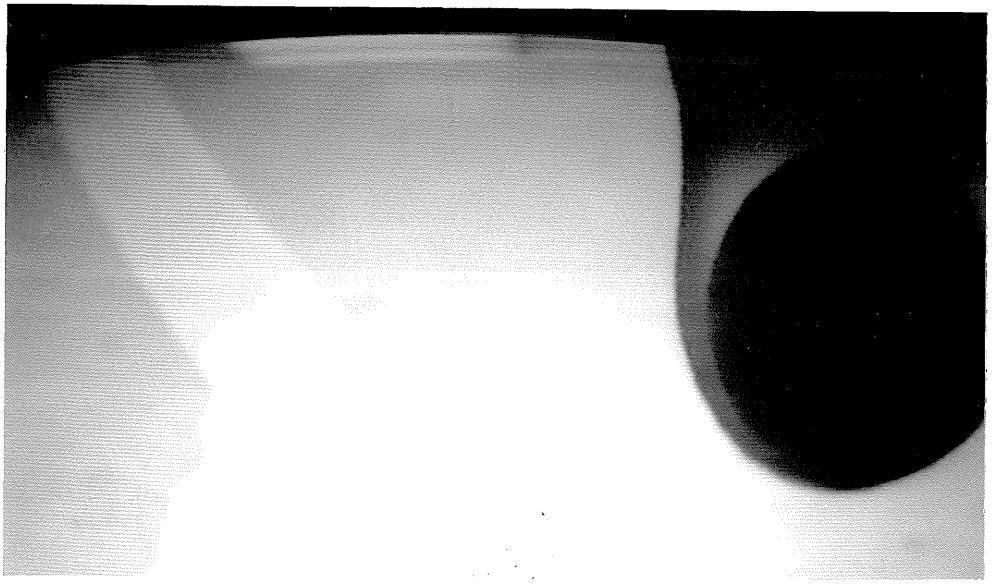

(e)

Figure XV: Photographs for Run B4. a.) l=3, b.) l=1, c.) l=0, d.) l=-1, e.) l=-3.

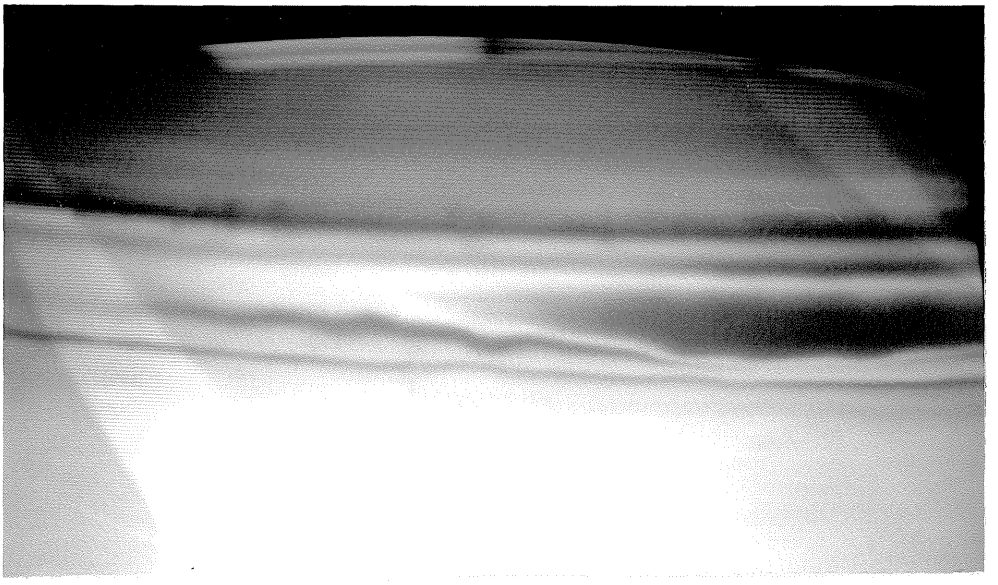

(a)

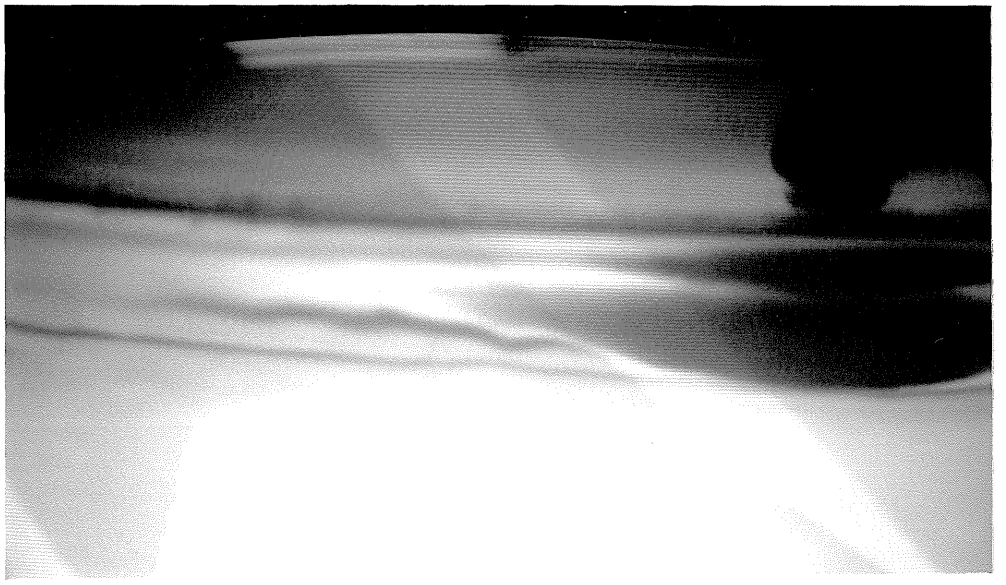

(b)

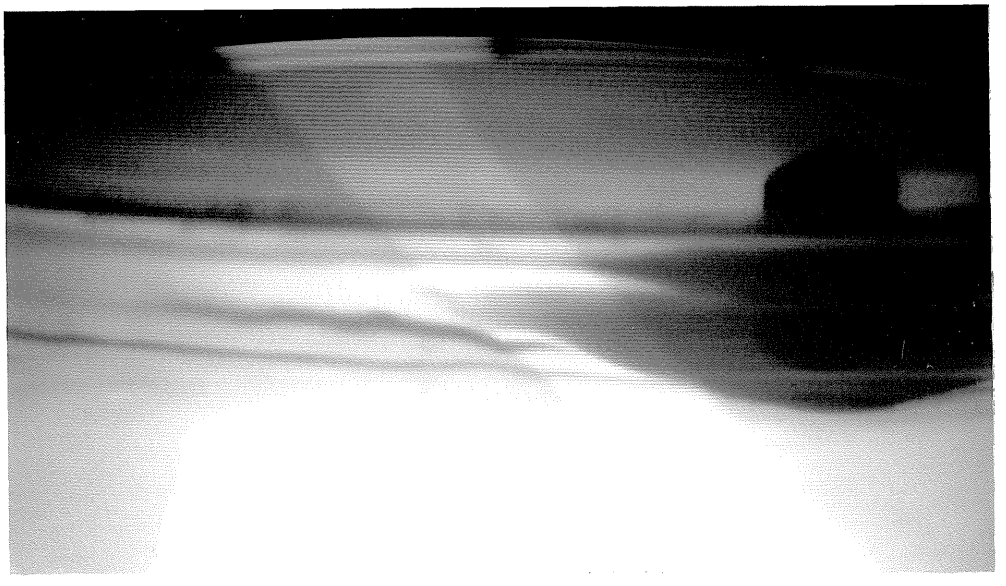

(c)

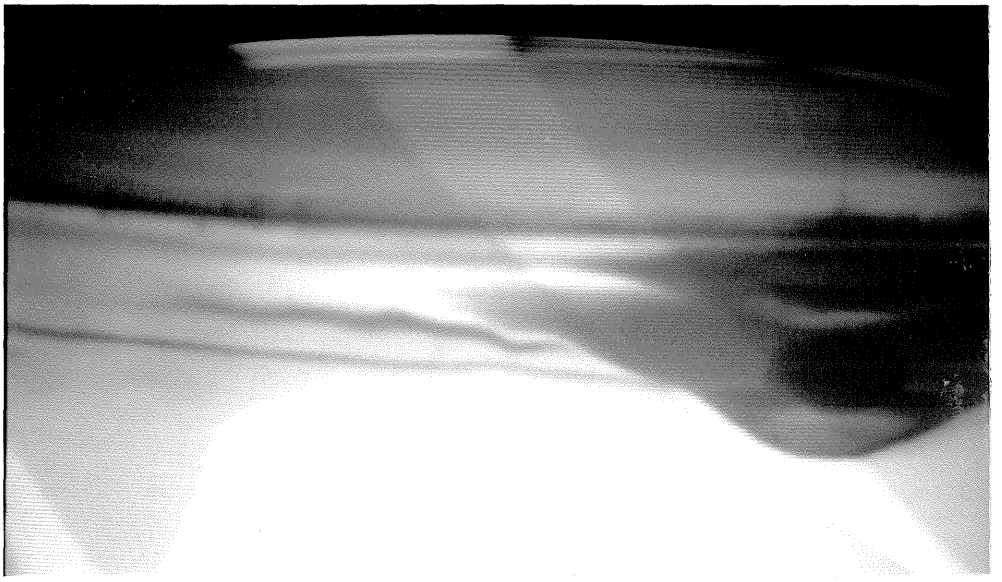

(d)

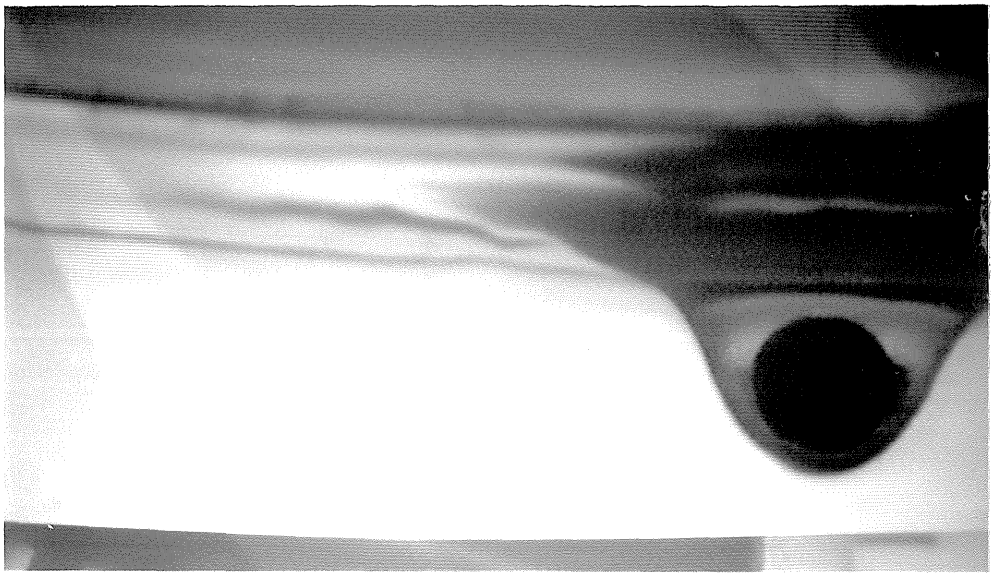

(e)

Figure XVI: Photographs for Run B8. a.) l=3, b.) l=1, c.) l=0, d.) l=-1, e.) l=-3.

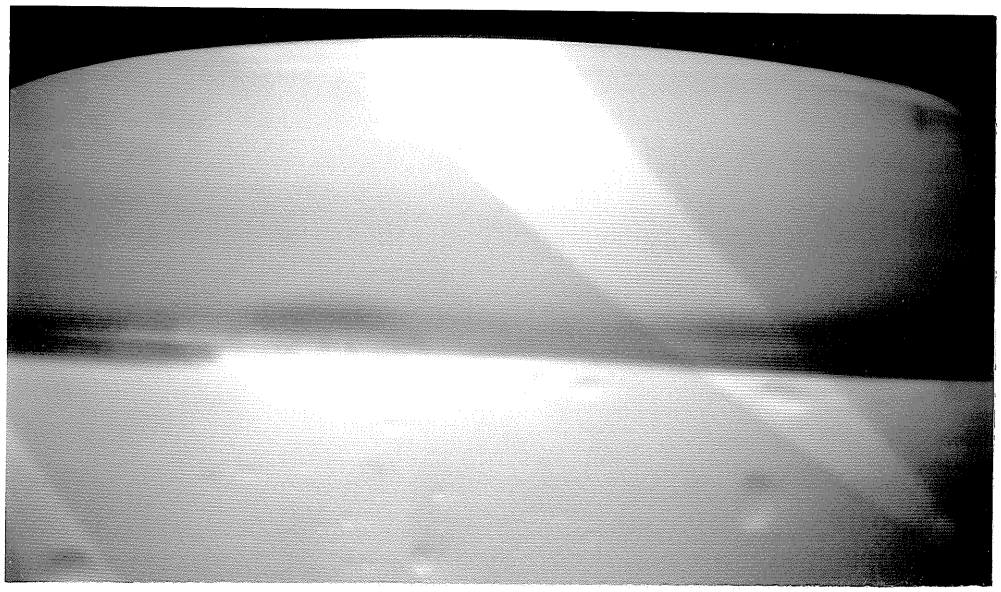

(a)

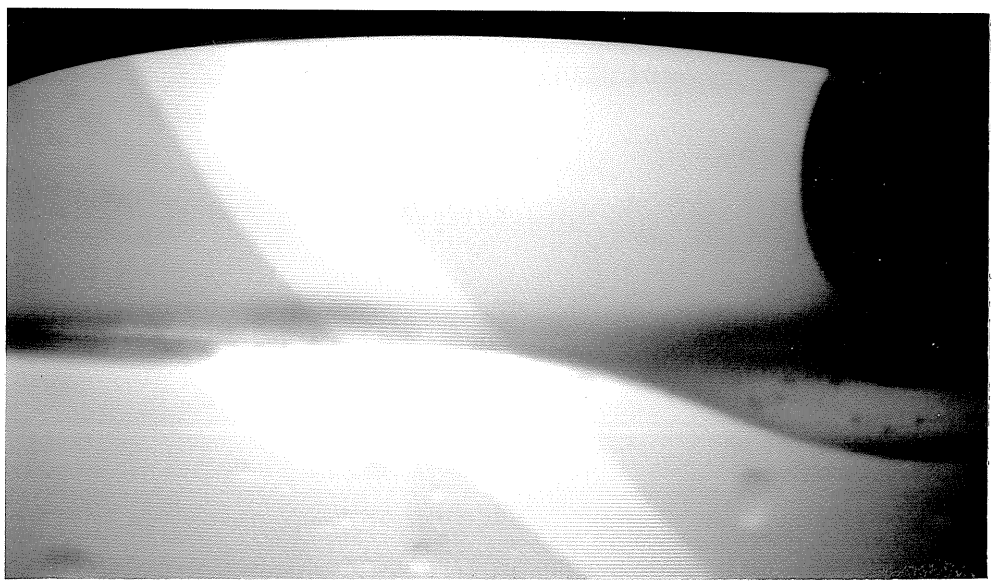

(b)

(c)

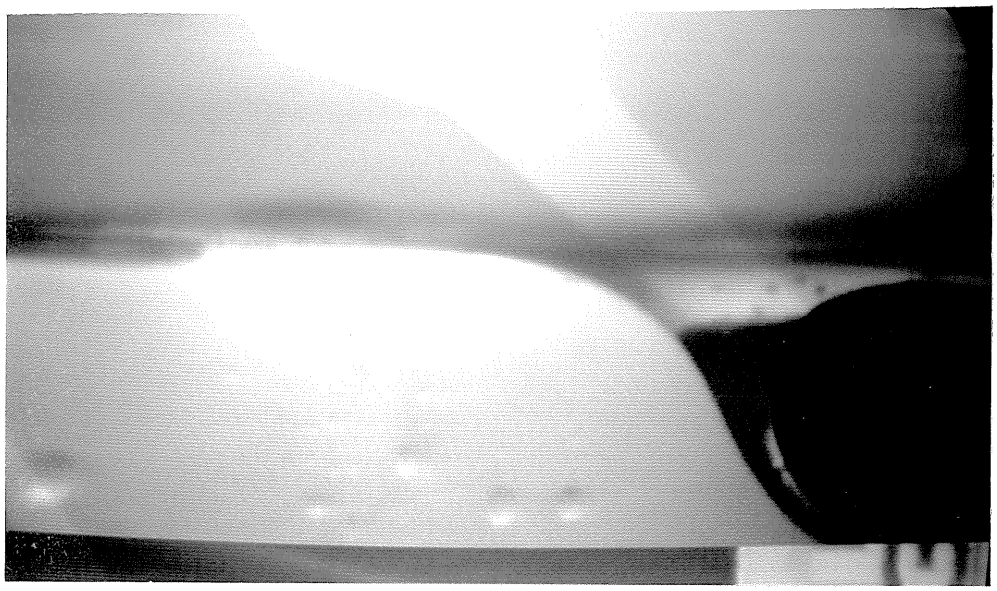

(d)

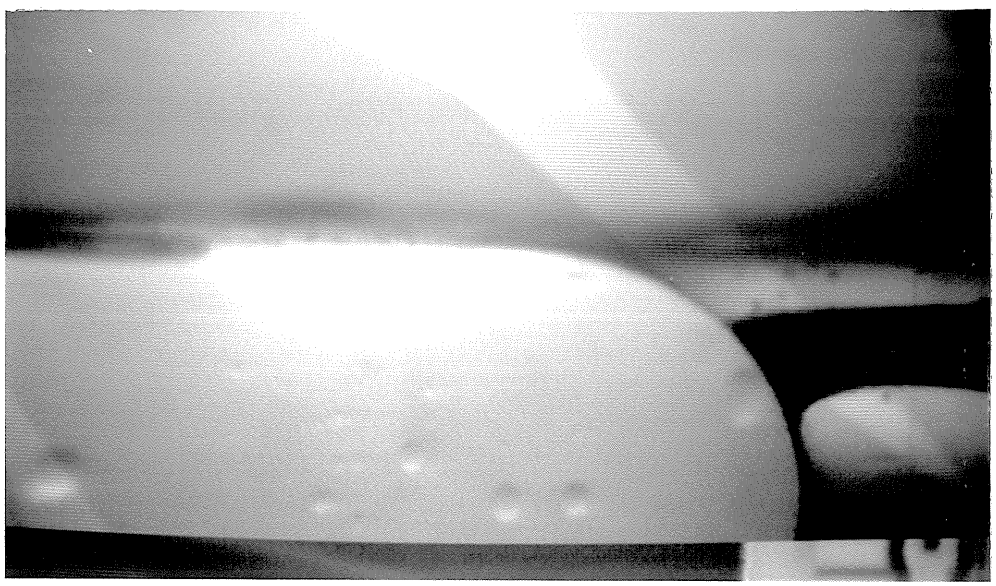

(e)

Figure XVII: Photographs for Run C4. a.) l=3, b.) l=1, c.) l=0, d.) l=-1, e.) l=-3.

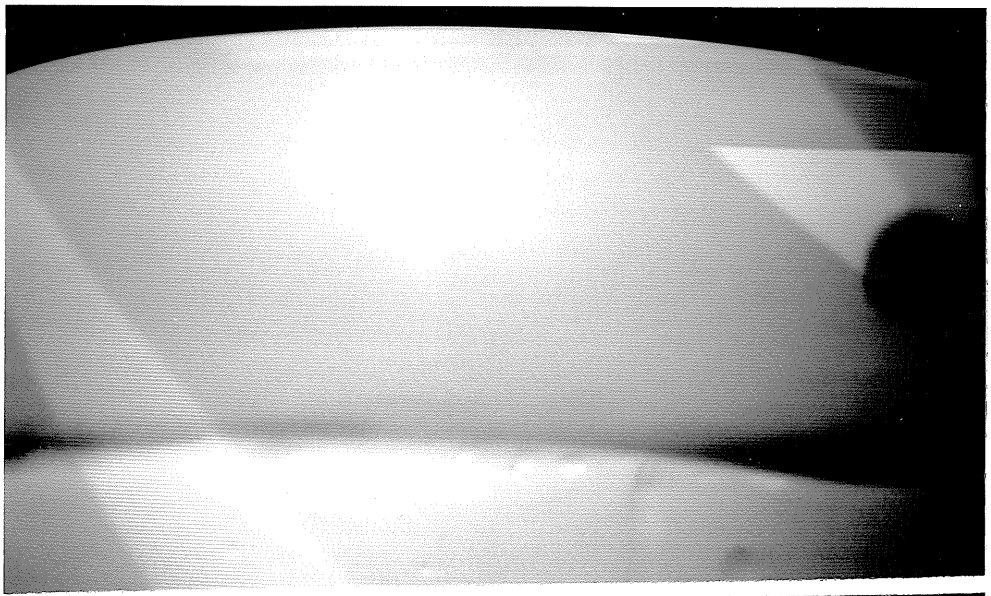

(a)

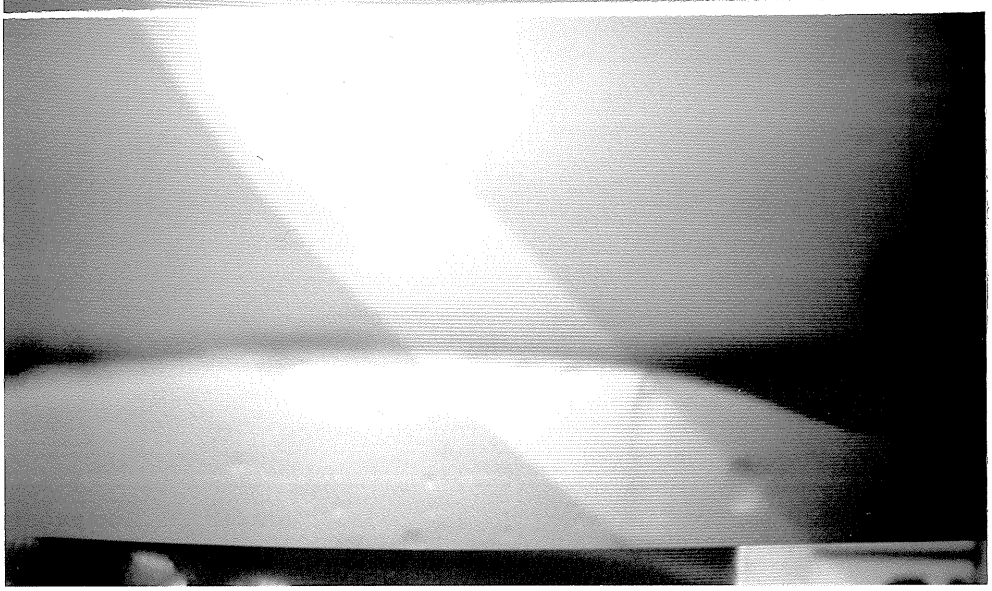

(b)

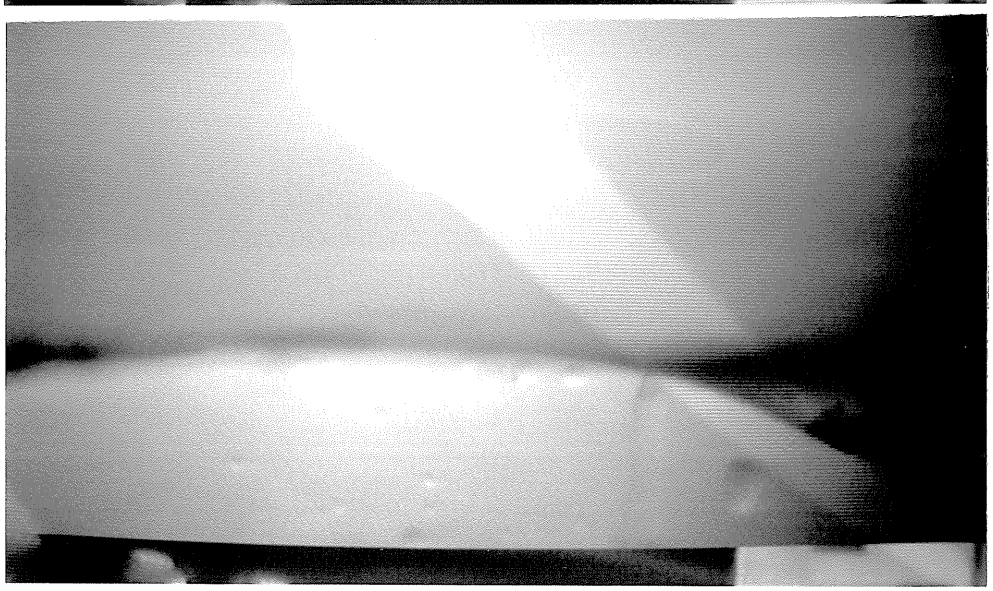

(c)

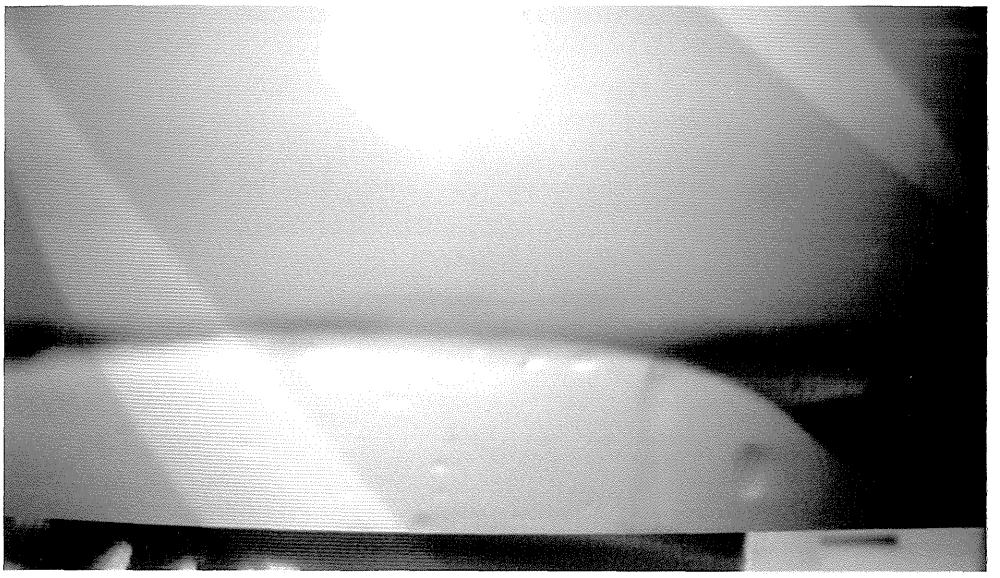

(d)

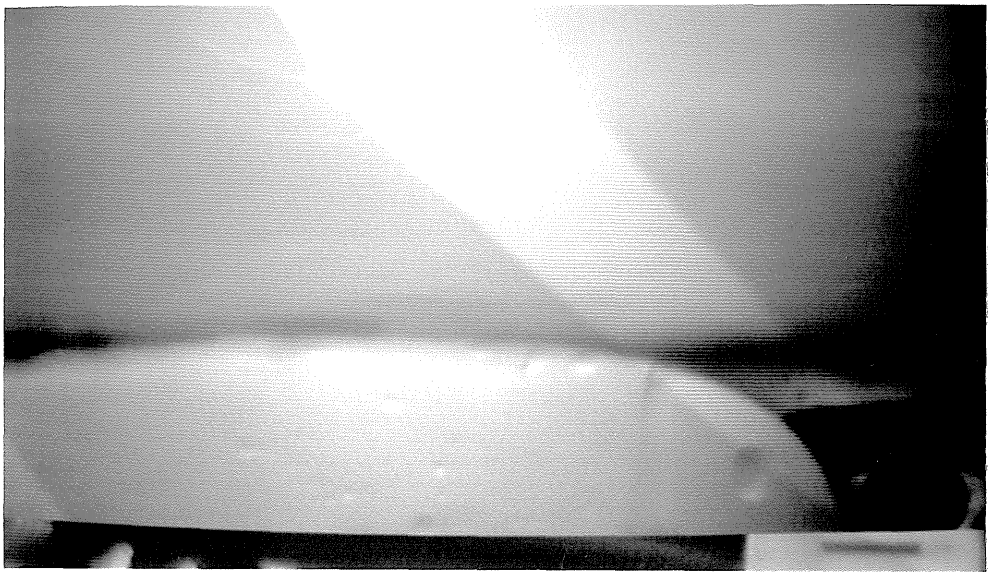

(e)

Figure XVIII: Photographs for Run C11. a.) l=3, b.) l=1, c.) l=0, d.) l=-1, e.) l=-3.

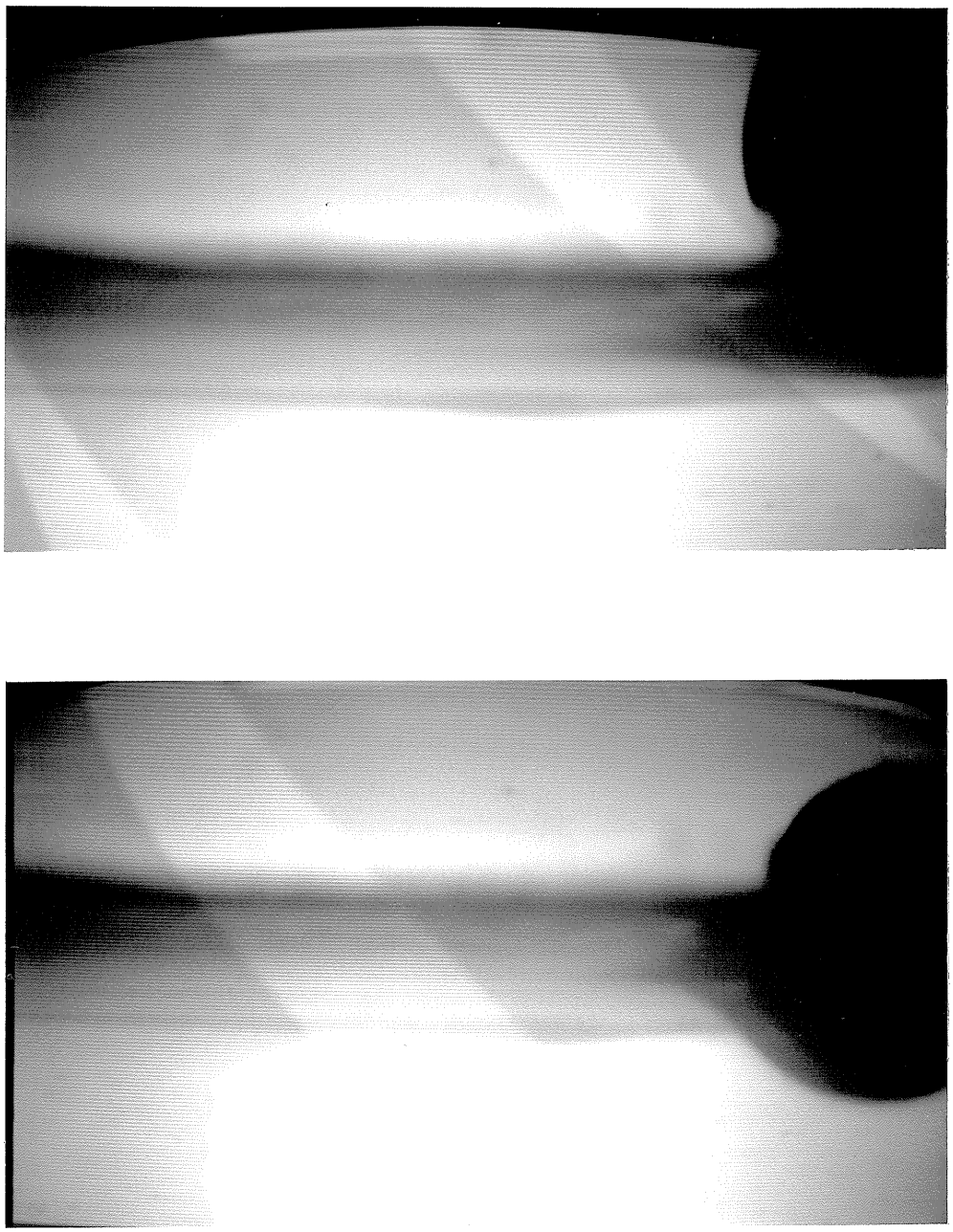

(a)

(b)

Figure XIX: Photographs for Run D2. a.) l=1, b.) l=0

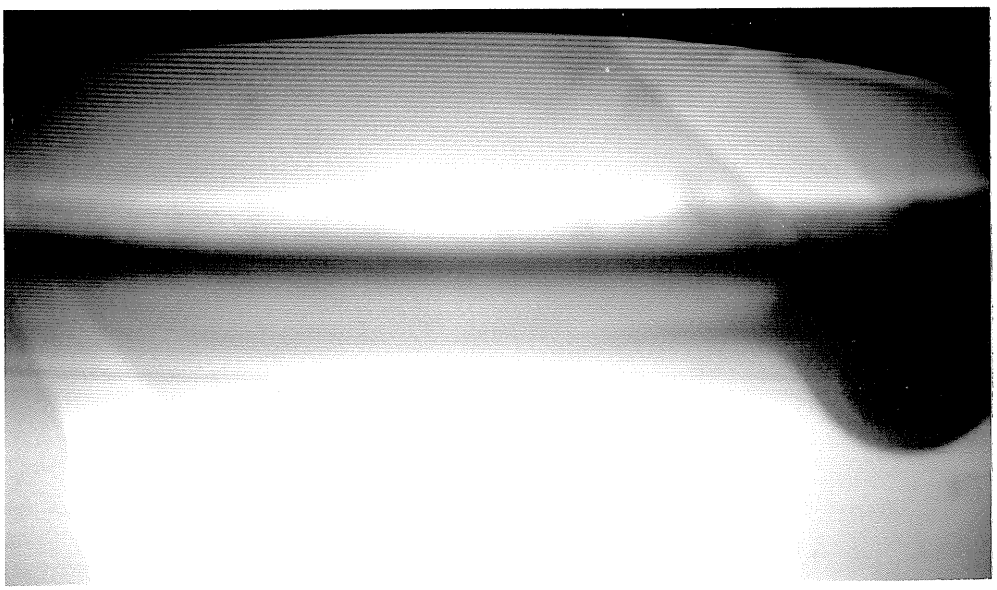

(a)

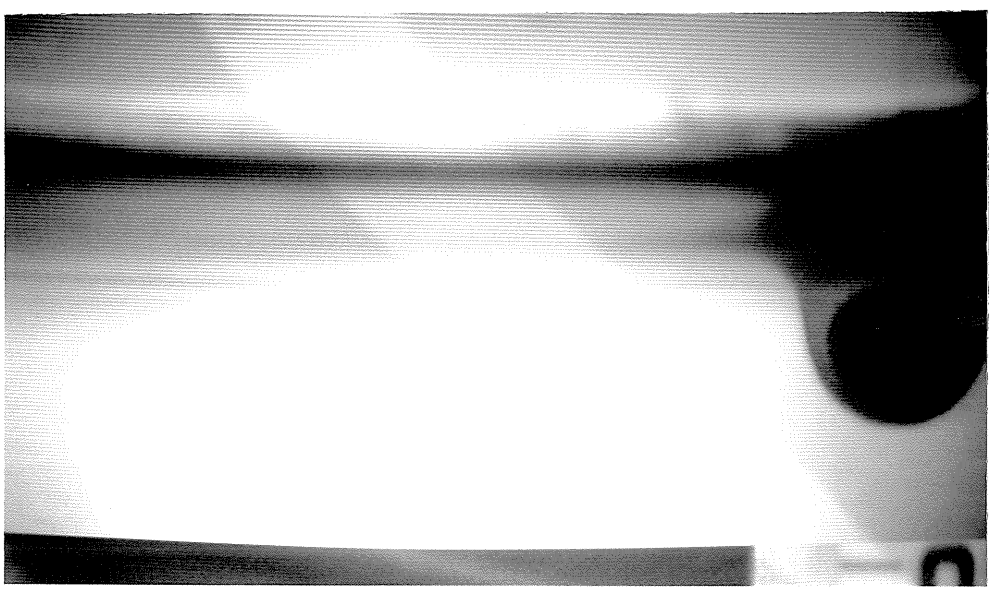

(b)

Figure XX: Photographs for Run D8. a.) l=-1, b.) l=-2

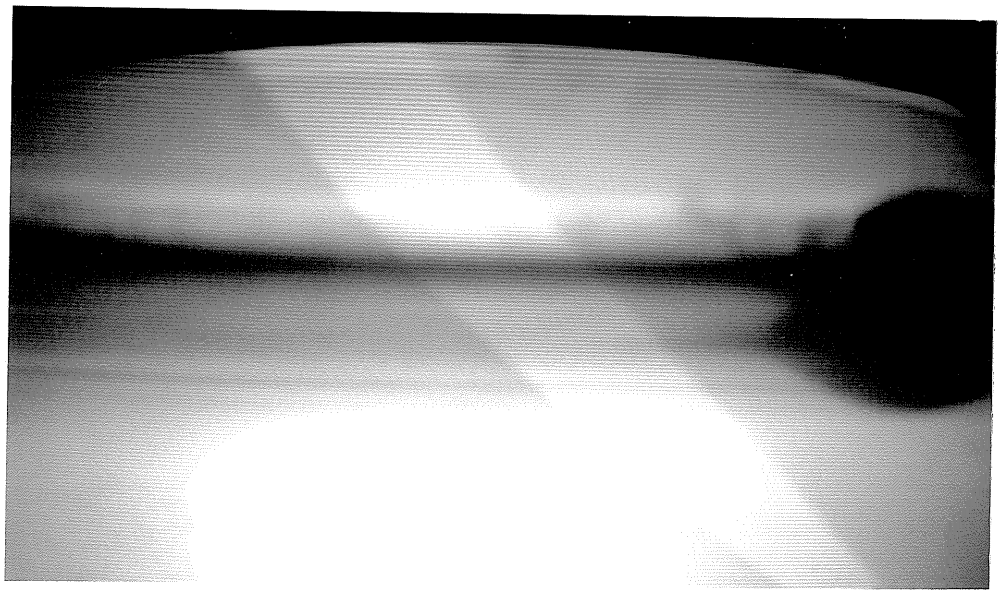

(a)

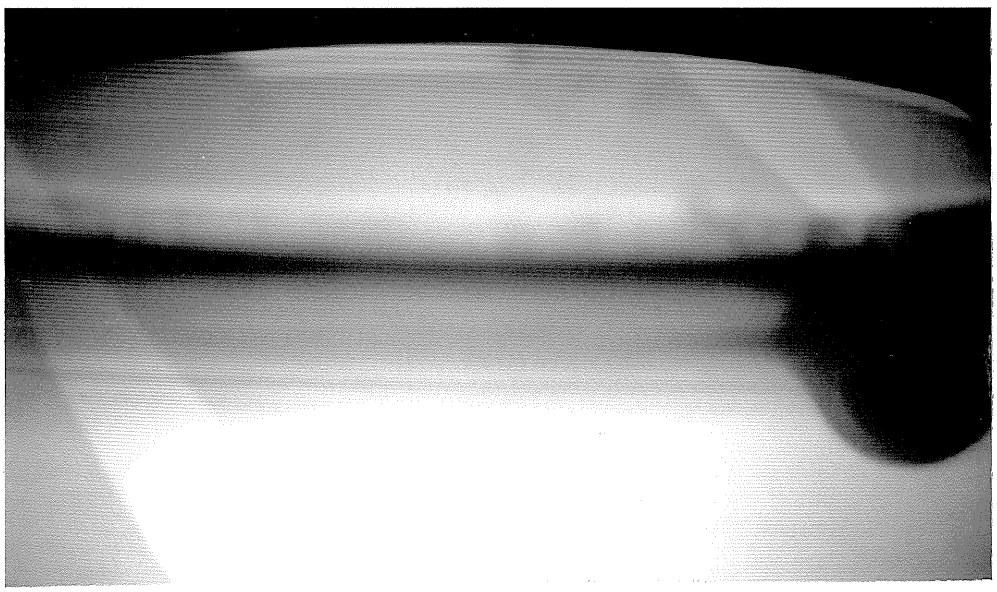

(b)

Figure XXI: Photographs for Run D10. a.) l=0, b.) l=-1

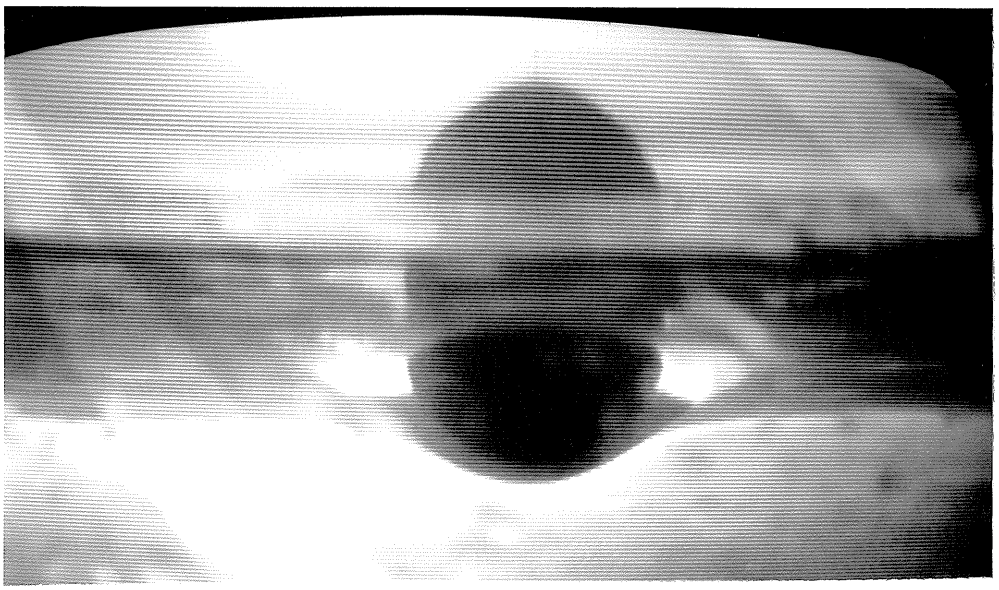

(a)

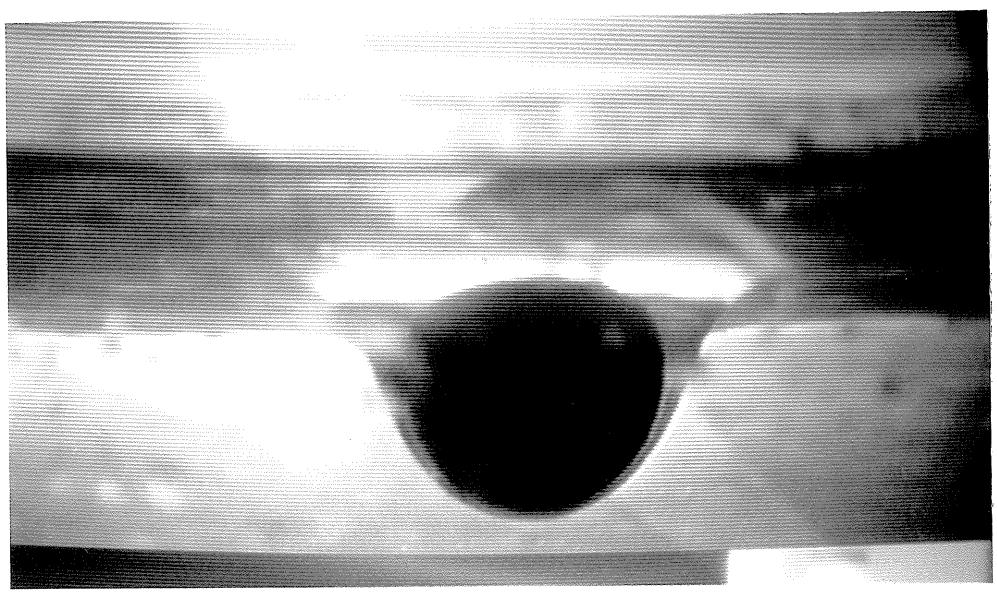

(b)

Figure XXII: Photographs for Run E2. a.) l=0, b.) l=-1

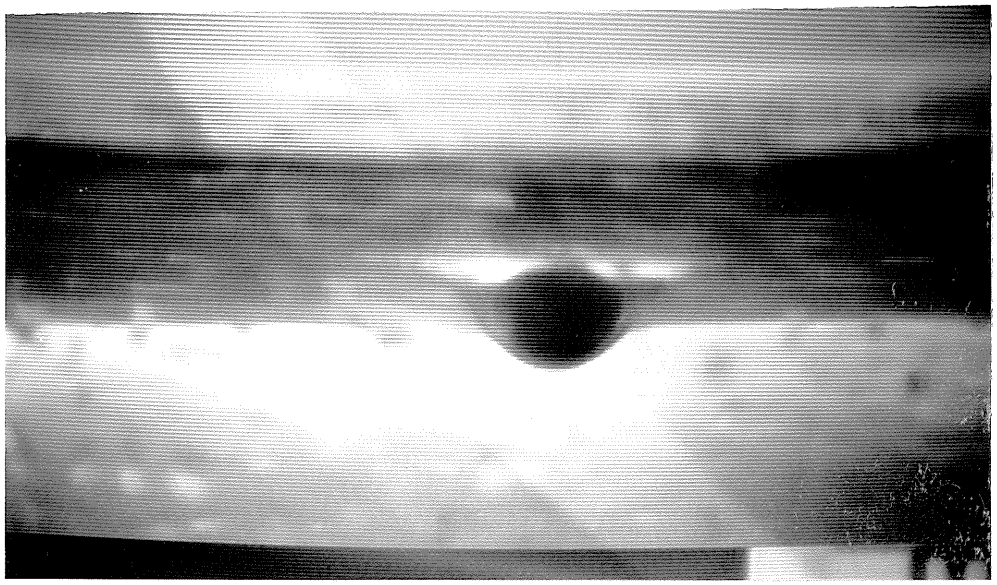

(a)

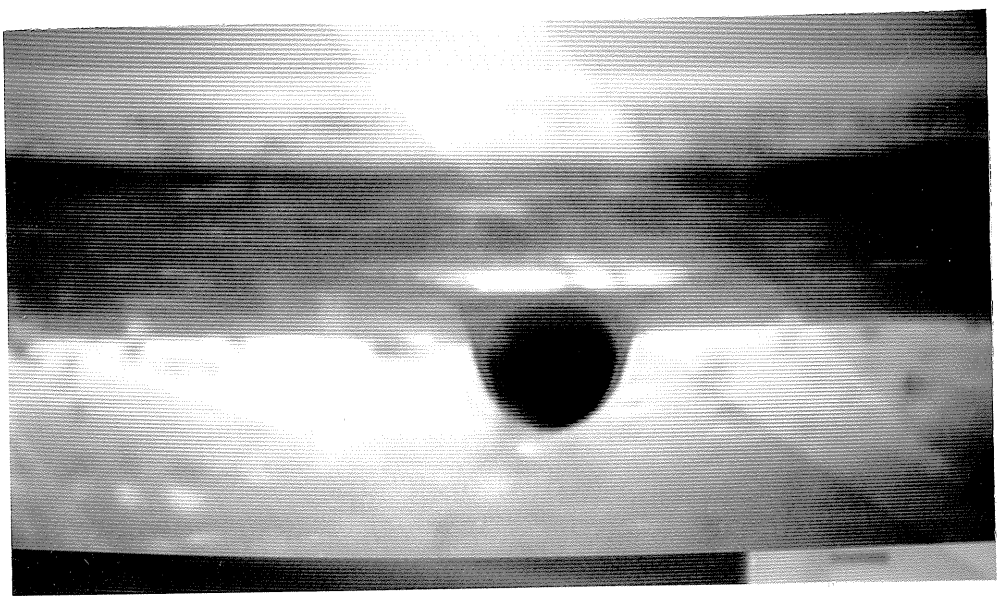

(b)

Figure XXIII: Photographs for Run E4. a.) l=-1, b.) l=-2

CHAPTER IV:

Numerical Investigation of the Parallel Motion of a Rigid Sphere Near a Deformable Interface

I: INTRODUCTION

Throughout the long history of solutions to creeping flow or inertialess problems, since the time of Stokes, researchers have been formulating problems which lead to analytical solutions. These problems necessarily fall into the class of problems with geometries in which, for example, the boundary is a coordinate surface as in the original work of Stokes (1851) for flow around a rigid sphere or near enough to a coordinate surface so that domain perturbation techniques can be used as in the work of Brenner (1964) for flow around a slightly deformed fluid drop. In Chapter I of this thesis, domain perturbation was again used to study the drag on a solid sphere as it rotated and translated relative to an infinite interface which was assumed to undergo only small deformation as a consequence of the large interfacial forces present. This work was extended by Lee and Leal (1981) to account for large deformations for translation of a rigid sphere normal to an infinite fluid/fluid interface. In this case, the boundary conditions cannot be easily satisfied analytically due both to the basic non-linearity of the problem and to the deviation of the true interface from coordinate surfaces in a simple coordinate system, and the problem was solved numerically for the force and torque on the sphere as well as the interface shape. Since the governing equations are still linear, however, it is possible to at least partially circumvent the difficulty of satisfying the boundary conditions on an arbitrary interface shape by using a general integral representation of the solution to Stokes' equation. An appropriate general solution is that obtained by Ladyzhenskaya (1963). Ladyzhenskaya (1963) used hydrodynamic potential functions to generate integral solutions to the creeping flow equations in terms of distributions of so-called single and double layer potentials over the boundary. Since the velocities and stresses on the boundaries are the weighting functions in the single and double layer integrals, their strengths can be

evaluated by inverting the system of linear equations generated by these single and double layer integrals when they are broken into finite sums.

Youngren and Acrivos (1975) were the first to use Ladyzhenskaya's solution in this manner to solve the problem of creeping flow of an unbounded fluid past a particle of arbitrary shape. Youngren and Acrivos (1976) and Rallison and Acrivos (1978) extended this work to consider the case of drops in extensional flow.

The present work is a continuation of Lee and Leal (1981) where instead of motion normal to the interface, we consider the translation of a rigid sphere parallel to an infinite, initially flat, interface in the *absence* of particle rotation. Our objective is an investigation of the drag and torque on a sphere and the interface shape caused by this parallel motion. In particular, we will investigate how these quantities are influenced by the interfacial deformation parameter, Cg (ratio of capillary number to Bond number), and the proximity of the sphere to the undeformed plane of the interface. It is our desire to determine the regions in which the small deformation results of Chapter I and flat interface work of Lee and Leal (1980) apply and also to extend these regions for the parameters studied. Specifically, one prediction which needs investigation comes from the small deformation results of Chapter I which show the existence of a normal force directed away from the interface for $l > 2$, but changing sign and directed towards the interface for $l < 2$ in some of the parallel motion studies.

It is important to note that for cases of large deformation, as discussed here, the general problem of translational motion is nonlinear and the solutions of normal and parallel motion *cannot* be superimposed to obtain results for arbitrary directions of translation as was the case for a flat or nearly flat interface (cf. Lee and Leal (1980) and Chapter I). The major difficulty in going from

the work of Lee and Leal (1981) to this problem is the fact that the flow field is no longer axisymmetric and there is thus one dimension more of complexity in the numerical equations.

II: PROBLEM FORMULATION AND METHOD OF SOLUTION

We consider here the parallel translation of a rigid nonrotating sphere near a deformable interface. The forces and torques on the sphere as well as the interface shape are to be calculated. The governing equations in each fluid are Stokes' equation and the equation of continuity

$$\nabla p_1 = \lambda \nabla^2 \mathbf{u}_1$$

$$\text{for Fluid 1} \tag{1}$$

$$\nabla \cdot \mathbf{u}_1 = 0$$

and

$$\nabla p_2 = \nabla^2 \mathbf{u}_2$$

$$\text{for Fluid 2} \tag{2}$$

$$\nabla \cdot \mathbf{u}_2 = 0$$

where $\lambda \equiv \frac{\mu_1}{\mu_2}$. The two fluids are designated by subscripts 1 and 2 where the sphere of radius, a, and velocity, U, is located in fluid 2. The pressure in equations (1) and (2) is the hydrodynamic pressure, that pressure which exists above the hydrostatic pressure of a stationary fluid at the same point. The equations (1) and (2) and the boundary conditions have been nondimensionalized with the characteristic velocity, U, length, a, and stress, $\mu_2 \frac{U}{a}$. The boundary conditions are,

$$\mathbf{u}_1, \mathbf{u}_2 \to 0 \qquad \text{as} |\mathbf{x}| \to \infty \tag{3}$$

$$\mathbf{u}_2 = \mathbf{i}_z \quad \text{on the sphere surface} \tag{4}$$

and on the interface, $z=f(\rho,\varphi,t)$,

$$\mathbf{u}_1 = \mathbf{u}_2 \tag{5}$$

$$\mathbf{n}\cdot\mathbf{u}_1 = \mathbf{n}\cdot\mathbf{u}_2 = \kappa\frac{\partial f}{\partial t} \tag{6}$$

$$[[\ \mathbf{n}\cdot\mathbf{T}\ ]] = \lambda\mathbf{n}\cdot\mathbf{T}_1 - \mathbf{n}\cdot\mathbf{T}_2 = \frac{1}{Cg}f\mathbf{n} - \frac{1}{Ca}\left(\frac{\kappa}{r}\frac{\partial f}{\partial r} + \kappa^3\frac{\partial^2 f}{\partial r^2} + \frac{\kappa^3}{r^2}\frac{\partial^2 f}{\partial \varphi^2}\right)\mathbf{n} \tag{7}$$

Equation (5) is the condition of velocity continuity across the interface while equation (6) is the kinematic condition relating the normal velocity of the interface and the change in interface shape with time. Finally in equation (7) we have the condition of matched shear stress across the interface, while the jump in the normal stress is balanced by the interfacial forces due to interfacial tension and to the jump in density across the interface. Ca and Cg are dimensionless interface parameters defined by

$$Ca \equiv \frac{\mu_2 U}{\gamma} \tag{8}$$

and

$$Cg \equiv \frac{Ca}{B} \equiv \frac{\mu_2 U}{ga^2(\rho_2-\rho_1)} \tag{9}$$

which are known, respectively, as the capillary number and the ratio of the capillary number to the Bond number, B. The interfacial tension of the interface is denoted as, γ, while, g, is the acceleration due to gravity.

As in Chapter I, the interface shape can be written in terms of a scalar function, F, where

$$F \equiv z - f(\rho,\varphi,t) = 0 \tag{10}$$

and the unit normal to the interface then calculated as

$$\mathbf{n} \equiv \frac{\nabla F}{|\nabla F|} = \kappa \left(\mathbf{i}_z - \frac{\partial f}{\partial \rho} \mathbf{i}_\rho - \frac{1}{\rho} \frac{\partial f}{\partial \varphi} \mathbf{i}_\varphi \right) \tag{11}$$

where

$$\kappa \equiv \frac{1}{|\nabla F|} = \left[1 + \left(\frac{\partial f}{\partial \rho} \right)^2 + \frac{1}{\rho^2} \left(\frac{\partial f}{\partial \varphi} \right)^2 \right]^{-\frac{1}{2}}. \tag{12}$$

In the preceding work of Chapter I we required that Ca and/or Cg be very small so that f remains small and the method of domain perturbations was then invoked to express the interface boundary conditions at z=f in terms of equivalent conditions applied at z=0. In the present work, we solve for the interface shape irrespective of the magnitude of the deformation. As indicated earlier, we use the single and double layer integral formulation of Ladyzhenskaya (1963) for the solution of Stokes' equations, together with the analysis of boundary conditions due to Lee and Leal (1981) to obtain a set of coupled integral equations for the stress and velocity components at the sphere surface and at the interface

$$\frac{1}{2}\mathbf{u}^F(x) = -\frac{3}{4}\int \frac{\mathbf{rrr}}{R^5} \cdot \mathbf{u}^F \cdot \mathbf{n}\, dS_F + \frac{1}{8\pi}\int \left(\frac{\mathbf{I}}{R} + \frac{\mathbf{rr}}{R^3} \right) \cdot \mathbf{T}_2^F \cdot \mathbf{n}\, dS_F$$

$$+ \frac{1}{8\pi}\int \left(\frac{\mathbf{I}}{R} + \frac{\mathbf{rr}}{R^3} \right) \cdot \mathbf{T}^S \cdot \mathbf{n}\, dS_S, \quad \mathbf{x} \in S_F \tag{13}$$

$$\mathbf{u}^S(x) = -\frac{3}{4}\int \frac{\mathbf{rrr}}{R^5} \cdot \mathbf{u}^F \cdot \mathbf{n}\, dS_F + \frac{1}{8\pi}\int \left(\frac{\mathbf{I}}{R} + \frac{\mathbf{rr}}{R^3} \right) \cdot \mathbf{T}_2^F \cdot \mathbf{n}\, dS_F$$

$$+ \frac{1}{8\pi}\int \left(\frac{\mathbf{I}}{R} + \frac{\mathbf{rr}}{R^3} \right) \cdot \mathbf{T}^S \cdot \mathbf{n}\, dS_S, \quad \mathbf{x} \in S_S \tag{14}$$

and

$$\frac{1}{2}(\lambda+1)\mathbf{u}^F(x) = \frac{3}{4}(\lambda-1)\int \frac{\mathbf{rrr}}{R^5} \cdot \mathbf{u}^F \cdot \mathbf{n}\, dS_F + \frac{1}{8\pi}\int \left(\frac{\mathbf{I}}{R} + \frac{\mathbf{rr}}{R^3} \right) \cdot \mathbf{T}^S \cdot \mathbf{n}\, dS_S$$

$$-\frac{1}{8\pi}\int\left[\frac{\mathbf{I}}{R}+\frac{\mathbf{rr}}{R^3}\right]\cdot\mathbf{F}(f)\,dS_F,\quad \mathbf{x}\in S_F \tag{15}$$

where

$$\mathbf{F}(f)\equiv\lambda\mathbf{n}\cdot\mathbf{T}_1-\mathbf{n}\cdot\mathbf{T}_2=\frac{1}{Cg}f\mathbf{n}-\frac{1}{Ca}\left[\frac{\kappa}{r}\frac{\partial f}{\partial r}+\kappa^3\frac{\partial^2 f}{\partial r^2}+\frac{\kappa^3}{r^2}\frac{\partial^2 f}{\partial\varphi^2}\right]\mathbf{n}.$$

The superscripts F and S designate quantities measured on the interface and sphere surface respectively. The quantity, $\mathbf{T}_2^F$, is the stress tensor evaluated in the limit as we approach the interface from fluid 2. The variable R is simply $|\mathbf{r}|$, where $\mathbf{r}$ is the interaction distance $\mathbf{x}-\eta$. $\mathbf{x}$ is the vector to the point at which the velocity and stress are to be determined and η is the vector to the point which is contributing to these quantities at $\mathbf{x}$. The integral equations govern how stresses and velocities at one location on either the sphere surface or interface affect those same quantities in another element. Thus we have interactions between any position and every other position of the system; we call the terms $\frac{\mathbf{I}}{R}$, $\frac{\mathbf{rr}}{R^3}$ and $\frac{\mathbf{rrr}}{R^5}$ the strengths of the interactions. The stresses and velocities act as weighting functions in the system of linear equations that is generated by these interactions when both the stresses and velocities are taken as constant over an entire grid element.

Now from equations (13)--(15), given the shape of the interface at some instant and the velocity of the particle, we can in principle evaluate the stress on the sphere surface, the stress at the interface and the velocity of the interface. In practice these equations are discretized and the integrals approximated as sums. In this process, the velocity or stress on an element of surface is approximated by its value at the center of the element. We thus obtain a system of linear equations in the unknown velocities and stresses, which can be solved by simple matrix inversion techniques. From the surface stresses, the

force on the sphere can be calculated and the interface velocities can be used with the kinematic boundary condition, equation (6), to march each element of the interface to a new position for a given choice of time step. The whole process can then be repeated with the new interface shape.

III: NUMERICAL DIFFICULTIES

In the first two sections we have described a problem which is formally similar to the normal motion problem solved by Lee and Leal (1981). As we have noted the primary difference is that their problem is axisymmetric and the present problem is not. In the process of solving equations (13)-(15) Lee and Leal (1981) used the axisymmetry of the normal motion problem to analytically evaluate the angular contribution to the integrals and then proceeded to partition the interface with respect only to ρ. Here, on the other hand, we must utilize a two dimensional partitioning of both the sphere and interface surfaces.

The number of grid elements thus becomes a key numerical problem and it is important to make every effort to minimize the total number. For motion of the sphere along the coordinate x direction with the undeformed interface being given as z equal to some constant, it is quite apparent that y=0 is a mirror plane of symmetry for the +y and -y half planes. We use this result to write all unknown stresses and velocities in the -y half plane in terms of their mirrored quantities in the +y half plane. This greatly increases the bookkeeping for the interactions of the elements but it does decrease the size of the matrix to be inverted by 75%.

The problem of evaluating the integrals near the singular points $\mathbf{x}=\eta$, corresponding to the self-interaction of an element, was handled in the same way as discussed by Lee and Leal (1981). In particular, the integrand was expanded in a small neighborhood of the singular point and the integral in this region was then evaluated analytically. The stress and velocity at other boundary elements (i.e. those whose center is located at $\eta \neq \mathbf{x}$) were assumed constant over the entire element for the calculation of the contribution to the stress and velocity at $\mathbf{x}$.

Each element on the interface has six unknowns (three components of velocity and three components of stress), while there are three unknowns per element on the surface of the sphere (three components of stress with the sphere velocity, **U**, specified). The half sphere was divided into 36 elements, six angular divisions between 0 and π in the φ direction and six equally spaced divisions in the z direction. This results in 36 elements covering the half sphere all with equal surface area as is readily apparent by noting that the area of any element is given in spherical coordinates by

$$\text{Element Area} = \int_{\varphi_1}^{\varphi_2}\int_{\vartheta_1}^{\vartheta_2} \sin\vartheta d\varphi\, d\vartheta = \Delta\varphi \int_{\vartheta_1}^{\vartheta_2} \sin\vartheta d\vartheta$$

$$= \Delta\varphi \int_{\cos\vartheta_1}^{\cos\vartheta_2} d\cos\vartheta = \Delta\varphi\Delta z$$

where $z=\cos\vartheta$ for a unit sphere. The interface half plane was covered with twenty elements, four divisions in the angular direction and five radial divisions. The positioning of the radial elements was such that the elements were smallest near the origin where the shape had the greatest slopes or displacements from flat and the elements were larger for large values of ρ. It was determined, for $l=6$, that it was not necessary to include effects of the interface for values of $\rho > 15$, thus the largest ρ in the outer most elements was kept at 15. As l decreased it was also possible to decrease the maximum value for ρ, so for $l < 3$ the greatest value for ρ evaluated was 10 which increased the density of grid points in the region of largest deformation. These results, for the truncation of the interface area included in the calculations, were shown in great detail to lead to accurate results by Lee and Leal (1981). Fewer grid points were positioned on the interface than on the sphere surface because each interfacial grid contributes twice as many unknowns as generated at the sphere surface for the

addition of a grid point. To show that this represents a sufficient number of interfacial grid points, we have compared solutions for the motion of a sphere at ℓ=2 for λ=1, Ca=∞ and Cg=1 evaluated using twenty interface elements extending out to ρ=15 in one case and twenty elements out to ρ=10 in the other. The results, as presented in Table II, show that increasing the density of the interface grid resulted in a 9% change in the normal force and even smaller changes in the parallel force and torque values.

Once the interactions of the elements (as called for in the integrals of Ladyzhenskaya (1963), equations (13)--(15)) have been evaluated, the matrix containing these interactions is inverted using a Gaussian elimination scheme done in double precision to minimize round-off errors. The forces and torques on the body are evaluated by summing the forces and torques on each of the individual sphere surface elements. The final step is then to calculate a new interface shape from the kinematic condition on the interface, equation (6). As the velocity and stress of each element greatly influences the motion of its neighboring elements it was found that the interface shape was very slow to converge. To enhance the convergence, an Adams-Moulton predictor-corrector scheme (see Carnahan, Luther and Wilkes (1969)) was added to try to minimize the number of steps taken to a steady shape.

IV: NUMERICAL RESULTS

To check for numerical accuracy of the calculation scheme we set ℓ =10,000 to remove all interactions between the sphere and the interface, thus reducing the problem to the motion of a sphere in an infinite fluid. For any direction of translation or rotation the forces and torques on the body in this case were within 0.6% of their theoretical values. The next point where comparison with theory is possible is to check forces, torques and interface shape for parallel translation for large values of ℓ when the flat interface results of Lee and Leal (1980) and the small deformation results of Chapter I apply. Table I shows the comparison for the forces and torques for Ca=∞, Cg=10 and λ=1, while the steady interface shapes from both theory and numerical work for these same parameters are presented in figure I. From these, it is apparent that the shapes are quite close, the forces agree to within 3% and the torque agrees to within 10% at ℓ=6. Figure II shows that the deviation in the shape from the theoretical shape has increased by ℓ=3, still for Cg=10, while table I shows that the normal forces are in significant disagreement. Thus our results for ℓ=6 show good agreement with theory but do point to the possibility that a finer mesh would bring even better agreement. For ℓ=3 the discrepancies are becoming larger and we expect the theoretical results to no longer apply.

The convergence of the numerical scheme proved slow even for the small deformation problem[1] when the interface starts from flat. For this reason the number of parameters varied was limited but judiciously chosen to make the most of the computation time available. The first thing to note is that we used

1. It is obvious that slow convergence is a minor problem for any case where the results are close to known small deformation calculations. In this case the small deformation results are used as the initial guess of the shape. The problem of convergence only becomes significant as the deformations become large. In fact guessing the shape to initialize large deformation cases commonly increased computation time when compared with the time for the initial guess of a flat interface, as the interface motion was very sensitive to any error in the shape.

$Ca=\infty$ (the interfacial tension was set to zero) for all cases. The interfacial tension forces depend on the curvature of the interface at a point and with the limited number of grid points on the interface, any result depending on calculated values of surface curvature would be of questionable accuracy at best. This omission of Ca as one of the independent parameters is not thought to be a serious void in the results, however, as the analytical results for a nearly flat interface and the numerical results for the normal motion problem (cf. Chapter I, Chapter II and Lee and Leal (1981)) indicate both that Ca is unimportant whenever $Ca > Cg$ and $Ca > 1$, and also that variations in Ca and Cg yield qualitatively similar results. The calculations have also used a fixed value of $\lambda=1$. The results in Chapter I predict a very limited dependence on λ for this problem when $\lambda \geq 1$. It is left for later studies to investigate results for $\lambda < 1$. The cases that were chosen studied the effects of the variation of l and Cg.

In figure III we compare the shapes for $\lambda=1$, $Ca=\infty$, and $Cg=1$ as l is varied from 3 down to 1.5. As the sphere gets closer to the interface the deformation obviously increases and becomes more localized. This localization of the normal stress difference for a close approach of the sphere to the interface allowed us to concentrate more grid points near the origin for cases with $l < 3$. Also, the fact that the deformation tends to be close to zero at the largest values for ρ which were calculated, again indicates that the grid did indeed include large enough values for ρ. Probably the most striking result relative to the earlier small deformation theories, is the absence of fore/aft symmetry in the interface shape. For example, the point at which the interface crosses the undeformed plane lies behind the center of the sphere. Thus the interface appears as a traveling wave which "trails" behind the sphere. Table II presents the force and torque data that correspond to figure III. The numbers show that the forces and torques increase monotonically as the sphere moves closer to the interface.

This is in conflict with the results in Chapter I insofar as the normal force is concerned. In Chapter I it was shown that the normal force in the parallel motion problem was directed away from the interface and increased in strength as l decreased from ∞ to 3. For $l<3$, however, the normal force began to decrease and finally was directed towards the interface for $l<2$. This change in sign for the force was attributed in Chapter I to the neglected terms in the small deformation solution for the flow field. With l small, it was anticipated that the neglected terms would be of the same order as the terms used to calculate the normal force. Table II confirms the existence of a monotonically increasing normal force directed away from the interface as l decreases.

The effects of changing Cg are considered in figure IV and table III. It is clear, as expected, that the interface becomes more deformed as the interfacial "restoring" force (the density difference in this case) is decreased. This larger deformation is also coupled with a much broader shape, quite the opposite result than was found for the variation of l. Table III shows that both the parallel force and parallel torque *decrease* as the deformation increases. This is simply a consequence of the locally greater mean distance between the sphere and the interface, and is expected for $\lambda \geq 1$. The corresponding results for small values of λ are not as apparent, and it is evident from the nondeformable interface problem that they cannot be deduced directly from the results for $\lambda \geq 1$. The most interesting result of varying Cg comes from the normal force. In this case the force is caused by the deformation and the proximity to the wall. But it can be seen that as the interface undergoes a larger deformation (for $Cg > 1$), some of the fore/aft symmetry of the interface disappears and the sphere appears locally further from the interface, yielding a smaller normal force for a given value of l.

V: CONCLUSIONS

The results clearly show that since the interface shapes were steady for parallel translation of a solid sphere the interface acts as a traveling wave. Thus the parallel motion problem can be solved here as a steady problem, where the forces and torques on the sphere and the shape of the interface will be constant as the sphere moves parallel to the interface displaced some fixed distance l. It was also determined that the wave form trails behind the sphere center and can deviate greatly from the symmetrical shapes obtained for the small deformation problem in Chapter I. Because of the skew in the interface shape, a symmetrical initial shape (i.e. a small deformation result whose magnitude was increased) is a poor starting guess for the numerical routine. The normal force results obtained here for small l are of some interest because they show that this force continues to be directed away from the interface even for small l, thus demonstrating that the peculiar sign change predicted for small l in the small deformation theory of Chapter I was, in fact, simply a consequence of a breakdown in the asymptotic expansion for too small values of l. Also, the dependence on the "degree" of deformation is not simple as was evident in the results for the variation in Cg. It was shown that (for Cg> 1) the normal force on the sphere began to decrease with increase in Cg, this appears to be a consequence of some combination of the decrease in the fore/aft symmetry and locally greater mean distance to the interface.

Finally there is a need to improve the numerical rate of convergence of the interface shape if a study of parallel motion near a deformable interface is to be performed for the case of deformation dominated by interfacial tension. As noted earlier, an increase in the number of grid points on the interface would be necessary if interfacial tension is to be studied. To increase the total number of grid points requires a faster scheme for the matrix inversion step. One

possibility for improved convergence might utilize the fact that some of the grid points for large ρ experience only very small movements relative to the maximum displacement of the interface. Thus computation time could possibly be reduced by converging the shape for small ρ, holding the normal velocity for large ρ at zero and the shear velocity and stresses at their zero deformation values. The matrix that is to be inverted will be small during the major part of the time necessary to deform the interface and this matrix will only grow as larger values of ρ are added to be converged.

References

Brenner, H. 1964 The Stokes resistance of a slightly deformed sphere. Chem. Eng. Sci. **19**, 519.

Carnahan, B., Luther, H. A. and Wilkes, J. O. 1969 "Applied Numerical Methods". Wiley & Sons, New York.

Lee, S. H., Chadwick, R. S. & Leal, L. G. 1979 Motion of a sphere in the presence of a plane interface. Part 1: An approximate solution by generalization of the method of Lorentz. J. Fluid Mech. **93**, 705.

Lee, S. H. and Leal, L. G. 1980 Motion of a sphere in the presence of a plane interface. Part 2: An exact solution in bipolar coordinates. J. Fluid Mech. **98**, 193.

Lee, S. H. and L. G. Leal 1981 The Motion of a Sphere in the Presence of a Deformable Interface Part 2: A Numerical Study of the Translation of a Sphere Normal to an Interface, Submitted **JCIS**.

Ladyzhenskaya, O. A. 1963 'The mathematical theory of viscous incompressible flow". Gordon and Breach, New York.

Rallison, J. M. and Acrivos, A. 1978 Numerical study of the deformation and burst of a viscous drop in an extensional flow. J. Fluid Mech. **89**, 191.

Stokes, G. G. 1851 On the effect of the internal friction of fluids on the motion of pendulums. Camb. Phil. Soc. **9**, Pt. II., 8.

Youngren, G. K. and Acrivos, A. 1975 Stokes flow past a particle of arbitrary shape: a numerical method of solution. J. Fluid Mech. **69**, 377.

Youngren, G. K. and Acrivos, A. 1976 On the shape of a gas bubble in a viscous extensional flow. J. Fluid Mech. **76**, 433.

TABLE I				
	l=6		l=3	
	Theory	Numerical	Theory	Numerical
Normal Force	0.000775	0.000794	0.0012	0.0061
Parallel Force	~ 1.015	1.0246	1.0294	1.0361
Parallel Torque	~ -0.003	-0.0033	-0.0103	-0.0113
Cg=10 Ca=∞ λ=1				

Comparison of forces and torques from theory and numerical results as a function of the distance to the interface.

TABLE II				
l=	1.5	2.0	2.0	3.0
Normal Force	0.0628	0.0440	0.0404	0.0219
Parallel Force	1.0369	1.0347	1.0290	1.0253
Parallel Torque	-0.0207	-0.0120	-0.0112	-0.0073
Elements out to ρ=	10	10	15	15
Cg=1 Ca=∞ λ=1				

Dependence of forces and torques on the distance to the interface for parallel motion to a deformable fluid/fluid interface and a comparison for the dependence of forces and torques on grid density at l=2.

TABLE III				
Cg=	0.001	0.1	1	10
Normal Force	0.0000075	0.0061	0.0219	0.0194
Parallel Force	1.0366	1.0361	1.0253	1.0117
Parallel Torque	-0.0115	-0.0113	-0.0073	-0.0025
Ca=∞ λ=1 ℓ=3				

Dependence of forces and torques on the density difference parameter, Cg, for parallel motion to a deformable fluid/fluid interface.

Figure Captions

Figure I: Comparison of shapes of the numerical results with theory in the small deformation region where $\lambda=1$, $l=6$, $Cg=10$, and $Ca=\infty$.

_____numerical results __ __ __ __theoretical results

Figure II: Comparison of shapes of the numerical results with theory in the small deformation region where $\lambda=1$, $l=3$, $Cg=10$, and $Ca=\infty$.

_____numerical results __ __ __ __theoretical results

Figure III: Interface shape comparison for the variation of l, with $\lambda=1$, $Cg=1$, and $Ca=\infty$.

_____$l=3$, __ __ __ __$l=2$, and - - - - - - - $l=1.5$

Figure IV: Interface shape comparison for the variation of Cg, with $\lambda=1$, $l=3$, and $Ca=\infty$.

_____$Cg=0.001$, __ __ __ __$Cg=0.1$, - - - - - - - $Cg=1$,

and ___ ___ ___ ___$Cg=10$

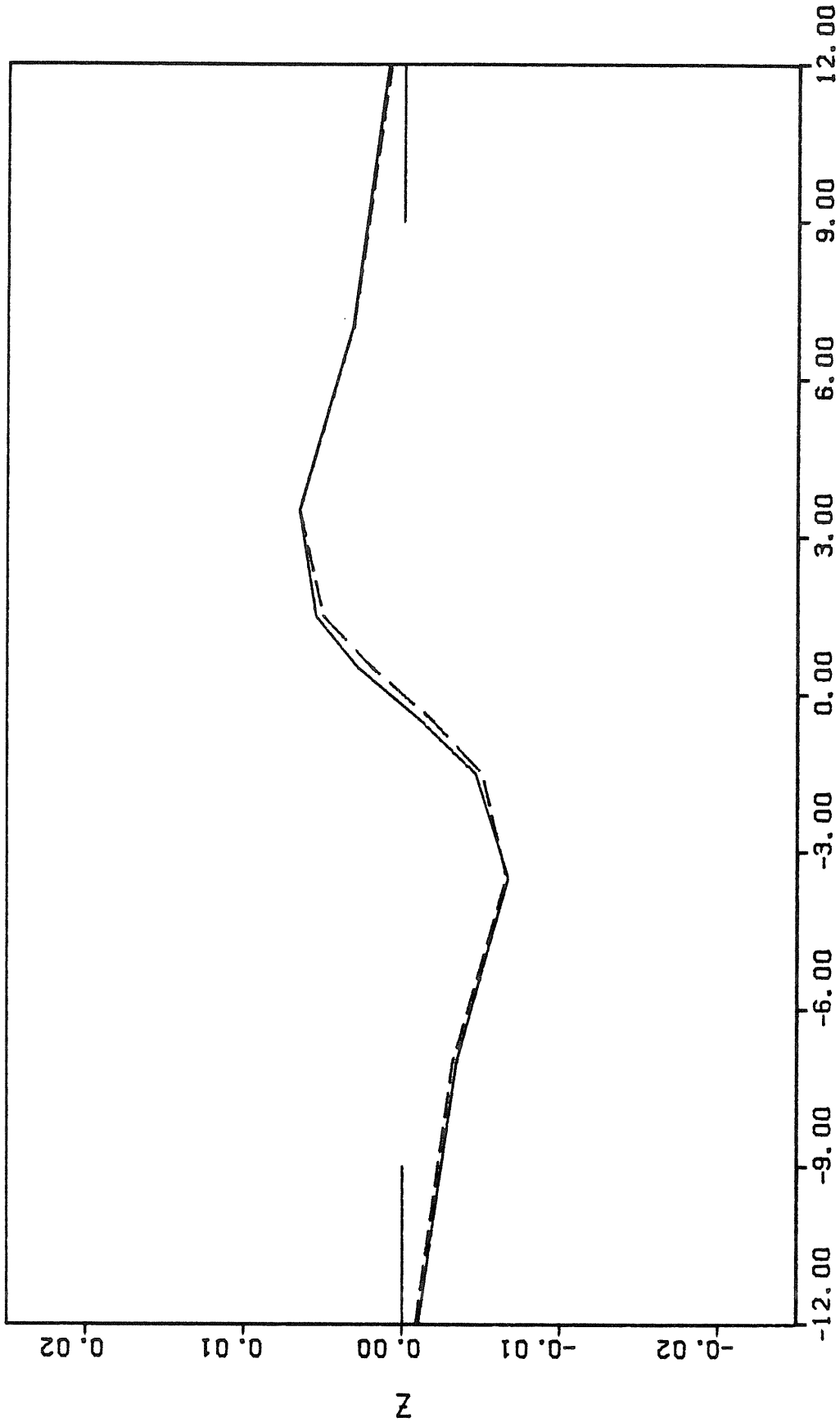

FIGURE I

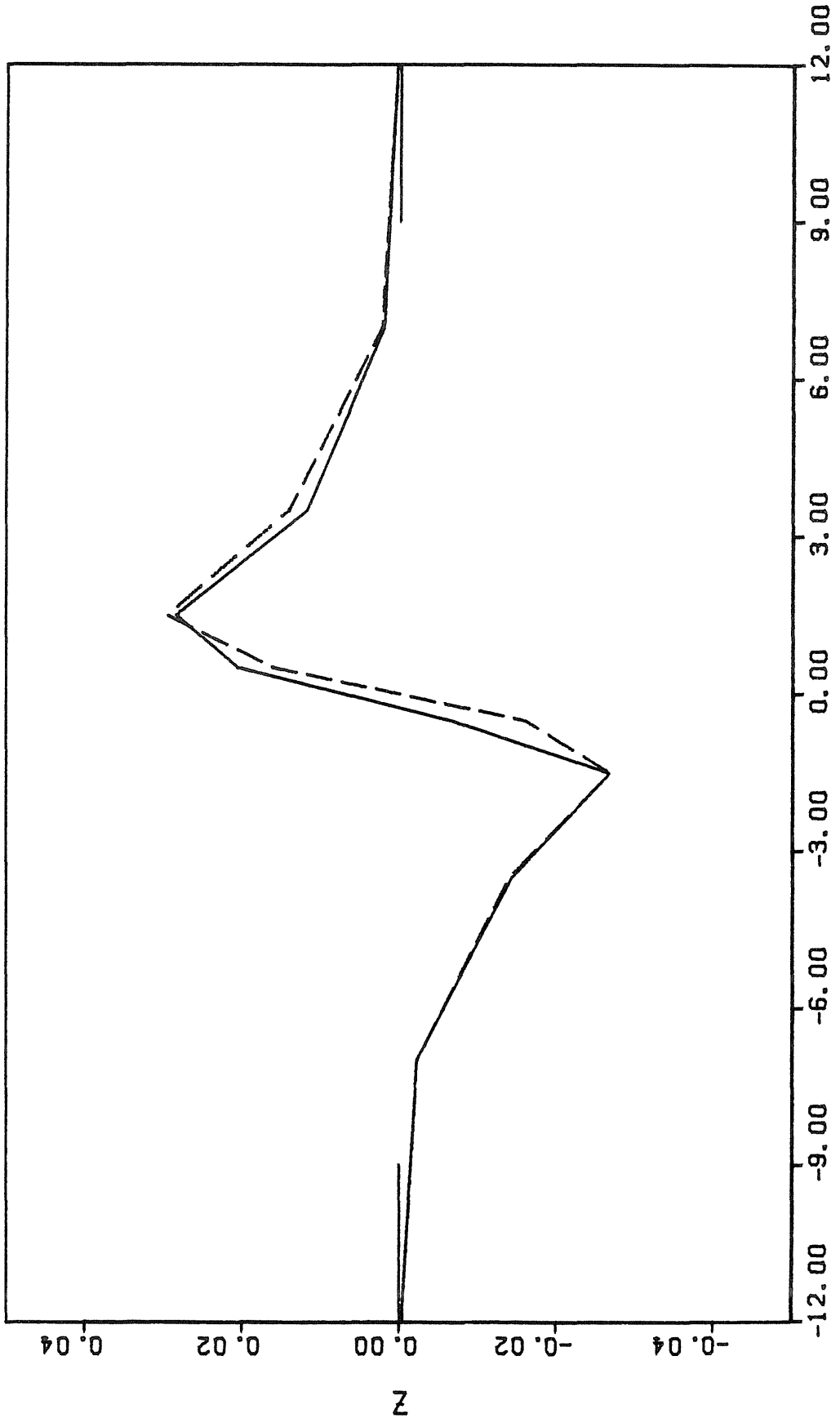

FIGURE II

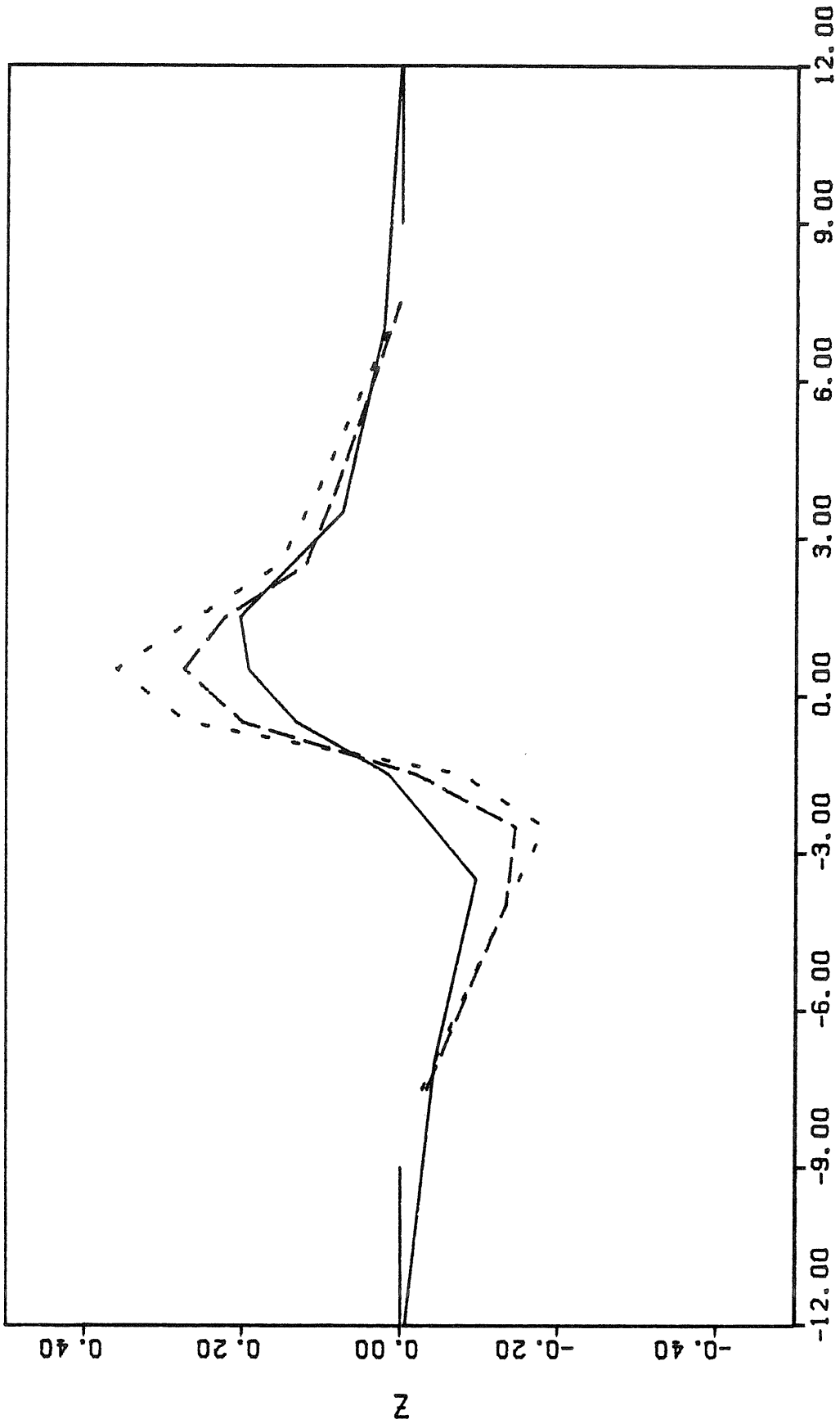

FIGURE III

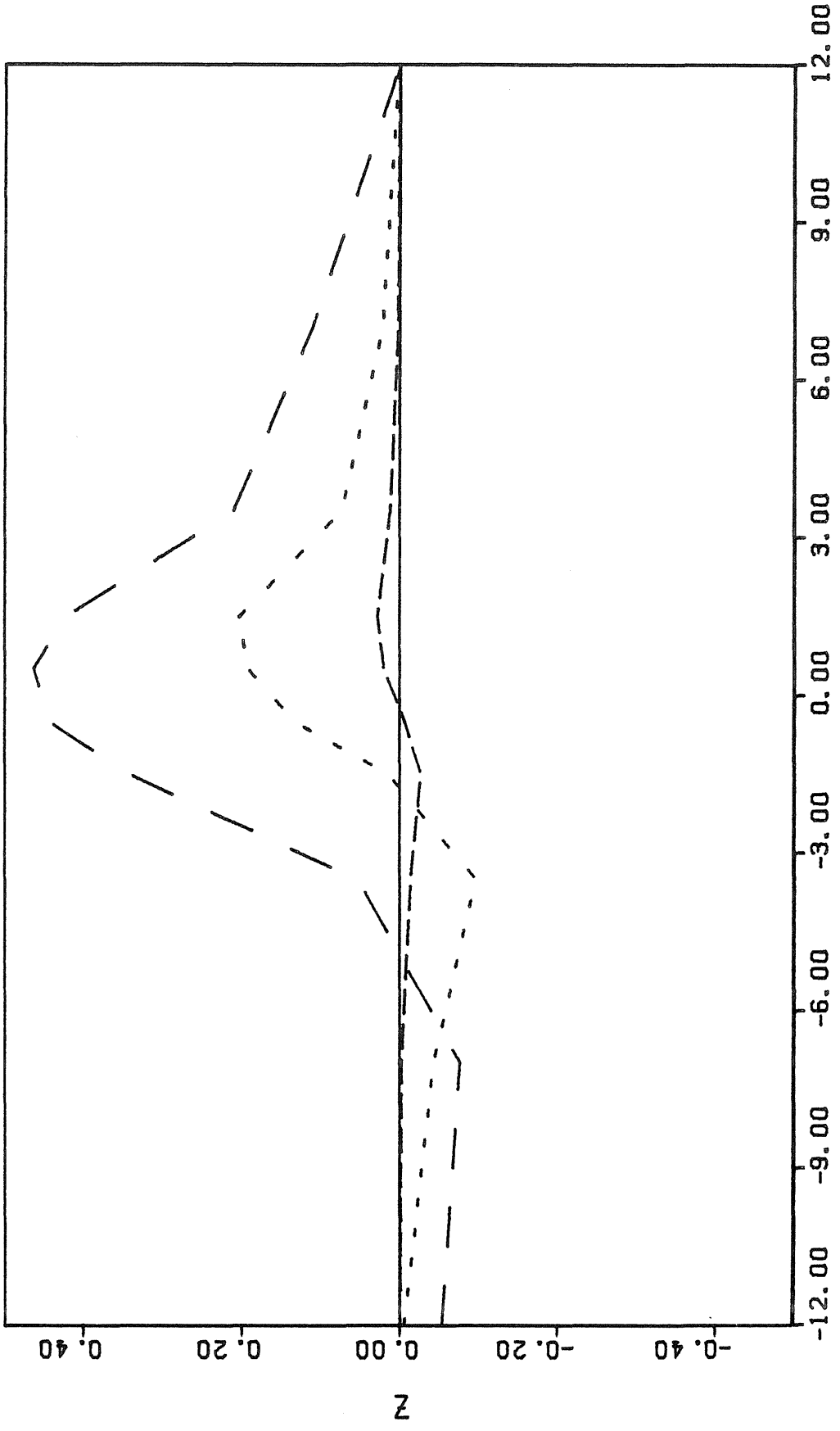

FIGURE IV